ICMRM9 - 2007

9th International Conference on Magnetic Resonance Microscopy
"*Heidelberg*" Conference

and the 7th Colloquium on Mobile NMR

September 3rd to 7th 2007
in Aachen, Germany

Edited by P. Blümler 2007

Detailed Program:　　Monday, 3rd of September

Invited talks are indicated by an asterix*

Time	Session (*Chair*)	No.	Presenter	Title
8:30 – 9:20	Educational Session I (*Blümich*)	1	Bernhard Blümich	Introduction to NMR and imaging
9:25 – 10:15		2*	Eiichi Fukushima	Hardware: Nuts and Bolts
10:15 – 10:45	Coffee Break			
10:45 – 11:35	Educational Session II (*Blümich*)	3*	Paul T. Callaghan	Diffusion and transport in NMR
11:40 – 12:30		4*	Xiao Lizhi	Some Important Issues for NMR Logging and Applications
12:30 – 14:15	Lunch Break			
14:15 – 14:45	Cultural Heritage (*Perlo*)	5*	Eleonora Del Federico	Unilateral NMR studies of Lead White Pigment with protinaceus binders
14:45 – 15:15		6	Donatella Capitani	Unilateral NMR for Monitoring Cultural Heritage
15:15 – 15:40		7	Bertram Manz	Three-dimensional MR Microimaging of fossils across taxa
15:40 – 16:00		8	Frank Rühli	Investigation of ancient mummies and bones by NMR and CT
16:00 – 16:30	Coffee Break			
16:30 – 17:00	Methods (*Song*)	9*	Petrik Galvosas	Experimental aspects of NMR diffusion exchange and diffusion-relaxation correlation spectroscopy
17:00 – 17:20		10	Juan Perlo	*Ex situ* NMR in highly homogeneous fields: ^{1}H spectroscopy
17:20 – 17:35		11	Johannes T. Schneider	CRAZED Imaging with RARE-Acquisition at High Fields
17:35 – 17:55		12	Louis-S. Bouchard	Geometry of Low-Field NMR
17:55 – 18:15		13	Xiaohong Ren	A rapid NMR method for measurements of a 3D flow velocity vector and a 3D diffusion tensor
18:15 – 18:30		14	Christoph H. Arns	Xray-CT enhanced interpretation of T_2-D-DG_0^2 NMR correlation experiments
18:30 – 21:00	Welcome Reception (*Bruker*)			

Detailed Program: Tuesday, 4th of September

Invited talks are indicated by an asterix*

Time	Session (*Chair*)	No.	Presenter	Title
8:30 - 9:00		15*	Pablo J. Prado	Compact MR Sensors: Who Pays for the Development?
9:00 - 9:20		16	Peter Blümler	The NMR-Cuff: Force free, hinged magnet arrangements for portable MRI and EPR
9:20 - 9:40	Hardware (*Fukushima*)	17	Peter J. McDonald	The Surface GARField and The Tree Hugger: Magnets designed for use in the built environment and with building materials
9:40 – 10:00		18	Shin Utsuzawa	Unilateral NMR apparatus with homogeneous B_0 field
10:00 – 10:15		19	Robin Dykstra	A Low Power High Performance Digital Transceiver for Mobile NMR
10:15 – 10:45	Coffee Break			
10:45 – 11:15		20*	Luisa Ciobanu	Spectroscopic Studies and High Resolution Imaging Applications
11:15 – 11:35	Small coils (*Stapf*)	21	Andrew McDowell	Toward a portable frequency-domain NMR spectrometer
11:35 – 11:55		22	Elad Harel	Beating the NMR time scale by remote detection flow imaging
11:55 – 12:15		23	Jeffrey H. Walton	A Small Planar Gradient Set for MRI Rheometry
12:15 – 12:35		24	Vasiliki Demas	Low Cost Ex Situ NMR with microcoils
12:35 – 14:00	Lunch Break		Meeting of the Executive Committee	
14:00 – 16:00	Poster Session I (*van Dusschoten*)		Even Poster numbers	
16:00 – 16:30	Coffee Break			
16:30 – 17:00		25	Yi-Qiao Song	Two-dimensional NMR of diffusion systems
17:00 – 17:30	Porous media (*Callaghan*)	26*	Rainer Kimmich	NMR mapping of ionic currents and electro-osmotic flow in microsystem channel networks
17:30 – 17:50		27	Rustem Valiullin	Fluid distribution in mesoporous materials
17:50 – 18:10		28	Ziheng Zhang	Magnetic Resonance Imaging of Water Content across the Nafion Membrane in Operational PEM Fuel Cells
18:10 – 18:30		29	Hans Adriaensen	Quantitative monitoring of liquid ingress in heterogeneous layered materials using a Mobile Universal Surface Explorer (MOUSE®)
18:30– 19:30	Division Committee		Meeting of the Committee of the Division of Spatially Resolved Magnetic Resonance of the Ampere Society: report, next meetings, elections	

Detailed Program: Wednesday, 5th of September

Invited talks are indicated by an asterix*

Time	Session (*Chair*)	No.	Presenter	Title
8:30 - 9:00	Materials and function (*Seymour*)	30*	Jeffrey A. Reimer	NMR Assessment of Polymer Mechanical Properties: Portable NMR and elastomeric moduli?
9:00 - 9:25		31*	Sarah L. Codd	Biopolymer and Water Dynamics in Microbial Biofilm Extracellular Polymeric Substance
9:25 - 9:45		32	Johannes Leisen	Fluid Distribution and Transport in Engineered Fibrous Substrates
9:45 – 10:00		33	M. L. Johns	MR Studies of Industrial Micelle Solutions
10:00 – 10:15		34	Steven D. Beyea	MR Microscopy of Resorbable Polymeric Bioceramics
10:15 – 10:45	Coffee Break			
10:45 – 11:05	Vendor Presentations (*Codd*)	35	Dieter Gross	New Hardware and Software Development and Optimization for NMR Microscopy
11:05 – 11:30		36	Michael Fey	NMR Microscopy with Isotropic Resolution below 10 um Using Dedicated Hardware and Optimised Methods
11:30 – 11:50		37	Andrew Coy	Curiosities from Earth's field and Low field NMR
11:50 – 12:10		38	Jürgen Kolz	The Profile NMR-MOUSE: Methods and Applications
12:10 – 12:30		39	Alexander Weisser	Customized Coils
12:30 – 14:00	Lunch Break			
14:00 – 16:00	Poster Session II (*van Dusschoten*)	Odd Poster numbers		
16:00 – 16:30	Coffee Break			
16:30 – 16:55	Young investigators (*Blümler*)	40	Nathalie Homan	MRI of axial and radial hydraulic conductivity in (woody) plants
16:55 – 17:20		41	Jennifer R. Brown	NMR measurement of irreversibility and particle migration in dilute sheared Brownian suspensions
17:20 – 17:45		42	Mark W. Hunter	Measurement and simulation of the non-local dispersion tensor in porous media
17:45 – 18:10		43	Paul P. Zänker	Spin echoes and intermolecular double-quantum coherences in gases in the fast diffusion regime
18:10 – 18:35		44	Meghan E. Halse	Novel Approaches to High-Resolution NMR Spectroscopy in Low and Ultra-low Fields
18:35 – 19:00		45	Shinya Handa	Development of compact MRI systems for specific diseases
19:00 – 19:30	General Meeting			General Meeting of the Ampere Division (all members): report, next meetings, elections

Detailed Program: Thursday, 6th of September

Invited talks are indicated by an asterix*

Time	Session (*Chair*)	No.	Presenter	Title
8:30 - 8:55		46*	Katsumi Kose	Compact MRI applications
8:55 - 9:15	Biomedicine (*Jakob/Haase*)	47	Lawrence L. Wald	Highly Parallel Array Detection for MRI
9:15 - 9:35		48	Thoralf Niendorf	Merits and Challenges of Clinical Cardiovascular MRI at 3.0 Tesla
9:35 – 9:55		49*	Oliver Speck	Highfield MRI: Human Applications at 7T
9:55 – 10:15		50	Peter Jakob	Molecular and cellular MRI
10:15 – 10:45	Coffee Break			
10:45 – 11:10	Structure and function relations in food and plants (*Van As*)	51	John van Duynhoven	Non-invasive Assessment of Moisture migration in Food Products by MRI
11:10 – 11:35		52	Martin D. Hürlimann	Encoding information in the CPMG echo shape
11:35 – 12:00		53	Dagmar van Dusschoten	Fitting Intrinsic Parameters to diffusion-relaxation data
12:00 – 12:15		54	Rebecca Milczarek	Mandarin Oranges Using Multivariate Analysis of MR Image Data
12:15 – 12:30		55	Gerd Melkus	Localized ^{1}H NMR and ^{1}H Spectroscopic Imaging on wild type and mutant pea
12:30 – 14:00	Lunch Break			
14:00 – 14:30	Chemical engineering (*Casanova*)	56*	Lynn F. Gladden	Recent Developments in Imaging Multi-Phase Reactors
14:30 – 14:50		57	Siegfried Stapf	MRI in Chemical Engineering – facts and promises
14:50 – 15:10		58	Melanie M. Britton	Probing and Controlling Chemical Waves Using Magnetic Resonance Imaging
15:10 – 15:30		59	Janez Stepišnik	Granular micro-dynamics by CPMG spin echo
15:30 – 15:45		60	Igor Mastikhin	Dynamics of gas and liquid during cavitation
15:45 – 16:00		61	K.V. Kovtunov	Observation of parahydrogen induced polarization in heterogeneous hydrogenation reaction and its MRT application
16:00 – 19:00	Excursion (*Fattah, van Dusschoten*)		Activities in Valkenburg, NL	
19:00 – 21:30	Lunch Break		Conference Dinner in *Feestgrot* in Valkenburg, NL Young Investigator Awards, Poster Prizes, Art Image Prizes	

Detailed Program:　　Friday, 7th of September

Invited talks are indicated by an asterix*

Time	Session (*Chair*)	No.	Presenter	Title
8:30 - 9:00	Polarization Enhancement (Demas)	62*	Song-I Han	Contrast and Sensitivity Enhanced Magnetic Resonance by Dynamic Nuclear Polarization
9:00 - 9:30		63*	Ross W. Mair	Improving ^{3}He polarization for human lung imaging in subjects in horizontal and vertical orientations
9:30 - 9:55		64*	Igor V. Koptyug	Bridging the gap between NMR Imaging and Catalysis
9:55 – 10:15		65	Luis Agulles Pedrós	Study of diffusion coefficient of hyperpolarized gases and their use as a contrast agent in MRI
10:15 – 10:45	Coffee Break			
10:45 – 11:15	Ultra-Low Fields (*Han*)	66*	John Clarke	SQUID-detected NMR and MRI in Microtesla Fields
11:15 – 11:35		67	Shoujun Xu	Laser-detected magnetic resonance imaging in the Earth's field
11:35 – 11:55		68	Andrei N. Matlashov	Multi-channel MRI at ultra-low fields compatible with MEG
11:55 – 12:15		69	Stephan Appelt	Long living spin states in the Earth's magnetic field
12:15 – 12:30		70*	Paul T. Callaghan	The Antarctic experience with Earth field NMR
12:30 – 12:45	Farewell (*Seymour*)			

Sponsors of the 9th ICMRM

We gratefully acknowledge financial support from:

Sanofi-Anventis
http://www.sanofi-aventis.de

Stelar
http://www.stelar.it

RAPID Biomedical GmbH
http://www.rapidbiomed.de/

BASF
http://corporate.basf.com/de

ACT
http://www.act-aachen.com/

Conference General Info:

Organizing Committee:
- Dr. Peter Blümler, ICG-3, Research Center Jülich, Germany
- Prof. Dr. Bernhard Blümich, ITMC, RWTH Aachen, Germany
- Prof. Dr. Henk Van As, NMR Centre, Wageningen University, The Netherlands
- Dr. Dagmar van Dusschoten, ICG-3, Research Center Jülich, Germany

Additional local organizers:
- Yasmin Abdel-Fattah, Research Center Jülich, Germany
- Dr. Markus Küppers, ITMC, RWTH Aachen, Germany
- João Martins, ITMC, RWTH Aachen, Germany

Venue, Conference Location: (see also maps)
Karman Auditorium, Eilfschornsteinstrasse 15,
52062 Aachen

Registration and Help Desk:
Registration starts on Monday (3rd Sep.) at 8:00 o'clock.
Registration is possible during the entire meeting.
Please note, that we can only accept cash (Euros) as
late payment. A teller machine and bank is close by
(2 min walking at *Templergraben*).
If you need help, please contact the registration desk or people wearing badges and
conference buttons.

Fees:
The registration fees apply to all participants including those with contributed papers:
Regular participant:
Ampere Member: 350.- €,   Non-Member: 385.- €
Students:
Ampere Member: 100.- €,   Non-Member: 120.- €

The fees cover the participation at the meeting, the conference booklet and the conference
dinner.

Conference Phone:
The registration desk can be reached under +49-241-80 90919.
(that is 0241-80-90919 from a local phone)

WLAN:
Wireless LAN will be provided
        Login: 9thICMRM
        Password: Aachen_2007

with the following services available:
World Wide Web: via HTTP/HTTPS
eMail: via SMTP/SMTPS, POP3/POP3S, IMAP/IMAPS
data exchange: via SSH, active FTP, VPN, ICQ, Lotus Notes

Conference Language:
The conference language is English.

Excursion (Thursday 6th Sep):

The excursion will take place in Valkenburg, just across the border in the Netherlands. A variety of tours can be selected from, each of roughly one and a half hours. Cycling in old mines, visiting an old coal mine or enjoying a visit to a 'ghost' mine. Other alternatives can be offered for those of you who are already familiar with (Dutch) coal mines. Transportation details will be announced during the conference.

Conference Dinner:

The conference dinner will take place in the *Feestgrot* (Party Cave) in Valkenburg (The Netherlands) within walking distance of each of the excursions. Please visit http://www.feestgrot.nl to get a good impression of the locality.

During the conference dinner the winners of the Image Art Competition, Poster Competition and of the Young Investigator Award will be announced.

Coffee Breaks:

All coffee breaks are held near the poster section and the vendor suits. Cookies and beverages will be organized.

Lunch/Dinner:

There will be no organized lunches and dinners (except the conference dinner). The Karman auditorium has a cafeteria for snacks, and the city of Aachen provides a variety of nice restaurants and snack bars. You might explore on your self or ask for suggestions at the help desk.

Babysitting during Conference:

We will provide a professional babysitter during the conference hours. Please contact the helpdesk for further information.

Instructions for Oral Lectures:

The duration of individual talks can be seen from the program. Please time your presentation such that 5 min for discussions are included.

The talk material can be either a computer-presentation (MS Office 2007, Open Office 2.2, Adobe Acrobat 8 or earlier versions) or using an overhead projector (standard will be computer presentation). You can bring and connect your own computer notebook or bring the presentation on memory sticks, CD or DVD.

Please contact a technical assistant to help you in preparing the presentation at least 1 hour ahead of your session and notify your chairman early before the session.

Instruction for Posters:

The poster sessions are on

- Tuesday, 4th Sep. from 14:00 – 16:00 o'clock for <u>even</u> poster numbers
- Wednesday, 5th Sep. from 14:00 – 16:00 o'clock for <u>odd</u> poster numbers

but the posters should stay mounted and displayed throughout the entire conference. The poster boards are located on the ground floor (see schematic drawing, next page) and will be marked with the poster number. Check the lists before the poster abstracts in this book in order to find your poster number.

<u>Poster size</u>: A0 portrait (841 * 1189 mm), max. size (1000 * 2200 mm). For fixation pushpins and magnets will be provided. Do not attach the poster with other material (e.g. tape etc.).

Manufacturer's Display:

Vendors can display their products throughout the conference in the designated area in the foyer (see schematic drawing, next page). Please contact Markus Küppers (mkueppers@mc.rwth-aachen.de or phone: ++49 241 80 26971) at least one week before the conference starts for special requests (no. desks, power outlet, extra space, etc.).

Aachen City Map:

①   Karman Auditorium (Conference) , Eilfschornsteinstrasse 15

②   Marketplace

③   Dome

④   Pontstrasse (Pubs, Snackbars)

⑤   Hotel Reichshof, Seilgraben 2, 52062 Aachen

⑥   Hotel Lousberg, Saarstraße 108, 52062 Aachen

⑦   Hotel IBIS Aachen Marschiertor, Friedlandstraße 8, 52064 Aachen

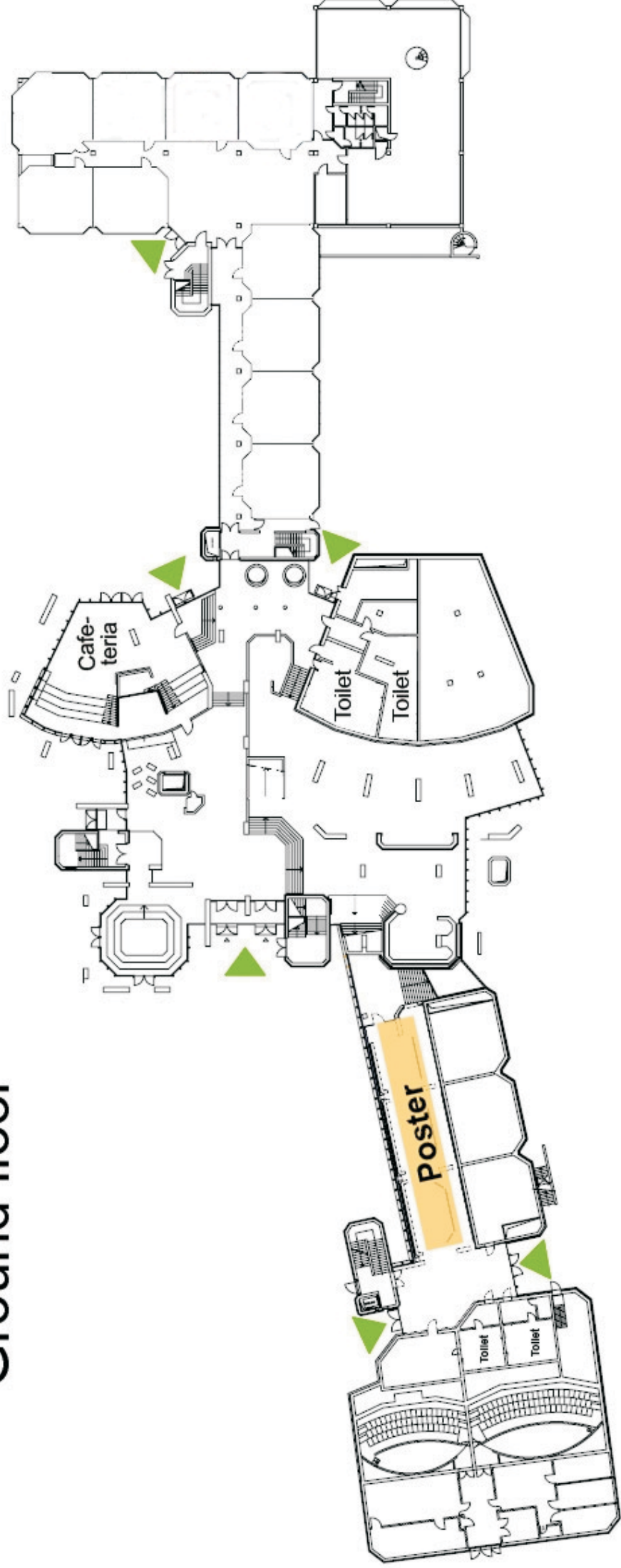⑧   Hotel Mercure Aachen City, Jülicher Straße 10 – 12, 52070 Aachen
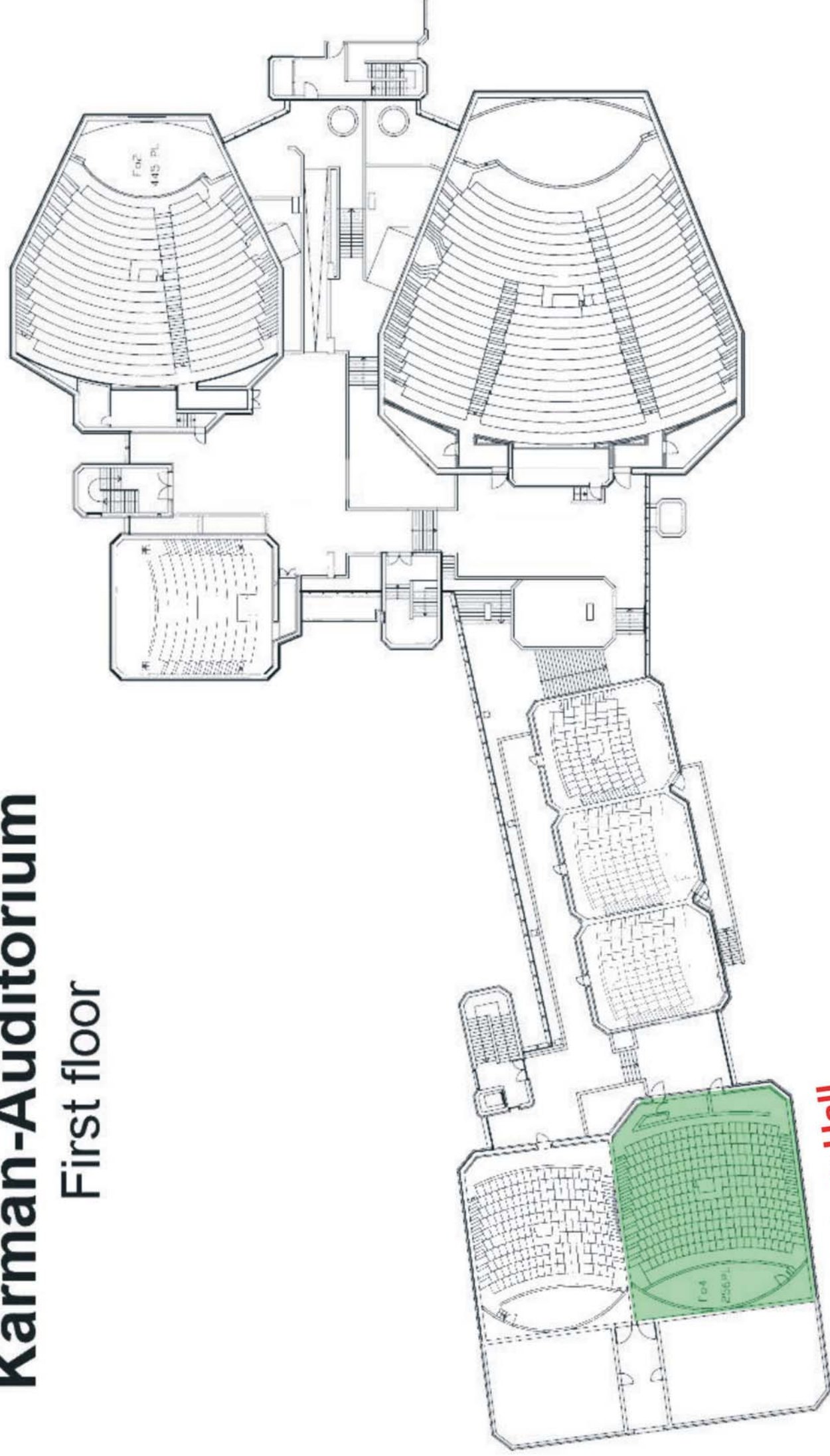
Kármán-Auditorium
Foyer

Toilet

Toilet

Vendor Exhibit

Cafeteria
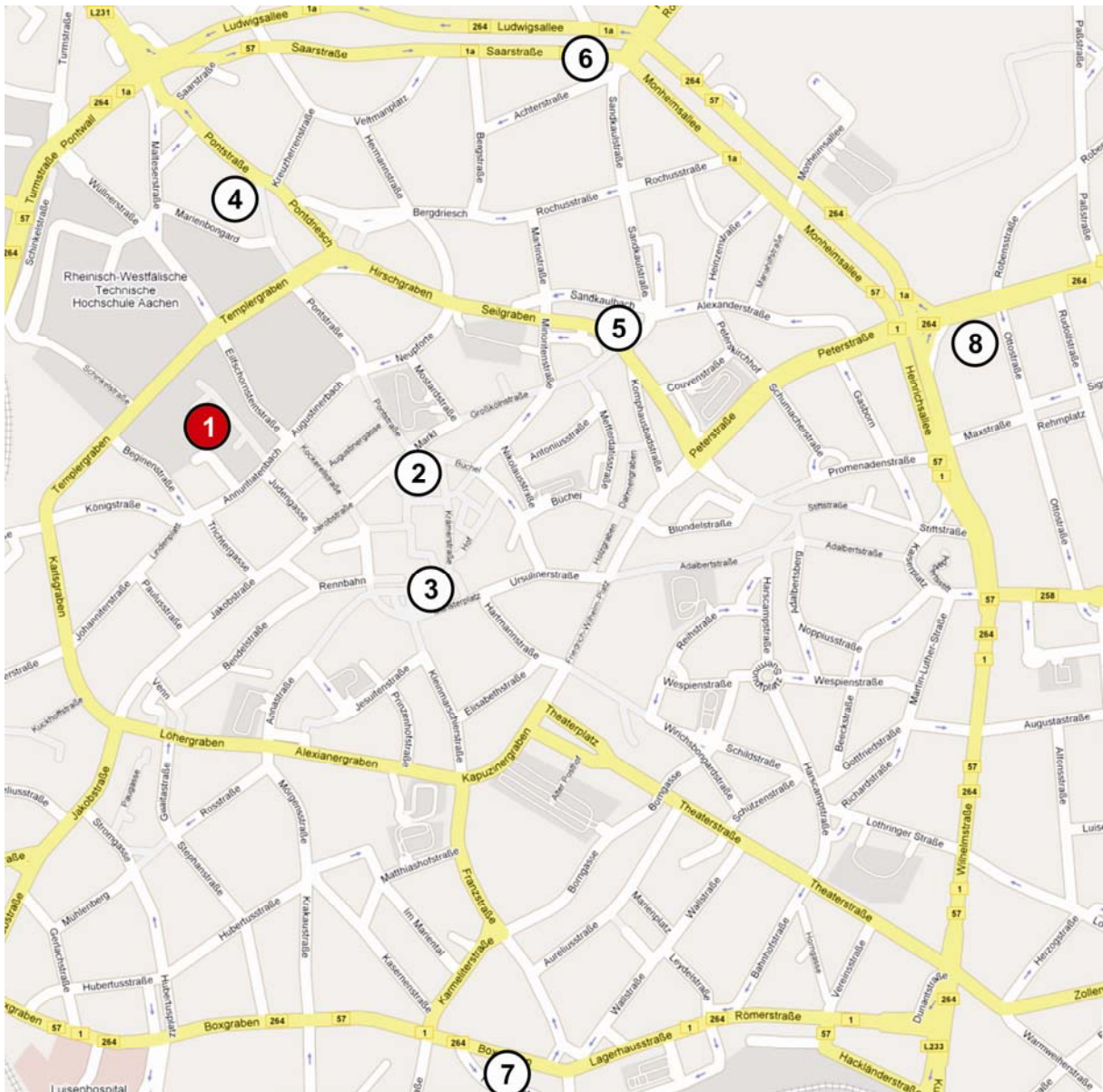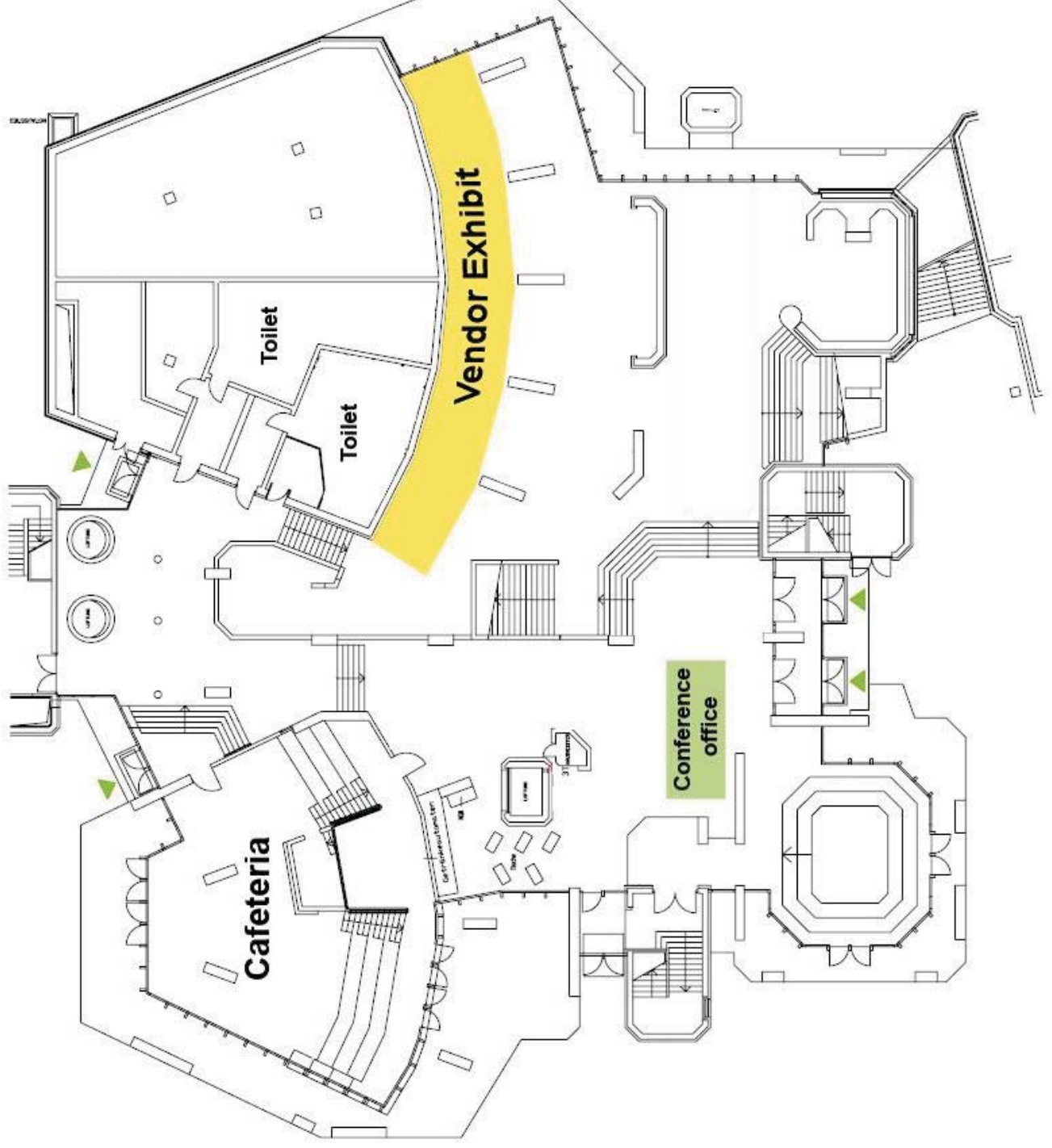
Conference office

Kármán-Auditorium
Ground floor

Cafe-teria

Toilet

Toilet

Poster

Toilet

Toilet

Kármán-Auditorium
First floor

Lecture Hall
Fo4

History of the ICMRM

In the year 1991 the 1st International Conference on Magnetic Resonance Microscopy (ICMRM) has been taken place in Heidelberg, Germany. Based on the contributions to this meeting the book Magnetic Resonance Microscopy: Methods and Applications in Materials Science, Agriculture and Biomedicine, VCH Wienheim, 1992, edited by Bernhard Blümich and Winfried Kuhn, provided an up-to-date reference on the subject of non-medical imaging. The next ICMRM meetings, now called Heidelberg Conference, were in 1993 (Heidelberg), 1995 (Würzburg).

The 4th ICMRM moved out to Albuquerque, New Mexico. By then it was felt that an update of the Microscopy Book was needed. During this time the field has advanced significantly, and several new techniques and hardware developments were introduced as well as interesting new (non-medical) applications covering such diverse areas as polymer and elastomer characterization, analysis of construction materials and material flow, various topics in biomedicine, foods and plant studies. The second book was titled: Spatially Resolved Magnetic Resonance: Methods, Materials, Medicine, Biology, Rheology, Geology, Ecology, Hardware, and edited by P. Blümler, B. Blümich, R. Botto and E. Fukushima (Wiley-VCH, 1998).

The Heidelberg Conference continued with very successful meetings: in 1999 the meeting was back in Heidelberg (chair B. Hull), moved out to Nottingham in 2001 (chairs R. Bowtell, P. McDonald), Snowbird, Utah, in 2003 (chairs D. Aylion, R. Botto) and Itsonomiya, Japan, in 2005 (chairs Y. Seo, K. Kose).

The phenomenon of spatially resolved Nuclear Magnetic Resonance, with or without imaging, has proven an essential tool in physics, it has revolutionized chemistry and biochemistry, it has made astonishing contributions to medicine, and is now making an impact in biology, biosciences, geophysics, chemical engineering, and food technology. It is even finding applications in new security technologies and in testing fundamental ideas concerning quantum computing. But the story of Magnetic Resonance is much more than the application of a well-established method to new areas of science. The technique itself continues to evolve. Magnetic Resonance has now garnered 6 Nobel prizes, the last one in 2003 (Paul Lauterbur and Sir Peter Mansfield). It is really quite extraordinary that such accolades are still being given to new developments in the methodology.

The 9th ICMRM meeting in Aachen will be held together with the 7th Colloquium on Mobile NMR (CMMR7). As such, it provides the international platform where (NMR, EPR, and MRI) scientists with a largely non-medical background meet to discuss advances in the diverse fields of Magnetic Resonance Microscopy and mobile NMR and MRI. It will be followed up by a new update of the Spatially Resolved Magnetic Resonance book, presenting the ongoing rapid developments of this field of research and its applications.

Henk Van As 2007

TALK ABSTRACTS

Talks indicated by an asterix* are invited

Introduction to NMR Imaging

Bernhard Blümich

Institute of Technical and Macromolecular Chemistry, RWTH Aachen University, Aachen, Germany

Abstract:

NMR (Nuclear Magnetic Resonance) is a form of resonant radio-frequency spectroscopy which probes the precession of nuclear spins in magnetic fields. The precession frequency is proportional to the strength of the magnetic field at the site of the nucleus. NMR imaging concerns NMR in magnetic fields, which are linearly inhomogeneous so that the NMR frequency is proportional to position. In conventional imaging, the gradient field is pulsed to mark the positions of nuclear spins at different times by their precession phase. Suitable successions of gradient field pulses are employed to encode time derivatives of spin positions and provide information about velocity and acceleration for example in terms of displacement distribution functions and velocity images.

The Physics of NMR are reviewed with particular attention to space encoding [1]. Essential concepts like the wave numbers for position and displacements, Fourier imaging, phase and frequency encoding, and the different ways of scanning k-space are introduced. The formal treatment is illustrated by representative examples from non-medical imaging.

1.   B. Blümich, *Essential NMR*, Springer, Berlin, 2005.

Hardware: Nuts and Bolts

Eiichi Fukushima[1]

[1] ABQMR, Albuquerque, USA

Abstract:

I shall first review the general requirements for NMR and then discuss several topics about or related to NMR hardware. These topics include aspects of magnets, transmitters, receivers, preamplifiers, probes & coils, and duplexers. Emphasis will be on my bias of knowledge that is important to either interpreting the results or in designing and performing experiments. These are facts that should be known by candidates taking qualifying examinations in physics. Digital circuits, data acquisition and processing, and pulse sequence generation are topics that will not be covered in this talk.

Diffusion and transport in NMR

Paul T. Callaghan,
MacDiarmid Institute for Advanced Materials and Nanotechnology
School of Chemical and Physical Sciences
Victoria University of Wellington, New Zealand

This talk will cover the basics of diffusion and flow. It will start with an explanation of what diffusion is, along with the diffusion tensor, and in addition, the Eulerian and Lagrangian descriptions of flow will be introduced, along with the concept of dispersion. From the NMR perspective the fundamental role of the spin echo will be explained. This will lead to the idea of q-space, diffusive diffraction, combined q-k imaging and NMR velocimetry and diffusion tensor imaging.   The talk will then move onto more advanced topics including the use of double PGSE NMR to measure fluctuations and correlations, the use of frequency domain analysis, and the use of multi-dimensional Fourier and inverse Laplace methods.

References

1. Einstein, Albert, *Investigations on the Theory of Brownian Movement*, ed. R. Fürth, translated by A.D. Cowper (1926, reprinted 1956); Einstein, *Collected Papers,* vol. 2, 170-82, 206-22.
2. Van Hove, L., *Phys. Rev.* 95, 249 (1954).
3. Callaghan, P.T., *Principles of Nuclear Magnetic Resonance Microscopy* (Oxford Univ. Press, Oxford/New York, 1991).
4. Hahn, E. L, *Phys. Rev.,* **1950,** *80*, 580-94.
5. Carr H.Y. and E.M. Purcell, *Phys. Rev*. 94, 630 (1954).
6. Stejskal E. O. and J. E. Tanner, *J. Chem. Phys.,* **1965,** *42*, 288-92.
7. Callaghan P.T. and J. Stepisnik, "Generalised Analysis of Motion using Magnetic Field Gradients", *Advances in Magnetic and Optical Resonanc*e, **19**, 325-388 (1996)
8. Callaghan, P.T. S.L. Codd and J.D. Seymour, *Concepts in Magnetic Resonance*, **11**, 181-202 (1999).
9. Basser, P.J,, J. Mattiello and D. LeBihan, *Biophys. J.* **66** 259-267 (1994).
10. Koch D. L. , and J. F. Brady, *AIChE J.,* **1987,** *180*, 387.
11. Callaghan P.T. and I Fúro, "Diffusion-diffusion correlation and exchange as a signature for local order and dynamics", *Journal of Chemical Physics*, **120**, 4032-4038 (2004)

Some Important Issues for

NMR Logging and Applications

Xiao Lizhi

Lab. of Petroleum Resources and Exploration,
China University of Petroleum, Beijing 102249, China

NMR logging has been successfully applied to petroleum reservoir evaluation for more than fifteen years. And it has made very positive contributions to complicated formation evaluation and to the development of well logging technology. There are many good things and bad things experienced. Issues related to NMR porosity, fluid-typing, irreducible water, permeability, tool feasibilities, job design, and data quality control are reviewed and discussed in details. The aim is to provide an outline and guides to NMR logging applications in various saturations based on author's theoretical considerations and application experiences.

Unilateral NMR studies of Lead White Pigment with protinaceus binders

Eleonora Del Federico[1] , Silvia Centeno[2], Akiko Yamazaki-Kleps[3] and Alexej Jerschow[4]

[1] Department of Mathematics and Science, Pratt Institute, Brooklyn, NY, USA.
[2] Department of Scientific Research, The Metropolitan Museum of Art, New York, NY, USA.
[3] The Sherman Fairchild Center for Works on Paper and Photograph Conservation, The Metropolitan Museum of Art , New York, NY, USA.
[4] Chemistry Department, New York University, New York, NY, USA.

Abstract:

The lead white pigment ($PbCO_3.Pb(OH)_2$) is thought to play a critical role in the degradation of illuminated manuscripts, such as The *Belles Heures of Jean of France, Duke of Berry* (Figure 1). Cracking, flaking, and separation of paint films containing lead white on parchment and other works of art have been reported by conservators, and have been attributed to the interaction of the pigment with the binding media.[1] Previous FTIR studies showed lead white to induce a change in the state of hydration of proteinaceus binders,[1] though the mechanism of this process is yet to be determined. An understanding of how the degradation occurs would provide crucial insight for the conservation, proper handling, and storage of these works of art on parchment. In this work we present ^{1}H spin-lattice (T_1) and spin-spin (T_2) relaxation studies on paint samples prepared following recipes recommended in medieval treatises using a profiler NMR MOUSE spectrometer. In the case of collagen-based media such as gelatine, fish glue, rabbit skin

Figure 1. Overall view (left) and detail (right) of a folio from the Medieval manuscript on parchment *The Belles Heures of Jean of France, Duke of Berry (ca. 1405-1409, MMA# 54.1.1),* showing lead white flaking paint.

glue, hide glue, and bone glue, the binding component is the protein collagen which is in a partially denatured state, including ordered regions of triple helix stabilized by water-mediated hydrogen bonds, and regions of random coils. We found that the presence of lead white causes an increase in T_2 relaxation in fish glue, and gelatines of low bloom index, however T_2 seems not to be affected by the addition of lead white in gelatines of high bloom index, rabbit skin glue, and hide glue. In gelatines of high bloom index, where the triple-helical content is larger,[3] no detectable changes were observed. This may indicate that the loss of mechanical strength causing flaking of the film upon addition of lead white could be related to the type of collagenous binder used, and particularly to its preparation method. This information is key for choosing a proper conservation treatment of the flaking paint; according to these results, high bloom index gelatines would give the best performance.

References:
1. S. Centeno, M. Guzman, A. Yamazaki-Kleps, C. Della Vedova, *JAIC* 43 (2004), 139- 150 .
2. G. Fullerton, E. Nes, M. Amurao, A. Rahal, L. Krasnosselskaia, I. Cameron, *Cell Biology International* 30 (2006) 66-73
3. A. Bigi, S. Panzavolta, K. Rubini, *Biomaterials* 25 (2004) 5675-5680.

Unilateral NMR for monitoring Cultural Heritage

Donatella Capitani [1] , Noemi Proietti[1], Sara Cozzolino [2] and Anna Laura Segre[1]

[1]Institute of Chemical Methodology, CNR Research Area of Rome, 00016 Monterotondo Stazione, Rome, Italy

[2] SMAArt Center and Department of Chemistry, University of Perugia, Via Elce di Sotto 8, 06123 Perugia, Italy

Abstract:

Although high resolution Nuclear Magnetic Resonance (NMR) spectroscopy is been an important analytical technique since many years, its application in the Cultural Heritage field is quite recent.

Standard NMR methods are particularly suitable for studying materials and are generally considered as non-invasive. However, they do require some sampling often

forbidden when studying rare and precious and/or unmovable objects belonging to the Cultural Heritage. The sampling can be avoided using a portable NMR instrumentation [1,2]. This instrument is portable and its use is fully non-invasive, allowing the measurement of a few NMR parameters such as the intensity of Hahn echo, the spin–spin and the spin–lattice relaxation times. The sensor can be positioned near intact objects in different positions. The main advantage of the unilateral NMR technique is that it is not only portable but can also be performed directly on large objects such as *frescoes*, monuments and in general any building [3]. The unilateral NMR is a suitable non-invasive technique for assessing the state of conservation of *fresco* paintings. In fact using unilateral NMR it is possible to evaluate the effect of consolidation treatments and to monitor the detachment of the painted layer from its support, the plaster, to observe the effect of salt outcropping, *i.e.* one of the major causes of *fresco* degradation [4]. Moreover the unilateral NMR can be used to monitor the distribution map of the dampness on a *fresco* [5]

Unilateral NMR is also useful for monitoring the water uptake and the effect and the quality of consolidation and restoration treatments performed on porous materials, and can be directly used on consolidated items which are of interest in the field of Cultural Heritage [6].

Unilateral NMR has been also used as a diagnostic tool for studying early degradation in cellulose-based materials [7].

1. G. Eidmann, R. Savelsberg, P. Blümer, and B. Blümich
   J. Magn. Reson. A **122,** (1996), 104.
2. B. Blümich, P. Blümer, G. Eidmann, A. Guthausen, R. Haken, U. Schmitz, K. Saito, and G. Zimmer *Magn. Reson. Imaging* **16**, (1998) , 479.
3. S. Sharma, F. Casanova, W. Wache, A. Segre, B. Blümich
   Magn. Reson. Imaging **21**, (2003), 249.
4. N. Proietti, D. Capitani, R. Lamanna, F. Presciutti, E. Rossi, A.L. Segre, *J. Magn. Reson.* **177**, (2005), 111.
5. N. Proietti, D.Capitani, E. Rossi, S.Cozzolino, and A.L.Segre
   J. Magn. Reson., **186**, (2007), 311.
6. N. Proietti, D. Capitani, S. Cozzolino, M. Valentini, E. Pedemonte, E. Princi, S. Vicini and A. L. Segre, *J. Phys. Chem. B*, **110**, (2006), 23719
7. N. Proietti, D. Capitani, E. Pedemonte, B. Blümich, and A.L. Segre, *J. Magn. Reson.* **170**, (2004), 113.

Three-dimensional MR Microimaging
of fossils across taxa

Daniel Mietchen[1,2,3], Bertram Manz[1] and Frank Volke[1]

[1] Fraunhofer-Institute for Biomedical Engineering, Ensheimer Str. 48, 66386 St. Ingbert, Germany
[2] Faculty of Physics and Mechatronics, University of the Saarland, 66123 Saarbrücken, Germany
[3] Present Address: Dept. of Psychiatry, Friedrich-Schiller University Jena, D-07743 Jena, Germany

Abstract:

The visibility of life forms in the fossil record is largely determined by the extent to which they were mineralised at the time of their death. In addition to mineral structures, many fossils nonetheless contain residual water and traces of organic molecules, the analysis of which has become an integral part of current palaeontological research. The methods available for this sort of investigations, though, typically require dissolution or ionisation of the fossil sample or parts thereof, which is an issue with rare taxa and outstanding materials like pathological or type specimens. In such cases, non-destructive techniques like MRI could provide an interesting methodological alternative.

In the present study, we show that three-dimensional MR images can be acquired from intact non-pathological invertebrate, vertebrate and plant fossils. Although fossils notoriously lack typical MRI contrast generators, namely water and soft tissue, ordinary liquid state pulse sequences lead to reasonable image contrast in rock-solid mineralized materials. At routine voxel resolutions in the range of several dozens to some hundreds of micrometers, these images reveal a host of anatomical details and thus highlight the potential of MR techniques to effectively complement existing methodological approaches for palaeontological investigations in a wide range of taxa.

On some anomalous guards of Jurassic and Cretaceous belemnites (Fig. 1), it is shown that pathological alterations of both the mineralized internal rostrum and the surrounding former soft tissue can be traced back in part to traumatic events of predator-prey-interactions, and partly to parasitism, creating a new palaeodiagnostics tool [1].
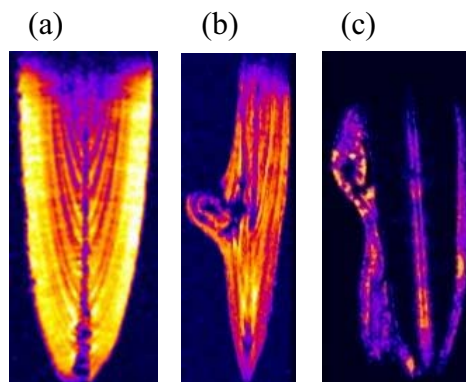
(a)   (b)   (c)

Fig. 1: MR Images of a normal (a) and anomalous (b, c) belemnite guards.

1. D. Mietchen, H. Keupp, B. Manz, F. Volke, *Biogeosciences* **2** (1995) 133-140.

Investigation of ancient mummies and bones by NMR and CT

Maria Baias[1], Juan Perlo[1], Federico Casanova[1], Kerstin Münnemann[2],
Frank Rühli[3], Hendrik von Waldburg[3], Bernhard Blümich[1]

[1] Institute for Technical and Macromolecular Chemistry, RWTH-Aachen, Germany
[2] Mainz University Medical School, Department of Radiology, Mainz, Germany
[3] Institute of Anatomy, University of Zürich, Switzerland

The natural glacier mummy Iceman, a mummified recent cadaver, a peruvian mummy, historic mummified body parts, historic bones, and living volunteers have been analyzed by non-invasive, single-sided NMR with the NMR-MOUSE®.

We aquired high-resolution depth profiles and T_2 relaxation curves of the head region of the Iceman mummy *in situ* in the storage room at the Museum and of a cadaver in the hospital. A spatial differentiation of surface ice layer, cutis, and skull bone up to a depth of 5 mm was possible. In ancient Egyptian mummified specimens, the thickness of a fingernail and a differentiation of a single bandage layer versus the skin underneath were possible. Depth profiles were aquired for the head, tibia and suprascapula of a Peruvian mummy as well as different historical tibiae and compared with CT images. A comparison of depth profiles through different foreheads of mummies, skulls, and living people gives strong evidence, that single-sided NMR with the NMR-MOUSE is a non-invasive technique to determine bone density. Our results demonstrate for the first time the feasibility of non-clinical MRI to visualize historic human tissue in a non-invasive approach.

We show for the first time completely non-invasive ^{1}H and ^{23}Na imaging of an ancient Egyptian mummified finger by NMR. Protons could be visualized by NMR only in the tissue close to surface and sodium primarily in the bone, while computer tomography images both, tissue and bone.

References:
Frank Rühli, Thomas Böni, Juan Perlo, Federico Casanova, Maria Baias, Eduard Egarter, Bernhard Blümich, *J. Cult. Heritage* – in press
Kerstin Münnemann, Thomas Böni, Giovanni Colacicco, Bernhard Blümich, Frank Rühli, *Magn. Reson. Imag.* – in press

Experimental aspects of NMR diffusion exchange and diffusion-relaxation correlation spectroscopy

P. Galvosas[1,2] , M. Gratz[1] , Y. Qiao[2], M. Schönhoff[3] and P. T. Callaghan[2]

[1] Faculty of Physics and Earth Sciences, University of Leipzig, Leipzig, Germany
[2] MacDiarmid Institute for Advanced Materials and Nanotechnology, School of Chemical and Physical Sciences, Victoria University of Wellington, Wellington, New Zealand
[3] Institut für Physikalische Chemie, Westfälische Wilhelms-Universität Münster, Münster, Germany

Abstract:

Two-dimensional (2D) NMR experiments involving inverse Laplace transformation [1] have become an important tool for the investigation of diffusional exchange as well as diffusion correlation in porous materials. Experimental results have been published frequently within the past years, demonstrating the potentials and opportunities of this method. In this contribution, we emphasize on the challenges and solutions related to the experimental aspects (NMR experiments and data processing) of the 2D methods.

Diffusion of dextran (77 kDa) has been investigated with diffusion exchange spectroscopy (DEXSY) [2], and molecular exchange has been found between the interior and exterior of hollow polyelectrolyte multilayer (PEM) capsules for a mixing time of 200 ms (see Fig. 1a). In this experiment, only a tiny fraction of the dextran molecules are involved in the exchange, thus the sensitivity of the method is demonstrated. Furthermore, due to the small molecular mobility, magnetic field gradients of about 10 T/m have to be used for a sufficient spacial encoding, demanding a special diffusion probe and appropriate gradient accuracy.

Anisotropic water diffusion in chive tissue is studied with the diffusion-relaxation correlation spectroscopy (DRCOSY) and diffusion-diffusion correlation spectroscopy (DDCOSY) respectively [3]. A joint interpretation of both experiments allows one to assign the peaks obtained by the DDCOSY (see Fig. 1b) to certain sites of the plant tissue on a scale beyond the resolution of standard NMR microscopy methods.

Furthermore, we present strategies for the combination of the aforementioned 2D methods with ultra high pulsed field gradients of up to 35 T/m, which reduces the observable molecular displacements to about 1 µm.
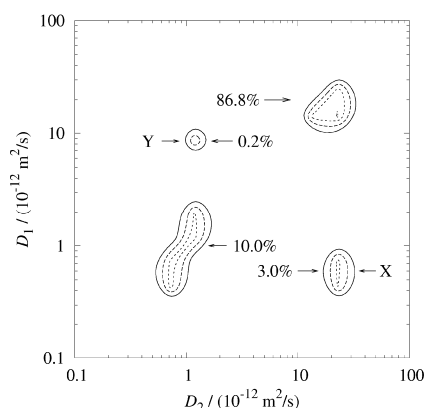
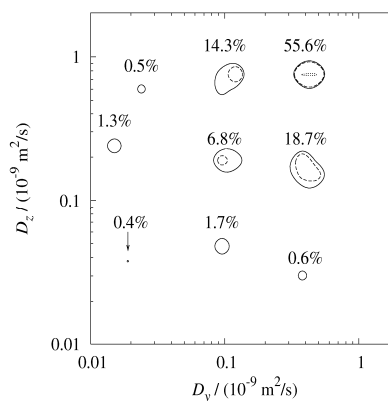Fig. 1a: Diffusional exchange of dextran   Fig. 1b: Anisotropy of diffusion in celluar tissue.

1. Y.-Q. Song, L. Venkataramanan, M. D. Hürlimann, M. Flaum, P. Frulla, and C. Straley, *J. Magn. Reson.* **154** (2002) 261-268.
2. Y. Qiao, P. Galvosas, T. Adalsteinsson, M. Schönhoff, and P. T. Callaghan, *Journ. Chem. Phys.* **122** (2005) 214912.
3 Y. Qiao, P. Galvosas, and P. T. Callaghan, *Biophys J.* **89** (2005) 2899-2905.

Ex situ NMR in highly homogeneous fields: ^{1}H spectroscopy

J. Perlo, F. Casanova, and B. Blümich

[1] ITMC, RWTH-Aachen, Aachen, Germany

Abstract:

Single-sided nuclear magnetic resonance sensors have been used for over two decades to characterize arbitrarily large samples. In contrast to conventional NMR apparatus, where the sample must be adapted to fit into the bore of large superconducting magnets, single-sided NMR experiments use portable open magnets placed on one side of an object to detect NMR signals ex situ. This configuration is convenient for nondestructive inspection of valuable objects, from which fragmentary samples cannot be drawn, but the convenience is bought at the expense of high and homogeneous magnetic fields that afford spectral resolution in conventional NMR studies. In fact, magnetic fields generated by open magnets are believed to be inherently inhomogeneous, precluding acquisition of chemical-shift resolved NMR spectra. In this work we break with this assumption, and demonstrate experimentally that the field of an open magnet can be shimmed to high homogeneity in a large volume external to the sensor.

To shim the highly inhomogeneous stray field of conventional open magnets, standard shim coils must be discarded simply because of excessive requirements for the shim currents. However, we demonstrate in this work that the required shim fields can be generated by means of a single-sided shim unit built from small permanent magnet blocks. The final shim unit geometry designed to homogenize the field of a conventional U-shaped magnet uses two pairs of movable magnet blocks with opposite polarization placed in the gap of the main magnet. By suitable displacement of the magnet block pairs with respect to the main magnet a total of eight shim components are generated (x, y, z, x^2, z^2, xy, xz, and yz). The unit includes also three single-sided coils generating x, y, and z gradient fields used for fine tuning of the field. This strategy made possible to shim to high homogeneity the magnetic field in a volume of 5×5 mm^2 along the lateral directions and 0.5 mm across, situated 2 mm above the rf coil surface. In combination with conventional volume selection techniques localized high-resolution proton spectra were measured outside a portable magnet with a spectral resolution of 0.25 parts per million (1).

1. J. Perlo, F. Casanova, and B. Blümich, *Science* **315** (2007) 1110-1112.

CRAZED Imaging with RARE-Acquisition at High Fields

Johannes T. Schneider[1], Cornelius Faber[1]

[1] Department of Experimental Physics 5, University of Würzburg, Würzburg, Germany

MR imaging, using the signal from intermolecular multiple quantum coherences (iMQC) can benefit from particular properties such as enhanced sensitivity to susceptibility differences or tunable structural contrast. On the other hand iMQC imaging suffers from low SNR.

The CRAZED sequence [1] was applied at 17.6 T on a water phantom to prepare and select signal from double-quantum coherences. The signal shows an initial build up for several tens of ms [2] as shown in Fig. 1 curve S(t). This time can be used to acquire multiple echoes with the RARE technique [3], in order to reduce acquisition time, or to enhance SNR. To this end we investigated and implemented an optimized k-space sampling and phase cycling within the echo train, which exploit and preserve the available signal.

Conventional RARE leads to exponentially T_2-weighted echoes, which makes centric-ordered phase encoding difficult because of Fourier transform artifacts (Fig. 2). The usual linear segmented sampling scheme provides good image quality but compared to spin echo (RARE-factor R=1), SNR decreased down to 79% and 50% at R=16 and R=32, respectively. In contrast, the rising CRAZED signal can be used to arrange those echoes with maximum signal and simultaneously minimum signal differences at the k-space centre (Fig. 2).

For the CRAZED signal both, transverse and longitudinal magnetization are essential, and both suffer from imperfections of the refocusing pulses. Applying the CPMG method [4] the errors are only refocused for transverse magnetization (Fig. 1). Alternating phases (x, $\bar{x}$) do not refocus unwanted transverse magnetization. Only four-step phase cycles refocus pulse errors and dephasing in both directions. Therefore, we implemented an MLEV-4 phase cycle (x, x, $\bar{x}$, $\bar{x}$) [5] and the cycle (x, y, x, y) on refocusing pulses (Fig. 1).

Combination of centric-ordered k-space sampling and four step phase cycling yields CRAZED images with optimum SNR and without FT artifacts (Fig. 2). Scaled to acquisition of a single echo at maximum signal, SNR decreased only to 97% and 88% at R=16 and R=32, respectively. Compared to the conventional RARE the CRAZED-SNR here is only 14% at spin echo acquisition (R=1) but increases up to 25% at R=32. With this two enhancements we obtained in vivo CRAZED images, e.g. for the purpose of fMRI, in less than one minute.
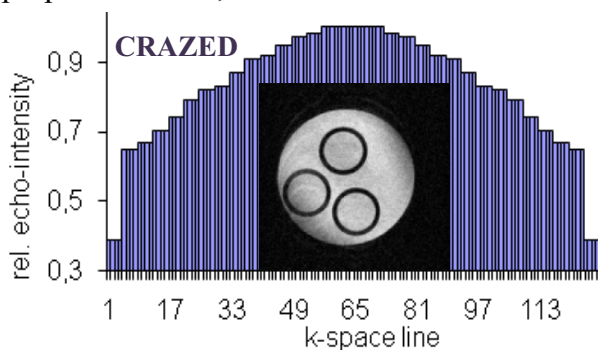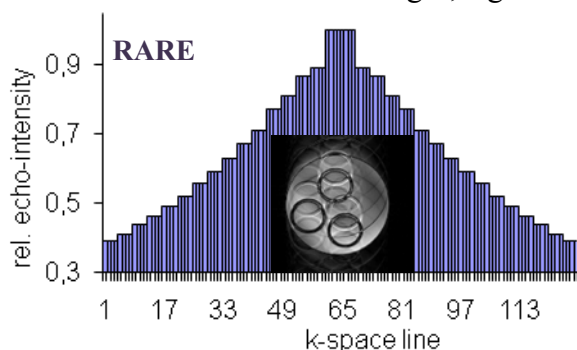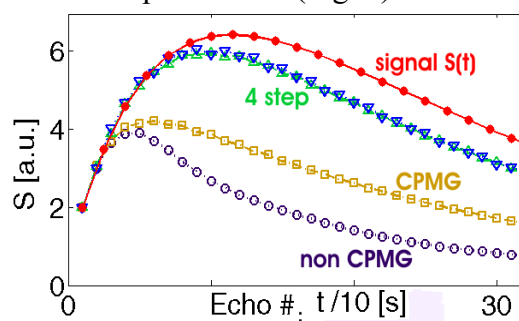
1. Warren W. et al., *Science* **265** (1993) 2005-2009./ 2. Ramanathan C. et al., *J Chem Phys* **114** (2001) 10854-10859./ 3. Hennig J. et al., *MRM* **3** (1986) 823-833./ 4. Meiboom S. et al., *Rev Sci Insrr* **28** (1958) 688-691./ 5. Levitt M. et al., *Advances in Magnetic Resonance*, Academic Press, New York (1983).

Geometry of Low-Field NMR

Louis-S. Bouchard[1,2], Vasiliki Demas[1,2,3], John Franck[1,2], Jeffrey L. Paulsen[1,2], N. Graziani[1,2], Bernhard Blümich[4], and Alexander Pines[1,2]

[1] College of Chemistry, University of California Berkeley, USA
[2] Materials Sciences Division, Lawrence Berkeley National Laboratory, USA
[3] Chemical & Materials Sciences, Lawrence Livermore National Laboratory, USA
[4] ICMC, RWTH-Aachen, Germany

Abstract

The fundamental limits to NMR/MRI in low magnetic fields will be reviewed in the context of portable NMR and future directions for imaging and spectroscopy applications will be discussed. The topics that will be discussed include alternative polarization and detection schemes; *ex situ* methodologies for counteracting static field inhomogeneities[1,2], and mitigation of concomitant field distortions.

New approaches for correcting Fourier encoding errors arising from concomitant fields will be discussed. In particular, we revisit Hoult's idea of rotating-frame MRI[3], where oscillating gradients are used for Fourier encoding in the rotating frame, and demonstrate its favorable properties for MRI in very low magnetic fields[4].

We also examine the problem of static field inhomogeneities, which is inevitable in one-sided magnet designs, and present new approaches to performing spin manipulations in magnetic fields with strong curvature. In particular, we examine the case of coil arrays and their ability to provide strongly matched RF excitations over a target volume[5]. As a practical application, the method of "shim pulses" will be discussed, whereby spin phases are stroboscopically "reset" using periodic phase corrections from RF/gradient pulses.

1. C.A. Meriles, D. Sakellariou, H.Heise, A.J. Moule, and A. Pines, Approach to High Resolution Ex Situ NMR Spectroscopy. *Science* **293**, 8 (2001)
2. D. Topgaard, R.W. Martin, D. Sakellariou, C. Meriles, and A. Pines, "Shim Pulses" for NMR Spectroscopy and imaging. *Proc. Natl. Acad. Sci. USA* **101**, 17576 (2004)
3. Hoult, D.I., Rotating frame zeugmatography. *J. Magn. Reson.* **33**, 183 (1979) *Philosophical Transactions of the Royal Society of London. Series B, Biological Sciences*. **289**, 543-547 (1980)
4. Bouchard, L.-S., Unidirectional magnetic-field gradients and geometric-phase errors during Fourier encoding using orthogonal ac fields. *Physical Review B* **74**, 054103 (2006)
5. Bouchard, L.-S., Anwar, M.S. Synthesis of matched magnetic fields for controlled spin precession. *Physical Review B* **76**, 014430 (2007)

A rapid NMR method for measurements of a 3D flow velocity vector and a 3D diffusion tensor

Xiaohong Ren[1] , HyungJoon Cho[1] , Eric E. Sigmund[2], and Yi-Qiao Song[1]

[1] Schlumberger-Doll Research, Cambridge, MA 02139, USA
[2] Department of Radiology, New York University, New York, NY 10016, USA

Abstract:

In the presence of a constant gradient field (g), a sequence of n hard RF pulses will allow multiple coherence pathways (q) to produce multiple signals. This class of sequences is called **m**ultiple **m**odulation **m**ultiple **e**choes (MMME). Different q creates different spatial phase modulation and yields an echo signal at different time. Consequently, in one scan of the sequence, different modulations with different diffusion weightings and phase shift coefficients can be measured. It has been shown that the MMME sequence can be used as an effective method for encodings of diffusion, flow and positional properties [1-4]. In this work, the authors demonstrate the capability of MMME method for rapid measurements of a 3D velocity vector and a 3D diffusion tensor within a few milliseconds without phase cycling.

A four-pulse MMME sequence with a static gradient along one direction and pulsed field gradients along other directions (Fig.1) can generate 13 distinct echoes and define a 13x3 flow induced phase shift coefficient matrix. Measurements of the echoes' phases with this encoding scheme allow an optimum solution for a 3D average flow velocity vector. The gradient pulse sequence is optimized by minimizing the well-known condition number in order to minimize error in the output parameters. Measured 1D, 2D and 3D vectors of the average flow velocities by the single-scan MMME sequence showed excellent agreements with the known flow velocities within ~5% error for a pipe flow. The signal decay in each echo due to a velocity distribution is also quantitatively verified with known laminar flow patterns.

In the static case, the attenuation of the spin magnetization due to anisotropic diffusion depends on the diffusion tensor and corresponding diffusion weighting matrix. With an optimized 4-pulse MMME sequence (Fig.1, Seq.B), one can obtain a 6x13 diffusion weighting matrix sufficient to determine a full diffusion tensor $D = (D_{xx}, D_{yy}, D_{zz}, D_{xy}, D_{yz}, D_{xz})$ in only two scans: a fully encoded scan and an equally timed reference scan. Both isotropic (water) and anisotropic (asparagus) systems were successfully tested within ~7% accuracy compared to the corresponding PFG measurements.
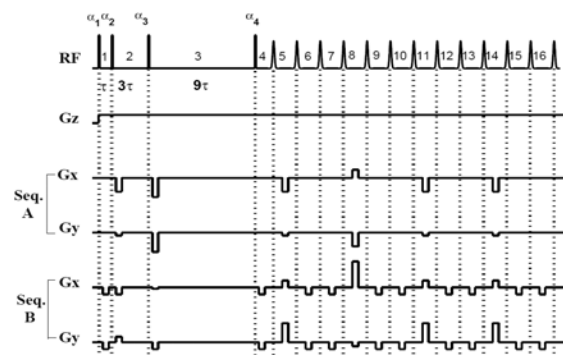
Fig.1 MMME sequences to encode 3D velocity vector (Seq. A) and 3D diffusion tensor (Seq. B)

1. Y.-Q. Song et al., *J. Magn. Reson.,* 170 (2004) 136.
2. Y.-Q. Song et al., *J. Magn. Reson.,* 172 (2005) 31.
3. H. Cho et al., *J. Magn. Reson.,* 180 (2006) 18.
4   E.E. Sigmund, *Magn. Reson. Imag.,* 24 (2006) 7.

Xray-CT enhanced interpretation of T_2-D-DG_0^2 NMR correlation experiments

C. H. Arns[1], K. E. Washburn[2], M. Hunter[2], and P. T. Callaghan[2]

[1] Dept. Applied Mathematics, RSPhysSE, Australian National University, Canberra, Australia
[2] MacDiarmid Institute, Victoria University Wellington, New Zealand

Abstract:

For NMR in porous media internal gradients are a major problem in the interpretation of both T_2-relaxation curves and higher-dimensional correlation maps (e.g. T_2-D, T_2-D-DG_0^2) with the aim of fluid-typing and/or spectral structure quantification. This is, because for rocks even with relatively weak susceptibility contrast but sharp corners and for many sandstones, internal gradients can range in strength to a point where they become comparable to the applied gradient, introducing distortions in measured diffusion coefficients, e.g. reducing the diffusion coefficient to an "apparent diffusion coefficient". For the pure T_2 relaxation time measurement, internal gradients can lead to a shorter T_2, thus suggesting smaller pore sizes than really present (potentially leading to an underprediction of reservoir quality). This apparent diffusion coefficient (apparent T_2) then needs to be corrected to facilitate more accurate distribution functions. Typically, either a single correction parameter is used, or an internal gradient distribution assumed [1].

If a high-resolution Xray-CT image is available, the internal gradient field can be calculated for linear media (magnetic permeability $\mu \approx 1$), assuming electric current density J=0, through a Poisson equation

$$\nabla\left(\mu\nabla\phi_m\right) = 0 \qquad (1)$$

with a scalar magnetic potential ϕ_m and appropriate internal and external boundary conditions [2]. Knowledge of the internal field allows to make corrections to the diffusion coefficients measured by NMR e.g. through a PGSE pulse sequence by considering applied gradient strength and cross-terms between internal and applied gradients. In addition, knowledge of the phase distribution and internal gradient field allows to simulate a T_2-D or T_2-D-DG_0^2 experiment.

In this work we calculate the internal magnetic fields of a set of sandstone and carbonate rock samples on the basis of susceptibility constrast from Xray-CT images and take diffusion weighted numerical averages of these fields to estimate the internal gradient distribution as seen through diffusion encoding over a fixed time interval (corresponding to a certain spatial support volume). Furthermore, we simulate T_2-D and T_2-D-DG_0^2 experiments directly on the Xray-CT images and compare with experimental results at low and high field.

1. R.C. Wilson and M. D. Hürlimann, *J. Magn. Res.,* **183** (2006) 1-12.
2. J.D. Jackson, Classical Electrodynamics, *John Wiley & Sons*, New York, 1962.

Compact MR Sensors: Who Pays for the Development?

Pablo J. Prado, Loganathan Doraisamy and Alejandro Bussandri

GE Security, Homeland Protection. San Diego, CA, USA

Abstract:

Developing state of the art compact Magnetic Resonance systems involves several technical advancements and in many instances costly and time demanding processes. We at GE have developed compact Magnetic Resonance and Quadrupole Resonance systems going from standard bench-top configurations to small, light and highly sensitive fieldable designs. Technical improvements were achieved as part of proof-of-concept and product platforms. This allowed us to support hardware and method advancements, in particular in dedicated electronics, signal processing, MR methods, and user interfaces.

A clear example of a successful high-risk development with significant impact across a family of RF products (Fig. 1) is provided by one of our compact RF spectrometer. The small embedded Power PC device operates over a wide frequency range with 24 digital output lines. The multi-channel, low noise spectrometer is controlled by a PC or laptop via Ethernet, facilitating versatility across applications. We have integrated this RF spectrometer into various Magnetic Resonance and Quadrupole Resonance sensors: 1) portable unit -UC Berkeley [1,2], 2) landmine detector – US DOD, 3) SRT Kiosk Shoe Scanner – GE Security, 4) Orange scanner – UC Davis. Each of these configurations had specific integration requirements, but highly benefited from the flexible spectrometer platform.
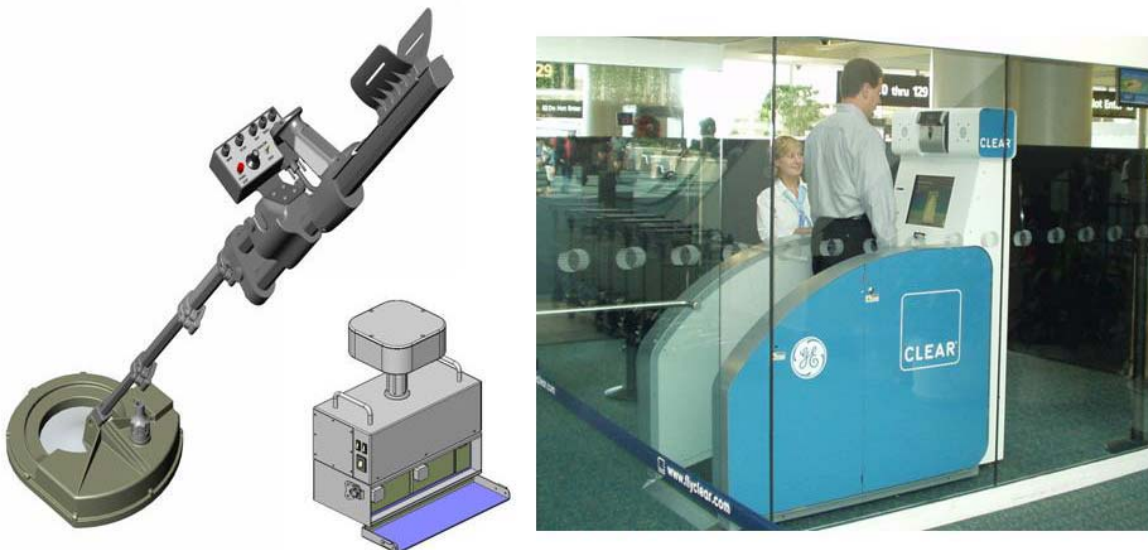

Fig. 1: Compact RF spectrometer integrated in a hand-portable Advanced Mine Detector (US DOD funded) and in the SRT Kiosk Shoe Scanner at an airport check point (GE NPI funded).

1. Bussandri A., Demas V., Prado P., Franck J., Reimer J., and Pines A, ENC, Asilomar, CA (2006).
2. Prado, P.J., 6th Colloquium on Mobile Magnetic Resonance, Aachen, Germany (2006)

The NMR-Cuff:
Force free, hinged magnet arrangements for portable MRI and EPR

H. Soltner[a] and P. Blümler[b]

[a] Central Department of Technology (ZAT), [b] Phytosphere (ICG-3),
Research Centre Jülich, 52425 Jülich, Germany

Samples with a waisted or concave shape (e.g. plants, tubes between fixed ends, extremities, neck etc.) are very problematic in NMR applications, because either the fill factor is low or single sided instrumentation has to be applied. One elegant solution is an arrangement of permanent magnets in the Halbach geometry which can be opened. This concept was realized for the first time in the NMR-cuff (**C**ut open, **U**niform, **F**orce **F**ree) which is an NMR-Mandhala[1] of four magnets, hinged along their diagonal (see Fig. 1). It generates a magnetic field of 0.57 T with a homogeneity better than 10^{-3}. A first prototype has an accessible opening of 3 cm, weights 4 kg and has two gradient sets. The necessary force to close this strong magnet is only 20 N at maximum.

Fig. 1 : NMR-cuff a) closed, b) opened. Top row: principle. Bottom row: first prototype applied to a plant stem.
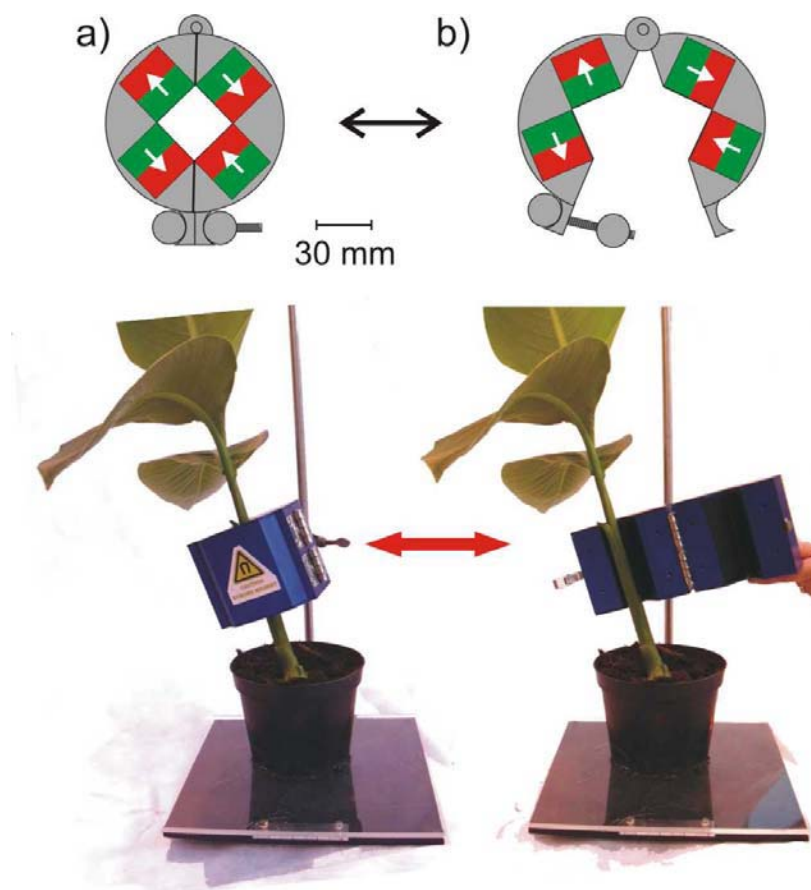
The methods for construction and optimization of such magnets will be explained. They are also perfectly suited for EPR, where two designs are presented. The first is a small desktop design (ca. 10 kg) optimized for S-Band EPR. The other uses two such NMR-Mandhalas, which are coaxially nested and designed for replacing standard electro-magnets for X-Band EPR. By mechanical rotation of one ring the magnetic field can be varied between 2000 and 5000 Gauss with an adjustment fine enough to use it even for field sweeps. Field and gradient coils complete both designs which have weights of about 6 and 60 kg, respectively.

---

[1] H. Raich and P. Blümler, Conc. Magn. Reson. B : Magn. Reson. Eng. **23B**(1) (2004) 16-25

The Surface GARField and The Tree Hugger:
Magnets designed for use in the built environment and with building materials.

Peter J McDonald[1] and Peter S Aptaker[2]

[1] Department of Physics, University of Surrey, Guildford, Surrey, GU2 7XH, UK.
[2] Laplacian Ltd, Culham Innovation Centre, D5 Culham Science Centre, Abingdon, Oxon, OX14 3DB, UK.

Abstract:

The Surface GARField[1] magnet is a medium sized unilateral permanent magnet NMR device that permits profile measurements to be made into the surface of materials to a depth of up to 50mm at a ^{1}H NMR frequency of 3 MHz. The magnet design is characterised by planes of magnetic field of constant magnitude (but varying direction) parallel to the device surface with a strong gradient in field strength in the orthogonal direction. A complementary radio frequency coil is used to produce an excitation field that is everywhere orthogonal to the static field. The magnet has been designed specifically for studies of concrete in the built environment. Results to date include curing, wetting and drying profiles with a spatial resolution of the order of 1 mm and also depth resolved one dimensional relaxation and two dimensional relaxation exchange spectra. These last prove to be very sensitive to the cement microstructure.

The Tree Hugger is a new homogeneous permanent magnet which, as its names implies, has been designed to fit around living trees; thought it is eqally suitable, in the built environemnt, for wooden or concrete pillars. The magnet operates at 1 MHz and has a homogeneous region of 200 mm diameter. The novel steel free NdFeB design utilises composite support materials, has open access and weighs 55 kg. A conventional steel framed 1 MHz C-core magnet with the same sample diameter would weigh circa 250 kg. A cylindrical Halbach magnet might potentially compete on weight, though one with this size and homogeneity and able to be opened has yet to be built.

The Tree Hugger magnet has an easily removable 2 piece 3D gradient set, enabling spatially resolved studies for ease of use and transportation. The gradients weigh a further 15 kg per pole. The magnet also has a hinged wrap around radio frequency coil for ease of access and maximum NMR sensitivity. Preliminary results will be shown.

1. P. J. McDonald, P. S. Aptaker, J. Mitchell, and M. Mulheron *J. Magn. Reson.* **185** (2007) 1-11, (2007).

Unilateral NMR apparatus with homogeneous B_0 field

Shin Utsuzawa[1], Eiichi Fukushima[2]

[1]New Mexico Resonance, Albuquerque, USA, [2]ABQMR, Inc., Albuquerque, USA

Introduction

Southwest Research Institute (San Antonio, TX) pioneered unilateral NMR for monitoring moisture content of drying concrete as well as of soil [1]. A group in Aachen took the identical idea but on a smaller scale to successfully make a series of unilateral NMR devices called NMR-MOUSE [2]. Both of these devices use the idea that the static magnetic field of a U-shaped magnet is strong enough close to the magnet that NMR signals can be obtained even in the decaying field. These devices work well but typically have an *effective depth*, which is defined as the distance to the sampled volume in units of the overall cross-section of the magnet, of only 0.01 to 0.05. Therefore, to date, they have principally been used to measure fairly thin objects, such as skin, paint, or membrane.

We, instead, use a barrel magnet that projects a region of homogeneous magnetic field (called *sweet spot*) outside of itself [3]. A consequence of working with a uniform field is that the sampled volume is greatly enlarged. Therefore, the *effective depth*, which is limited by signal-to-noise ratio, increases. With an additional bar magnet inserted in the bore, the *sweet spot* enlarge further, although the distance to the *sweet spot* decreases (Fig. 1).

Materials and methods

The prototype probe head consists of a barrel magnet and a double-D coil (Fig. 2). The barrel magnet generates B_0 parallel to the cylinder axis, whereas the double-D coil generates B_1 orthogonal to the axis around the *sweet spot*. The barrel magnet was constructed from ten commercially available NdFeB rings. Assembled magnet has the dimensions of 10.2 cm diameter, 1.9 cm wall thickness, and is 8.2 cm long. The weight is about 3 kg. We tested two bar magnet inserts, both made of NdFeB, with 2.54 cm diameter and 2.54 cm long (bar magnet (a)) as well as 3.81 cm diameter and 3.81 cm long (bar magnet (b)). The insert's axial position can be adjusted with a screw.

Results

Figure 3 shows frequency dependences of the sum of 96 echoes in a CPMG train obtained with and without a bar magnet insert. With a bar magnet insert, it possessed sharper peaks, which reflects improvement of B_0 homogeneity. The peak for the bar magnet (b) was approximately 4.4 times larger that that for the barrel magnet without bar magnet, and 1.5 times larger than that for the barrel magnet with bar magnet (a).

References

[1] R.F. Paetzold, *et al.*, *Soil. Sci. Soc. Am. J.* **49** (1985) 537-540.
[2] G. Eidmann, *et al.*, *J. Magn. Reson. A* **122** (1996) 104-109.
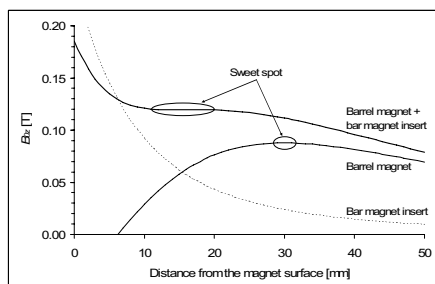[3] E. Fukushima and J.A. Jackson. U.S.Patent No. 6,489,872 (2002).
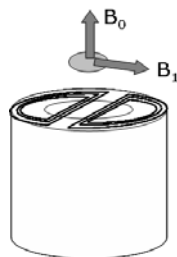
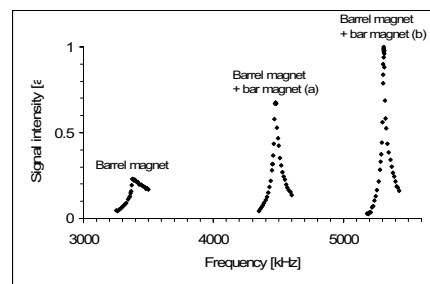Fig. 1. B_{0z} profile along z axis.

Fig. 2. Probe head.

Fig. 3. Frequency response.

A Low Power High Performance Digital Transceiver for Mobile NMR

R. Dykstra[1], T. Southern[1] and M. Van Der Werff[2]

[1] Institute of Fundamental Science, Massey University, Palmerston North, New Zealand
[2] Institute of Technology and Engineering, Massey University, Palmerston North, New Zealand

Abstract:

Mobile NMR probes are often inhomogeneous and typically operate from 100 kHz to 50 MHz. The use of a digital receiver is ideal as it can operate over a wide frequency range, provide the necessary wide bandwidth as well as having features such as excellent linearity, wide dynamic range, no DC offsets or gain mismatch between channels and no thermal dependence. Digital receiver integrated circuits are available, but now it is relatively easy to implement one in a Field Programmable Gate Array (FPGA). This provides maximum flexibility as the receiver can easily be tailored to many applications.

A digital receiver was constructed using a 100 MHz, 16-bit Analogue to Digital Converter (ADC), a FPGA and 512 kB of high speed memory resulting in a maximum receiver bandwidth of 50 MHz and an input frequency range of 100 kHz to several hundred MHz. A bandpass filter was included before the ADC to restrict the bandwidth to the 50 MHz Nyquist limit. Special care was taken to minimise the phase noise of the ADC clock to guarantee good signal to noise performance and to allow the subsampling of signals. Decimating digital filters limit the final bandwidth of the quadrature channels. Considerable effort was made to minimise the delay introduced by the filters and a filter reset function was also implemented to rapidly set all the data within the filters to zero. These two features are important for many experiments as the filter delay can limit the minimum echo time used and the residual data in the filters often interfere with new data. These issues have been a problem with a lot of digital receiver integrated circuits. A transmitter section was constructed by implementing a Direct Digital Synthesiser within the FPGA, with a clock frequency of 200 MHz, and interfacing it to a high speed Digital to Analogue Converter.

Mobile NMR requires systems to be power efficient, but most digital receivers consume considerable amounts of power due to the high speed logic and ADC. To reduce power consumption the receiver section was shut down when not required. One simple way to shut down the receiver is to halt the clock going to the logic and ADC. The problem with this is that gating the clock increases the phase noise as logic is introduced between the pure reference oscillator and the ADC clock input. To overcome this, a new ADC device that had a shut down option which didn't interfere with the clock was used. The transmitter and the RF power amplifier are also shut down when not required.

Small scale NMR: Spectroscopic Studies and High Resolution Imaging Applications

Luisa Ciobanu

Pfizer Inc, Ann Arbor, Michigan, USA

Abstract:

The applicability of nuclear magnetic resonance to the study of mass/volume limited samples suffers from low sensitivity. In recent years efforts to improve the sensitivity in NMR spectroscopy have been focused on designing single or multiple miniature NMR coils (microcoils), where the increase in sensitivity is provided by the reduction in size. The main practical considerations in placing several microcoils within the same probe head are the avoidance of coupling between the coils and the maintenance of high spectral resolution. These two issues have been resolved by a careful arrangement of the microcoils (typically 90^0 with respect to each other) and their placement within a medium whose magnetic susceptibility matches the susceptibility of copper wire from which they are manufactured. The development of multiple microcoil NMR probes has enabled the reduction of data acquisition time and the increase in sensitivity in a variety of experiments such as: 2D NMR spectroscopy [1], reaction kinetics monitoring [2], and high-throughput screening of chemical compounds [3].

Microcoils have also been used for MR microscopy. Through a combination of microcoil receivers, strong magnetic field gradients and pulse sequences that maximize the signal to noise ratio, MR images with spatial resolution as high as 3.7 μm by 3.3 μm by 3.3 μm (~40 femtoliters) have been reported [4]. Despite these advances the application of MR microscopy to the study of biological cells is still limited. The combination of microcoils with new pulse sequences designed to take advantage of diffusion (Diffusion Enhancement of SIgnal and REsolution [5]) or flow (Flow ENhanced SIgnal [6]) at small length scales could significantly increase the signal-to-noise ratio and the resolution in MR microscopy and localized NMR spectroscopy.

1. Wang H, Ciobanu L, Webb AG, *J. Magn. Reson.*, **173** (2005) 134-139.
2. Ciobanu L, Jayawickrama DA, Zhang X, Webb AG, Sweedler JV, *Angew. Chem. Int. Ed*. **42** (2003) 4669-4672.
3. Wang H, Ciobanu L, Edison AS, Webb AG, *J. Magn. Reson*. **170** (2004) 206-212.
4. Ciobanu L, Seeber DA, Pennington CH, *J. Magn. Reson*. **158** (2002) 178 -182;
5. Ciobanu L, Webb AG, Pennington CH, *J. Magn. Reson*. **170** (2004), 252- 256;
6. Sutton BP, Ouyang C, Ching BL, Ciobanu L, *Magn. Reson. Med*. in press (2007).

Toward a portable frequency-domain NMR spectrometer

Andrew McDowell[1]

[1] ABQMR, Inc., Albuquerque, NM, USA

Abstract:

The theoretical promise [1] of microcoils as optimal detectors for mass-limited samples has been realized in a wide range of applications, including high-resolution spectroscopy, imaging of single cells, and integration of NMR with liquid chromatography and other separation techniques. In addition to these high-field applications, other workers have paired microcoil detectors with compact bench-top magnets to create a platform attractive for industrial users.[e.g.,2] Low-field systems using moderately sized coils have been demonstrated.[3] In our work, we explore the possibilities for operating very small coils in miniature low-field permanent magnets.

The magnet design determines the overall capabilities of any NMR system. Our first miniature magnet (from Aster Enterprises) is a 1 Tesla dipole design, roughly a 5 cm cube weighing 600 g. This magnet has a 5 mm x 10 mm gap access and a specified working volume of 0.5 mm DSV. We are challenged to (1) build efficient microcoil probes for operation in this low field, (2) fit the probe into the tightly constrained available space, and (3) achieve useable SNR and resolution. In addition, we seek to meet these challenges using simple, low-cost, robust designs.

In this talk, we discuss our proposal [4] of a novel tuning circuit to facilitate the operation of very small coils in low-field/low-frequency magnets. We also demonstrate [5] that the circuit allows the detection of nano-liter volume samples in a single shot at 1 Tesla. The circuit also has significant collateral benefits that greatly ease the use of the smallest coils. We also present our recent success in repackaging the efficient probe circuit into a form factor compatible with our magnet, using very simple construction techniques.

Our first magnet achieves only 10 ppm homogeneity, due to a slight misalignment of the pole faces, while our probes are capable of at least 0.1ppm. We demonstrate the potential of our system by acquiring the spectra of a number of fluids (including ethanol, food oils, crude oil, juice concentrates and shoyu) using the homogeneous field of a larger 1 Tesla permanent magnet. Simple design improvements will upgrade the tiny magnet to match this performance.

Sufficient miniaturization will open a new cost/size/siting regime for NMR. We will speculate on future possibilities and implications.

1. Peck, TL, Magin, RL. and Lauterbur, PC *J. Magn. Reson. B* **108** (1995) 114-124.
2. Moresi, G and Magin, RL *Concept. Magn. Res*., **19B** (2003) 35-43.
3. Goloshevsky, AG, Walton, JH, Shutov, MV, de Ropp, JS, Collins, SD, McCarthy, MJ, *Rev. Sci. Inst.,* **76** (2005) 024101.
4. Sillerud, LO, McDowell, AF, Adolphi, NL, Serda, RE, Adams, DP, Vaslie, MJ, and Alam, TM, *J. Magn. Reson.* **181** (2006) 181-190.
5. McDowell, AF and Adolphi, NL, *J. Magn. Reson.* (2007, in press).

Beating the NMR time scale by remote detection flow imaging

Elad Harel,[1] Christian Hilty,[1*,2] Erin E. McDonnell,[1*] Ville-Veikko Telkki,[1*] Katherine Koen,[1*] Josef Granwehr,[1*] Sandra Garcia,[1*] Kimberly L. Pierce,[1*] Song-I Han[1*] and Alex Pines[1]

[1]Department of Chemistry, University of California, Berkeley and Materials Sciences Division, Lawrence Berkeley National Laboratory, Berkeley, CA 94720 (* former members).

[2]Now at: Department of Chemistry, Texas A&M University, College Station, TX 77843.

Microfluidics holds great promise for advancing research in the biological and physical sciences due to its unique ability to control very small amounts of fluid with high precision. In analogy with miniaturization technology in the semiconductor industry, microfluidics promises to bring large scale chemistry and biology to a lab-on-a-chip environment where many advantages can be realized, in particular, the level of control over which fluids can be readily manipulated. By far, the most utilized method for analyzing properties of the fluids flowing inside a microfluidic device is fluorescence due to its high sensitivity. However, optical techniques suffer serious drawbacks, primarily, that they require tracers and, in general, preclude chemical identification. The few methods that do allow spectroscopy on a microfluidic device suffer from low sensitivity due to the short optical pathlength through the microchannels. A few groups have attempted to utilize the analytical power of NMR on microfluidic chips by placing small surface coils directly on the chip. Unfortunately, doing so is a tremendous challenge in terms of fabrication. Additionally, the large fingerprint of the coil makes placing more than a few on a chip difficult. With this method only a few select regions of the device can be monitored. Here, we demonstrate a new method based on remote detection which allows the entire chip to be imaged with high resolution and with high sensitivity. Furthermore, we show that high-resolution spectroscopy can be achieved on the chip, and, even in the case of grossly inhomogeneous fields, off the chip. This has allowed us to acquire high spatial resolution, time-resolved spectroscopic flow images. Our most recent work has shown that we can even use this method to circumvent what appears to be NMR's inherent time resolution. In principle, any time-resolution can be achieved up to the detection limit. We demonstrate this by looking at the flow of two miscible fluids inside a complex 3D mixer chip. This time slicing methodology allows a resolution below 2 ms. We believe that with simple optimization we can bring the time resolution below 100 us.

A Small Planar Gradient Set for MRI Rheometry

J. H. Walton[1]; A. G. Goloshevsky[2]; Y. J. Choi[2]; Adan Roa[4], J. S. de Ropp[1]; S. D. Collins[3]; M. J. McCarthy[2]

[1]Department of Food Science and Technology, UC Davis, Davis, CA, USA
[2]NMR Facility, UC Davis, Davis, CA, USA
[3]MicroInstruments and Systems Laboratory (MISL), University of Maine, Orono, ME, USA
[4]Department of Biomedical Engineering, UC Davis, Davis, CA, USA

The non-invasive nature NMR/MRI is ideal for on-line/in-line monitoring of fluid rheological properties during industrial production in real time. Miniaturization of the probe components confers several advantages in the industrial environment. Smaller RF coils use much less RF power to produce a given B_1. This in turn reduces the size and cost of the RF amplifier necessary for the system. Smaller Gradient coils produce much more gradient per unit current. Furthermore, smaller gradients have inherently lower inductance, which permits faster gradient switching times which lead to shorter echo times. Smaller probes can be put in smaller magnets at lower field to drastically cut the cost of maintenance while improving safety while reducing both costs and the footprint on the industrial process floor.

The miniaturized nuclear magnetic resonance system we have developed includes miniaturized RF and gradient microcoils coils combined with low field magnets and a capillary tube for sample delivery. Measurements useful to process control applications include spectroscopic identification and monitoring of reaction products, monitoring of product rheological properties, and monitoring extent of mixing. We have developed a package of consisting of a microfabricated Helmholtz RF coil and a microfabricated Gradient set for use in a low field magnet. Here we focus on the gradient coils we have developed and their use in viscosity measurements.

Tube flow viscosity measurements require only two gradients – one in the direction of the flow and one perpendicular to it. This enables the easy microfabrication of a planer gradient system[1]. The gradient system we constructed achieved a strength of 28.9 ± 0.1 mT/m/A and 37 ± 1 mT/m/A for the flow and perpendicular which compares favorably with calculated values of 32 mT/m/A and 39 mT/m/A. Viscosity was successfully measured for two CMC solutions. The less viscous CMC solution (1% with MW = 700k) was found to have the power index $n = 0.77 \pm 0.06$ and the flow consistency coefficient $K = 1.68$, whereas the more viscous CMC solution (2% with MW = 250k) exhibited $n = 0.5 \pm 0.03$ and $K = 7.23$. The MRI measurements compared well with measurements of the same samples performed on a conventional rotational rheometer. The range of shear rates covered by the obtained MRI viscosity data was 3–20 s-1.

[1]Zupancic I. and Pirs J., J. Phys. E: Sci. Instrum. **9** 79–80 (1976)

Low Cost Ex Situ NMR with microcoils

Vasiliki Demas[1,2,3], Julie Herberg[1], Vince Malba[1], Anthony Bernhardt[1], Lee Evans[1], Robert Maxwell[1], John Franck[2,3], Alexander Pines[2,3]Jeffrey Reimer[2,3]

[1]Lawrence Livermore National Laboratory, Livermore CA, USA
[2]University of California, Berkeley, CA, USA
[3]Larence Berkeley National Laboratory, Berkeley, CA USA

Abstract:

We are currently developing a low-cost NMR system for *in situ* chemical analysis of trace samples. The main limitations that need to be overcome for commercialization of such a system are sensitivity and resolution of the system, despite the low strength and quality of the fields typically present in permanent magnet arrangements. We will discuss our efforts towards overcoming these limitations.

Laser-lathe lithography and three dimensional micro fabrication technology available at LLNL is being used to construct high sensitivity RF microcoils for NMR analysis [1]. Electrical characterization as a function of design parameters (diameter, length, inter-turn spacing and wire thickness) of the lithographically produced microcoils has been performed and compared to handwound microcoils. LLNL's microcoils have been incorporated in NMR probes, and have been used to evaluate the field of various permanent magnets. Optimization of the probe configuration, identification of an existing suitable spectrometer, and new magnet design remain the focus of our work. In addition field corrections based both on hardware shimming and the series of "*ex situ*" methodologies developed in UC Berkeley [2, 3] are being implemented to increase the resolution.
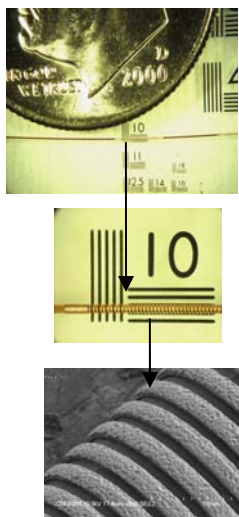
Fig. 1: Laser Lathe Lithographically produced RF solenoidal microcoils.

1. V. Malba, R. Maxwell, L.B. Evans, A.F. Bernhardt, M. Cosman, K. Yan, "Laser-Lathe Lithography-a Novel Method for Manufacturing Nuclear Magnetic Resonance Microcoils," Biomed. Microdevices 5 (2003) 21.
2. C.A. Meriles, D. Sakellariou, H.Heise, A.J. Moule, and A. Pines, "Approach to High Resolution Ex Situ NMR Spectroscopy," Science 293 (2001) 8.
3. D. Topgaard, R.W. Martin, D. Sakellariou, C. Meriles, and A. Pines, "Shim Pulses" for NMR Spectroscopy and imaging, Proc. Natl. Acad. Scie. 101 (5) (2004) 17576.

Two-dimensional NMR of Diffusion Systems

Yi-Qiao Song and Lukasz Zielinski

Schlumberger-Doll Research, Cambridge MA 02139

Abstract:

2D NMR of relaxation and diffusion is a significant advance in the study of porous materials. There have been many applications of 2D NMR as a way to distinguish signals from different phases e.g. oil, water and gases, and different geometries. In these applications, the key is the enhanced resolution of such techniques.

2D NMR has also been used to probe water diffusing from one pore to another. The analogy of such experiments is the conventional NOESY, the 2D NMR in frequency domain. Such experiments offer the potential to probe the connectivity of pore structures, permeability of membranes,

We show that the diffusion system itself, without the artificial exchange, shows a variety of behaviors in 2D NMR and we provide the complete theoretical approach to understand such experiments. The molecular diffusion is governed by the Torrey-Bloch equation for the longitudinal magnetization:

$$\frac{\partial}{\partial u} m(\mathbf{r},t) = D\nabla^2 m(\mathbf{r},t), \text{ and } m(\mathbf{r},t) = \sum_n a_n \phi_n(r) \exp(-\frac{t}{\tau_n})$$

where m is the magnetization deviation from its equilibrium. Any solution can be written as a sum of the eigenfunctions.

The spectroscopy of these eigenfunctions ϕ_n and eigenvalues τ_n uniquely define the pore system. In fact, with different surface relaxivity for longitudinal and transverse magnetization decays, two sets of eigenfunctions and eigenvalues are relevant, corresponding to each relaxation mode respectively. We call them L-modes and T-modes. Both modes are a complete set of functions and orthogonal within each set. However, the overlap between the L-modes and T-modes depends on the surface relaxivity. And such overlap is critical for the variety of behavior of the 2D NMR results, including the lack of off-diagonal peaks. This approach allows numerical simulation of 2D NMR for arbitrary 3D pore geometry. Examples of a single pore and connected pores are shown in the figures below.

Single pore, T1-T2 and T2-T2 experiments

Two coupled pores
T1-T2 experiments
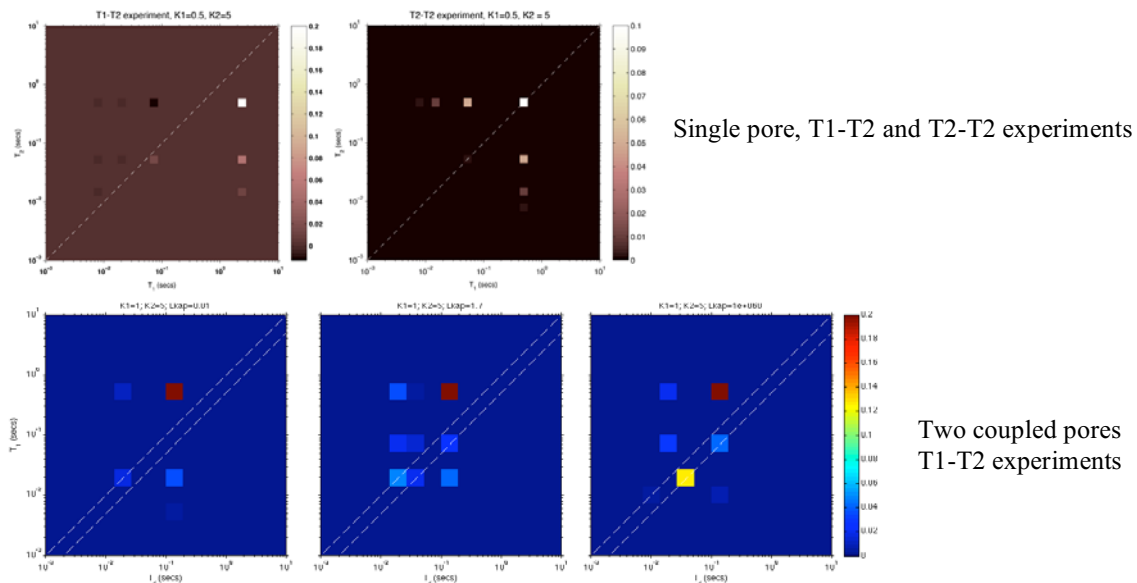
NMR mapping of ionic currents and electro-osmotic flow in microsystem channel networks

Rainer Kimmich, Bogdan Buhai, Yujie Li

Sektion Kernresonanzspektroskopie, Universität Ulm, 89069 Ulm, Germany

rainer.kimmich@nmr-ulm.de

The main objective of this study was to examine and compare maps of the ionic current density and electro-osmotic flow in channel networks on a microscopic length scale (1). As a paradigm for complex pore spaces, model objects of random and correlated site percolation clusters were fabricated and filled with electrolyte solutions. The experimental maps were compared with computational fluid dynamics simulations based on finite element techniques. The patterns observed in maps of the current density, pressure induced and electro-osmotic flow velocity strongly deviate from each other. This is due to the different transport resistance characteristics and the different nature of the driving forces. The patterns of the spatial distribution of the electric current density measured in the pore space of plastic objects (no electro-osmotic flow superimposed), for example, is entirely different from those found in ceramic objects (electro-osmotic flow superimposed). Vortices and recirculation patterns have been observed for all transport quantities, but at different sites. The findings can be explained and elucidated with the aid of the computational fluid dynamics simulations and experiments with test objects especially designed for this purpose (2).

Fluid transport by flow in random porous media is subject to hydrodynamic dispersion (3). In another series of pulsed field-gradient NMR experiments, we have compared flow driven by pressure gradients on the one hand and by electroosmosis on the other. The media were porous glasses with pore dimensions from 1 to 100 μm. With increasing flow rates, a crossover from subdiffusive to superdiffusive mean-squared displacement laws was observed in both cases. This demonstrates the competition between molecular diffusion and convection, and is a typical example of anomalous transport.

(1) B. Buhai and R. Kimmich, *Phys. Rev. Letters* **96** (2006) 174501.

(2) B. Buhai, T. Binser, and R. Kimmich, *Appl. Magn. Reson.*, in press, (2007).

(3) Y. Li, G. Farrher, and R. Kimmich, *Phys. Rev. E* **74** (2006) 066309.

Fluid distribution in mesoporous materials

Rustem Valiullin, Muslim Dvoyashkin, Alexey Khokhlov and Jörg Kärger

Department of Interface Physics, University of Leipzig, Leipzig, Germany

Abstract:

Due to a variety of attractive properties, porous materials with typical pore sizes in the mesoscalic range are in the focus of current research. To date, an enormous number of such materials with different pore morphologies have been produced [1, 2]. However, the number of experimental techniques for their structural characterization is rather limited and often is confined to analysis of the adsorption isotherms. This is even more crucial concerning "visualization" of various physico-chemical phenomena occurring in these materials, for example, the processes of phase separation. In this contribution, we discuss potentials of NMR to probe characteristics of fluid distribution during adsorption/desorption and melting/freezing transitions, which, in turn, reveal important information on the porous material properties.

Concerning phase transitions of fluids in mesopores, the most essential processes occur on a length scale from a few to thousands of nanometers, making conventional NMR microscopy not applicable. One of the approaches to circumvent this problem could be "dynamical" imaging, i.e. assessing structure and dynamical features of the phase-separated domains basing on the dynamical properties of the individual molecules in the pores. The most informative realizations of this approach are diffusion diffraction phenomenon [3] and restricted diffusion [4] but their applicability is limited to a very narrow class of materials.

One of the routes we have followed was to simultaneously measure the amount of a fluid and the molecular diffusivities during continuous filling and drying the mesoporous material. In this way, on the length scale of the order of micrometers probed using PFG NMR, one measures diffusivities averaged over an intentionally created inhomogeneous distribution of the fluid. However, the observed patterns in diffusivities as a function of the history, how a particular state had been attained, reveal the specific character of the distribution, in agreement with the results provided by other scattering techniques [5]. More interestingly, it is found that under certain conditions the thus measured diffusivities exhibit patterns of restricted diffusion, providing more detailed information on the structure of the capillary-condensed domains.

Similar studies could also be done along the freezing and melting transitions of fluids in mesopores. By exploiting samples with a well-defined structure, namely mesochannels with varying diameter along the channel axis, we show that, in complete similarity to the information provided by the shape of the adsorption/desorption hysteresis, the shape of the freezing/melting hysteresis can be affected by the interconnectivity of pores with different dimensions. The diffusion behavior may be quite complex depending on many factors. However, further studies concentrating on finding of suitable probe molecules may provide a novel informative experimental approach to the reconstruction of the structure of mesoporous materials.

1. T. J. Barton, *et al.*, *Chemistry of Materials*, **11** (1999) 2633.
2. A. Taguchi, F. Schüth, *Microporous and Mesoporous Materials*, **77** (2005) 1.
3. P. T. Callaghan, *et al.*, *Nature* **351**, (1991) 467.
4. P. N. Sen, *Concepts Magn. Reson. Part A* (2004) **23A**, 1.
5. J. H. Page, *et al.*, *Phys. Rev. Lett.* **71**, (1993) 1216.

Magnetic Resonance Imaging of Water Content across the Nafion Membrane in Operational PEM Fuel Cells

Ziheng Zhang[1], Jonathan Martin[2], Haijiang Wang[2], Keith Promislow[3], Bruce J. Balcom[1]

[1]MRI Centre, Department of Physics, University of New Brunswick, Fredericton, New Brunswick, Canada E3B 5A3
[2] Institute for Fuel Cell Innovation (IFCI) National Research Council Canada (NRC), 4250 Wesbrook Mall, Vancouver, BC, Canada, V6T 1W5
[3]Department of Mathematics, Michigan State University, East Lansing, MI 48824

Abstract:

Double half k-space (DHK) spin echo (SE) single point imaging (SPI) [1], has recently been developed for high resolution imaging of thin films. The specific intent of this method is quantitative water content measurements across nafion membranes.

In this presentation, we report preliminary water content mapping in the Nafion membrane of a home-made operational fuel cell specially designed for these experiments, as shown in Fig. 1. In this apparatus, we incorporate the function of the RF resonator into the electrodes of the fuel cell [2]. The integrated assembly functions as a TEM resonator for magnetic resonance at RF frequencies while still operating as a DC fuel cell, which avoids the sensitivity loss associated with other MRI measurements where the RF probe is outside of the conductive fuel cell electrodes.

An operational fuel cell will develop variable water content boundary conditions on each side of the nafion membrane in a manner dependent on the operating conditions. In the preliminary experiments, the resultant depth profiles, as shown in Fig. 2, clearly reveal the time dependent process of cathode flooding and water removal with increased air flow. The ability to rapidly and non-invasively measure the evolution of the water content distribution should dramatically improve our understanding of water transport behavior [3] and water management in PEM fuel cell [4].
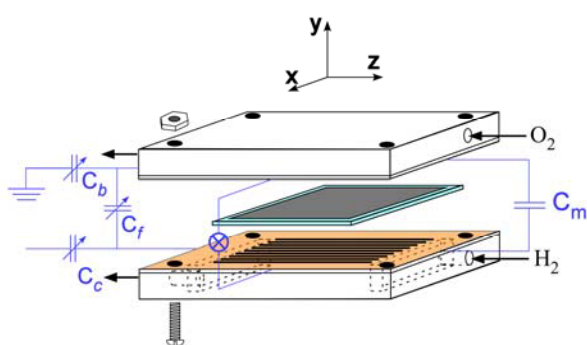
Fig. 1: Schematic of RF Resonator and DC Fuel Cell. The gold coated PC boards, which sandwich gas diffusion layer (carbon paper coated with catalyst layer) and nafion 1110 as PEM, are also the plates of the RF resonator. The B_1 field it generated is parallel to plates.
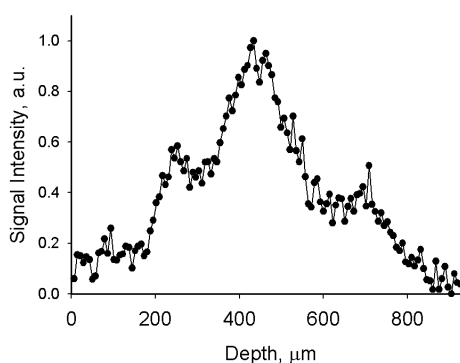

Fig. 2: A one-dimensional depth profile with 128 pixels. Two discernable gaps on the profile identify the GDL. The water signal from the gas channels on the other side of the GDL is observable. The water content distribution across the Nafion membrane is inhomogeneous.

1. A. V. Ouriadov, R. P. MacGregor, and B. J. Balcom, J. Magn. Reson. 169 (2004) 174.
2. Ziheng Zhang, A. E. Marble, R. D. MacGregor, B. J. Balcom, proceedings of ICMRM 2007.
3. G. Hoogers, Fuel Cell Technology Handbook, CRC Press, New York, 2000.
4. R. J. Bellows, M. Y. Lin, M. Arif, A. K. Thompson and D. Jacobson, J. Electrochem. Soc., 146 (1999) 1099.

Quantitative monitoring of liquid ingress in heterogeneous layered materials using a Mobile Universal Surface Explorer (MOUSE®)

Hans Adriaensen[1], Martin Bencsik[1], Stuart Brewer[2] and Glen Mc Hale[1].

[1]School of Biomedical and Natural Science, Nottingham Trent University, NG11 8NS, UK
[2]DSTL, Porton Down, Salisbury, Wiltshire, SP4 0JQ, UK

Abstract:

The design of liquid repellent fabrics is extremely important to industrial and domestic applications that seek to minimise, or prevent, liquid ingress from contaminating materials and personnel[1,2,3,4,5]. In this work we have developed an experimental protocol by which a known volume (7 µL) of a given liquid is deposited on a three layered fabric and a known weight is vertically applied for a time duration of 30 to 90 seconds on top of the liquid. We have then explored and optimised the ability unilateral NMR (Nuclear Magnetic Resonance) has, to spatially resolve the liquid penetration, with one-dimensional Fourier-transformed NMR of standard CPMG spin echoes. This was achieved using the *profile* MR MObile Universal Surface Explorer[6] (MOUSE®) at a field strength of 0.25 T. By placing the investigated sample in the middle of the selected slice (2 mm above the instrument) across which resides a very strong (11.4 T/m) built-in vertical field gradient, vertical loads can be placed without the restrictions that a tubular NMR system usually exhibits, and an elegant match is obtained between the features of the unilateral instrument and the geometry of this particular experiment.

We successfully measured the ingress of a commercially available oil (DUCKHAMS 15W/40 Mineral formula) into a fabric made of three stacked individual 80 µm thick layers. The top and bottom layers have been treated and are strongly repellent to the oil, whilst the middle layer is non-repellent.

A spatial resolution of approximately 15 µm is obtained, over a field of view exceeding 500 µm. Good SNR (> 15) is obtained in four minutes by using a liquid exhibiting a short T_1. The CPMG sequence is used with 40 echoes and an echo time of 510 µs.

We show that the absolute amount of oil in each individual layer can be monitored as a function of the applied pressure and of the timings used to apply those pressures. This preliminary study opens a new range of possible explorations into the ingress of liquids in intelligent heterogeneous layered fabrics.
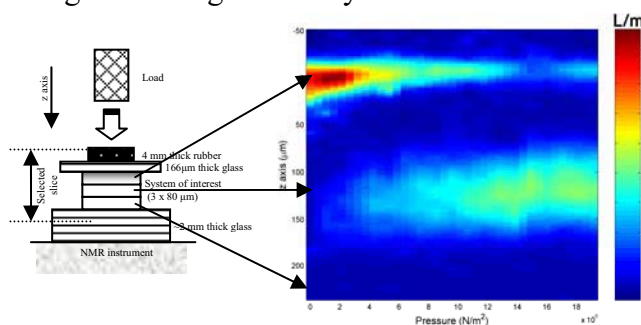
Figure 1.(a) Sketch of experimental set up. (b) color-coded linear oil volume density as a function of z (vertical axis) and applied pressure (horizontal axis) revealing the dynamics of the ingress of the liquid into the system. Note the absence of signal in the first 80 microns of the system, due to the repellent layer. The origin of the z axis was made to coincide with the interface between the top of the system under investigation and the glass microscopy slide.

[1] E. Kissa, In *Handbook of Fibre Science and Technology*; edited by M. Lewin, S. B. Sello (Marcel and Dekker Inc. New York, 1984). **[2]** S.A. Brewer, S.R. Coulson, I.S. Woodward, J.P.S. Badyal, C. Willis, J. Phys Chem B 104 (37): 8836-8840 21 (2000). **[3]** S.A. Brewer, S.R. Coulson, I.S. Woodward, J.P.S. Badyal, C. Willis, *Langmuir* 16 (15): 6287-6293 25 (2000). **[4]** S.A. Brewer, S.R. Coulson, I.S. Woodward, J.P.S. Badyal, C. Willis, Chem Materials 12 (7): 2031-2038 (2000). **[5]** *Adv. Mater.* 2006, *18*, 3063–3078 *Xinjian Feng* and *Lei Jiang*. **[6]** Perlo J. et al., J. Mag. Res. 176 (1): 64-70 2005

NMR Assessment of Polymer Mechanical Properties:

Portable NMR and elastomeric moduli?

Jeffrey A Reimer[1]

[1] University of California, Berkeley, USA

Abstract:

In this paper I seek to demonstrate the application of residual dipolar couplings towards the imaging of mechanical properties in radiation-damaged silica-filled elastomeric materials. We determine residual couplings for elastomers subjected to eight different exposures of gamma-radiation, correlate these couplings to moduli obtained from dynamical mechanical analysis, and show that moduli can then be imagined using simple MRI methodologies. The correlation between residual dipolar couplings and moduli are scalable down to magnetic fields typically used in portable MR devices, thus portending the development of standoff *in-situ* assessment of elastomeric moduli.
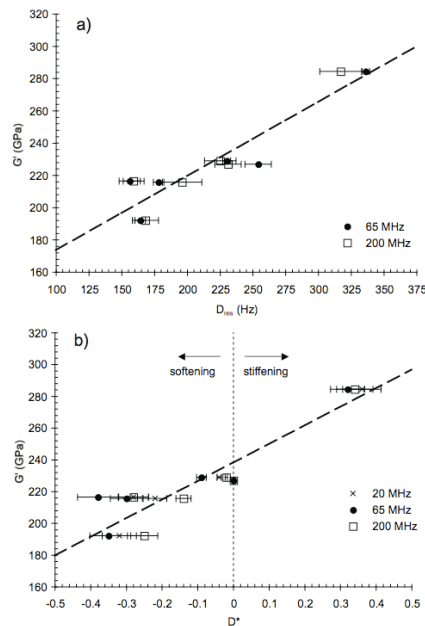
Biopolymer and Water Dynamics in Microbial Biofilm Extracellular Polymeric Substance

Sarah L Codd

*Department of Mechanical Engineering
and Center for Biofilm Engineering
Montana State University
Bozeman MT 59717 USA*

Microbial bacteria in the presence of surfaces and water will form biofilms. Biofilms have detrimental impacts in many medical applications and both detrimental and useful impacts in environmental and industry applications. Biofilms are generated by formation of a hydrogel matrix composed of biopolymers, the extracellular polymeric substance (EPS). The EPS is composed primarily of polysaccharides with DNA, proteins and other biopolymer elements present. The EPS provides resistance and increases the survival of microbes through a variety of mechanisms including an ability to both increase and limit mass transfer of nutrients and antimicrobials. It is widely evidenced that the biofilm growth is impacted by and alters the hydrodynamics in flowing systems. NMR studies have demonstrated their ability to aid our understanding in this regard [1-4].

There is still much debate about the exact nature of the EPS and the way in which environmental and chemical challenges impact the matrix. *Staphylococcus Epidermis* biofilm has been studied using spectrally resolved PGSE experiments as initially demonstrated by Vogt et al [5]. The results from our recent work provide insight into the mechanisms by which the EPS and cell structure changes due to environmental and antimicrobial challenges [6]. *Pseudomonas aeruginosa* and its associated biofilm structure are associated with cystic fibrosis and are one of the most studied biofilm forming organisms. Alginate is the primary component of *P. aeruginosa* EPS and genetic modification can vary the degree of O-acetylation of the alginate chains and impact biofilm development. The degree of O-acetylation varies the EPS hydration and material properties however the molecular mechanisms involved are poorly understood. Understanding the water and polymer dynamics within the hydrogel and their impact on material properties provides the prospect of connecting chemical structure of the EPS to biological function and could lead to new ways to control biofilms. The application of magnetic resonance methods to measure the molecular dynamics is considered.

References:
1. Manz, B., Volke, F., Goll, D., Horn, H., *Investigation of biofilm structure, flow patterns and detachment with magnetic resonance imaging.* Water Science and Technology, 2005. 52(7): p. 1-6.
2. Seymour, J.D., Gage, J. P., Codd, S.L., and Gerlach, R., *Anomalous fluid transport in porous media induced by biofilm growth* Physical Review Letters, 2004. 93(19): p. 198103.
3. Gjersing, E.L., Codd, S.L., Seymour, J.D. and Stewart, P.S., *Magnetic resonance microscopy analysis of advective transport in a biofilm reactor.* Biotechnology and Bioengineering, 2005. 89(7): p. 822-834.
4. Majors, P.D., McLean, J.S., Fredrickson, J.K., and Wind, R.A., *HMR methods for in-situ biofilm metabolism studies: spatial and temporal resolved measurements* Water Science and Technology, 2005. 52(7): p. 7-12.
5. Vogt, M., Flemming, H.-C., Veeman, W. S., *Diffusion in Pseudomaonas aeruginosa biofilms: a pulsed field gradient NMR study*. Journal of Biotechnology, 2000. 77: p. 137-146.
6. Hornemann, J.A., Lysova, A. A., Codd, S.L., Seymour, J.D., Brown, J.R., Stewart, P.S. and Busse, S.C. To be submitted.

Fluid Distribution and Transport in Engineered Fibrous Substrates

Johannes Leisen and Haskell W. Beckham
School of Polymer, Textile and Fiber Engineering
Georgia Institute of Technology, Atlanta, USA

The interaction of fluids with engineered fibrous substrates, including textiles, carpet, paper, and absorbent products, is important for their manufacture as well as end-use properties. Magnetic resonance microscopy (MRM) is uniquely suited for nondestructive studies of fluid distribution and movement in these often opaque fibrous materials. Depending on the fibers, binding of the fluid to the fiber surfaces can lead to complex T_2 relaxation behavior, significantly affecting the image contrast and making it difficult to extract quantitative information when using conventional spin-echo sequences. Image contrast is further influenced by the self-diffusion of the fluid through complex hierarchical porous environments characteristic of fibrous substrates. Quantitative information has been obtained by two means: (i) establishment of calibration curves to relate image intensities to concentrations, or (ii) phase-encoding sequences such as single-point imaging or SPRITE. We have utilized MRM to study a variety of industrially relevant engineered fibrous substrates:

(1) Nonwovens are used extensively in personal care products and in disposable garments for health care personnel. The pore size distribution governs fluid ingress and distribution. We have used MRM to measure the equilibrium fluid distribution after vertical wicking into nonwovens, and used this distribution to determine the pore size distribution.[1]

(2) Carpet manufacturing relies on the efficient removal of water as the last step after coloration. We simulated an industrial dryer within an MRM probe and used single-point imaging to quantitatively and rapidly follow moisture distribution within carpet as a function of drying time.[2]

(3) The mechanical properties of cardboard are significantly affected by moisture, even at low levels. We used spin-echo imaging, for sufficient sensitivity at low moisture levels, to examine ingress of moisture into dry cardboard from high-humidity environments. A calibration curve was used along with simulations of moisture concentration profiles to analyze the data.[3]

(4) Fiber tows and fabrics are commonly used to reinforce polymer composites, in which the wicking of viscous fluids into the fibrous reinforcement must occur without leaving entrapped air defects. We have used MRM to study transverse flow across aligned micro-cylindrical fibers and compared these experimental results to theoretical predictions.[4]

(5) Woven fabrics are used in a variety of technical applications, including de-watering in paper manufacturing. We used flow MRI to examine steady-state flow through complex woven fabrics. Using a sequence very similar to diffusion-weighted imaging, velocity maps were measured and compared to those constructed from computational fluid dynamics simulations.

References
1. Leisen, J.; Landeryou, M.; Cottenden, A. "Measurements of moisture distribution within nonwoven fabrics using NMR imaging"; *IMechE, Incontinence: The Engineering Challenge* **2003**.
2. Leisen, J.; Beckham, H. W. "Quantitative Magnetic Resonance Imaging of Fluid Distribution and Movement in Textiles"; *Textile Research Journal* **2001**, *71*, 1033-1045.
3. Leisen, J.; Hojjatie, B.; Coffin, D. W.; Lavrykov, S. A.; Ramarao, B. V.; Beckham, H. W. "Through-Plane Diffusion of Moisture in Paper Detected by Magnetic Resonance Imaging"; *Ind. Eng. Chem. Res.* **2002**, *41*, 6555-6565.
4. Neacsu, V.; Leisen, J.; Beckham, H. W.; Advani, S. G. "Use of Magnetic Resonance Imaging to Visualize Impregnation across Aligned Cylinders Due to Capillary Forces"; *Exp. Fluids* **2007**, *42*, 425-440.

MR Studies of Industrial Micelle Solutions

M.L. Johns, J.D. Griffith, C.J. Davies, A.J. Sederman[1]

[1]Department of Chemical Engineering, University of Cambridge, Cambridge, UK

Particulate solid detergents are complex mixture of various materials (polymers, surfactants, salts, solids) with a range of functions; the primary necessary ingredient however is a surfactant with the most common industrial example being linear alkylbenzene sulfonate (LAS). In this presentation, we will consider the application of various Magnetic Resonance (MR) techniques to elucidate the drying behaviour during formation of such LAS-based detergent particles from a wet paste. This will include quantification of the drying rate and regime as well as quantitative descriptions of the evolving microstructure in the drying paste. In particular, we will present an overview of the following uses of MR techniques in this capacity which contains both novel application and novel pulse sequence development:

- The combined use of 1D spin-echo imaging and SPI techniques has been used to quantify the moisture profiles in suspended 2 ml droplets as they dry *in-situ*. We demonstrate that a combination of these two methods is able to provide quantitative limits on the moisture content profiles of the sample as it dries. The data has been used for the verification of droplet drying models, in the process requiring a double inverse Abel transform; preliminary data will be presented.
- The use of rapid self-diffusion measurement has been used to determine the surface-to-volume ratio and tortuosity of the pore space within these detergent paste systems as they dry (1). Such geometric parameters dictate the drying regime, the microstructure and hence the functionality of the final product. To this end we have implemented a potentially single shot version of the Difftrain pulse sequence (2), modified to optimise use of the available signal. The evolution of these microstructural parameters during drying will be presented and discussed.
- Relaxation measurements have been conducted on the drying material and via interpretation of the T_1 probability distribution we were able to determine the order and rate of water loss from the various phases within the sample. This technique was successfully implemented on a bench-top spectrometer for routine sample analysis.

The rheology of the material is also of general interest as it determines the particulate size and shape as formed from the wet paste. We will present preliminary results for the application of Rheo-NMR to such systems. This will feature the combined application of rapid velocimetry (3) and triggered acquisition to track the evolution in the flow field as a function of time following the cessation of imposed shear. For the case of visco-elastic fluids in a reasonably wide-gap Couette cell, this results in the reversal of the flow direction, forming a wave that propagates across the cell gap width.

References
(1) P.P. Mitra, P.N. Sen, L.M. Schwartz, Phys. Rev. B 47 (1993) 8565.
(2) C.J. Davies, J.D. Griffith, A.J. Sederman, L.F. Gladden and M.L. Johns, J. Magn. Reson. 187 (2007) 170.
(3) A.J. Sederman, M.D. Mantle, C. Buckley and L.F. Gladden, J. Magn. Reson. 166 (2007) 182.

MR Microscopy of Resorbable Polymeric Bioceramics

Josh M. Bray[1,2], Carl Petrone[3], M. Filiaggi[3] and <u>Steven D. Beyea</u>[1,2,4]

[1] Institute for Biodiagnostics (Atlantic), National Research Council, Halifax, Nova Scotia, Canada
[2] Department of Physics, [3] School of Biomedical Engineering, [4] Department of Radiology, Dalhousie University, Halifax, Nova Scotia, Canada

Abstract:

While novel and innovative interventions in regenerative medicine hold great promise, such methods are only as effective as the ability to develop an empirical and mechanistic understanding of how/why they work. One such example is the use of resorbable bioceramics, which have potential to provide large, sustained concentrations of therapeutic agents to a specific tissue, while not exceeding the minimum toxic concentration in other tissues.

Optimization of resorbable bioceramic design requires methods that will permit the non-invasive and non-destructive study of the spatially and temporally varying physicochemical changes that occur due to material degradation. The study of drug delivery biomaterials using MRI therefore has the potential to significantly improve the understanding of the performance of such devices.

The current study focuses on the use of MR imaging and relaxometry at 11.7 Tesla to characterize the spatial-temporal evolution of amorphous Calcium Polyphosphate (CPP) bioceramics, intended for implantation into bone fractures for treatment of osteomyelitis. The ability of MR microscopy to resolve the internal network reorganization will be demonstrated by comparing the results obtained as a function of initial biomaterial processing.
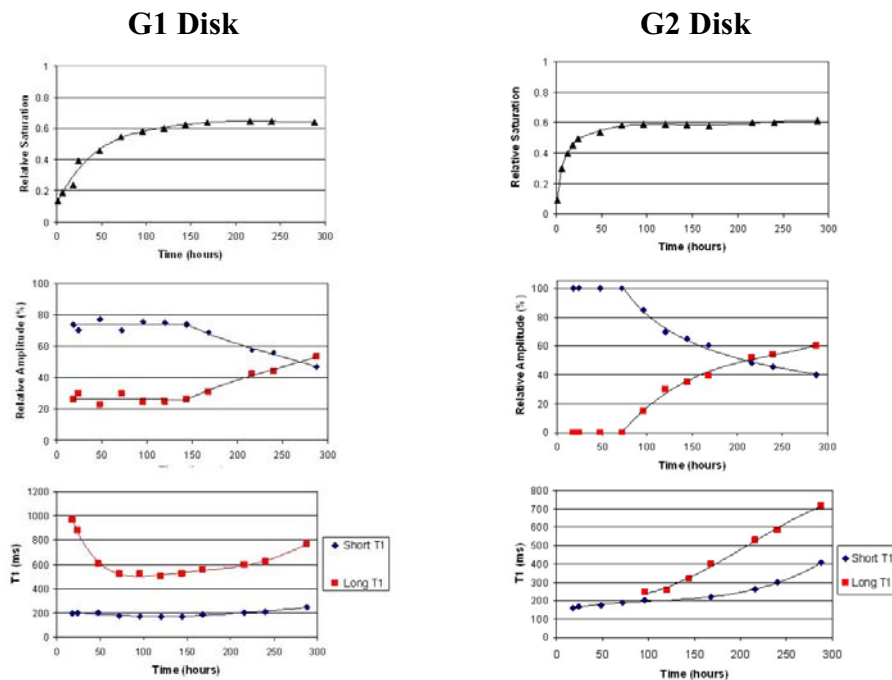
G1 Disk   **G2 Disk**

Fig. 1: Data extracted from a single pixel internal to a CPP disk, shown as a function of time during 1D fluid transport into the material. Plots of Fluid Saturation, T1 relaxation time, and T1 component relative amplitude are shown. Data for CPP disks produced using two different processes are shown, with the "G2" disks having undergone a secondary re-compaction/gelling step.

New Hardware and Software Development and Optimization for NMR Microscopy

D. Gross, V. Lehmann, T. Oerther and K. Zick

Bruker Biospin GmbH, Rheinstetten, Germany

Abstract:

NMR Microscopy has become a well established field of research and the number of applications is increasing continuously. Thus far the hardware components have not substantially changed but the process of improvement and optimization is ongoing. The design of gradient systems was changed from unshielded to shielded versions. This reduced the distortion caused by eddy currents by more than an order of magnitude. Nevertheless, such effects can still play a role in some imaging, localized spectroscopy and diffusion methods where it would help for them to be reduced even further. To that end a new digital preemphasis and B0 shift compensation unit has been developed.

Another important factor in NMR Microscopy is the signal to noise ratio in the experiments. This is often the limiting factor in many practical applications. Great effort has been made to improve the signal to noise ratio. But due to the wide range of different properties in the objects under investigation there is no standard solution for this. Various options exist which have to be adapted on a case by case basis. Some examples are shown: optimized quadrature probes; Cryoprobes; micro-coils; dedicated surface coils and multi-receive systems.

In order to cover the wide and rapidly expanding range of applications the various hardware and software components have to be of a modular design. Examples are shown for MAS NMR combined with diffusion gradients, imaging and localized spectroscopy of small animals (Drosophila flies and spiders), and cardiac movies without the need for triggering by ecg electrodes and respiratory sensors.

NMR Microscopy with Isotropic Resolution below 10 μm Using Dedicated Hardware and Optimised Methods

Michael Fey[1], Daniel Schmidig[1], Schimun Denoth[1], Charles Massin[1], Franck Vincent[1], Michael Schenkel[1], and Markus Weiger[1]

[1] Bruker BioSpin AG, Faellanden, Switzerland

Abstract:

NMR microscopy [1,2] has the great potential of providing the plurality of NMR contrast mechanisms also to very small biological samples. However, at a spatial resolution of a few micrometers it is increasingly difficult to obtain sufficiently high SNR within a reasonable measurement time. Furthermore, conventional Fourier techniques suffer from loss of true resolution due to diffusion under the encoding field gradients and the associated filter in k-space [3]. This effect can be reduced by the use of very strong gradients. However, during frequency-encoding this leads to a decrease of the SNR, favouring purely phase-encoded methods such as constant time imaging (CTI) [4,5].

In this work, dedicated hardware and optimised imaging methods were used to push the isotropic resolution of NMR imaging below 10 μm. For high sensitivity, micro-fabricated planar surface RF coils with a multi-turn spiral [6] were used and evaluated for different diameters D, confirming an approximate inversely proportional behaviour of the SNR with respect to D. Furthermore, imaging was performed at B0 field strengths up to 18.8 T, actually providing the theoretically expected SNR increase proportional to $B0^{7/4}$. To overcome diffusion-related resolution problems a planar triple-axis gradient capable of providing up to 6500 G/cm was employed. For parameter optimisation of CTI the analysis of [7] was further developed, and also diffusion effects after the gradient application were considered. With the described setup 3D phantom images were acquired with isotropic resolution down to 3.0 μm.
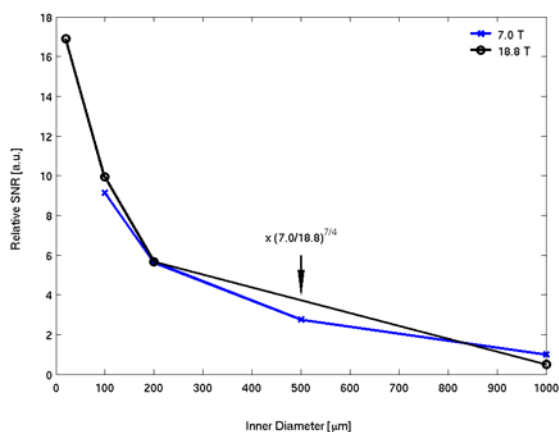
Fig. 1: Relative SNR as a function of the inner diameter of the RF microcoil measured at two different B0 field strengths.

Fig. 2: Slice parallel to the 20 μm surface coil taken from a 3D CTI data set with 3.0 μm isotropic resolution acquired in 58 h and showing glass fibres in doped water.

1. L. Ciobanu, A.G. Webb, C.H. Pennington, *Prog. Nucl. Magn. Res. Spectrosc.* **42** (2003) 69-93
2. S.-C. Lee, K. Kim, et al., *J. Magn. Reson.* **150** (2001) 207-213
3. P.T. Callaghan, C.D. Eccles, *J. Magn. Reson.* **78** (1988) 1-8
4. S. Gravina, D.G. Cory, *J. Magn. Reson. B* **104** (1994) 53-61
5. S. Choi, X.-W. Tang, D.G. Cory, *Int. J. Imaging Syst. Technol.* **8** (1997) 263-276
6. C. Massin, F. Vincent, et al., *J. Magn. Reson.* **164** (2003) 242-255
7. A.G. Webb, *Concept. Magn. Reson.* **22A** (2004) 25-36

Curiosities from Earth's field and Low field NMR

Andrew Coy[1], Robin Dykstra[2], Craig D. Eccles[1], Meghan E. Halse[3], Mark W. Hunter[3], B. Parkinson[3] and Paul T. Callaghan[3]

[1] Magritek Limited, 32 Salamanca Road, Wellington, New Zealand.
[2] Institute of Fundamental Sciences, Massey University, Palmerston North, New Zealand.
[3] MacDiarmid Institute, School of Chemical and Physical Sciences, Victoria University of Wellington, Wellington, New Zealand.

Abstract:

The use of small, cheap permanent magnets to create portable NMR systems has resulted in an ever increasing number of novel probe designs and geometries. These NMR probes are each designed with the goal of promoting one or more specific characteristics of the probe at the expense of others. For instance a particular design and geometry may result in lower size and weight but consequently have lower field homogeneity. This mutation and evolution of designs has resulted in a growing ecosystem of probes, quite dramatically different in design, each with particular advantages and disadvantages. We present here a subset of results from a range of NMR systems we have built around probes such as the NMR-MOUSE, Profile NMR-MOUSE, NMR-CUFF, Halbach and NMR-MOLE[1] designs which demonstrate the specific advantages of each design.

For a truly portable and magnet-free solution the use of the Earth's magnetic field is particularly attractive. However, the use of the Earth's magnet field as the basis of an NMR system has traditionally been limited by the very low signal-to-noise available. By taking advantage of the high natural homogeneity of the Earth's field, and by incorporating other signal-to-noise enhancement techniques, we have developed systems that can perform a range of NMR experiments, including advanced techniques such as MRI and 2D spectroscopy[2]. A selection of results obtained using a Terranova-MRI Earth's field NMR and MRI system will be presented along with some of the new methods being used to improve the performance of the instrument.

1. B. Manz et al., J. Magn. Reson. 183 (2006) 25 - 31.
2. Robinson, J., et. al.. Magn. Reson. 182 (2006) 343-347.

The Profile NMR-MOUSE: Methods and Applications

Jürgen Kolz[1,2], Juan Perlo[1,2], Federico Casanova[1,2], and Bernhard Blümich[2]

[1] ACT GmbH, Roetgen, Germany
[2] ITMC, RWTH-Aachen, Aachen, Germany

Abstract:

Single-sided NMR technology has considerably evolved during the last decade and many different sensor geometries are available nowadays. Among them the *profile* NMR-MOUSE, which is able to resolve depth structure with microscopic resolution [1], is proving to be a powerful analytical tool applicable in diverse fields spread across many disciplines. For example, in the field of conservation of the cultural heritage it is used to study pigments paintings, frescos, ancient manuscripts, mummies, and stones of roman buildings. In medicine, it is used to resolve in vivo the structure of human skin in order to improve the effect of treatments for skin diseases, to study the effect of cosmetics, and to monitor skin regeneration. In the rubber industry, it is used for quality control of tires, determining the cross-link density, and by selective imaging of certain composites. For building material analysis, it is used to determine the thickness of coatings applied to the surface of porous materials and to measure quantitatively the moisture profile through multilayer structures. The requirements to study such a diversity of materials, which present extremely different NMR properties, are met by a suitable combination of optimum magnet design, right methodologies and sensitive contrast parameters. In this work we present a number of examples that illustrate the flexibility to adapt the sensor for specific applications.

1.   J. Perlo, F. Casanova, and B. Blümich, *Journal of Magnetic Resonance* **176** (2005) 64-70.

Customized Coils

Alexander Weisser

RAPID Biomedizinische Geräte, RAPID Biomedical GmbH
Technologiepark Pav. 4, Kettelerstraße 3-11, D-97222 Rimpar, Germany
Phone: +49-93 65-88 26-0, Fax: +49-93 65-88 26-99, www.rapidbiomed.de

RAPID Biomedical GmbH is specialised in the research and production of custom made probeheads for MRI and NMR spectroscopy. The company collaborates with research institutions, hospitals and MR system manufacturers worldwide. Our products include ^{1}H MR resonators for clinical studies at all magnetic field strengths and for all organs. We also supply multi-nuclear (e.g. ^{1}H / ^{31}P) MR-probeheads for combined MRI and MRS in clinical and basic science investigations. Our product range includes MR probeheads for routine animal research (RAPID COMPLETE™) and various accessory devices, as well.

Our recent work concentrates on multi array coils for parallel MRI both for human (e.g. 32 channel cardiac array) as well as for animal studies (e.g. 8 channel whole body mouse array).

MRI of axial and radial hydraulic conductivity in (woody) plants.

N. Homan, E. Gerkema, F.J. Vergeldt, H. Van As,

Laboratory of Biophysics and Wageningen NMR Centre, Wageningen University, Wageningen, the Netherlands.

Abstract:

Hydraulic conductivity of (axial) long distance xylem and phloem transport and radial water transport in plants and trees provides key information to validate biophysical structure-function plant models. Such models are in use to address water stress-induced effects and growth limitations. In addition, such models are used to quantify the contribution of plant evapotranspiration and carbon exchange within global atmospheric circulation models. Flow in (woody) plants can be described by a combination of Darcy's law and the continuity equation, with the conductivity regarded as a function of structure. However, there are many violations to Darcy's law when applied to water in living (woody) plants and key aspects of the relationships between pressure and flow rates/flow conducting area are not well understood. Using conventional methods it is very difficult to determine radial transport and sapwood specific conductivity (active flow conducting area) *in situ* and to study the dynamics (e.g. day-night, stress responses) therein.

A very promising and attractive method for providing detailed, quantitative information on flow and effective flow conducting area in intact plants is flow MRI based on PFG methods. Because the diameter of flow conducting vessels and tracheids is small in comparison to the pixel size, a crucial step in quantification is to discriminate non-flowing and flowing water within a single pixel. The fact that the propagator for non-flowing water is symmetrical around zero is used to separate it from the flowing water. In this way the active flow conducting area can be obtained. By combined propagator-T_2 measurements [1] active and non-active xylem can be discriminated. Measuring T_2 fractions as a function of propagator labelling time (Δ) gives access to (radial) exchange or radial transport, containing information on the pit connections between conduits. Pit membranes determine a large part of hydraulic resistance.

Further information on radial transport can be obtained by applying the PFG in the radial direction. Now apparent diffusion coefficients are observed as a function of Δ [2]. On the basis of combined T_2 information in central parenchyma, xylem and phloem regions different fractions can be discriminated with different restricted diffusion behaviour. From this restricted diffusion information tissue permeability is obtained.

We have applied this approach to different (genetically modified) plants and trees. Some striking lessons emerge from the results, which demonstrate that (woody) plants are dynamic, unsaturated porous media and that MRI can reveal unexpected differences in hydraulic conductance between wild type and modified plants.

1. C.W Windt, F.J. Vergeldt, H. Van As, *J Magn Reson* 185 (2007) 230-239.
2. H. Van As, J *Exp Bot* 58 (2007) 743-756.

NMR measurement of irreversibility and particle migration in dilute sheared Brownian suspensions

Jennifer R. Brown[1], Joseph D. Seymour[1], Sarah L. Codd[2],
Einar Orn Fridjonsson[1], Giles R. Cokelet[1] and Magnus Nydén[3]

[1]Department of Chemical and Biological Engineering, Montana State University Bozeman MT USA

[2]Department of Mechanical and Industrial Engineering, Montana State University Bozeman MT USA

[3]Department of Chemical and Biological Engineering, Chalmers University of Technology Göteborg, Sweden

Abstract:

   PGSE NMR measurements for a dilute ($\phi < 0.10$) suspension of ~2.5 mm Brownian particles under shear flow in a 1 mm diameter glass capillary suggest particle migration and irreversible dynamics, effects typically associated with concentrated non-colloidal suspensions. The use of "core-shell" particles[1] allows differentiation between the particulate and fluid phases of this multi-phase flow system due to the spectral resolution between particle core oil and suspending water possible with PGSE techniques. Propagators were obtained showing an increased probability of finding the particle at higher velocities. In addition, velocity imaging shows a parabolic or nearly parabolic bulk velocity profile characteristic of Poiseuille flow where the highest velocity streamlines are located at the centre of the capillary, indicating that particles are migrating inward. Particle migration of Brownian suspensions under pressure driven flow has been shown previously with optical techniques[2]. However, at dilute concentrations ($\phi \sim 0.05$), evidence of migration was not greater than the measurement uncertainty, unlike the NMR results presented here. Flow models generally only account for particle migration in non-colloidal or concentrated suspensions, but this work implies that theoretical concepts could be applicable to dilute Brownian suspensions. Dispersion coefficients as a function of observation time for the Brownian particles were also measured via flow-compensated PGSE and indicate the onset of irreversible dynamics with increasing total strain. Chaotic dynamics are an indication that many body hydrodynamics impacts the motion of the particles. It appears that concepts governing the time reversibility of shear flows previously applied to concentrated non colloidal suspensions[3] again could apply to dilute Brownian suspensions.

1.   Wassenius, H. and P.T. Callaghan, *Journal of Magnetic Resonance*, **169**(2004): p. 250-256.
2.   Frank, M., et al., *Journal of Fluid Mechanics*, **493**(2003): p. 363-378.
3.   Pine, D.J., et al., *Nature*, **438**(2005): p. 997-1000.

Measurement and simulation of the non-local dispersion tensor in porous media

M.W. Hunter[1], A.N. Jackson,[2] and P.T. Callaghan[1]

[1] MacDiarmid Institute for Advanced Materials and Nanotechnology, Victoria University of Wellington, Wellington, New Zealand.
[2] SUPA. School of Physics, University of Edinburgh, Edinburgh EH9 3JZ, Scotland, United Kingdom

Abstract: Dispersion describes the phenomenon whereby particles on the same streamline separate during flow. The physics of dispersion is governed by stochastic processes arising from the interplay between advective velocity gradients, molecular diffusion and boundary layer effects [1]. The dispersion tensor, $\mathbf{D}^*$, is a local measurement in the sense that it does not depend on positional relationships and is measured as time asymptotes [2]. For situations where the length- and time-scales on which transport occurs are not much larger than the scale of the fluctuations in the velocity field, a non-local description is required [3]. The tensor is written as

$$\mathbf{D}^*_{NL}(\mathbf{R},\tau) = \left\langle \mathbf{u}(\mathbf{r},0)\,\overline{P_{\mathbf{r}}}(\mathbf{R},\tau)\,\mathbf{u}(\mathbf{r}+\mathbf{R},\tau) \right\rangle.$$

Pulsed Gradient Spin Echo (PGSE)-NMR provides a wealth of information about the velocity correlations in porous media. Presented here is a set of NMR pulse sequences and a superposition designed to extract the velocity correlations necessary to calculate the dispersion as a function of displacement and hence the non-local dispersion. The experimental method will be tested against the calculable non-local dispersion in a Couette cell [4]. Further experiments are performed on porous media.

The Lattice-Boltzmann algorithm has been shown to successfully predict the flow field in porous media [5], and has been used to model the flow field through our model porous medium. This flow field is used to simulate a large ensemble of virtual tracer particles, from which numerical estimates for both the local and non-local dispersion can be determined. Our implementation of this approach is presented here along with a comparison between the experimental and computational results.
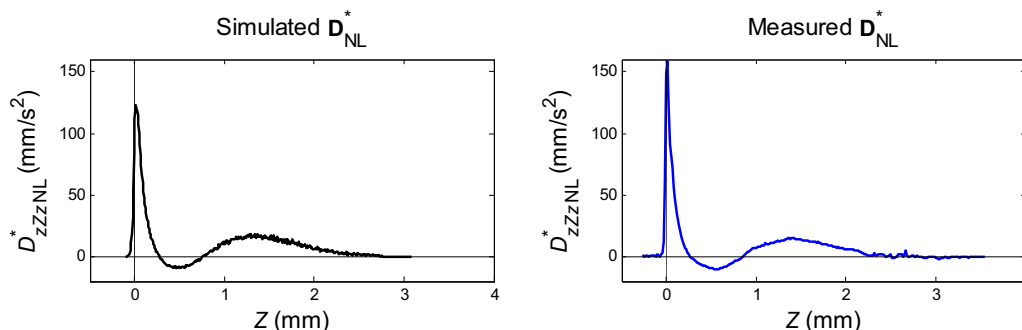
The non-local dispersion of flow through a beadpack, Pe = 2000, $V_t = 8mm/s$, $\tau = \tau_v$, $d_{bead} = .5mm$.

[1] A. A. Khrapitchev and P. T. Callaghan, Phys. Fluids, **15**, 9 (2003)
[2] J. D. Seymour and P. T. Callaghan, AIChE J. **43**, 8 (1997).
[3] D. L. Koch and J. F. Brady, J. Fluid Mech. **180** (1987)
[4] M.W. Hunter and P. T. Callaghan *submitted*
[5] B. Manz *et al.*, AIChE J. **45**, 9 (1999).

Spin echoes and intermolecular double-quantum coherences in gases in the fast diffusion regime

P.P. Zänker[a], J. Schmidt[a], R.H. Acosta[b], L. Agulles-Pedrós[a],
J. Schmiedeskamp[a], H.W. Spiess[a]

[a] *Max Planck Institute for Polymer Research, Mainz, Ackermannweg 10, D-55128,Germany.*
[b] *FaMAF- National University of Córdoba, Ciudad Universitaria, Córdoba, X5016LAE, Argentina.*

The spin echo (SE) phenomenon, which was first discovered by Hahn in 1950 [1], provides the basis of numerous pulse sequences in modern NMR and MRI. The reduction of the SE signal due to spin motion has already been subject of many theoretical and experimental studies in liquids [2,3]. In gases, however, translational motion affects the SE signal on much shorter timescales, even shorter than the pulse distance. This regime of very fast diffusion has not been studied yet, although it is of special interest for example in the field of gas MRI. Here, for the first time, a detailed theoretical and experimental examination of the SE time evolution under the fast motion in the gas phase is presented.

The experiments were realized using hyperpolarized (HP) ^{3}He (provided by the Physics Department of the University of Mainz [4]) and a self-constructed gas mixing setup, which allows a precise variation of the diffusion coefficient by admixing HP ^{3}He with heavier buffer gases at different pressures. The influence of fast motion on the echo formation was found to be much more dramatic than in the regimes considered so far. It results in a change of the SE signal in terms of amplitude, shape and echo position (so-called *pseudo SE effect* [5]). These effects were described by an extension of the Stejskal-Tanner equation to arbitrary times for linear gradients. The more general case of non-linear gradients, where an analytical solution cannot be easily obtained, was simulated using computer calculations.

While on the one hand the understanding of this phenomenon is of general theoretical interest, it is, on the other hand, a prerequisite for different applications, e.g. SE imaging sequences in MRI of HP gases. Here, diffusion suppression used to be one of the major obstacles. Additionally, the developed setup and the awareness of fast diffusion effects on echo signals allowed for the first time the detection of *intermolecular double-quantum coherences* (iDQCs) in the gas phase, which arise from the distant dipolar field induced by remote spins. Since the discovery of such couplings in solution NMR [6], great attention has been paid to this subject, resulting in several novel biomedical applications [7]. The possibility to detect iDQCs also in the gas phase will allow new experiments, e.g. in structure determination of porous materials or human lungs, similar to studies that have been performed on model systems for liquids [8].

[1]   E.L. Hahn. *Physical Review*, 80:580–594, 1950.
[2]   H.Y. Carr and E.M. Purcell. *Physical Review*, 94(3):630–638, 1954.
[3]   E.O. Stejskal and J.E. Tanner. *Journal of Chemical Physics*, 42(1):288–292, 1965.
[4]   E.W. Otten. *Europhysics News*, 35(1), 2004.
[5]   J.Collignon, H.Sillescu, and H.W. Spiess. *Colloid & Polymer Science*, 259:220–226, 1981.
[6]   W.S. Warren, W. Richter, A.H. Andreotti and S. Farmer, *Science* 267:2005-2009 (1993).
[7]   W.S. Warren et al. *Science*, 281:247–251, 1998.
[8]   L.-S. Bouchard and W.S. Warren *J. Magn. Reson.* 170:299-309 (2004).

E-mail: zaenker@mpip-mainz.mpg.de

Novel Approaches to High-Resolution NMR Spectroscopy in Low and Ultra-low Fields

Meghan E. Halse[1] and Paul T. Callaghan[1]

[1] MacDiarmid Institute, School of Chemical and Physical Sciences, Victoria University of Wellington, Wellington, New Zealand

Abstract:

One of the biggest challenges of low field and ultra-low field NMR research is the problem of how to maximise the information, particularly spectral information, which can be obtained from an NMR device with limited sensitivity and/or resolution. In this work we will present several approaches to obaining high-resolution spectroscopic information with a range of low and ultra-low field NMR devices.

First we will present a frequency stabilised approach to high-resolution (sub-hertz) multi-dimensional NMR spectroscopy in the Earth's magnetic field. It has recently been demonstrated by Appelt *et al.* [1] that not only hetero-nuclear but also homo-nuclear J couplings are observable in ultra-low fields, thus greatly increasing the potential information content of Earth's field (EF) NMR spectroscopy. It is anticipated that 2D EFNMR techniques will be valuable for the elucidation of complex coupling networks. The viability of 2D EFNMR spectroscopy has been demonstrated by Robinson *et al*. [2]; however achieving high-resolution (sub-hertz) results has hitherto been limited by several technical challenges, such as the significant temporal variation in the Earth's field over the course of 2D measurements. We have devised a highly effective solution to this problem of field drift and will show that the frequency of the EFNMR signal can be reliably stabilised to better than 0.2 Hz. Our most recent 2D EFNMR spectroscopy results, utilising this stabilisation method, will be presented and compared to simulation.

Second we will evaluate the imaged deconvolution technique [3] using the inhomogeneous B_0 field of a one-sided-access type NMR device. In this technique the ability of phase encode gradients to provide spatial resolution is combined with the powerful post-processing technique of reference deconvolution in order to significantly improve the achievable spectral resolution of an NMR device beyond that set by the B_0 inhomogeneity limited spectral line-width. The spectral resolution gain which can be achieved using this technique will be explored and the issues relating to its practical implementation will be discussed.

Third we will discuss the prospects for the elucidation of both chemical shift and scalar coupling in inhomogeneous fields using an unconventional approach to both the acquisition of the data in the time domain and the interpretation of the corresponding data in the Fourier domain.

1. Appelt, S., Haising F.W., Kuhn, H., Sieling U. and Blümich B., *Chem. Phys. Lett.* **440** (2007) 308 - 312.
2. Robinson, J., Coy A., Dykstra R., Eccles C., Hunter M. and Callaghan P.T., *J. Magn. Reson.* **182** (2006) 343-347.
3. M.E. Halse and P.T. Callaghan, *J. Magn. Reson.* **185** (2006) 130 - 137.

Development of compact MRI systems for specific diseases

Shinya Handa[1] , Katsumi Kose[1] and Tomoyuki Haishi[2]

[1] Institute of Applied Physics, University of Tsukuba, Tsukuba, Japan

[2] MRTechnology, Inc., Tsukuba, Japan

Introduction High field (1.5~3.0 T) whole body MRI (WB-MRI) systems are now widely available for diagnosis of various diseases. Moreover, recent developments of gradient and RF coil have made the WB-MRI systems much more powerful. Under this situation, clinical applications of small MRI systems are very limited. However, compact MRI systems have definite advantages over the WB-MRI systems for diagnosis of osteoporosis (OP) and rheumatoid arthritis (RA). In this study, we report compact MRI systems developed for trabecular bone (TB) microstructure measurements (1) and whole hand imaging (2).

Compact MRI for OP We have developed a compact MRI system (FIG.1) for TB microstructure measurements of the distal radius using a 1.0 T permanent magnet (gap width = 100 mm, homogeneity 16.4 ppm over 60 mm dsv). Figure 2 shows a 2D cross section selected from a 3D dataset of the distal radius acquired using a slice selective driven equilibrium 3D spin-echo sequence (TR/TE = 80 ms / 10 ms). This system achieved 150 μm × 150 μm × 500 μm spatial resolution in practical measurement times (17 or 23 minutes). Bone microstructure analysis results were demonstrated usefulness of our system.

Compact whole hand scanner for RA We also have developed a compact whole hand scanner using a 0.30 T permanent magnet (gap width = 130 mm, homogeneity 50 ppm over 220 mm × 80 mm diameter ellipsoidal volume). Hand examinations of normal volunteers were performed using a 3D T1-weighted GRE sequence (TR/TE = 35 ms/6 ms, acquisition time: 7 min) and STIR 3D-FSE sequence (TR/TI/TE = 1000 ms/110 ms/40 ms, acquisition time: 6 min 30 sec). Figure 3 shows 2D cross sections selected from a 3D datasets of the whole hand image acquired with respective sequences. These images have a sufficient quality for diagnosis of RA

Discussion and Conclusion We have developed compact MRI systems for diagnosis of OP and RA. These systems have advantages in installation space, patient comfort, and patient safety over the WB-MRI systems. At present these MRI systems are optimally designed for respective diseases using two different types of magnets. However, a "unified" compact MRI system with an intermediate magnetic field strength would be more preferable because osteoporosis is frequently observed in RA patients.
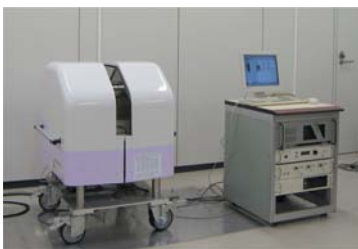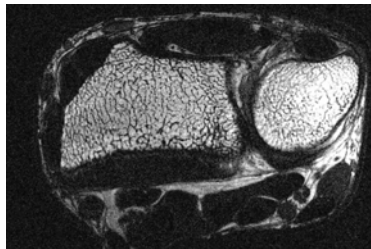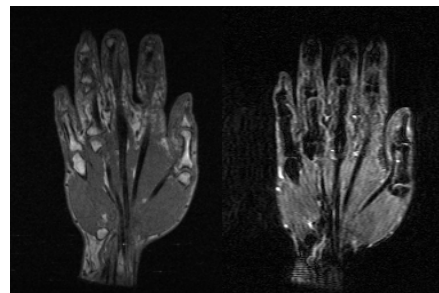

FIG.1.   FIG.2.   FIG.3.

References
1. Handa, S. Tomiha, T Haishi, K. Kose, Magn Res Med 58, (2007), in press.
2. Handa, S. H. Yoshioka, Tomiha, T Haishi, K. Kose, Magn Reson Med Sci 6, 113-120 (2007).

Compact MRI applications

Katsumi Kose[1], Tomoyuki Haishi[2], and Shinya Handa[1]

[1] Institute of Applied Physics, University of Tsukuba, Tsukuba, Japan

[2] MRTechnology, Inc., Tsukuba, Japan

Introduction About ten years ago, we established key technologies to built small MRI systems using permanent magnets (1-4). Since then, we have developed various compact MRI systems for academic research, industrial applications, and clinical diagnosis. In this talk we review compact MRI applications performed in our group. The compact MRI applications can be divided into two major categories: clinical and non-clinical applications.

Clinical applications Because many high-field (1.5-3.0 T) and advanced whole body MRI systems are now widely available, clinical applications of small MRI systems are very limited. However, some compact MRI systems have definite advantages over the WB-MRI systems. Among them two compact MRI applications are promising: trabecular bone (TB) microstructure measurements and hand imaging.

We have developed two compact MRI systems for TB microstructure measurements using 1.0 T permanent magnets (5,6). One measures TB of the finger and the other measures TB of the distal radius. These systems achieved $(160~\mu m)^3$ and $150\mu m \times 150\mu m \times 500\mu m$ spatial resolution in practical measurement times (15-20 minutes) using 3D driven equilibrium spin-echo sequences. We have developed two whole-hand MR scanners for diagnosis of rheumatoid arthritis (7). One system uses a 0.21 T permanent magnet and the other system uses a 0.30 T permanent magnet. The former system are now used for clinical evaluation in our university hospital.

Non-clinical applications Compact MRI systems are widely used for non-clinical applications. They are animal (mouse/rat) imaging (8), food science/engineering, flow measurements, plant science, microstructure measurements, and so on. The remarkable advantages of the permanent magnet MRI systems over the superconducting magnet MRI systems are their "openness" and "portability". So we can take MR images of live trees in outdoor environments (9). We can set up an MRI system even in a low temperature (-5°C) room for snow 3D structure measurements. Many mouse/rat MRI systems are now operated within "biologically clean" areas.

Conclusion Although the absolute SNR of the NMR signal is limited by the available magnetic field strength (at most 2 T), we believe the compact MRI systems using permanent magnets will continue to create novel applications in MRI.

References
(1) K. Kose, T. Haishi, A. Caprihan, E. Fukushima, J. Magn. Reson. 124, 35-41(1997).
(2) T. Haishi, K. Kose, J. Magn. Reson. 134, 138-141 (1998).
(3) K. Kose, T. Haishi, Spatially Resolved Magnetic Resonance, Edited by P. Blumler, B. Blumich, R. Botto, E. Fukushima, WILEY-VCH, 703-709 (1998).
(4) T. Haishi, T. Uematsu, Y. Matsuda, K. Kose, Magn Reson Imaging 19, 875-880 (2001).
(5) N. Iita, S. Handa, S. Tomiha, K. Kose, Magn Res Med 57, 272-277(2007).
(6) Handa, S. Tomiha, T Haishi, K. Kose, Magn Res Med 58, (2007), in press.
(7) Handa, S. H. Yoshioka, Tomiha, T Haishi, K. Kose, Magn Reson Med Sci 6, 113-120 (2007).
(8) T. Shirai, T. Haishi, S. Utsuzawa, Y. Matsuda, K. Kose. Magn Reson Med Sci 4,137-143 (2005).
(9) F. Okada, et al. Abstract of the 7th CMMR 2006.

Highly Parallel Array Detection for MRI

Lawrence L. Wald[1,2] and Graham C. Wiggins[,1]

[1] A.A. Martinos Center, Dept. of Radiology, Massachusetts General Hospital, Harvard Medical School Boston, USA.
[2] Harvard MIT Division of Health Sciences and Technology.

Abstract:

While advances in the "primary" technologies of MR such as increased field strength and improved gradient performance have been substantial, advances in Radio Frequency (RF) detection technology, have also proved to be a valuable and cost-effective way to improve sensitivity and encoding capabilities in Magnetic Resonance Imaging (MRI). Utilizing the phased array concept, and adapting it to the near-field limit applicable in MRI, previous work has shown the value of using multiple (usually 4 or 8) parallel detectors for improving sensitivity and encoding. While theoretical work has suggested that although there appear to be intrinsic limits in the parallel detection approach for both sensitivity and encoding ability, there are still substantial gains possible with the use of more highly parallel detection (greater than 32 elements).

We have therefore sought to determine the limitations and engineering issues of the highly parallel detection method and to explore how parallel imaging detector array might be constructed if the coil designer was essentially unconstrained by the number of parallel RF detection channels available on the instrument. The basic approach combines some of the lessons of micro-imaging (small, tightly coupled coils) with mass-manufacturing and attention to channel-to-channel interactions. We have developed a prototype MR scanner with 128 simultaneous reception channels and developed 96 channel detectors for the brain and 128 channel arrays for cardiac imaging. The expansion in parallelism allows substantial gains in sensitivity and nearly order of magnitude advances in our ability to accelerate image encoding. The latter allows us to contemplate new forms of image encoding and methods which have been previously dismissed as impractically lengthy such as echo volumnar imaging.
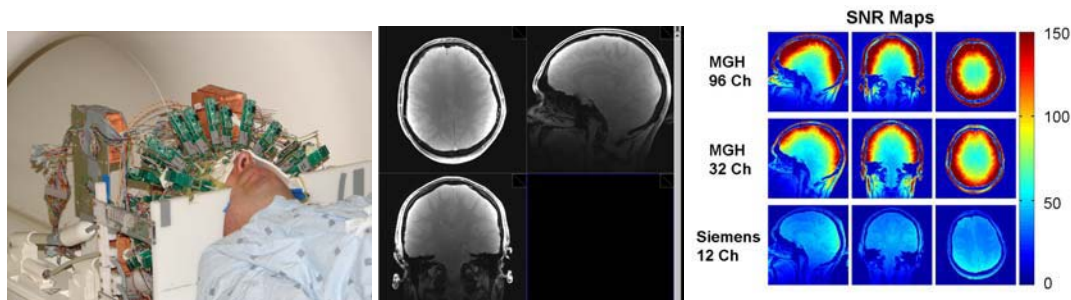
Fig.1   96 channel head array, coverage and SNR comparison to a 12 and 32 channel array.
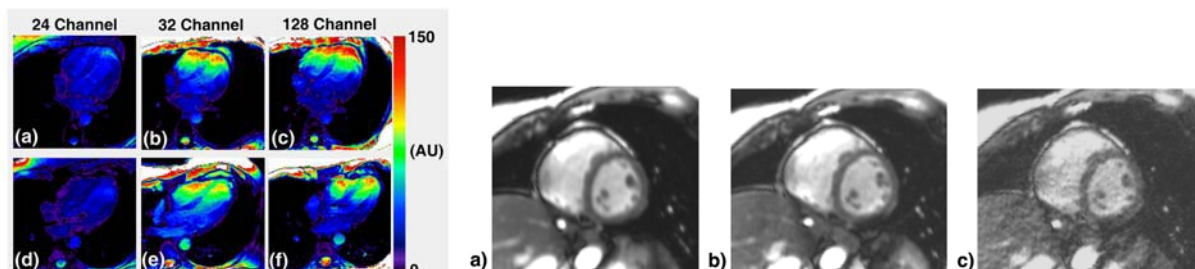

Fig.2   128 channel cardiac array SNR comparison to 24 and 32 channel commercial coils and highly accelerated imaging (R=1,4,7) cardiac cine imaging.

Prof. Thoralf Niendorf
Division of Experimental Magnetic Resonance Imaging
RWTH Aachen, Aachen, Germany

UNIVERSITÄTSKLINIKUM AACHEN

Merits and Challenges of Clinical Cardiovascular MRI at 3.0 Tesla

Cardiovascular MR imaging (CVMR) has become a valuable diagnostic imaging modality for the non-invasive detection of cardiovascular diseases. CVMR has conventionally been regarded as among the most challenging for 3.0 T, because of constraints associated with cardiac and respiratory motion artifacts, magnetic field inhomogeneities and localized tissue heating from RF power deposition. But CVMR at 3.0 T is also an area where the increased signal could overcome some of the problems experienced at 1.5T. A higher magnetic field strength may, for example, make it easier to differentiate healthy and infarcted tissue during delayed-enhancement imaging to assess myocardial viability. Switching from 1.5T to 3T could also improve the visibility of tagging bands used to track regional myocardial wall motion and extend their longevity. High-field imaging strategies are also appealing for the pursuit of whole heart coverage acquisitions in clinically acceptable breath-hold times or short free-breathing examinations. The merits of otherwise unattainable SNR paralleled by acquisition speed improvements promise to further advance clinical first pass myocardial perfusion imaging at 3.0 T. High-field imaging also provides means of improving MR angiography of the coronary arteries and large vessels by minimizing the impact of physiological motion and by permitting an improvement in the spatial resolution and anatomic coverage. There is also a powerful potential synergy between high-field MRI and parallel imaging, which is another driving force for the broad move towards clinical CVMR at 3.0 T. In this presentation, examples of these strategies will be provided including free breathing and breath-hold applications. But first, this presentation addresses the technology, key concepts and practical considerations of (accelerated) high-field CVMRI.

In summary, the capacity for rapid CVMR enabled by high magnetic field strengths promise to be beneficial to translate MR technology into extra diagnostic value not only by streamlining structural and functional imaging but also by facilitating targeted tissue characterization through molecular imaging and parametric mapping and by opening a broader access to physiologic information. It stands to reason that all these developments might culminate in another shift of paradigm when transitioning routine cardiac MRI from the current comprehensive cardiovascular MR examination focusing on cardiac anatomy and cardiac function to an even advanced imaging protocol including vessel wall imaging, plaque characterization and detection of arteriothrombosis.

Highfield MRI: Human Applications at 7T

Oliver Speck

Dept. Biomedical MR, FNW, Otto-von-Guericke-University, Magdeburg, Germany

Abstract:

Magnetic resonance imaging of the human body has been widely introduced some 25 years ago and is still one of the fastest developing fields in clinical diagnostic, clinical research, and neuroscientific studies. While 1.5T has been accepted as the best compromise for clinical imaging for many years, the introduction of 3T clinical MRI over the past few years has shown to clearly improve image quality. Currently, 7T whole body MRI systems are being installed in a number of research laboratories. The main driving argument behind the quest for ever higher field strength is the increased signal to noise ration obtainable. In neuroscientific applications the increased BOLD (blood oxygen level dependent) effect that allows the detection of brain activity in another driving force. However, in contrast to MR microscopy or small animal MRI, a number of obstacles have to be overcome in order to make ultra-high field MRI a valuable tool for a wide range of applications. The main limitations are the RF-energy deposited in the subject and the RF-homogeneity across the object. The latter is especially hindering since the extension of the body or head is larger than the wavelength in the body corresponding to the larmor frequency.

With the development of multi-receiver systems and new RF-coils some of these limitations are addressed. For measurements of the human brain new methods have been developed that reduce the RF-power deposited, minimize the sensitivity of the signal and contrast to RF-inhomogeneities and thus allow very high resolution imaging with high signal-to-noise ratio. Currently, applications of ultra-high field MRI are still focused on functional brain imaging in small regions of interest. New developments allow examinations of larger regions of the head and the clinical potential of the methods is being evaluated.

The larger susceptibility induced frequency spread between different tissue types, which has previously been expected to be a major challenge in ultra-high field MRI, has recently been used to generate novel contrast that dramatically exceeds the commonly exploited tissue differences in T1 or T2. This may open up new insights into neuro-anatomical microstructures that were not accessible in the living human brain until now. An example is shown in the Figure.
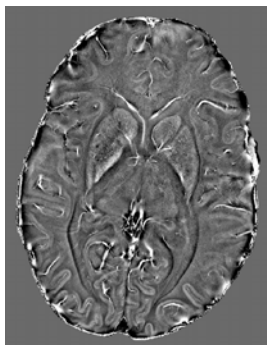
Figure 1: A single slice out of a 3D phase data set covering the human brain. The in-plane resolution is 200*200 µm, the slice thickness 2mm. The image intensity corresponds to the local magnetic field strength as a result of the tissue susceptibility. The image shows strong contrast between gray and white matter and also pronounced structures of fiber bundles within the white matter. This contrast is far stronger than conventionally achievable with gradient echo or spin echo magnitude imaging.

Molecular and cellular MRI

P.M. Jakob

Department of Experimental Physics V & Research Center Magnetic-Resonance Bavaria, University of Würzburg, 97074 Würzburg, Germany

Abstract:

Molecular & Cellular Imaging (MCI) is "the in-vivo characterization and measurement of biological processes at the cellular and molecular level" and aims to image molecular abnormalities associated with diseases and to monitor cell assemblys such as macrophages or stem cells.

MRI (magnetic resonance imaging), PET, and optical imaging are currently the modalities of choice, which can be used for MCI in the living system. Among the different non-invasive modalities, MRI has a number of characteristics that makes it an ideal candidate: (1) an extraordinary 3-dimensional capabilities, (2) a superb spatial and temporal resolution and (3) a high safety profile. In addition, MRI appears very attractive for MCI, since current MRI protocols already provide anatomic, functional and biochemical information in excellent image quality. Combining this high spatial resolution/high contrast imaging modality with specific MR molecular imaging agents for MCI is current focus in many research laboratories, in particular small animal imaging centers, worldwide.

Molecular and cellular MRI, which is principally performed by using (actively or passively) targeted exogeneous MRI-contrast agents, has the potential to undergo a transition from being a basic sciences discipline to one recognized as a important component of future medical practice. However, so far, since MRI compared to other imaging techniques is traditionally a low sensitivity modality (micromolar range!), a major objective of current research is (1) to increase the sensitivity and (2) to detect unambiguously target structures beyond the resolution limit of current MRI techniques. In this context, it is important to remember, that MRI contrast agents (such as coated superparamagnetic iron oxide nanoparticles) are not detected directly, but indirectly, since they only influence the MR signal. This makes a one-to-one identification of labeled structures in many cases difficult, if not impossible. Therefore, new approaches, which allow for a "background-free" identification and imaging of the labeled structures, are currently being developed. In summary, besides the fact that MRI currently has several limitations, a number of applications, such as stem cell imaging, imaging of apoptosis, plaque and other biological targets of interest, can already be envisaged that expand the potential of MRI techniques in the field of MCI.

Non-invasive Assessment of Moisture migration in Food Products by MRI

J. van Duynhoven[1], W. Weglarz[1], C. Windt[2], P. Ramos Cabrer[2], A. Mohoric[2], H. van As[2]

[1] Unilever Food and Health Research Institute, Vlaardingen, The Netherlands
[2] Wageningen University and Research Centre, Wageningen, The Netherlands
[3] University Clinical Hospital, Santiago de Compostela, Spain

Abstract:

For many food products, water is critical for establishing a texture that is well appreciated by consumers. This is not only the case for soft and smooth textures, but also for dry and crisp ones. In order to engineer desired food textures, food technologists attempt to control location and mobility of water within food structures. In order to assess the efficacy of such technologies, there is a need to assess water status in a non-invasive and real-time manner. NMR and MRI have unique advantages in this respect, but in their application to food systems one is challenged with respect to sensitivity, and resolution in terms of time, space and molecular mobility. Conventional spin-echo imaging techniques do not perform adequately, and one has to take recourse to more specific methods.

For applications within the area of food processing, where technologies aim at bringing water into a desired location as fast as possible, one typically needs to focus on time and spatial resolution. Here application of RARE is appropriate. This will be illustrated by monitoring rice kernels during cooking, where the kernels were engineered in such a way that their microstructures facilitated water ingress. In a second example, water ingress in soup inclusions was studied, where microstructures were manipulated in order to impede migration. For both cases it will be shown how the MRI observations could be interpreted using simulations of water migration.

For applications in the area of enhancing shelf life of food products, one aims at maintaining water in a low mobility state within the food matrix. Here one typically needs to address challenges with respect to resolving molecular mobilities. Here SPI methods are called for, and this will be illustrated by shelf life studies on multi-component food systems. In one example, efficacy of moisture barriers in sandwiches was monitored, with relatively high time resolution, at the expense of resolving molecular mobilities. In a second example, moisture migration in so-called Aw matched snack systems was monitored, where resolution in terms of molecular mobility was emphasized. Also in this case we will illustrate how modelling can be used to interpret the MRI observations.

1. W.P. Wêglarz; M. Hemelaar; N. Franciosi; G. van Dalen; H. Blonk; C. Windt; J. van Duynhoven, Food Chemistry, in press.
2. P. Ramos-Cabrer, P, van Duynhoven, JPM, Timmer, H, Nicolay, K, J. Agric Food Chem. (2006) 54(3) 672-677.
3. A. Mohoric, F. Vergeldt, E. Gerkema, A. de Jager, J.P.M. van Duynhoven, G. van Dalen, H. van As, J. Magn. Reson. 171 (2004) 157-162

Encoding information in the CPMG echo shape

M. D. Hürlimann

Schlumberger – Doll Research, Cambridge MA 02139, USA; hurlimann@slb.com

Abstract:

Two-dimensional diffusion and relaxation measurements are well suited for the study of complex systems. This method is particularly powerful in heterogeneous samples such as complex fluids, mixtures, or fluid filled porous media. Such systems are ubiquitous and examples include hydrocarbon bearing geological formations, biological samples such as plants and wood, food products, and construction materials such as concrete. The method has the additional advantage that it does not require high magnetic fields of high homogeneity, but it can be applied in experimental set-ups of low field strength and with 'inside-out' configurations.

The standard implementation is analogous to conventional two-dimensional measurements. The pulse sequence consists of an initial encoding sequence followed by a long CPMG train. In subsequent acquisitions, parameters in the initial encoding sequence are systematically varied to change the sensitivity to the parameter of interest, e.g. diffusion or longitudinal relaxation time. This leads to a characteristic reduction in the echo amplitudes of the CPMG train that is used to extract the diffusion or T_1 information. We discuss here a new approach [1] where the information is encoded in the echo shape, rather than the amplitude, of the CPMG trains. The method uses sequences with initial encoding sequences that generate echoes with contributions from at least two different coherence pathways. These contributions are then refocused many times by a long string of closely spaced identical pulses. The generated echoes quickly assume an asymptotic shape that encodes the information of interest. High signal-to-noise ratios can be achieved by averaging the large number of echoes. We demonstrate this approach with different implementations of the measurements of longitudinal relaxation time, T_1, and diffusion coefficient, D. The method can be used for novel single-shot measurements in inhomogeneous fields.

1. M. D. Hürlimann, *J. Magn. Reson.* **184**, 114-129 (2007).

Fitting Intrinsic Parameters to diffusion-relaxation data

D. van Dusschoten[1] , F. J.Vergeldt[2] and H. Van As[2]

[1] ICG-3, Research Center Jülich, Jülich, Germany
[2] Lab. Biophysics, Wageningen University, Wageningen, the Netherlands

Abstract:

2D NMR experiments in non-spectroscopy mode are beginning to show significant value for investigation of microscopic properties of heterogeneous systems of varying nature. The problem that still needs to be solved is the translation of the data analysis results with respect to important, intrinsic properties, like compartment sizes (a or r) in porous media or membrane permeability (H or P_d) for cells. Currently the usage of 2D Inverse Laplace Transformation (ILT) of diffusion-relaxation experiments has gained in attention significantly. Although the resolution of the fitted parameters appears to increase using this approach, it still does not yield the desired microscopic properties. Here we show that parameters like compartment size and membrane permeability can, in principle, be obtained from this hybrid experiment, using as a starting point a NMR-specific, numerical solution of Fick's second law of diffusion for a 1D multi-compartment system.

First, we generated 2D diffusion-relaxation data by means of a numerical solution for Fick's second law for diffusion in a single compartment with relaxing walls, as described elsewhere [1]. This results in a data surface that is nearly identical to a data surface as calculated by means of an analytical solution for either a T_2 or a diffusion experiment. To this, noise was added. In order to get to the intrinsic parameters we used a 2D fitting routine in IDL that calls the same numerical program that generates the data and incorporated it in a Marquart-Levenberg NLLS fit-routine, starting with guess-parameters that where at least a factor 2 to 10 off. Typically, it took 2 to 3 minutes before a solution was found. At the same time the data surface was fitted with a 2D fitting routine described elsewhere [2] with sufficient fractions for a reasonable fit. This procedure was repeated 5 times while adding different noise (SNR 10.000) to estimate the precision and the repeatability of the fit. Obviously the outcome of the fit procedures is rather different: Whereas a traditional 2D fit yields 3 fractions with 2 T_2's and 3 D's, similar to results obtained by Callaghan [3] using 2D ILT, the intrinsic fit yields P_d or H (m/s) , a or r (m), the intrinsic diffusion constant and the intrinsic relaxation constant, with a precision better than 0.1 % and a standard deviation below that mark. The normal fit routine, like a 2D ILT requires further interpretation with regard to the above intrinsic parameters; a procedure that nessecitates another fit using a root finding routine and is limited to simple cases, Furthermore we have extended our approach to a two compartment system for which the permeability and the compartment sizes could be found with sufficient (< 10 % deviation) precision for several variations of P_d and a, where normal 2D fit yield results that can not be further interpreted quantitatively. Fitting 2D geometries will become available when the efficiency of the computer code is significantly enhanced.

1. E.G. Novikov, D. van Dusschoten and H. Van As, J. Magn. Reson. 135, 522 (1998).
2. D. van Dusschoten, C.T.W. Moone. P.A. de Jager and H. Van As, Magn. Reson. Med. 36, 907 (1996).
3. P.T. Callaghan, S. Godefroy and B.N. Ryland, J. Magn. Reson. 162, 320 (2003).

Seed Detection in Mandarin Oranges Using Multivariate Analysis of MR Image Data

Rebecca Milczarek[1] , Michael McCarthy[1]

[1] Biological and Agricultural Engineering, University of California, Davis, United States of America

Abstract:

The state of California produces 2.5 million tons of fresh-market orange crop per season, accounting for 80% of the supply in the United States [1]. Of this crop, seedless mandarin orange varieties are experiencing an increase in both popularity among consumers and total planted acreage [2]. While mandarin cultivars have been carefully bred to eliminate the seed-producing trait, unintended pollination from other cultivars can result in seeded fruit that is unacceptable to the consumer. Thus, nondestructive detection of seeds during fruit sorting is an important goal for citrus fruit processors. In this study, 140 (109 seeded, 31 unseeded) 'W. Murcott' mandarin oranges (*Citrus reticulata*) were imaged using 3 different MR sequence types: Turbo Fast Low-Angle Shot [Turbo FLASH], Fast Spin Echo [FSE], and Gradient Recalled Echo [GRE]. Imaging was performed on a 1 Tesla industrial-grade ASPECT AI MR system. Shortly after imaging, the presence and count of seeds were verified by a grader through destructive testing. The 3 congruent images of each fruit sample were combined to create a multivariate image data set. A Partial Least Squares [PLS] analysis was performed using the 3-level data set as the "x-block" and a binary mask indicating the positions of the seeds as the "y-block". The resulting model, using 1 latent variable, was applied to the raw data to create a prediction image in which seeds appeared hyperintense and orange pulp appeared hypointense. In this prediction image, the ratio of average seed intensity to average pulp intensity was 2.90. This is a clear improvement in seed/pulp contrast compared to that of the Turbo FLASH (1.40), FSE (1.21), and GRE (1.05) images taken separately. Several technical challenges remain to be addressed in order to automate the imaging and seed detection process, but the multivariate approach shows promise as a method for enhancing image contrast without extensive pulse sequence optimization. Thus, the multivariate analysis of MR image data has been shown to be a feasible approach for quality assurance of citrus fruit.

1. United States Department of Agriculture Economic Research Service, "California's Citrus Industry", (accessed 10 July 2007), http://www.ers.usda.gov/News/CAcitrus.htm
2. California Agricultural Statistics Service, "2004 California Citrus Acreage Report" (accessed 10 July 2007), http://www.calcitrusgrowers.com/200412citac.pdf

Localized ^{1}H NMR and ^{1}H Spectroscopic Imaging on wild type and mutant pea

Gerd Melkus[1], Ljudmilla Borisjuk[2], Hardy Rolletschek[2], Michael Flentje[3], Peter M. Jakob[1]

[1] Department of Physics, EP5 (Biophysics), University of Würzburg, Würzburg, Germany
[2] Institut of Plant Genetics and Crop Plant Research, Gatersleben, Germany
[3] Department of Radiation Oncology, University of Würzburg, Würzburg, Germany

Abstract

Introduction: Plant seeds accumulate storage products like starch, protein and oil. Despite millenarian domestication history, the regulation of storage processes in the seed is less understood. One of the main obstacles is the lack of methods appropriate for measurement and visualization of crop seeds *in vivo*. Here we applied localized ^{1}H NMR Spectroscopy and ^{1}H Spectroscopic Imaging for monitoring of the structural development and storage processes in seeds of pea (*Pisum sativum)*.

Material and Methods: NMR experiments on wild type and mutant pea [1] of different weights (30mg to 280mg) were performed on a Bruker 17.6T widebore spectrometer equipped with a 200mT/m gradient system and a 15mm diameter birdcage resonator. Localized, water suppressed 1D (PRESS [2], TR=15s, TE=20ms, voxel=$(1mm)^3$, NA=32) and 2D (L-COSY [3], TR=2s, TE=20ms, voxel=$(1.5mm)^3$, t1-increment=1024, NA=1) methods were used to identify the different metabolites in the pea endosperm. The local distributions of the metabolites were imaged using a chemical shift imaging sequence (CSI [4], TR=1.5s, TE=2ms, NS=5000, resolution in plane = $200\mu m^2$, slice = $250\mu m$). Different metabolites were quantified using a phantom replacement method [5]. The NMR methods were combined with conventional biochemical methods for analysis of liquid endosperm in developing seeds.

Results and Discussion: Fig. 1 shows a FLASH image of a wild type pea seed. The growing embryo (em) is surrounded by the seed coat (sc, maternal organ) which nurses the embryo until maturation. Metabolite exchange between the two generations occurs via liquid endosperm (le). Endosperm is a key determinant of seed size and quality [6]. In the L-COSY spectrum (Fig. 2) different metabolites are visible. NMR metabolites values were compared with photometric and HPLC measurements (Fig. 3). The high B_0 field allows a good separation of the chemical shift and the localized NMR methods enable the *in vivo* metabolite quantification of the selected region. The derived data are essential for understanding of maternal/filial interactions during seed filling, which actually determines seed yield.
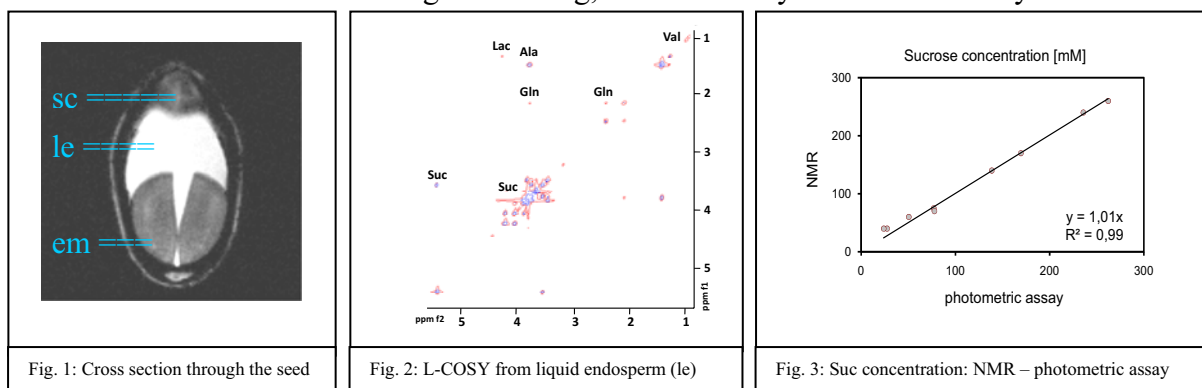
Fig. 1: Cross section through the seed

Fig. 2: L-COSY from liquid endosperm (le)

Fig. 3: Suc concentration: NMR – photometric assay

References: [1] Borisjuk L et al., *Development* **129** (2002)1595-1607. [2] Bottomley PA, U.S. Patent 4,480,228 (1984). [3] Thomas MA et al., *Magn Reson Med* **46** (2001) 58-67. [4] Brown TR et al, Proc Natl Acad Sci USA **79** (1982) 3523-3526. [5] Soher BJ et al, *Magn Reson Med* **35** (1996) 356-363. [6] Alonso-Blanco C et al., *Proc Natl Acad Sci* USA **96** (1999) 4710-4717.

Recent Developments in Imaging Multi-Phase Reactors

Lynn F. Gladden , Laura D. Anadon , Chris P. Dunckley, Daniel J. Holland, Zhenyu Huang, Mick D. Mantle, Christoph Müller, Thoa Nguyen and Andrew J. Sederman

University of Cambridge, Department of Chemical Engineering, Pembroke Street, Cambridge CB2 3RA, U.K.

Abstract:

This presentation will review some of the most recent developments in the application of magnetic resonance imaging (MRI) to the field of reaction engineering. Illustrative examples will include: (i) the implementation of ultra-fast MRI methods to image unsteady-state flows; (ii) *in situ* spatial mapping of chemical species within reactors, and (iii) the direct imaging of solids which allows us to image the distribution and velocity of solids in fluidised-bed reactors. As well as giving immediate insight to how reactors work, MRI provides invaluable data to aid the development and validation of numerical codes to predict the behaviour of these systems.

Imaging unsteady-state flows
A number of MRI techniques can be used to image liquid flows that vary in time. We have used RARE methods extensively to characterise hydrodynamic instabilities in various process engineering environments. Amongst the examples presented will be:

(i) 3D RARE has provided experimental data which clearly identifies the mechanism of the hydrodynamic transition from trickle to pulsing flow in fixed-bed reactors.
(ii) Application of RARE to measure the velocities of liquid pulses in fixed-bed reactors.
(iii) Demonstration of how RARE can be used to provide new insights into how reactors might be operated in the unsteady–state as opposed to steady state, to obtain enhanced catalytic conversion.

Chemical mapping inside catalytic reactors
Previously we have shown that ^{13}C DEPT MRI can be used to map conversion within a heterogenous catalytic reactor [1]. This work has now been extended to provide quantitative maps of local rate and selectivity of chemical reactions occurring inside reactors. Deactivation of the catalyst can also be studied *in situ*.

Imaging granular flows
Granular flows are of widespread interest to physicists and engineers. In chemical engineering, an area of particular interest is in gas-fluidised beds. This presentation will give a brief overview of some of our initial work in this field, focussing on how direct imaging of solids' motion enables us to study these 3D optically opaque systems at high spatial resolution for the first time. Data are acquired sufficiently fast that movment of individual gas bubbles within the reactor can be imaged.

1. A.J. Sederman et al., Catal. Letters. **103** (2005) 1-8.

MRI in Chemical Engineering – facts and promises

Siegfried Stapf

Dept. Technical Physics II, TU Ilmenau, 98684 Ilmenau, Germany

The potential use of NMR microscopy in a technical and industrial environment mostly relies on three powerful items out of the NMR toolbox: the determination of material properties from a range of specifically available parameters; the non-invasive quantification and visualization of transport phenomena; and the exploitation of the spectroscopic selectivity for control of multicomponent systems with and without reactions. In recent years, the first two of these fields have reached rather mature states while the third one is currently at a point where obstacles such as inhomogeneous fields and low signal intensities are being overcome.
This contribution attempts to give an overview of the status quo of NMR in Chemical Engineering, summarizing dedicated studies out of recent literature, and demonstrating the feasibility of performing investigations into transport and reaction processes with commercial as well as purpose-built technology. A focus of these studies is on the observation of processes in technically relevant systems, ranging from down-sized and simplified set-ups to real online measurements of transport and/or reaction in actual reactors. The future and commercial success of MRI will be discussed in the light of time- and cost-efficiency of performance control of realistic reactor and production conditions.

Probing and Controlling Chemical Waves Using Magnetic Resonance Imaging

Melanie M. Britton[1]

[1] School of Chemistry, University of Birmingham, Birmingham, B15 2TT, UK

Abstract:

Magnetic Resonance Imaging is a powerful tool, able to probe complex chemical systems and is even able to 'visualise' chemistry directly [1]. In addition to this, MRI is also providing some exciting new methods for controlling chemistry [2]. The chemical systems studied in the group are ones which form waves and patterns. Travelling waves can form in chemical reactions where autocatalysis couples with diffusion [3]. Initiation of the wave is performed through addition of an autocatalyst to a localised region. Concentration of this species increases rapidly and a wave is then propagated as the autocatalyst diffusions into neighbouring regions. There are a number of chemical reactions that can form waves and they are increasingly used as models for studying wave formation in biological systems.

Visualisation of chemical waves is possible using MRI in reactions where there is a transition between oxidative states of a transition metal ion [4]. Protons in water molecules surrounding these ions are sensitive to the oxidative state of the transition metal and there is a reduction in the T_1 and T_2 relaxation times, particularly for molecules surrounding paramagnetic ions [5]. This difference in relaxation time produces the image contrast necessary to observe the wave, but it also enables the concentration of these species [1] to be directly measured and hence enable reaction mechanisms to be probed. An area of increasing interest is in the control of chemical wave formation using flow. Greater understanding into how flow couples with non-linear reactions is possible through MRI measurements of flow and diffusion [6].

In addition to MRI's ability to visualise flow and chemistry, it is also providing new means of controlling chemistry, by applying precise, controlled magnetic field gradients across heterogeneous chemical systems. The $Co(II)EDTA^{2-}$-hydrogen peroxide reaction [7] produces heterogeneity through a travelling front. This front can easily be visualised using MRI, because paramagnetic Co(II) ions are converted to diamagnetic Co(III) ions, producing excellent image contrast. Interestingly, this change in magnetic susceptibility also produces heterogeneous magnetic susceptibility within the sample. The heterogeneity of concentration and susceptibility allows this chemical wave to be manipulated by the application of magnetic field gradients. Using the magnetic field gradients of the MR imager it was possible to control the velocity and direction of the propagating wave [2].

1. M. M. Britton, *J. Phys. Chem. A* **110** (2006) 2579-82.
2. R. Evans, C. R. Timmel, P. J. Hore, M. M. Britton, *J. Am. Chem. Soc.* **128** (2006) 7309-14.
3. I. R. Epstein, J. A. Pojman: An Introduction to Nonlinear Chemical Dynamics, OUP, Oxford, 1998.
4. M. M. Britton, *J. Phys. Chem. A* **107** (2003) 5033-41.
5. M. M. Britton, *J. Phys. Chem. A* **110** (2006) 13209-14.
6. M. M. Britton, A. J. Sederman, A. Taylor, S. K. Scott, L. F. Gladden, *J. Phys. Chem. A* **109** (2005) 8306-13.
7. R. Evans, C. R. Timmel, P. J. Hore, M. M. Britton, *Chem. Phys. Lett.* **397** (2004) 67-72.

Granular micro-dynamics by CPMG spin echo

Janez Stepišnik[1] , Samo Lasič[,1] , Aleš Mohorič[,1], Igor Serša[2], and Gorazd Planinšič[1]

[1] University of Ljubljana, Ljubljana, Slovenia
[2] J. Stefan Institute, Ljubljana, Slovenia

Abstract:

NMR technique of modulated gradient spin echo (MGSE) enables the direct measurement of the velocity autocorrelation function[1] (VCF), which is a fundamental quantity relating the dynamical processes on the microscopic level to the macroscopic transport properties of system. CPMG train of π–rf pulses applied to spins in the steady magnetic field gradient is a variant of MGSE sequence, if all coherent pathways[2], but the direct one, are filtered out from the signal[3]. By changing the period of applied π-rf pulses, the novel method can modulate spin dephasing to the frequencies above 10 kHz and thus enables the measurement of motion spectrum in the frequency range that is approaching the low frequency limit of the another method for the direct measurement of VCF, i.e. the inelastic neutron scattering.

Measurement of grain motion in the system of air-fluidized oil-filled spheres and mustard seeds at different degrees of fluidization and filling fractions shows that the frequency range of the method is wide enough to scan the entire dynamic range of grain fluctuations. It provides VCF that differs from the exponential Enskog decay that is commonly anticipated for granular dynamics. The obtained spectra confirm the model of grain caging at collisions with adjacent beads and give a cognition that the grain autocorrelation memory decay τ_c is an event driven by inelastic collision. The result of NMR measurements is the VCF spectrum in the form[4] $D(\omega) = \dfrac{D + \omega^2 \left\langle \xi^2 \right\rangle \tau_c}{\omega^2} e^{-\tau_c \omega}$ where $<\xi^2>$is the squared free path between collisions and D is the cage-breaking rate or the diffusion-like constant.
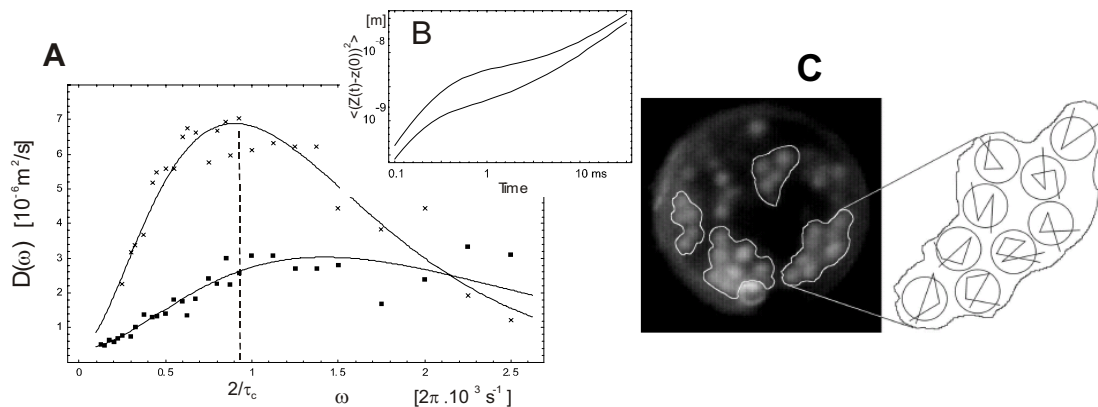
Fig. 1: A) VCF spectra of fluidized granular systems at different degrees of fluidization, B) the relating grain mean-squared grain displacement and C) the visual inspection of grain motional caging by using high-speed video recording.

1.   P.T. Callaghan and J. Stepišnik, J. of Mag. Res. **A 117**, (1995), 118-122
2.   M.D. Hurlimman, J. of Mag. Res. **148**, (2001), 367-378
3.   J. Stepišnik, S. Lasič, A. Mohorič, I. Serša and A. Sepe, J. of Mag. Res.., **182**, (2006), 195-199
4.   S. Lasič, J. Stepišnik, A. Mohorič, I. Serša and G. Planinšič, Europhys. Lett. **75**, (2006), 887–893

Dynamics of gas and liquid during cavitation

Igor Mastikhin and Benedict Newling

MRI Centre, Physics Department, University of New Brunswick, Fredericton, Canada.

Gaseous cavitation in water begins via formation of gaseous bubbles in the body of liquid from the previously dissolved gas due to an external pressure drop. Activity of cavitation depends on presence of nucleation sites which are thought to be mostly particles of dust, irregularities of surfaces and stabilized micro/nanobubbles [1,2].

Commonly employed optical and acoustical methods are not suited well to obtain quantitative information of gas behaviour, and they fail to answer such questions as: what fraction of gas participates in cavitation, how long gas molecules reside inside the bubbles, and what is the nature of the nucleation sites. Engaging NMR relaxation paramaters as a "spin memory" can help to get integral information of fluid dynamics during cavitation [3].

In this work, we performed comparative studies of both liquid and gaseous fractions of cavitating fluid. Tap, 0.2μm-filtered tap and distilled/deionized water samples were saturated with highly soluble gas chlorodifluoromethane (Freon-22) which F-19 NMR relaxation parameters depend dramatically on its state and pressure: T1 changes from 2 ms for the gaseous state in to 3.5 s for the dissolved state at 2.35 T and 1Atm. These two states have also different chemical shifts, permitting a control of potential degassing. PFG SE sequence with 1D-resolution along the acoustical axis of the sample was performed before, during, and after acoustic cavitation at 19.7 kHz, with 7 min per measurement. Measurements of both gas and liquid were done with the same diffusion gradients and delays to compare their dynamic behaviour. Diffusive delays of 28, 48, and 88 ms were chosen. Experiments were usually repeated with delays from 2 min to 1 hour.

We found that gas dynamics strongly depended on the state of water. In water samples with high concentration of nucleation sites, gas mobility resembled that of water, and amount of gas participating in motion was low, indicating a high localization of bubbles within cavitation cloud and an expected depletion of near-bubble layers of water. However, in filtered water, the gas mobility suddenly increased, with almost no stationary dissolved gas during the diffusion evolution time. At the same time, neither NMR signal amplitude nor NMR relaxation of gas changed substantially during cavitation, so only a very small fraction of cavitating bubbles underwent violent collapses that could destroy or affect the NMR magnetization. Repetition of experiments with filtered water showed a dependence of delays between cavitation periods for the filtered water samples which can be interpreted as an increase in number of nucleation sites thanks to stabilized micro/nanobubbles from previous series.

1. Vuong VQ, Szeri AJ Sonoluminescence and diffusive transport PHYSICS OF FLUIDS 8 (9): 2354-2364 SEP 1996.
2. Louisnard O, Gomez F. Growth by rectified diffusion of strongly acoustically forced gas bubbles in nearly saturated liquids PHYSICAL REVIEW E 67 (3): Art. No. 036610 Part 2 MAR 2003
3. Mastikhin IV, Newling B. MRI measurements of an acoustically cavitated fluid in a standing wave. PHYSICAL REVIEW E 72 (5): Art. No. 056310 Part 2 NOV 2005

Observation of parahydrogen induced polarization in heterogeneous hydrogenation reaction and its MRT application

K.V. Kovtunov[1], M.S. Anwar[2], S.R. Burt[2], I.V. Koptyug[1],
L.-S. Bouchard[2], R.Z. Sagdeev[1], A. Pines[2]

[1] International Tomography Center, Novosibirsk, Russia
[2] Materials Sciences Division, Lawrence Berkeley National Laboratory College of Chemistry, University of California, Berkeley, USA

Abstract:

NMR is a superior tool for investigations of catalytic reactions, because the chemical shift, coupling constant, and relaxation time yield useful information about chemical structures, as well as mechanisms of the reaction. However, the macroscopic magnetization generated by the nuclear spins at thermal equilibrium in magnetic field of a typical NMR spectrometer is only about 10^{-5} of what it could be if all spins were aligned in parallel. It is well know that correlation of nuclear spins of parahydrogen can be utilized for MNR signal enhancement via homogeneous hydrogenation of an appropriate substrate. Unfortunately, the fact that homogeneous catalyst is present in the reaction mixture along with products can be main disadvantage for much wider use of the homogeneous catalysts. One of the effective routes to solve this problem is immobilization of homogeneous (Wilkinson, etc) catalysts on solid supports.

We demonstrate, for the first time, parahydrogen induced polarization in heterogeneous hydrogenation reactions. Using Wilkinson's catalyst, supported on either silica gel or a polymer, we hydrogenate styrene in solution with para-H_2 and produce polarized ethylbenzene. We use three Rh catalysts, supported on silica gel, to hydrogenate propylene gas with para-H_2. In all cases, both PASADENA and ALTADENA are demonstrated. These experiments serve as a direct verification of the mechanism of heterogeneous hydrogenation reactions involving immobilized metal complexes. The clear PASADENA and ALTADENA spectral patterns confirm the preservation of the longitudinal spin order between the protons derived from the same para-hydrogen molecule, proving that the addition is, indeed, pairwise. Moreover, the immobilized complex will produce polarization in the gas phase due to the mechanism of the chemical reaction remains essentially the same as in homogeneous solution. Hence, supported metal complex can be successfully applied to produce catalyst-free fluids with highly polarized nuclear spins for a broad range of hyperpolarized NMR and MRI applications.

Gas-phase MRI of void spaces suffers from the problem of low sensitivity. This has led to the use of expensive hyperpolarized gases such as ^{129}Xe, ^{3}He and, more recently, ^{83}Kr. Other approaches have used fast-relaxing inert fluorinated gases or higher gas pressures. We present the first magnetic resonance images of hyperpolarized gas using parahydrogen. The propylene and p-H_2 mixture flows through a reactor cell which contains a supported catalyst. Enhancement factors on the order of ~300 were observed with unoptimized parameters.

Contrast and Sensitivity Enhanced Magnetic Resonance by Dynamic Nuclear Polarization

Songi Han, Evan McCarney, Brandon Armstrong, Mark Lingwood

Department of Chemistry and Biochemistry, University of California Santa Barbara, CA, USA

We present new applications for NMR and MRI analysis enabled by signal enhancement through dynamic nuclear polarization (DNP) [1-3]. We employ the Overhauser mechanism at 0.35 Tesla and under ambient condition to directly and instantaneously achieve enhanced ^1H polarization of water that corresponds to thermal polarization at 45 Tesla field [1,4,5]. Maximum signal enhancement is achieved using our home-built DNP setup that shows optimum performance and is also fully portable [5]. An improved theoretical model quantifies and predicts the maximum possible Overhauser enhancement at 0.35 Tesla when utilizing stable nitroxide radicals as the electron spin polarization source [4]. We introduce two applications enabled through the production of highly polarized water which polarization builds up instantaneously within the relevant time scale, and with any residual radicals contained, if needed: (1) the use of hyperpolarized water in continuous flow as a tracer-free and physiologically applicable MRI contrast agent to monitor blood perfusion [1], and (2) to employ the amplitude of ^1H water enhancement as a unique probe to monitor water exclusion—a key phenomena in numerous biological processes, e.g. the aggregation of the *tau* protein that is closely related to neurodegenerative brain diseases [2].

[1] E. R. McCarney, B. L. Armstrong, M. D. Lingwood, S. Han , "Hyperpolarized water as an authentic magnetic resonance imaging contrast agent", *Proc. Nat. Acad. Sci. USA.* **104 (6)** 1754-1759 (2007).
[2] E. R. McCarney, S. Han, "A unique tool for detecting local water in bulk water: water content and mobility inside self assembled micelle-vesicle systems", *Proc. Nat. Acad. Sci. USA*, submitted.
[3] E. R. McCarney, S. Han, "A polarization matrix for the production of radical-free, dynamic nuclear polarization enhanced molecules for NMR spectroscopy and imaging", submitted.
[4] B. L. Armstrong, S. Han, "A New Model for Overhauser Enhanced Nuclear Magnetic Resonance Using Nitroxide Radicals", *J. Chem. Phys.*, in press (2007).
[5] B. D. Armstrong, M. D. Lingwood, E. R. McCarney, E. Brown, S. Han, "Portable X-Band DNP Device to achieve >45 T 1H Polarization in Solution State", *J. Magn. Reson.*, submitted.

Improving ^{3}He polarization for human lung imaging in subjects in horizontal and vertical orientations

Ross W. Mair[1], Leo L. Tsai[1,2], R. Scheidegger[1,3], Chih-Hao Li[1,4], Michael J. Barlow[5], Matthew S. Rosen[1,4], Samuel Patz[2,5] and Ronald L. Walsworth[1,4]

[1] Harvard-Smithsonian Center for Astrophysics, Cambridge, MA, USA.
[2] Harvard Medical School, Boston, MA, USA.
[3] Harvard-MIT Division of Health Sciences and Technology, Cambridge, MA, USA.
[4] Department of Physics, Harvard University, Cambridge, MA, USA.
[5] Sir Peter Mansfield Magnetic Resonance Centre, University of Nottingham. Nottingham. UK.
[6] Department of Radiology, Brigham and Women's Hospital, Boston, MA, USA.

Abstract:

In NMR experiments with hyperpolarized noble gases, signal-to-noise is generally limited by either low polarization or slow production rates. We have modified our system used for producing spin-polarized ^{3}He gas by incorporating Volume Holographic Grating (VHG)-line-narrowed lasers and multiple storage cells.

Although the Laser Diode Arrays typically used in ^{3}He optical-pumping may be rated at 60 W or higher, their optical spectra are broad. The desired wavelength of 794.7 nm appears as a broad peak of ~ 3 nm width, resulting in relatively little of the laser power being resonant for the Rb transition in spin exchange. The recent development of VHG's [1] that can be incorporated directly with Laser Diode bars result in a ~ 0.3 nm resonant line without additional hardware. We have incorporated such a laser into our ^{3}He polarization apparatus, resulting in ~ 50% improvements in production rate, similar to results observed by others [2]. The faster production rate, combined with storage cells with long polarization lifetimes, allow the production of multiple batches of polarized ^{3}He for use in a single imaging session.

The ^{3}He is inhaled by subjects sitting or lying in a novel, open-access MRI system that operates at $B_0 = 6.5$ mT. This scanner, combined with highly polarized ^{3}He, allows us to study lung function at variable postures or orientations. This is a novel and important tool for pulmonary physiology, and one not provided by any common radiological imaging modality. Using this system, we have we have, for the first time, imaged the regional partial pressure of O_2 in the human lung with a subject in the vertical position [3]. Such experiments will provide vital insights into the variations in pulmonary perfusion and ventilation [4].
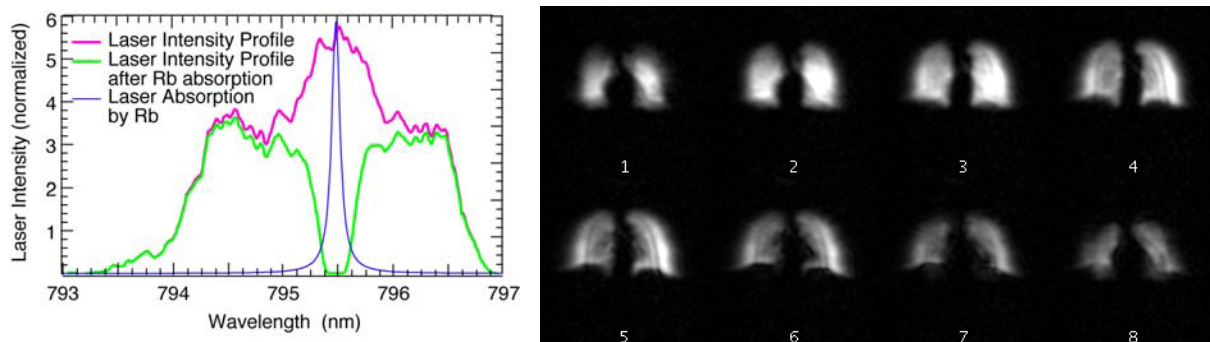
Fig. 1: Laser line-shape from a typical laser diode array, before and after transmission through a standard optical pumping cell used for ^{3}He polarization. Right: ~ 1.5 cm thick horizontal slices from a 3D image of human lungs obtained using the open-access human MRI system while the subject is supine. Slices are plotted from the subject's back to their front.

1.   F. Havermeyer, W. Liu, C. Moser et al., *Opt. Eng.*, **43** (2004), 2017-2021.
2.   B. Chann, E. Babcock, L. W. Anderson, T. G. Walker et al., *J. App. Phys.,* **94** (2003) 6908-6914.
3.   L. L. Tsai, R. W. Mair, M. S. Rosen et al., *Proc 15th ISMRM, Berlin, Germany*, **15** (2007) 943.
4.   J. B. West, C. T. Dollery and A. Naimark, *J. Appl. Physiol.,* **19** (1964) 713-724.
5.   R. W. Glenny, W. J. Lamm, R. K. Albert and H. T. Robertson, *J. Appl. Physiol.*, **71** (1991) 620-629.

Bridging the gap between NMR Imaging and Catalysis

Igor V. Koptyug, Anna A. Lysova, Kirill V. Kovtunov,
Vladimir V. Zhivonitko and Alexey V. Khomichev

International Tomography Center, Novosibirsk, Russia

NMR imaging (MRI) holds a significant promise for catalytic research, but the bridge between MRI and catalysis is still under construction. Despite that, a number of interesting applications have been developed. Dynamic visualization of the transport of diamagnetic as well as paramagnetic compounds in porous catalyst supports was performed upon the preparation of hydrodesulfurization catalysts by solution impregnation. The character of mass transport in a reactor can change dramatically under reactive conditions, making the studies of operating catalytic reactors imperative. We have performed dynamic MRI studies of catalytic hydrogenation of α-methylstyrene or 1-octene in a packed bed reactor with continuous or modulated reactant feed. One of the issues of paramount importance in exothermic processes such as hydrogenation is that of heat transport. Based on the direct imaging of the solid phase (^{27}Al MRI of the Pd/Al$_2$O$_3$ catalyst bed), we are developing the approach for the spatially resolved NMR thermometry of operating catalytic reactors. A pronounced temperature dependence of the ^{27}Al NMR signal was used to reveal the variations of the temperature along the catalyst bed in the course of hydrogenation of propylene into propane. While homogeneous systems are not generally suitable for MRI studies, there are essential exceptions, including propagation of chemical waves in autocatalytic homogeneous reactions. We have employed both conventional MRI and spatially resolved NMR thermometry of aqueous solutions to investigate the effect of liquid flow and convection on the propagation of chemical waves in a number of such reactions.

Catalytic research can thus benefit greatly from the utilization of the MRI technique, but in fact the benefits can be mutual. Indeed, it has been demonstrated [1] that homogeneous catalytic hydrogenation of unsaturated compounds with parahydrogen can be utilized to enhance sensitivity and contrast in MRI by several orders of magnitude. However, having the catalyst as a separate (solid) phase could greatly facilitate catalyst removal from the polarized fluid. At the same time, observation of PHIP in heterogeneous hydrogenations is often considered to be impossible. Indeed, the dissociative chemisorption of H$_2$ on metal particles and migration of H atoms on the surface of the catalyst (e.g., Pd/Al$_2$O$_3$) destroys the initial correlation of the nuclear spins of the parahydrogen (or orthohydrogen) molecule. One of the ways to achieve PHIP in heterogeneous hydrogenation reactions is to immobilize conventional homogeneous catalysts on a suitable solid support [2,3]. Such heterogenized catalysts combine the reaction mechanism of the homogeneous catalysts with the ease of separation of the heterogeneous catalysts. Our recent studies have demonstrated, however, that observation of PHIP in heterogeneous hydrogenation reactions is not limited to the processes involving heterogenized metal complexes but is feasible with other types of heterogeneous catalysts as well.

1. K. Golman, O. Axelsson, H. Johannesson, S. Mansson, C. Olofsson, J.S. Petersson, *Magn. Reson. Med.* **46** (2001) 1-5.
2. I.V. Koptyug, K.V. Kovtunov, S.R. Burt, M.S. Anwar, C. Hilty, S. Han, A. Pines, R.Z. Sagdeev, *J. Amer. Chem. Soc.* **129** (2007) 5580-5586.
3. L.-S. Bouchard, K.V. Kovtunov, S.R. Burt, M.S. Anwar, I.V. Koptyug, R.Z. Sagdeev, A. Pines, *Angew. Chem. Int. Ed.* **46** (2007) 4064-4068.

Study of diffusion coefficient of hyperpolarized gases and their use as a contrast agent in MRI

Luis Agulles Pedrós[b], Rodolfo H. Acosta[a], Peter Blümler[b,c],
Jörg Schmiedeskamp[b], Hans Wolfgang Spiess[b]

a. Universidad Nacional de Córdoba, Ciudad Universitaria X5016LAE, Córdoba, Argentina.
b. Max Planck Institute for Polymer Research, Ackermannweg 10, 55128 Mainz, Germany
c. Forschungszentrum Jülich GmbH,   52425 Jülich, Germany

The use of MRI as diagnostic tool is increasingly employing functional contrast agents to study or contrast entire mechanisms. Contrast agents in MRI can be classified in two categories. One type of contrast agents alters the NMR signal of the protons in its surrounding, e.g. lowers the T1 relaxation time. The other type enhances the NMR signal of specific nuclei. For hyperpolarized gases the NMR signal is improved several orders of magnitude. The most interesting question in spatially resolved experiments is of course the achievable resolution and contrast by controlling the diffusivity of the gas. However, gases have a high diffusivity which strongly influences the NMR signal strength, hence the resolution and appearance of the images.

The influence of such diffusive processes scales with the diffusion coefficient, the strength of the magnetic field gradients and timing used in the experiment. Diffusion may not only limit the MRI resolution, but also distort the line shape of MR images for samples, which contain boundaries or diffusion barriers within the sampled space [1,2].

In addition, due to the large polarization in gaseous ^{3}He and ^{129}Xe, spin diffusion (different from particle diffusion) could play a role in MRI experiments. It is demonstrated that for low temperatures some corrections to the NMR measured diffusion coefficient have to be done, which depend on quantum exchange effects for indistinguishable particles [3]. Physically, if these effects can not change spin current, they can do it indirectly by modifying the velocity distribution of spin up or down atoms separately, so that the subsequent collisions between atoms with opposite spins can eventually be affected

A detailed study of the hyperpolarized gas diffusion coefficient is presented, demonstrating the no influence of spin diffusion (different from particle diffusion) in MRI. A novel procedure is proposed to control the diffusion coefficient of gases in MRI by admixture of inert buffer gases and results agree with theoretical simulations. The molecular mass and concentration enter as additional parameters into the equations that describe structural contrast. This allows for setting a structural threshold up to which structures contribute to the image. For MRI of the lung this enables images of very small structural elements (alveoli) only, or in the other extreme, all airways can be displayed with minimal signal loss due to diffusion.

[1] B.Saam, N.Drukker, W.Happer, *Chem. Phys. Lett.,* (1996). 263, 481-487
[2] T.M. de Swiet , *J. Magn. Reson. B*, (1995).109, 12-18
[3] V.J.Emery "Spin Diffusion in Gases at Low Temperatures" Physical Review
    133:3A A661-A664 (1963)

SQUID-detected NMR and MRI in Microtesla Fields

John Clarke[1]

[1]Department of Physics, University of California, Berkeley CA 94720 USA
and
Materials Sciences Division, Lawrence Berkeley National Laboratory, Berkeley CA 94720 USA

Abstract:

The principles of the Superconducting QUantum Interference Device (SQUID) are briefly reviewed. We describe the use of a SQUID, coupled to an untuned gradiometer, to detect nuclear magnetic resonance (NMR) and magnetic resonance imaging (MRI) in microtesla magnetic fields. The nuclei are prepolarized in a much higher magnetic field, and the oscillating signal produced by the precessing spins is detected after the polarizing field is removed. This technique enables us to perform NMR spectroscopy of protons in liquids with a high signal-to-noise ratio and a 1-Hz spectral resolution at frequencies as low as 80 Hz. We have constructed an MRI system that operates at 5.6 kHz, corresponding to a magnetic field of 132 μT. The magnetic field noise, referred to the lowest loop of the second-derivative gradiometer coupled to the SQUID, is about 0.8 fT Hz$^{-1/2}$ at the imaging frequency. We have imaged phantoms containing water with an in-plane resolution of better than 1 mm, and acquired three-dimensional *in vivo* images of a human forearm with an in-plane resolution of about 2 mm. The low magnetic field implies that magnetic susceptibility variations within the sample are much less important than in conventional high-field MRI, enabling us to obtain distortion-free images in the presence of metals. We have measured the longitudinal relaxation time T_1 of different concentrations of agarose gel in water, and find much greater T_1-contrast in low fields (below 1 mT) than in high fields. This enhanced contrast has potential medical applications, for example imaging tumors. In preliminary experiments we have measured T_1 in specimens of normal and cancerous prostate tissue removed surgically. The measured values of T_1 in normal tissue are typically 60% higher than in tumors; by comparison, there is no significant difference in high-field MRI. These results suggest that low-field MRI may well find an application in medical diagnosis.

Laser-detected Magnetic Resonance Imaging in the Earth's field

Shoujun Xu[1], Charles Crawford[2], David Michalak[2], Dmitry Budker[3], and Alexander Pines[2]

[1]Department of Chemistry, University of Houston, Houston, TX 77204
[2]Materials Sciences Division, Lawrence Berkeley National Laboratory, Berkeley, CA 94720
[3]Department of Physics, University of California, Berkeley, CA 94720

Magnetic resonance imaging (MRI) is usually performed in a strong magnetic field with Faraday induction detection. However the cost and immobility of the system impose restrictions on its applications. We present a novel laser-detection technique using atomic magnetometers for MRI. This technique possesses a high sensitivity that is independent on the strength of the encoding magnetic field, allowing MRI to be conveniently performed in the Earth's magnetic field. It also operates at virtually room temperature, eliminating the necessity of cryogenics.

The characteristics of our recently-constructed atomic magnetometer and its applications for MRI in the Earth's magnetic field are exhibited. Various flow images are obtained, with spatial resolution reaching sub-millimeter regime. Additional applications and future developments are discussed.

Multi-channel MRI at ultra-low fields compatible with MEG

Andrei N. Matlashov, Vadim S. Zotev, Petr L. Volegov, Michelle A. Espy, John C. Mosher, and Robert H. Kraus, Jr.

Los Alamos National Laboratory, Group of Applied Modern Physics, Los Alamos, NM, USA

Magnetic resonance imaging at ultra-low fields (ULF MRI) is a new imaging method that uses SQUID (superconducting quantum interference device) sensors to measure the spatially encoded precession of pre-polarized nuclear spin populations at a microtesla-range measurement field. ULF MRI has two important advantages over conventional high-field MRI. First, it greatly simplifies coil design and makes it possible to construct portable low-cost imaging systems. Second, it can be naturally combined with SQUID-based multi-channel techniques for biomagnetic measurements such as magnetoencephalography (MEG). This allows development of new instruments for multi-modal imaging, such as next-generation MEG systems with ULF MRI capability. Here, the latest results of our work on multi-channel ULF MRI are presented. Design and performance of our seven-channel SQUID system for simultaneous 3D ULF MRI and MEG are described. The system consists of seven axial second-order SQUID gradiometers, with 37 mm diameter and 60 mm baseline, characterized by magnetic field resolutions of 1.2 – 2.8 fT/rtHz. It also includes five sets of coils for 3D Fourier imaging with pre-polarization. The system's ULF MRI performance is demonstrated by multi-channel 3D images of a human hand and a preserved sheep brain acquired at 46 microtesla measurement field with pre-polarization at 40 mT. Imaging resolution is 3 mm × 3 mm × 6 mm for the human hand and 2.5 mm × 2.5 mm × 5 mm for the sheep brain. Benefits on multi-channel imaging such as increased FOV and improved SNR are illustrated. Imaging acceleration by using the sensor array is demonstrated at ULF for the first time. Multi-channel images of a large 2D water phantom are acquired with different degrees of undersampling, and 1D SENSE (Sensitivity Encoding) method is used to reconstruct correct full-FOV images. It is shown that our seven-channel system allows true 3-fold imaging acceleration in comparison to single-shot fully-encoded Fourier imaging. Auditory MEG experiments with the same system are also described. Our results demonstrate that ULF MRI can potentially be as efficient as high-field MRI, and should be very useful in practice, particularly in combination with MEG.

Long living spin states in the Earth's magnetic field

Stephan Appelt[1], F. Wolfgang Häsing[1], Holger Kühn[1], Ulrich Sieling[1] and Bernhard Blümich[2]

[1] Zentralinstitut für Elektronik, Forschungszentrum Jülich, Jülich, Germany
[2] Institut für Technische und Makromolekulare Chemie, RWTH Aachen, Aachen, Germany

Abstract:
We present a new way of J-coupled NMR spectroscopy in low magnetic fields. The network of all homo- and hetero-nuclear *J*-coupling constants can be measured in the Earth's magnetic field, thus revealing the whole molecular structure even in the absence of any chemical shift information. The line widths of the different NMR lines inside one multiplet are measured to be substantially different and depend on the total spin state of the molecule. Narrow lines are associated to singlet states, which are formed automatically in the Earth's field.

The Antarctic experience with Earth field NMR

Paul Callaghan[1], Robin Dykstra[1], Craig Eccles[1], Mark Hunter[1],
Ocean Mercier[2] and Joe Seymour[3]

[1] MacDiarmid Institute for Advanced Materials and Nanotechnology, School of Chemical and Physical Sciences, Victoria University of Wellington, New Zealand
[2] School of Māori Studies, Kelburn Campus, Victoria University of Wellington, New Zealand
[3] Department of Chemical and Biological Engineerng, Montana State University, Bozeman, USA

For several years (1994, 1995, 1997, 1999, 2002 and 2006) a New Zealand team from Victoria University of Wellington and Massey University, joined on occasions by Joe Seymour from the US, has been travelling to the Antarctic as part of the New Zealand Sea-Ice project. We have spent periods of up to three weeks in the McMurdo Sound Delbridge Islands area near Mt Erebus, "camping" on the 2 m thick sea ice, and taking NMR measurements of brine content and mobility with home-made Earth field NMR apparatus. Our work was a component of a larger project aimed at understanding sea ice from the micron scale to the 100's of kilometre scale, the motivation being the crucial role that Antarctic sea ice plays in global climate models. The surprising outcome of these Antarctic forays was never quite anticipated. That human story, with its strange entrepreneurial twist, is the subject of this talk.

POSTER ABSTRACTS

Posters sorted by number and topic

Nr.	Presenter	Title
1	Behr, V.	Mapping the flux density of a coil with an optical detector
2	Ciarrocchi, M.	Design of an Elliptical Permanent Magnet for Surface MRI
3	Gädke, A.	Open source NMR spectrometer control software DAMARIS – a common basis for home-built NMR systems?
4	Glückler, H	How to produce small gradient coils
5	Glückler, H.	Design of a MRT spectrometer for investigations on trees
6	Halse, M.	NMR-MOLE: Field stabilisation, shimming and improvement of spectral resolution
7	Handa, S.	Development of planar gradient coils for a whole hand MRI system
8	Köllisch, U.	Design of a double-resonant ^{19}F-^{1}H resonator for in vivo MRI detection of amyloid plaques at 17.6T
9	Kusima, S.	B_1 concentration by surface resonator for MR microimaging on a clinical system
10	Lopez, M.	Four-Channel Mouse Volume Array at 7 Tesla
11	Manz, B.	A Simple, Small and Low Cost Permanent Magnet Design to Produce Homogeneous Magnetic Fields
12	Marble, A.	Surface coils for unilateral NMR
13	Marble, A.	Unilateral NMR with homogeneous magnetic fields
14	Mauler, J.	Soil Moisture Measurements with a Mobile NMR Sensor
15	Neuberger, T.	High field magnetic resonance microimaging using ceramic dielectric resonators
16	Ozeki, T.	Development of a compact MRI system in –5 °C cold room for visualization of sea-spray icing
17	Rommel, E.	Battery operated pocket-size nmr imaging machine
18	Sell, J.	Plug-and-Play Preamplifier for Mobile MR
19	Tymofiyeva, O.	Intraoral Receiver Coil for Dental Impression using MRI
20	Zhang, Z.	Zero Mode TEM Parallel Plate for High Resolution Thin Film Depth Magnetic Resonance Imaging
21	Qiu, L.	Earth's Magnetic Field NMR Using a SQUID Sensor
22	Amar, A.	Velocity maps measured in a single-shot using multi.echoes independently encoded
23	Bühler, J	Combined Image Processing Tools for MRI- and PET-data
24	Basser, P.	Rheo-NMR micro-imaging in natural coordinates
25	Basser, P.	On the Observation of (Remote) Anisotropy due to Macroscopic Restrictions
26	Böhme, U.	Charge determination by electrophoresis NMR
27	Chandrasekera, T.	Towards the Design of PFG-NMR Experiments for Emulsion Droplet Sizing
28	Ferrante, G.	Measurement of the spin-spin relaxation time T_2 at very low magnetic field by means of the Fast Field Cycling NMR method
29	Franchi, D.	Design of an acquisition-reconstruction algorithm for Magnetic Resonance surface Imaging
30	Gädke, A.	Inverse DESIRE: enhanced apparent longitudinal relaxation in thin excited slices
31	Franck, J	Ex Situ Pulse Design and Implementation
32	Golzi, P.	NMR Data Accumulation in Polar Coordinates Numerical Methods to minimize Systematic Errors
33	Balcom, B.	Magnetic Field Gradient Waveform Mapping and Shaping
34	Kampf, T.	Computation of inter and intra voxel diffusion using MC-simulations in frequency and spatial domain: a comparison
35	Khomichev, A.	Solid state ^{27}Al MRI and its applications.
36	Kusmia, S.	^{1}H IP-DQF imaging on a clinical MR scanner
37	Mertens, D.	Evaluating and Avoiding Transient and Permanent Effects of Gradient Pulses on an NMR Permanent Magnet

Nr.	Presenter	Title
38	Schneider, J.T.	Enhanced BOLD effect with iMQCs at high field
39	Weiger, M.	A Closer Look into DESIRE for NMR Microscopy
40	Wölk, K.	Accurate Spin-Echo Inversion in Imaging with Inhomogeneous B1 Fields
41	Zhang, Z.	Centric Scan MR T_1 Contrast Imaging
42	Ziener, C.	Diffusion Dependent Frequency Distribution
43	Anferova, S.	NMR of Geophysical Drill Cores with a Mobile Halbach Magnet
44	Ardelean, I.	Surface effects on the dynamics of molecules confined in core – shell nanocapsules
45	Balcom, B.	Spatially Resolved Tracer Distributions in a Rock Core Diffusion Experiment
46	Haber-Pohlmeier, S.	NMR relaxation in natural soils: Fast Field Cycling and T_1-T_2 Determination by IR-MEMS
47	Mitchell, J.	Measuring Flow Propagator Moments using DiffTrain
48	Morris, R.	Ultra-fast quantitative MRI of novel advection-free polysaccharide preparations, retaining high sensitivity to local fluid pressure using gas filled liposomes
49	Sagidullin, A.	Pore Geometry from Internal Magnetic Fields. Simulations and Experiments of CPMG Trains
50	Song, Y.	NMR measurement of magnetic field correlation function in porous media
51	Stingaciu, L.	Relaxation Measurements and Water Flux Imaging in Sand/Clay Phantom
52	Sturm, V.	NMR diffraction in partially ordered lattices – towards detection of Alzheimer plaques in the brain
53	Baias, M.	Investigation of ancient mummies and bones by NMR and CT
54	Nestle, N.	Unilateral and conventional NMR relaxation studies on hydrating gypsum: Experimental evidence for vapour phase diffusion in strong gradients and signal/noise benefits in a sensor with reduced gradient
55	Adams, A.	Study of Aging Process in Polyethylene
56	Fathima, N. N.	Studies on Hydration of Leather: One and Two Dimensional NMR using Mobile NMR MOUSE®
57	Blümich, A.	Relaxation Anisotropy of Tendon and Strained Rubber
58	Dahlberg, C.	Mobilization of Drug and Polymer During Dissolution of Pharmaceutical Tablets
59	Dvinskikh, S	NMR cryoporometry and imaging of swelling clays
60	Garnov, N.	Determination of load influenced mean collagen fiber orientation by means of NMR microscopy
61	Goga, N.	Surface UV aging of elastomers investigated with microscopic resolution by single-sided NMR
62	Hunger, K.	Water percolation studied in hydrogel filled elastomer matrices using fast imaging techniques
63	Kolz, J.	Investigation of water dynamics and diffusion processes in polyacrylate hydrogels using low-field NMR techniques
64	Mastikhin, I.	NMR and MRI measurements of stable, surfactant-free emulsions
65	Nestle, N.	Quantitative relaxation time measurements on aqueous polymer solutions by unilateral NMR
66	Ogawa, K.	Local water-content measurement of PEM for fuel cell applications using planar surface coils
67	Amar, A	Diffusion profiles to study reactions in solvent-gel systems
68	Broadbent, A.	Quantifying Mass Transfer & Velocity in Two Phase Taylor-Couette Flow
69	Brosten, T.	NMR velocity phase encoded measurements within unidirectional tapered-pore ceramic structures
70	Buljubasich, L.	Investigation of H_2O_2 decomposition in heterogeneous catalysts
71	Davies, C.	Velocity Imaging of Two-Phase Flow in Microchannels
72	Englert, S.	NMR-Imaging at µ-Mixers
73	Feindel, K.	Investigation of shear banding fluctuations in wormlike micelles using rapid NMR velocimetry

Nr.	Presenter	Title
74	Fridjonsson, E.	Study of flow and particle distribution in a bifurcation using dynamic NMR Microscopy
75	Gong, Q.	Diffusion Studies on the Ionic Liquid-CO_2 System
76	Holland, D.	Measurement of Granular Temperature in Gas-Solid Systems
77	Hornemann, J.	Analysis of Biofilm Extracellular Polymeric Substance (EPS) Diffusion
78	Li, L.	Visualization of Polymer Flooding in Heterogeneous Cores by SPRITE Imaging Methodology
79	Li, L.	Velocity Imaging of Single Phase Flow in Porous Media by Magnetization Prepared Centric-scan SPRITE
80	Manz, B.	Investigation of Biofilm Detachment Using MR Microscopy and ^{13}C-MAS NMR Spectroscopy
81	Maddinelli, G.	MRI study of complex flows of viscoelastic fluids
82	Newling, B.	Turbulent, Two-Phase Flow Measurements
83	Sankey, M.	MR velocimetry of liquid flow in trickle-bed reactors
84	Scheler, U.	Flow NMR of complex fluids
85	Schulenburg, D.	Biofilm-mediated Ion Exchanger Optimisation using MRI
86	Schulenburg, D.	Impact of biofilm growth on displacement statistics studied using enhanced ^{13}C PFG-NMR
87	Tsushima, S.	MRI-based D_2O/H_2O-Contrast Method to Visualize Membrane Hydration Path in a Temperature-Controlled Polymer Electrolyte Membrane Fuel Cell
88	Vergeldt, F.	Counter Hagen-Poiseuille flow of two liquids
89	Voda, M.	Quantitative analysis of interdiffusion in a binary liquid system
90	Zhang, Z.	Spatial and Temporal Mapping of Water Content across Nafion Membranes under Wetting and Drying Conditions
91	Zhivonitko, V.	Transport influence on chemical waves: an MRM study
92	Adolphi, N.	Detecting Magnetic Nanoparticles that Selectively Bind to Cancer Cells: the complementary aspects of SQUID Magnetometry and Magnetic Resonance Imaging
93	Beyea, S.	Can MRI Signals Be Recovered During Rapid Imaging in Regions of Magnetic Susceptibility Distortion?
94	Ciampi, E.	Dynamic *in vivo* GARField Magnetic Resonance Profiling of Skin Hydration
95	Guillot, G.	Characterization by MRI of glenoid trabecular bone
96	Helluy, X.	Assessing the detection sensitivity of iron loaded cells in spoiled gradient echo imaging
97	Hörr, V.	In vivo intra-oocyte NMR spectroscopy
98	Lang, E.	Rapid 3D MR Histology on Murine Embryos using a Contrast Agent
99	Neuberger, T.	Morphological imaging of the in vivo mouse eye: application to diabetic retinopathy
100	Neuberger, T.	Morphometric and air flow analysis of the nasal airways of the dog using magnetic resonance microscopy
101	Oya, K.	Measurements of NMR parameter weighted images in chemically fixed human embryos
102	Sanfratello, L.	Using MR Elastography to Image Force Chains in a Quasi-Static Granular Assembly
103	Schmid, F.	Dental Impression using MRI
104	Schröder, M.	Evaluation of Scars and Skin Tissue using the new NMR Mouse® Technology
105	Seo, Y.	Lateral diffusion of Mn^{2+} ion in the brain determined by T_1 relaxation time measured by ^{1}H MRI
106	Sersa, I.	MR Microscopy of Blood Clot Dissolution
107	Shah, N.	Imaging of bound water in the frozen rat brain
108	Xia, Y.	Imaging the Molecular Concentrations in Articular Cartilage
109	Goudappel, G.	Probing the meso- and microstructural heterogeneity of low dense networks with dendrimer probes and NMR/MRI diffusometry
110	Jahnke, S.	Positron Emission Tomography of plants meets NMR Imaging
111	Mikac, U.	MR Study of Moisture Content and Water Distribution in Tree Tissues

Nr.	Presenter	Title
112	Neuberger, T.	MR microscopy of lipid depositions in developing seeds
113	Parasoglou, P.	MRI studies of moisture absorption of food wafers
114	Petrov, O.	The fat content determination with unilateral NMR
115	Pohlmeier, A.	Root water uptake and root system architecture monitored by MRI-MSME and RARE
116	Schulze-Till, T.	Imaging of water transport in Coffee Beans after roasting and quenching
117	Schulze-Till, T.	Slow flow quantification using the inflow effect
118	Spindler, N.	High resolution NMR Imaging and Relaxation Mapping to study the transition of activity of wood garlic (*Allium ursinum)* in natural soils: A Feasibility Study
119	Veliyulin, E.	Rapid Determination of the Fat Content in Packaged Dairy Products by Unilateral NMR
120	Veliyulin, E.	Rapid Determination of the Moisture Content in Wood Shavings Using Time Domain NMR
121	Veliyulin, E.	Quantitative ^{23}Na MRI of muscle foods
122	Venne, B.	Investigating cheese pressing by NMR and MRI
123	Danieli, E.	Single-shot depth profiling with a single-sided NMR sensor: Application to skin measurements
124	Danieli, E.	Improving the field homogeneity of a Halbach array using an efficient shim unit based on permanent magnets
125	Schöfberger, W.	Investigation of coated particle boards with the profile NMR-MOUSE

Posters sorted by name

Presenter	Title	Nr.
Adams, A.	Study of Aging Process in Polyethylene	55
Adolphi, N.	Detecting Magnetic Nanoparticles that Selectively Bind to Cancer Cells: the complementary aspects of SQUID Magnetometry and Magnetic Resonance Imaging	92
Amar, A	Diffusion profiles to study reactions in solvent-gel systems	67
Amar, A.	Velocity maps measured in a single-shot using multi.echoes independently encoded	22
Anferova, S.	NMR of Geophysical Drill Cores with a Mobile Halbach Magnet	43
Ardelean, I.	Surface effects on the dynamics of molecules confined in core – shell nanocapsules	44
Baias, M.	Investigation of ancient mummies and bones by NMR and CT	53
Balcom, B.	Spatially Resolved Tracer Distributions in a Rock Core Diffusion Experiment	45
Balcom, B.	Magnetic Field Gradient Waveform Mapping and Shaping	33
Basser, P.	Rheo-NMR micro-imaging in natural coordinates	24
Basser, P.	On the Observation of (Remote) Anisotropy due to Macroscopic Restrictions	25
Behr, V.	Mapping the flux density of a coil with an optical detector	1
Beyea, S.	Can MRI Signals Be Recovered During Rapid Imaging in Regions of Magnetic Susceptibility Distortion?	93
Blümich, A.	Relaxation Anisotropy of Tendon and Strained Rubber	57
Böhme, U.	Charge determination by electrophoresis NMR	26
Broadbent, A.	Quantifying Mass Transfer & Velocity in Two Phase Taylor-Couette Flow	68
Brosten, T.	NMR velocity phase encoded measurements within unidirectional tapered-pore ceramic structures	69
Bühler, J	Combined Image Processing Tools for MRI- and PET-data	23
Buljubasich, L.	Investigation of H_2O_2 decomposition in heterogeneous catalysts	70
Chandrasekera, T.	Towards the Design of PFG-NMR Experiments for Emulsion Droplet Sizing	27
Ciampi, E.	Dynamic *in vivo* GARField Magnetic Resonance Profiling of Skin Hydration	94
Ciarrocchi, M.	Design of an Elliptical Permanent Magnet for Surface MRI	2
Dahlberg, C.	Mobilization of Drug and Polymer During Dissolution of Pharmaceutical Tablets	58
Danieli, E.	Single-shot depth profiling with a single-sided NMR sensor: Application to skin measurements	123
Danieli, E.	Improving the field homogeneity of a Halbach array using an efficient shim unit based on permanent magnets	124
Davies, C.	Velocity Imaging of Two-Phase Flow in Microchannels	71
Dvinskikh, S	NMR cryoporometry and imaging of swelling clays	59
Englert, S.	NMR-Imaging at µ-Mixers	72
Fathima, N. N.	Studies on Hydration of Leather: One and Two Dimensional NMR using Mobile NMR MOUSE®	56
Feindel, K.	Investigation of shear banding fluctuations in wormlike micelles using rapid NMR velocimetry	73
Ferrante, G.	Measurement of the spin-spin relaxation time T_2 at very low magnetic field by means of the Fast Field Cycling NMR method	28
Franchi, D.	Design of an acquisition-reconstruction algorithm for Magnetic Resonance surface Imaging	29
Franck, J	Ex Situ Pulse Design and Implementation	31
Fridjonsson, E.	Study of flow and particle distribution in a bifurcation using dynamic NMR Microscopy	74
Gädke, A.	Open source NMR spectrometer control software DAMARIS – a common basis for home-built NMR systems?	3
Gädke, A.	Inverse DESIRE: enhanced apparent longitudinal relaxation in thin excited slices	30

Presenter	Title	Nr.
Garnov, N.	Determination of load influenced mean collagen fiber orientation by means of NMR microscopy	60
Glückler, H	How to produce small gradient coils	4
Glückler, H.	Design of a MRT spectrometer for investigations on trees	5
Goga, N.	Surface UV aging of elastomers investigated with microscopic resolution by single-sided NMR	61
Golzi, P.	NMR Data Accumulation in Polar Coordinates Numerical Methods to minimize Systematic Errors	32
Gong, Q.	Diffusion Studies on the Ionic Liquid-CO_2 System	75
Goudappel, G.	Probing the meso- and microstructural heterogeneity of low dense networks with dendrimer probes and NMR/MRI diffusometry	109
Guillot, G.	Characterization by MRI of glenoid trabecular bone	95
Haber-Pohlmeier, S.	NMR relaxation in natural soils: Fast Field Cycling and T_1-T_2 Determination by IR-MEMS	46
Halse, M.	NMR-MOLE: Field stabilisation, shimming and improvement of spectral resolution	6
Handa, S.	Development of planar gradient coils for a whole hand MRI system	7
Helluy, X.	Assessing the detection sensitivity of iron loaded cells in spoiled gradient echo imaging	96
Holland, D.	Measurement of Granular Temperature in Gas-Solid Systems	76
Hornemann, J.	Analysis of Biofilm Extracellular Polymeric Substance (EPS) Diffusion	77
Hörr, V.	In vivo intra-oocyte NMR spectroscopy	97
Hunger, K.	Water percolation studied in hydrogel filled elastomer matrices using fast imaging techniques	62
Jahnke, S.	Positron Emission Tomography of plants meets NMR Imaging	110
Kampf, T.	Computation of inter and intra voxel diffusion using MC-simulations in frequency and spatial domain: a comparison	34
Khomichev, A.	Solid state ^{27}Al MRI and its applications.	35
Köllisch, U.	Design of a double-resonant ^{19}F-^{1}H resonator for in vivo MRI detection of amyloid plaques at 17.6T	8
Kolz, J.	Investigation of water dynamics and diffusion processes in polyacrylate hydrogels using low-field NMR techniques	63
Kusima, S.	B_1 concentration by surface resonator for MR microimaging on a clinical system	9
Kusmia, S.	^{1}H IP-DQF imaging on a clinical MR scanner	36
Lang, E.	Rapid 3D MR Histology on Murine Embryos using a Contrast Agent	98
Li, L.	Visualization of Polymer Flooding in Heterogeneous Cores by SPRITE Imaging Methodology	78
Li, L.	Velocity Imaging of Single Phase Flow in Porous Media by Magnetization Prepared Centric-scan SPRITE	79
Lopez, M.	Four-Channel Mouse Volume Array at 7 Tesla	10
Maddinelli, G.	MRI study of complex flows of viscoelastic fluids	81
Manz, B.	A Simple, Small and Low Cost Permanent Magnet Design to Produce Homogeneous Magnetic Fields	11
Manz, B.	Investigation of Biofilm Detachment Using MR Microscopy and ^{13}C-MAS NMR Spectroscopy	80
Marble, A.	Surface coils for unilateral NMR	12
Marble, A.	Unilateral NMR with homogeneous magnetic fields	13
Mastikhin, I.	NMR and MRI measurements of stable, surfactant-free emulsions	64
Mauler, J.	Soil Moisture Measurements with a Mobile NMR Sensor	14
Mertens, D.	Evaluating and Avoiding Transient and Permanent Effects of Gradient Pulses on an NMR Permanent Magnet	37

Presenter	Title	Nr.
Mikac, U.	MR Study of Moisture Content and Water Distribution in Tree Tissues	111
Mitchell, J.	Measuring Flow Propagator Moments using DiffTrain	47
Morris, R.	Ultra-fast quantitative MRI of novel advection-free polysaccharide preparations, retaining high sensitivity to local fluid pressure using gas filled liposomes	48
Nestle, N.	Unilateral and conventional NMR relaxation studies on hydrating gypsum: Experimental evidence for vapour phase diffusion in strong gradients and signal/noise benefits in a sensor with reduced gradient	54
Nestle, N.	Quantitative relaxation time measurements on aqueous polymer solutions by unilateral NMR	65
Neuberger, T.	High field magnetic resonance microimaging using ceramic dielectric resonators	15
Neuberger, T.	Morphological imaging of the in vivo mouse eye: application to diabetic retinopathy	99
Neuberger, T.	Morphometric and air flow analysis of the nasal airways of the dog using magnetic resonance microscopy	100
Neuberger, T.	MR microscopy of lipid depositions in developing seeds	112
Newling, B.	Turbulent, Two-Phase Flow Measurements	82
Ogawa, K.	Local water-content measurement of PEM for fuel cell applications using planar surface coils	66
Oya, K.	Measurements of NMR parameter weighted images in chemically fixed human embryos	101
Ozeki, T.	Development of a compact MRI system in –5 °C cold room for visualization of sea-spray icing	16
Parasoglou, P.	MRI studies of moisture absorption of food wafers	113
Petrov, O.	The fat content determination with unilateral NMR	114
Pohlmeier, A.	Root water uptake and root system architecture monitored by MRI-MSME and RARE	115
Qiu, L.	Earth's Magnetic Field NMR Using a SQUID Sensor	21
Rommel, E.	Battery operated pocket-size nmr imaging machine	17
Sagidullin, A.	Pore Geometry from Internal Magnetic Fields. Simulations and Experiments of CPMG Trains	49
Sanfratello, L.	Using MR Elastography to Image Force Chains in a Quasi-Static Granular Assembly	102
Sankey, M.	MR velocimetry of liquid flow in trickle-bed reactors	83
Scheler, U.	Flow NMR of complex fluids	84
Schmid, F.	Dental Impression using MRI	103
Schneider, J.T.	Enhanced BOLD effect with iMQCs at high field	38
Schöfberger, W.	Investigation of coated particle boards with the profile NMR-MOUSE	125
Schröder, M.	Evaluation of Scars and Skin Tissue using the new NMR Mouse® Technology	104
Schulenburg, D.	Biofilm-mediated Ion Exchanger Optimisation using MRI	85
Schulenburg, D.	Impact of biofilm growth on displacement statistics studied using enhanced ^{13}C PFG-NMR	86
Schulze-Till, T.	Imaging of water transport in Coffee Beans after roasting and quenching	116
Schulze-Till, T.	Slow flow quantification using the inflow effect	117
Sell, J.	Plug-and-Play Preamplifier for Mobile MR	18
Seo, Y.	Lateral diffusion of Mn^{2+} ion in the brain determined by T_1 relaxation time measured by ^{1}H MRI	105
Sersa, I.	MR Microscopy of Blood Clot Dissolution	106
Shah, N.	Imaging of bound water in the frozen rat brain	107
Song, Y.	NMR measurement of magnetic field correlation function in porous media	50
Spindler, N.	High resolution NMR Imaging and Relaxation Mapping to study the transition of activity of wood garlic (*Allium ursinum)* in natural soils: A Feasibility Study	118
Stingaciu, L.	Relaxation Measurements and Water Flux Imaging in Sand/Clay Phantom	51

Presenter	Title	Nr.
Sturm, V.	NMR diffraction in partially ordered lattices – towards detection of Alzheimer plaques in the brain	52
Tsushima, S.	MRI-based D_2O/H_2O-Contrast Method to Visualize Membrane Hydration Path in a Temperature-Controlled Polymer Electrolyte Membrane Fuel Cell	87
Tymofiyeva, O.	Intraoral Receiver Coil for Dental Impression using MRI	19
Veliyulin, E.	Rapid Determination of the Fat Content in Packaged Dairy Products by Unilateral NMR	119
Veliyulin, E.	Rapid Determination of the Moisture Content in Wood Shavings Using Time Domain NMR	120
Veliyulin, E.	Quantitative ^{23}Na MRI of muscle foods	121
Venne, B.	Investigating cheese pressing by NMR and MRI	122
Vergeldt, F.	Counter Hagen-Poiseuille flow of two liquids	88
Voda, M.	Quantitative analysis of interdiffusion in a binary liquid system	89
Weiger, M.	A Closer Look into DESIRE for NMR Microscopy	39
Wölk, K.	Accurate Spin-Echo Inversion in Imaging with Inhomogeneous B1 Fields	40
Xia, Y.	Imaging the Molecular Concentrations in Articular Cartilage	108
Zhang, Z.	Zero Mode TEM Parallel Plate for High Resolution Thin Film Depth Magnetic Resonance Imaging	20
Zhang, Z.	Centric Scan MR T_1 Contrast Imaging	41
Zhang, Z.	Spatial and Temporal Mapping of Water Content across Nafion Membranes under Wetting and Drying Conditions	90
Zhivonitko, V.	Transport influence on chemical waves: an MRM study	91
Ziener, C.	Diffusion Dependent Frequency Distribution	42

Mapping the flux density of a coil with an optical detector

Volker C. Behr , Peter M. Jakob

Experimental Physics 5, University of Würzburg, Würzburg, Germany

Abstract:

A detector for mapping the magnetic field generated by a radio frequency (rf) coil using the Faraday effect is presented. As opposed to B_1-maps created by rotating-frame-imaging [1,2], this method does not require the coil to be within a spectrometer in order to measure the generated flux density.

For this setup, a red laser diode (laser class I, ≤ 25 µW) and a polarizer were used. The linearly polarized beam penetrated a 15 mm rod of SF6-flintglass (Verdet constant at 595 nm: V=21.1 rad T^{-1} m^{-1}) in which the plane of polarization is rotated proportionally to the longitudinal component of the surrounding flux density. An analyzer converted this rotation into an amplitude modulation, which was then acquired using a home-built detector based on an avalanche diode. For the first studies, a threefold loop coil with a radius of 66 mm was used, which created a flux density of approx. 80 µT in its center at 15 kHz.

Data were acquired at a sampling rate of 44.1 kHz for 1 second. These yielded a signal-to-noise ratio of above 20 at the center of the coil. Since the glass rod had a length of 15 mm, the measured values represent the averaged value of the flux density over this distance. With the current setup, flux densities down to the order of 1 µT are detectable, which covers flux densities of typical resonators employed in NMR. Currently frequencies are limited to audio range by the audio amplifier generating the current for the coil and the audio input of the computer used for sampling the signal. The detector itself is capable of frequencies up to 100 MHz.

Fig. 1 shows the axial distribution of the magnetic flux density B starting from the center of the coil moving along the axis. The red line is a calculation of the expected values using Biot-Savart with a correction for a possible systematic error in the positioning of the detector and the baseline-offset of the receiver. Fig. 2 shows a 3D-plot of values measured starting from the center of the coil and moving radially outwards.

Since they do not couple into neighboring sensor elements, arrays of high densities can be realized using optical detection.
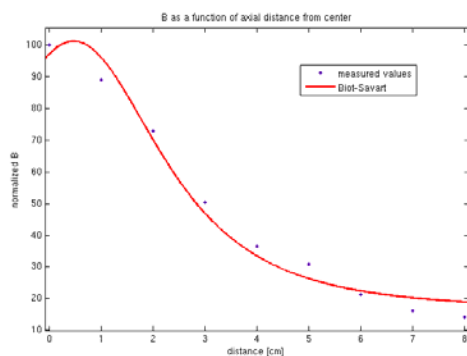
Fig. 1: B as a function of axial distance from center (blue dots) and values computed according to Biot-Savart (red line).
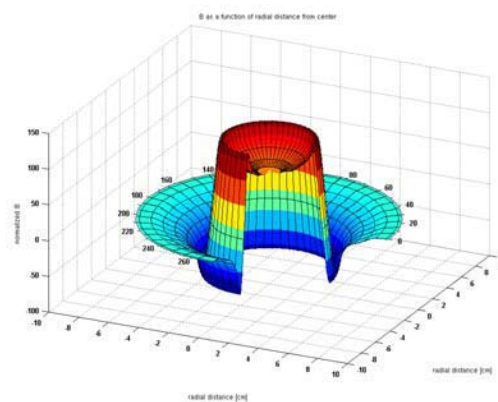
Fig. 2: B as a function of radial distance from center. The sharp drop in B occurs at the position of the loop.

1. D.I. Hoult, *J Magn Reson* **33**(1) (1979) 183-197.
2. J. Murphy-Bosch et al., *J Magn Reson* **73**(2) (1987) 293-303.

Design of an Elliptical Permanent Magnet for Surface MRI

Ciarrocchi M.[1], Galante A.[1], V. Di Miccoli[2], Alecci M.[1], Sotgiu A.[1]

[1]Dipartimento di Scienze e Tecnologie Biomediche, Università dell'Aquila, L'Aquila, Italy
[2]Itel Telecomunicazioni, Ruvo di Puglia, Bari, Italy

Abstract. The unilateral MRS/MRI sensor has several applications in materials [1] and in biomedicine [2] studies. We have studied a new design for a hand-size permanent magnet suitable for 1D-MRI [3] that should be useful for skin and ancient frescoes analyses. The magnet has been optimized to achieve a relatively high B_0 field uniformity in a volume of about $20 \times 2 \times 4$ mm^3 at a distance up to 8 mm from the magnet surface. The device is composed of an elliptical iron base, four identical NdFeB bar magnets with residual induction of 1.4 T with polarities and angular separations along x and y axis (α_x, α_y) respect to the center, as shown in Fig. 1. Optimization has been performed from field contributions by an open source program (Radia) as a function of the seven main geometrical parameters of the magnets and of the iron base. The requirement of a good uniformity in a relative large volume has constrained the field strength intensity that in the present model, at a distance of $z = 8$ mm from the surface, is $B_{0x} = 1137$ G. In the observed volume maximum field inhomogeneity is about 10^3 ppm over a region from 4 to 8 mm away from the probe with maximum sensitivity at a depth of 8 mm, see Fig. 2. Imaging capabilities will be achieved by adding a field gradient $\partial B_{0x}/\partial x$ coil. Fig. 2 shows also how at different distances from the surface the magnetic field has similar distribution, but different intensities. This paves the way to obtain stratigraphic images by using multi-channel receivers.
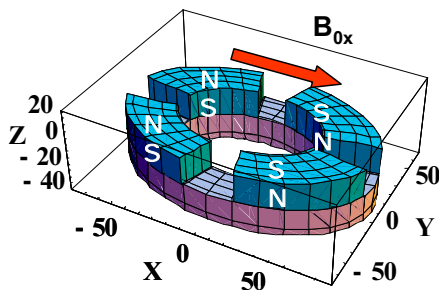
Inner Ellipse:	Base Height = 20 mm
Major radius = 49 mm	Magnets Height = 20 mm
Minor radius = 31 mm	Weight = 3.47 kg
External Ellipse:	$\alpha_x = 23.7°$ $\alpha_y = 25.8°$
Major radius = 85 mm	
Minor radius = 54 mm	

Figure 1 Elliptical permanent magnet model.

Figure 2 Field intensity along the directions (a) x (at y = 0) and (b) y (at x = 0) for distance from the surface: z = 8 mm (black line), z = 7 mm (red line), z = 6 mm (green line), z = 5 mm (blue line), z = 4 mm (cyan line).
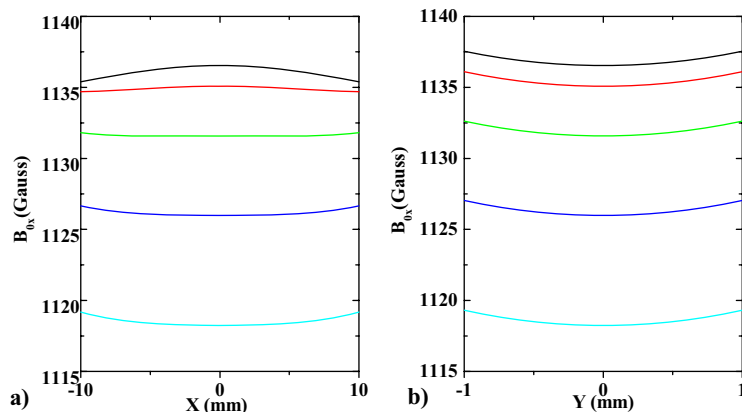
References: [1] Blumich B. et al, Advances of unilateral mobile NMR in non-destructive materials testing, Magn Res Imag, 2005, 23, 197-201; [2] Haken R. et al, Anisotropy in tendon Investigated in Vivo by a Portable NMR Scanner, the NMR-MOUSE, JMR 2000, 144, 195,199; [3] Prado P. J. et al, One-Dimensional Imaging with a Palm-Size Probe, JMR, 2000, 144, 200-206.

Open source NMR spectrometer control software DAMARIS – a common basis for home-built NMR systems?

Achim Gädke[1], Christopher Schmitt[2], Holger Stork[1], Markus Rosenstihl[1], Nikolaus Nestle[1,3]

[1] Institute of Condensed Matter Physics, TU Darmstadt, Darmstadt, Germany
[2] Department of informatics, Frankfurt University of Applied Sciences, Frankfurt, Germany
[2] BASF Aktiengesellschaft, Ludwigshafen, Germany

Abstract:

The DArmstadt MAgnetic Resonance Instrument Software (DAMARIS) [1,2] is developed as an open source project which aims at serving the needs of NMR research groups who build their own equipment on the basis of hardware components such as pulse programmer cards and ADCs.

Over the years, both computer programming and the parameter space covered in NMR experiments have strongly increased in complexity. This makes the development of an appropriate spectrometer control software a more and more demanding task. Instead of starting from scratch, adapting and extending a common basic spectrometer control software for the special requirements of a given hardware configuration or experiment is a time-saving alternative.

DAMARIS is developed to provide such a basis. Due to the modular design of the software, it is possible to exchange individual components such as the user interface or drivers for individual hardware components with minimal need for adapting the rest of the system. Like that, DAMARIS offers plenty of options for future developments and is not prone to become obsolete along with the present generation of NMR hardware and computer systems. The modular design of DAMARIS also allows to use is both on Windows and Linux based computer systems in order to meet restrictions posed by the availability of vendor drivers or individual institutions' rules with respect to computer operating systems.

With its Python-based script language [4] for pulse programming and experiment control and the possibilities to store every individual acquired NMR signal for further *ex-post* processing, DAMARIS offers options for novel signal averaging and data evaluation schemes which are almost impossible to realize on commercial NMR spectrometers using the vendor software. As the same time, DAMARIS can also be used with other "front-ends" such as LabVIEW [4] or with dedicated "single-button"-programs for specialized applications.

DAMARIS is now used on about 10 NMR spectrometers in different labs. One installation runs with LabVIEW as a "front-end", the others use the Python-based script language along with a GTK-based [5] graphical user interface. In the contribution, we will resume the present state of development of the software and the experience built up in different use cases along with an outlook on possibilities of its further development.

1. DAMARIS user page and documentation http://www.fkp.physik.tu-darmstadt.de/damaris/
2. DAMARIS - A flexible and open software platform for NMR spectrometer control, Diffusion Fundamentals, Special Issue 2007 (in print)
3. Python scripting language homepage http://www.python.org/
4. LabVIEW by National Instuments http://www.ni.com/labview
5. GTK "The GIMP Toolkit" http://www.gtk.org/

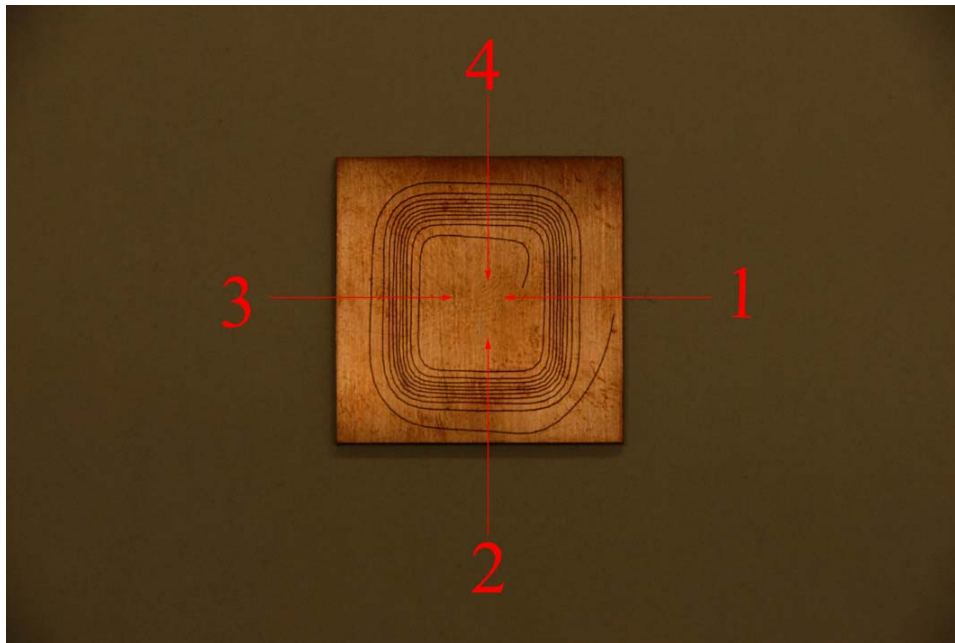# How to produce small gradient coils

J. Collienne[1], H. Peerenboom[1], H. M. Schmitz[1], and H. Glückler [1,2]

[1] Central Department of Technology, Forschungszentrum Jülich GmbH, Jülich, Germany
[2] VIP-NMR, Virtual Institute for Portable NMR

Abstract:
Based on a theoretical optimized design of small gradient coils for a MRT spectrometer [1] we describe the production procedure of these coils. Some of the coils will be shown at the conference.

Picture of a manufactured gradient coil. The outer dimensions of the coil are 30 mm x 30 mm.

1. P. Blümler, private communication (2007).

Design of a MRT spectrometer for investigations on trees

Th. Ortmanns [1], H. Soltner[1,2], and <u>H. Glückler</u>[1,2]

[1] Central Department of Technology, Forschungszentrum Jülich GmbH, Jülich, Germany
[2] VIP-NMR, Virtual Institute for Portable NMR

Abstract:

The design of a movable MRT spectrometer for field studies on trees will be shown on our poster. The spectrometer has a total weight of approximately 350 kg and can be easily handled by two persons.

The DC magnetic field is made by several stacked rings of permanent magnets in an optimized Mandhalas geometry. The spectrometer can be mechanically opened to take up the tree to be investigated. The inner diameter of the spectrometer is approximately 110 mm.

Several safety installations are included into the spectrometer design to maintain an easy-to-use and safe instrument.
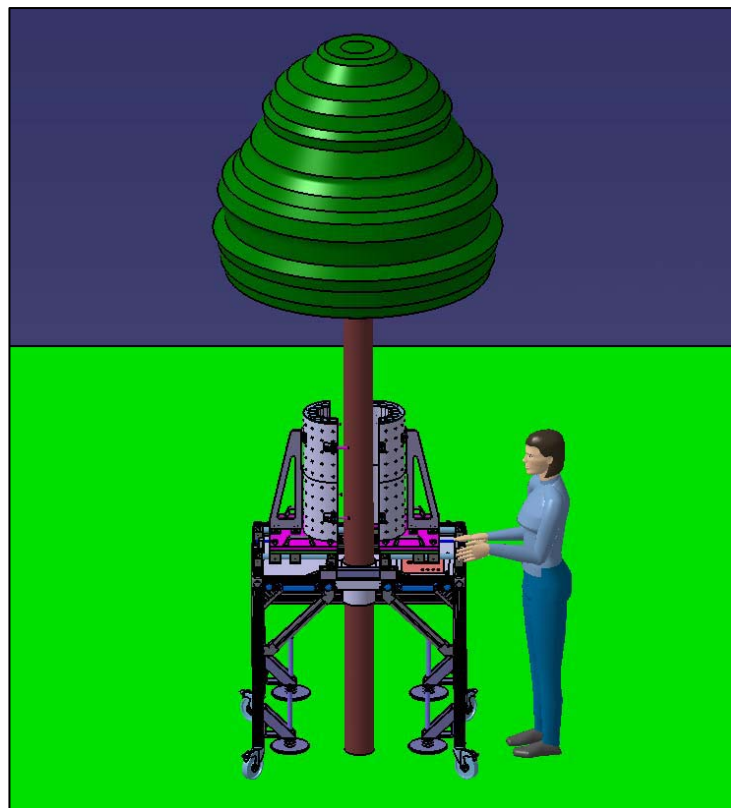
Sketch of the "Tree Scanner"- MRT spectrometer design.

NMR-MOLE: Field stabilisation, shimming and improvement of spectral resolution

M.E. Halse, M.W. Hunter, and P.T. Callaghan

MacDiarmid Institute for Advanced Materials and Nanotechnology, Victoria University of Wellington, Wellington, New Zealand.

Abstract:

The NMR-MOLE [1] is a probe designed to give a large homogenous region with a resonant frequency of 3.2 MHz at a depth of approximately 12 mm. Like all permanent magnet systems, the field, and hence frequency, is temperature dependant and therefore long time experiments or industrial applications are difficult to realise. Furthermore, variations in the residual induction from permanent magnets means some shimming, either mechanical or electromagnetic is desirable to optimise field homogeneity.

Presented here is a body of work demonstrating how the B_0 field of the NMR-MOLE can be shimmed and stabilised to better than 50 ppm. As a proof of concept a conventional gradient set is used for 3-axis first-order shimming with a small sample (2.5 mm in diameter and 10 mm in length) inside a solenoidal transmit and receive coil. In addition to electromagnetic shimming, the mechanical adjustment of one magnet is used to obtain a fourth-order B_0 field. Long-term frequency stabilisation is achieved through the use of a B_0 offset coil and a rapid reference scan, which can easily be incorporated into any NMR experiment. Figure 1 presents a time series of complex 1D spectra acquired over a period of 14 hours using the NMR-MOLE with (a) B_0 compensation and (b) no B_0 compensation.
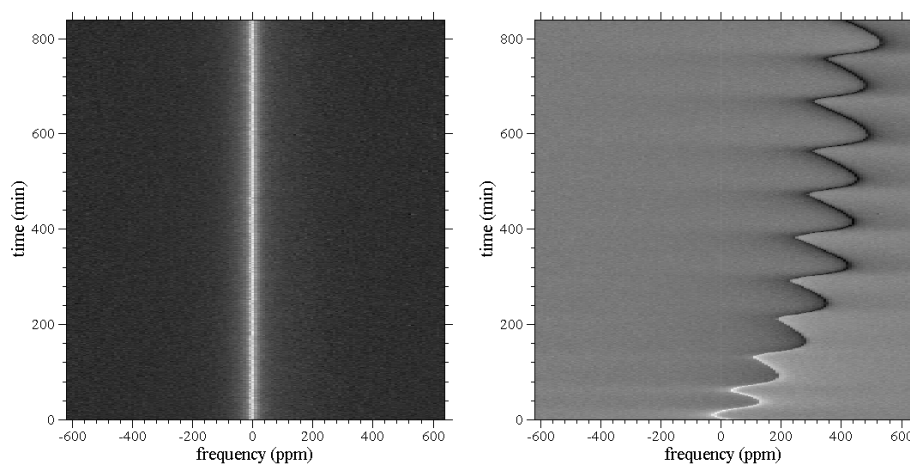
Figure 1: Time series of complex NMR spectra acquired using the NMR-MOLE
(a) with B_0 compensation and (b) without B_0 compensation.

Having surmounted the difficulty of frequency stabilisation and also greatly improved the field homogeneity via first-order shimming and mechanical magnet adjustment, it is now possible to implement techniques such as imaged deconvolution [2] on the NMR-MOLE. Our most recent results using this technique to obtain significant spectral resolution improvements will be presented.

1.   B. Manz *et al., J. Magn. Reson.* **183** (2006) 25 - 31.
2.   M.E. Halse and P.T. Callaghan, *J. Magn. Reson.* **185** (2006) 130 - 137.

Development of planar gradient coils for a whole hand MRI system

Shinya Handa[1] , Katsumi Kose[,1] and Tomoyuki Haishi[2]

[1] Institute of Applied Physics, University of Tsukuba, Tsukuba, Japan
[2] MRTechnology Inc., Tsukuba, Japan

Introduction: Whole hand MR imaging is essential for early detection and follow-up of rheumatoid arthritis (1,2). We already reported a compact MRI system using a permanent magnet (field strength: 0.21 T, gap: 160 mm) for this purpose (2). To achieve better image quality or shorter examination time, a permanent magnet with a higher magnetic field is desired for the whole hand MRI system. In this study, we have developed a planar gradient coil set for a narrower-gap (130 mm) and higher magnetic field (0.30 T) permanent magnet.

Materials and Methods: For whole hand MRI, the field of view (FOV) should include the wrist and the distal end of phalanx. Therefore, the target region for homogeneous magnetic field (within 10 % inhomogeneity) was determined to be a 22 cm × 22 cm × 8 cm diameter ellipsoidal volume. The transverse gradient coils (FIG.1) were designed using the target-field approach (3) and the axial (z) gradient coil (FIG.2) was designed using a genetic algorithm (4).

Geometric distortion was measured using a 3D phantom consisted of 64 acrylic cubic containers (outer size = $(24 \text{ mm})^3$, inner size = $(20 \text{ mm})^3$ filled with aqueous $CuSO_4$ solution. The 3D phantom was imaged with a 3D-SE sequence (TR/TE = 80 ms/10 ms, voxel size = $(0.4 \text{ mm})^2 \times 0.8$ mm, 512 × 256 × 64, FOV = 20.48 cm × 10.24 cm × 6.4 cm). Geometric distortion in three dimensions was characterized as follows;

$$\Delta x = x'_{ijk} - x_{ijk}, \quad \Delta y = y'_{ijk} - y_{ijk}, \quad \Delta z = z'_{ijk} - z_{ijk}, \quad \Delta r = \sqrt{\Delta x^2 + \Delta y^2 + \Delta z^2}$$

where x'_{ijk} , y'_{ijk} , and z'_{ijk} are coordinates in the image space and x, y, and z are coordinates in real space. The real space coordinates are characterized by vertex points of the 3D phantom.

Results and Discussion: The measured gradient coil efficiencies are 0.18, 0.18, 0.29 G/cm/A for Gx, Gy, Gz respectively. Figure 3 shows the 2D cross sections selected from 3D dataset of the 3D phantom. Large geometrical distortions were observed in the outer region of the FOV. The statistical analysis of the geometrical distortions is summarized in Table 1.

The maximum displacement (Δr) is 24.6 voxel lengths (9.84 mm). However, because the spatial variation of the geometric distortion is relatively small compared with the former system (2), the distortion can be easily corrected for clinical applications.

Conclusion: A gradient coil set for a narrower-gap and higher magnetic field permanent magnet optimized for whole hand MRI was developed and the geometrical properties was quantitatively evaluated. We have therefore concluded that the gradient coil set has a sufficient spatial performance for clinical applications of the whole hand MRI system.

FIG.1   FIG.2   FIG.3   Table 1

	RMS (mm)	σ	Max (mm)
Δx	2.44	2.30	7.24
Δy	1.18	1.11	4.31
Δz	0.21	0.212	0.392
Δr	2.73	1.98	9.65
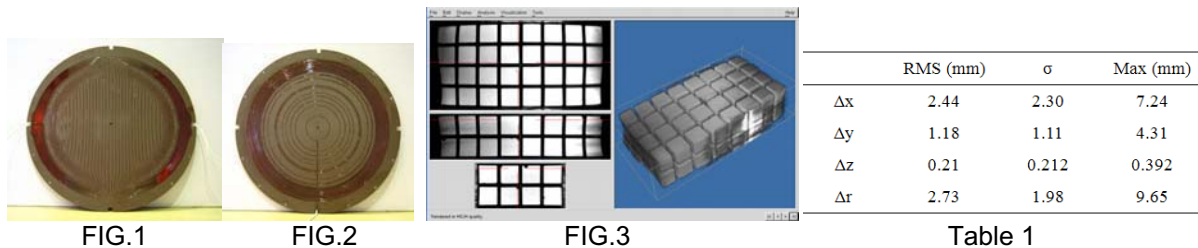
References
1. Sugimoto H, Takeda A, Masuyama J, Furuse M. Radiology 1996;198:185-192.
2. Handa S, Yoshioka H, Tomiha S, Haishi T, Kose K, Magn Reson Med Sci 6, 113-120 (2007).
3. Turner R. J Phys D: Appl Phys 1986;19:147-151
4. Goldberg DE. Genetic algorithms in search, optimization and machine learning, 1st edition. 1989 Addison-Wesley Longman Publishing, Boston.

Design of a double-resonant ^{19}F-^{1}H resonator for in vivo MRI detection of amyloid plaques at 17.6T

Ulrich Köllisch, Volker C. Behr, Cornelius Faber

Department of Experimental Physics V, University of Würzburg, Germany

Abstract:

Senile plaques composed of amyloid-β peptides are characteristic for the pathology of Alzheimers' disease. Detecting and monitoring amyloid plaques in vivo with MRI may become a helpful tool in diagnosis as well as in developing medication against the disease.

It has been shown, that it is possible to label amyloid plaques with the compound FSB [1], which was shown to be of low toxicity and crosses the blood brain barrier. The aim of this work is to establish this procedure on a 17.6 T tomograph with a 57 mm diameter 200 mT/m gradient system, for investigation of a novel double transgenic mouse model of Alzheimer.

For detection of the ^{19}F signal and localization by use of a ^{1}H reference image, a double-resonant crosscage resonator with 45mm length was built. It is composed of two linear operating concentric highpass birdcages, each twice disconnected on opposing sides of the ring. The diameter of the inner ^{19}F coil is 26 mm, and 36 mm for the ^{1}H coil. The resonator is screened with a copper RF-shield with a diameter of 55 mm. The birdcages are rotated by 90°, thus producing orthogonal Eigenmodes as shown in Figure 1. The unloaded/loaded quality factors were determined in reflection as 178/62 for the ^{19}F channel, and 80/62 for the ^{1}H channel. The design offers excellent field homogeneity for the ^{19}F frequency and good homogeneity for ^{1}H measurements. The sensitivity of the resonator was examined (Figure 2) with a 3D RARE sequence using tubes filled with different FSB concentration solved in DMSO as a phantom. 10 mm FSB was detectable in a 1 mm slice in 2 h scan time. In a transgenic mouse model [2] plaques in the thalamus were observed in vivo with ^{1}H gradient echo imaging (Figure 3).
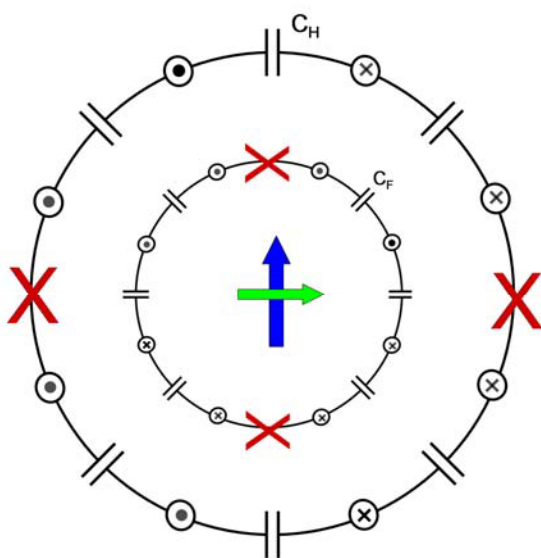
Figure 1: Scheme of the crosscage resonator
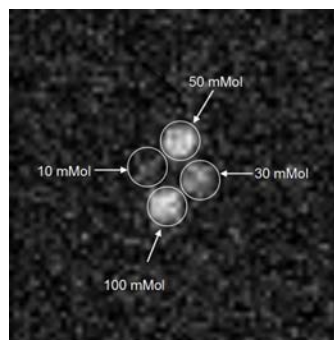
Figure 2: ^{19}F 3D RARE of FSB phantom (5 mm tubes) RARE factor 32 Slice 1mm FOV (25mm)^{2} Resolution (391μm)^{2} 400 averages scan time 2h 8min
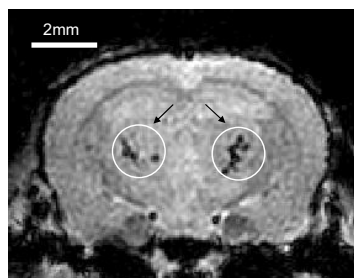
Figure 3: ^{1}H in vivo 3D GE of double transgenic Alzheimer mouse model. Iron-containing thalamic plaques are visible. Slice 90 μm; resolution (152μm)^{2}; scan time 11min

1. M. Higuchi et al., *Nature Neuroscience* **8** (2005) 527 - 533
2. R. Postina et al., *J. Clin. Invest.* **113** (2004) 1456-1464

B_1 concentration by surface resonator for MR microimaging on a clinical system

S. Kusmia[1], O Girard[2], M. Poirier-Quinot[2], J.-C. Ginefri[2], L Darrasse[2], G. Guillot[2]

1-U2R2M UMR8081 CNRS Univ Paris-Sud, CIERM-Hôp Bicetre, 94275 Le Kremlin Bicetre, France
2-U2R2M UMR8081 Univ Paris-Sud, Bât 220, 91405 Orsay, France

Signal to noise (*SNR*) improvement from surface coils used for signal reception and fitted to the size of the region of interest (ROI) is a well known practice. When the ROI becomes so small that the sample noise is lower than the intrinsic coil noise, *SNR* can still be improved by lowering the coil temperature[1]. Using such coils in combination with the standard transmission coil of the scanner (whole-body coil), in absence of decoupling, a strong transmit field can be realized locally. We used MRI methods to evaluate the B_1 concentration thus obtained, in view of using routinely sequences with short RF 90° pulses.

A copper Multi-turn Transmission Line Resonator (MTLR) working at the proton frequency of a 1.5 T scanner was used[2]. The MTLR mean diameter is 11.8 mm. The whole-body coil of the clinical scanner was used to transmit radio frequency (RF) pulses, the B_1 concentration factor was defined as the ratio of the B_1 amplitude generated with MTLR inside the body coil to the B_1 amplitude generated by the body coil alone. From the dependence of the MRI signal intensity on the RF pulse flip angle, the B_1 concentration factor was about 30 for our resonator, as shown on Fig. 1. RF pulses with 90° flip angle and duration shorter than 15 µs can thus be used on a clinical MRI system. MR images with very high in-plane resolution were acquired with the resonator (Fig. 2), *SNR* was 2 times higher than with the Philips micro coil (23 mm) and the same sequence parameters. In future work, we can take advantage of the high B_1 concentration for *in vivo* MRI of ordered and more rigid structures, such as in human skin or tendons[3]. In case of limited *SNR*, superconducting coils with the same geometry can be used to get also higher reception sensitivity[4].
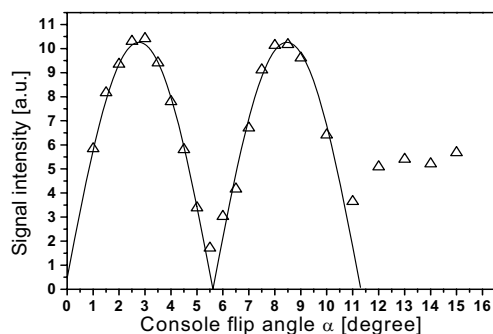
Fig.1. NMR signal against the B_1 level (the control parameter is the RF flip angle α computed by the console) for the copper MTLR at room temperature. The RF pulse duration was fixed at 12.8 µs. The black line shows the best fit of the |sinus| function to the data (open triangles).
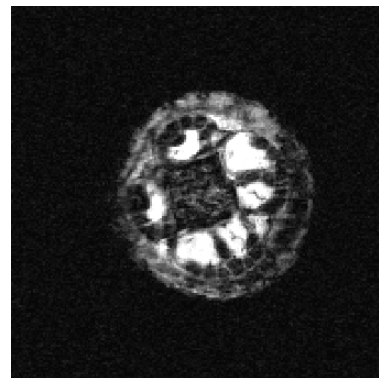

Fig.2. GE MR image of a rat tail obtained with the Multi-turn Transmission Line Resonator on a clinical 1.5 T MRI system: FOV 13x13 mm^2, MTX 192x192, BW/pixel 120 Hz, slice thickness 1 mm, TE/TR 12/500 ms, , NSA 4, total experiment time 6 min.

1- L. Darrasse, J. C. Ginefri Biochimie 85 (2003) 915-937.
2- A-L Coutrot, E Dufour-Gergam, J-M Quemper, E Martincic, J-P Gilles, J-P Grandchamp, M Matlosz, A Sanchez, L Darasse, J-C Ginefri. Sensors and Actuators, A: Physical 99(2002) 49-54.
3- G. Navon, U.Eliav, D.E. Demco, B. Blümich J Magn Reson Imaging 25 (2007) 362-380.
4- M. Poirier-Quinot, J. C. Ginefri, F. Ledru, P. Fornes, L. Darrasse MAGMA 18 (2005) 89-95.

Four-Channel Mouse Volume Array at 7 Tesla

M. A. Lopez[1], F. Breuer[2], N. Seiberlich[1], D. Gareis[1], P. Ehses[3],S. Voll[1], and P. M. Jakob[1,2]

[1]Experimental Physics 5, University of Wuerzburg, Wuerzburg, Bavaria, Germany,
[2]Research Centre Magnetic Resonance Bavaria (MRB), Wuerzburg, Bavaria, Germany
[3]Medizinische Klinik I, University of Wuerzburg, Wuerzburg, Germany

Abstract:

A four-channel volume array for mouse imaging at 7 T [1, 2] is presented, which is 29 mm in diameter, 27 mm long in z-direction and is suitable for measuring mice with weights between 20 and 35 g. Each element is decoupled using the capacitive decoupling technique [3]. The volume array is actively decoupled by a 300.3 MHz tuned trap circuit. As a transmitter, a Bruker 1H Quadrature birdcage coil with a diameter of 72 mm was used. The decoupling achieved between the elements is -26 to -34dB, and active decoupling by the traps is -28 to -34dB. In Fig.1 different views of the four-channel array are depicted.
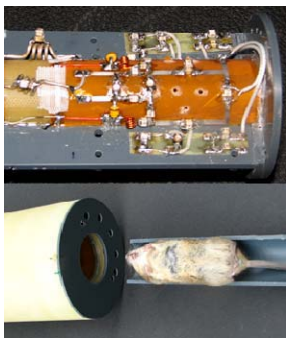
Fig. 1: Different views of the 4-channel volume array.
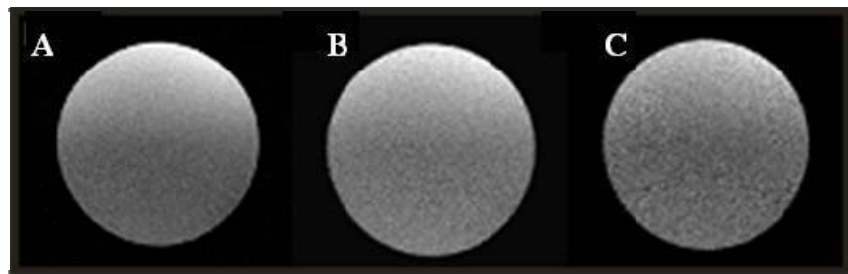
Fig. 2: Axial image of a phantom (4.7g/mol NaCl) after SENSE reconstruction for different acceleration factors, (A) R=1, (B) R=2, (C) R=2x2.

Conclusion:

The array presented exhibits both good homogeneity and RF penetration, as well as good performance and decoupling between each element without preamplifiers. This allows the use of volume array without additional interfaces between the coil and the system. In addition, the cylindrical geometry of the four channel coil is well-suited for the use of parallel imaging. In Fig. 2B, a SENSE [4] reconstruction of an accelerated R=2 phantom experiment is shown. In addition, in 3D imaging, the data can be reduced by an additional factor of 2 in a second dimension, yielding a total acceleration of R=4, fig. 2C.
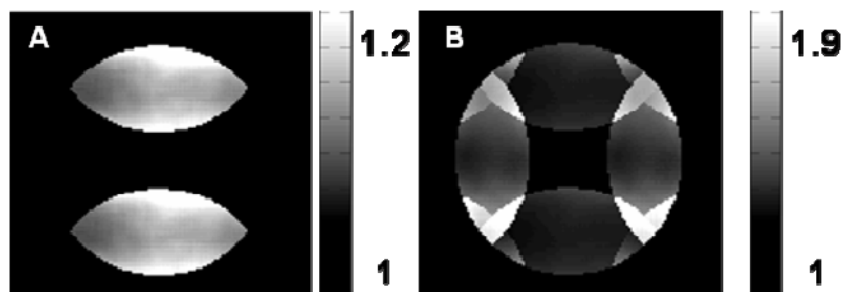

Fig. 3: g-maps of the four-channel volume array, (A) R=2, (B) R=4.

1.PB. Roemer etal. **MRM16**: 192-225 (1990).
2. T. Lanz etal. **Proceedings ISMRM 2006**. Seattle, Wa, USA.
3. R.F. Lee etal. **MRM48**: 203-213(2002).
4. K. Pruessmann etal. **MRM42**: 952-962 (1999)

A Simple, Small and Low Cost Permanent Magnet Design to Produce Homogeneous Magnetic Fields

B. Manz, M. Benecke and F. Volke

Fraunhofer-Institute for Biomedical Engineering, Ensheimer Str. 48, 66386 St. Ingbert, Germany

Abstract:

Using permanent magnets, a strong magnetic field can be created in the gap between two unidirectionally oriented bar magnets. Along the axis, the magnetic field strength takes on an extremum (maximum or minimum) at the centre between both magnets (2nd order homogeneity). The homogeneity can be further improved to 4th order by adjusting the separation between both bar magnets. However, for normal, commercially available magnet dimensions, the optimum separation is often too small to place a sample and RF coil in the gap and therefore be useful for NMR experiments. In this study we show that by placing a commercially available ring magnet around the arrangement of bar magnets (Fig. 1), 4th order homogeneity can be achieved with a larger gap. By using custom-made ring magnets with specific dimensions, even higher order homogeneity can be achieved.

A prototype magnet was built with a resulting magnetic field strength of 1 T. The gap width was with approx. 4 mm large enough to accommodate a 2 mm sample tube with a solenoid RF coil. First preliminary spectra will be shown to demonstrate the potential of this new magnet design for microfluidic applications in biomedical or materials research.
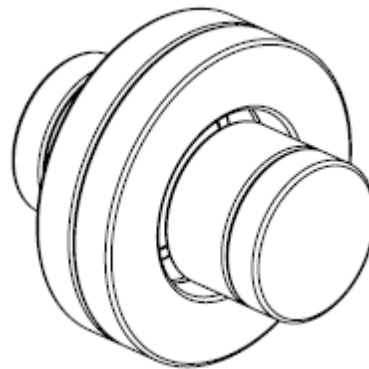
Fig. 1: Arrangement of the proposed magnet design.

Surface coils for unilateral NMR

Andrew E. Marble, Igor V. Mastikhin, and Bruce J. Balcom

MRI Centre, Department of Physics,
University of New Brunswick, Box 4400, Fredericton, NB, Canada

Abstract:

Single-sided magnetic resonance measurements require single-sided or surface coils for B_1 generation and signal detection. The fundamental constraint in coil design is that B_1 must be orthogonal to B_0. For the case where B_1 must be normal to the magnet surface, a circular surface coil is the clear choice. This design is simple, well studied, and offers superior sensitivity. This last point results from the fact that all wire in the coil is involved in generating 'useful' RF field, and no additional wire is needed for current return paths.

In many cases, it is desirable to have B_0 normal to the magnet surface, and B_1 must therefore be generated parallel to the surface of the coil. This can be achieved in practice by a sheet of RF current, approximated by several parallel wires. However, in this arrangement, additional wire is necessary to form a closed loop of current. Along with increasing the resistance of the coil, this additional wire generates a spurious B_1 field. This field can be parallel to B_0, and therefore not useable for NMR purposes, or outside the desired sensitive volume of the coil. In the first case, the field effectively reduces the filling factor (volume ratio of MR sensitive field to total field) and directly increases the measurement noise. In the second case, signal from unwanted regions of a sample may be measured, affecting experimental results.

This work compares several different coil designs, generating a field parallel to their surface. The goal is to generate the strongest possible field in a ROI, while reducing spurious fields as much as possible. The coils' magnetic fields are studied through simulation, and sensitivity maps of candidate coils are obtained through magnetic resonance imaging of phantom samples. A new 'bowtie' coil configuration is introduced which offers shorter return paths, and a stronger B_1 field in a well defined central region over the coil. While not as sensitive as a circular surface coil, this coil is found to be superior to other previously employed designs.
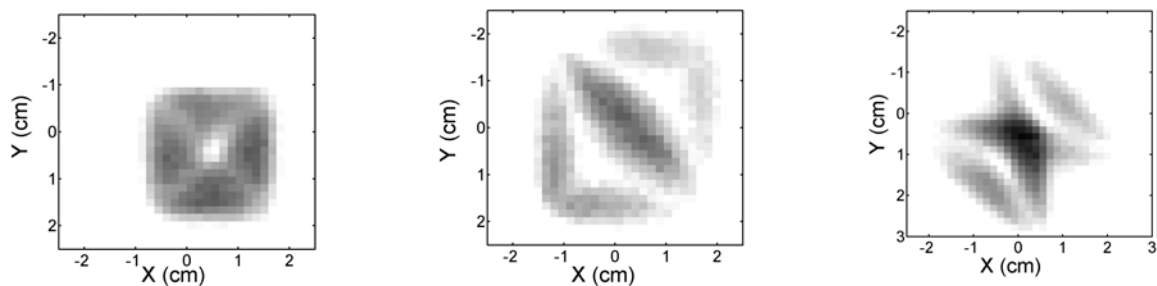
Figure 1: Sensitivity maps of different coil configurations (left-right: spiral, double-D, bowtie) measured by MRI. The color scale is the same for each, with darker regions indicating higher sensitivity. The sensitivity of the spiral coil is a uniform ring, but there is no signal from the central region. The double-D coil has a stronger signal in the central region, but suffers from a relatively large spurious signal from the return loops. The bowtie coil features a much higher sensitivity over the central region of the coil, with comparatively little spurious signal.

Unilateral NMR with homogeneous magnetic fields

Andrew E. Marble, Igor V. Mastikhin, and Bruce J. Balcom

MRI Centre, Department of Physics,
University of New Brunswick, Box 4400, Fredericton, NB, Canada

Abstract:

This presentation discusses two new unilateral magnets, designed to have homogeneous B_0 fields. The first magnet generates a spot removed 1 cm from its face with a field uniformity of several Gauss over an extent of nearly 1 cm. The field uniformity is achieved by adjusting the position and spacing of three magnet blocks, resulting in a magnet array only 10 cm by 11.5 cm by 6 cm in size. The B_0 field of this magnet is oriented parallel to its surface, allowing a simple circular surface coil to be used for signal transduction. This allows substantially improved sensitivity compared to more complicated coil configurations.

The second magnet uses a shaped pole piece to generate a B_0 field with a homogeneity of several hundred ppm over a disk 1 cm in diameter and several millimeters thick. This magnet allows FID measurements with a natural T_2^* of ~200 us. This linewidth allows unilateral time domain NMR measurements of short T_2^* systems, for example solid fat. By virtue of an improved design technique, the magnet is remarkably compact, occupying an 11 cm diameter cylinder.

The presentation focuses on the techniques used to design these magnets, and the resulting magnetic field characteristics. Experimental results showing sensitivity and linewidth will also be presented.
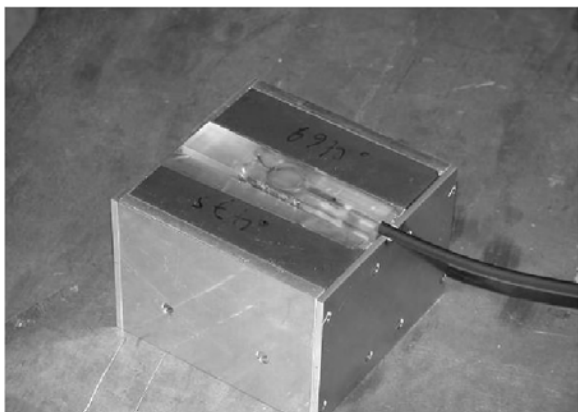
Figure 1: High-sensitivity magnet array, shown with RF coil.
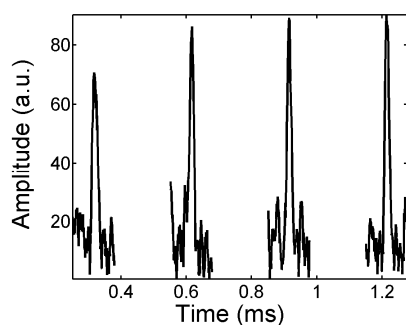

Figure 2: Compact TD-NMR magnet.

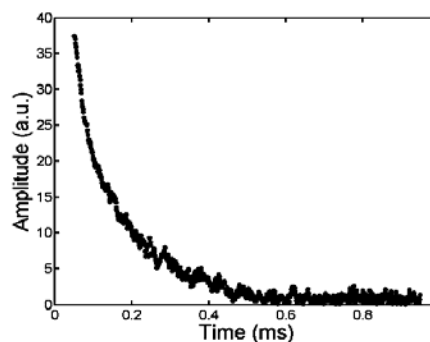Figure 3: Spin echoes, acquired in a single scan with the high-sensitivity magnet above.

Figure 4: FID acquired from a large sample using the compact TD-NMR magnet.

Soil Moisture Measurements with a Mobile NMR Sensor

Jörg Mauler, Federico Casanova, and Bernhard Blümich

Institute for Macromolecular Chemistry, Worringerweg 1, D-52056 Aachen

Abstract

In this work a miniature NMR sensor for moisture measurements in soil is presented. The magnet geometry (Fig. 1a) consists of two cylindrical blocks (length $l = 37.5$ mm, diameter $d = 18$ mm) magnetized perpendicular to the long axis [1] and separated by a small gap ($g = 1.7$ mm). The sensor provides a magnetic field intensity of 0.25 T with a gradient of 30 T/m at a distance of 5 mm from the magnet surface. The iso-B surfaces of the magnetic field are cylindrical shells concentric to the magnet. Moreover, the small gap can be varied to minimize the field variation along the long axis. The radial gradient can be exploited to select slices at different depths into the soil. The coil has a diameter of 20 mm^2 (c).

As a test sample for moisture measurements a cylinder of 10 cm inner diameter was filled with sand up to a height of 40 cm. To lower the probe into the column, a plastic tube was placed in the center of the cylinder. The sand was initially saturated with water. Depth profiles along the tube were measured every third day in order to monitor the drying process (Fig. 1b). The results clearly show that soil layers close to the surface dry faster than the deeper ones. The sensor proves to have potential applications in the field of studying root soil interaction where the dynamic of water in soil needs to be measured.

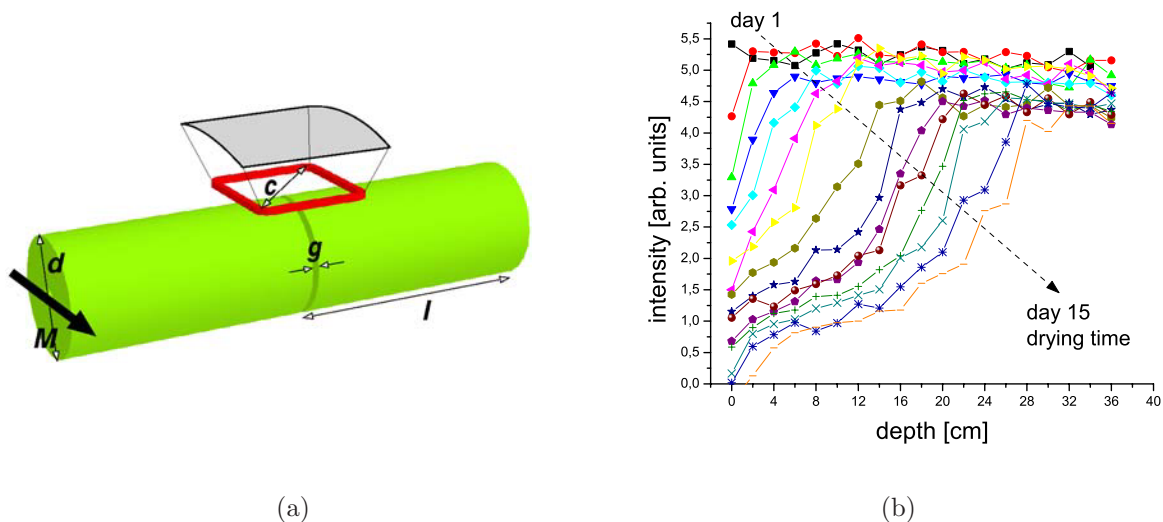(a)   (b)

Figure 1: a) Geometry of the sensor b) Depth profiles of different days reveal the time dependency of the moisture of the soil depending on the depth.

[1] Dunn, K. J., *Nuclear Magnetic Resonance Petrophysical and Logging Applications, Pergamon* (2002)1-10

High field magnetic resonance microimaging using ceramic dielectric resonators.

T.Neuberger[1], E.Semouchkina[2], V.Tyagi[2], M.Lanagan[2], A.Baker[2], A.G.Webb[1]

[1] Huck Institute for Life Sciences, Penn State University, University Park, PA, USA
[2] Materials Research Laboratory, Penn State University, University Park, PA, USA

Abstract:
The design of RF coils for magnetic resonance microimaging becomes increasingly challenging at high magnetic fields. Radiation loss, wavelength effects, self-resonance and decreased Q of typical components all contribute to increased losses in conventional designs based on conductive metals. High permittivity ceramic dielectric resonators are able to create strong uniform magnetic fields in a compact structure at high frequencies, and have very high Q values. They have previously been used in EPR studies, showing enhanced performance over conventional designs [1-3]. In our initial work at 600 MHz, two barium strontium titanate (BST) ceramic disc resonators were produced in-house with the following characteristics : diameter 28.45 mm, thickness 12.2 mm, relative permittivity (ε_r) = 323 (measured using the Hakki-Coleman apparatus), and magnetic susceptibility (300K) = -4.15e-6 (measured on a SQUID magnetometer). The Q value was measured to be ~1000. Magnetic field distributions at 600 MHz (14.1 tesla) were calculated and visualized using finite difference time domain (FDTD) electromagnetic simulation software. The design incorporated frequency tuning via copper sheets that can be partially overlapped with the resonators, as well as providing optimum parameters for the production of a uniform oscillating magnetic field within the sample. Initial results, summarized in Figure 1, showed a very uniform B1 field between the disks, and an improvement in signal-to-noise of approximately a factor-of-two over similarly sized saddle coils.
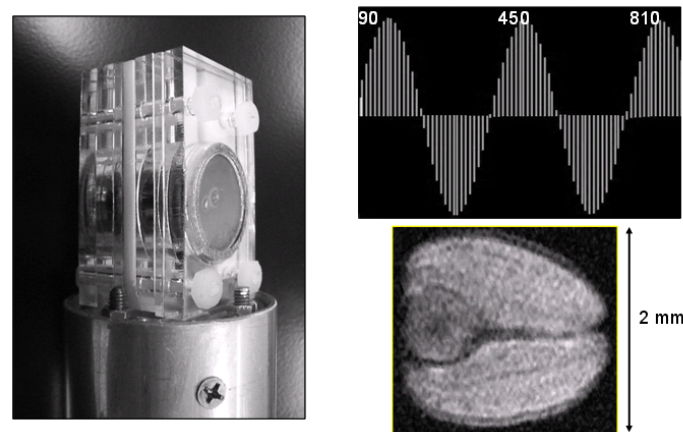
Fig. 1: (left) Probehead for 600 MHz with two coupled dielectric disks: a single loop inductive feed is used for matching. (right) Top: Pulse width calibration for a 2.8 mm wide sample within a 3.2 mm gap. Bottom: One slice from a 3D lipid image of soybean: spatial resolution 20 x 20 x 30 mm, TR=1s, TE=10 ms, 192 x 192 x 144 data matrix, 4 signal averages.

1. Dykstra RW, Markham GD. *J.Magn.Reson.* **69** (1986) 350-355. 2. Walsh WM, Rupp LW. *Rev.Sci.Instr.* **57** (1986) 2278-2279. 3. Jaworski M, Sienkiewicz A, Scholes CP. *J.Magn.Reson.* **124** (1997) 87-96.

Development of a compact MRI system in –5 °C cold room for visualization of sea-spray icing

Toshihiro Ozeki[1] , Satoru Adachi[2], Tomoyuki Haishi[3], Katsumi Kose[2] and Shinya Handa[2]

[1] Hokkaido University of Education, Iwamizawa, Japan
[2] Institute of Applied Physics, University of Tsukuba, Tsukuba, Japan
[3] MR Technology Co., Tsukuba, Japan

Abstract:

Sea-spray ice accretion is a major problem for the operation of lighthouses in northern harbors. Reduced stability due to spray icing on trawlers and vessels can also lead to marine disasters in cold seas. Brine pockets trapped in spray-ice matrices during wet growth are one of the structural features of sea-spray icing, and brine drainage control, one of the physical properties of spray ice. Ozeki *et al*. [1] designed an NMR imaging system to measure the three-dimensional microstructure of sea-spray icing. It comprised a 4.74-T superconducting magnet and a specimen-cooling system controlled by adjusting the volume of cold airflow. However, the system was set up at room temperature, and hence, temperature control of the ice sample was difficult. To address this problem we have developed a compact NMR imaging system set up in a cold room to maintain the sample at a constant temperature.

The system consists of a permanent magnet, a gradient coil set, and an RF probe installed in –5 °C cold room, as shown in Fig. 1. A compact MRI console was set up at room temperature beside the cold room. The permanent magnet is a yokeless magnet with the following specifications: field strength = 1.04 T, gap width = 60 mm, homogeneity = 15.3 ppm over 30 mm DSV at 25 °C, and weight = 300 kg. The RF coil is a 30-mm-diameter ten-turn solenoid.

We obtained sea-spray icing samples from the ice accretion on a lighthouse on the west coast of Hokkaido, Japan. Because the brine in the spray ice had drained out, using a suction pump, we filled the air gaps in the drainage channels with dodecane ($C_{12}H_{26}$). The signal from dodecane doped with iron acetylacetonate ($C_{15}H_{21}O_6Fe$) was sufficient to detect the location of the drainage channels.

A three-dimensional driven equilibrium spin-echo (3D-DESE) sequence (repetition time (TR)/echo time (TE) = 200 ms/8 ms, image matrix = 256^3, voxel size = $(123\ \mu m)^3$, total imaging time = 16 h, NEX = 4) was used for 3D high-resolution imaging [2]. Fig. 2 shows a 2D slice selected from the 3D image data set. Since the NMR signal from the ice was negligible compared with that from dodecane, the drainage channels appeared as bright regions.
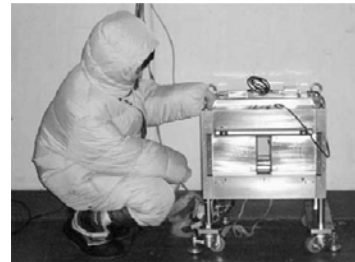

Fig.1. The compact MRI system for cold room. Size = 45 cm (W) × 38 cm (D) × 58 cm (H).
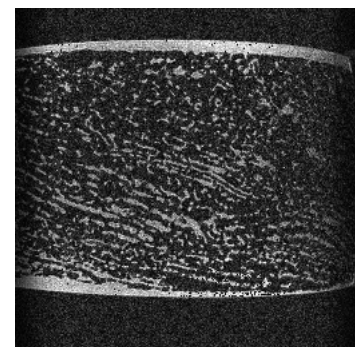

Fig.2. A cross-sectional image of the sea-spray icing acquired from the 3D-DESE sequence.
TR = 200 ms; TE = 8 ms; NEX = 4; image matrix size = 256 × 256; pixel size = $(123\ \mu m)^2$.

1. Ozeki,T., Kose,K., Haishi,T., Nakatsubo,S., Matsuda,Y., *Magnetic Resonance Imaging* **23** (2005) 333–335.
2. Iita,N., Handa,S., Tomiha,S., Kose,K., *Magnetic Resonance in Medicine* **57** (2007) 272–277.

Battery operated pocket-size nmr imaging machine

Eberhard Rommel

Physikalisches Institut, Universität Würzburg, Germany

Abstract:

A battery operated pocket-size NMR imaging system is presented which is suited for teaching purposes and also for plant imaging. The whole electronic system including batteries is placed in a box with the measurements 20cm x 15.5 cm x 6 cm. The magnet is a C-type magnet (11cm x 7 cm x 14 cm, pole caps 7 cm diameter), which was already presented last year at the CMMR6 meeting [1]. The B_0 field is 0.235 T, corresponding to a proton resonance frequency of 10 MHz.

In spite of the small size the system contains everything an imaging system needs:
- RF: quadrature transmitter, low noise preamplifier, quadrature receiver
- AD-converter for data acquisition with 32 k RAM
- microcontroller for timing, pulse shapes, communication, data transfer (serial)
- three 16 bit gradient D/As and three gradient power supplies (4A for 200mT/m).

The latest version, which is in beeing delevopped, also contains a programmable frequency synthesizer and fast USB interface.

fig.1 Complete nmr imaging machine (without notebook computer) including electronic box (lower board with preeamp, receiver, transmitter, gradient D/A, RAM, microcontroller, upper board with gradient power supply and batteries) and magnet.

The main controlling program typically runs on a notebook computer, which is also used for data processing.

Pulse programs can be written in a very simple pulse program language and can be downloaded to the microcontroller during normal operation. Up to 32 different pulse programs can be selected in the microcontroller without downloading.

In order to demonstrate the capabilities of the machine we have performed several tests, among them e.g.:
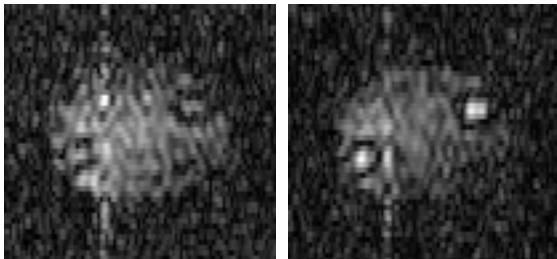

fig. 2: Inflow-weighted TSE images of a phantom sample (two small tubes, inner diameter 1 mm, surrounded by non-flowing water) without flow (left) and flow velocity of ca 2 mm/s in the small tubes (right)

The machine will be presented live at the poster.

References:

1. E. Rommel, CMMR6, Aachen, 2006

Plug-and-Play Preamplifier for Mobile MR

Johannes Sell[1], Florian Fidler[2], Toni Hippmann[3], Michael Ledwig[2], Peter M. Jakob[1,2]

[1] Department of Experimental Physics 5, University of Würzburg, Würzburg, Germany
[2] Research Center Magnetic-Resonance-Bavaria, Würzburg, Germany
[3] Department of Electrical Engineering, FH Würzburg-Schweinfurt, Würzburg, Germany

In MRI devices, transmit receive coils with preamplifiers usually are connected with two or three wires. Receive only coils with an integrated preamplifier can not be tuned and matched with typical standard equipment. We invented a novel design for a 20/40 MHz low noise preamplifier which only requires a single wire. Having small dimensions (11.2mmx26.7mm) the amplifier can be connected to virtually any transmission-reception chain.

The preamplifier design is based on the use of a low noise GaAs-FET (MGF-1302). The input is optimized to a high pass matching network, behaving similar to a $\lambda/4$ phase shifter. This in combination with crossed diodes protects the amplifier from high powers. The amplifier is bypassed by crossed diodes. The output is realized as a resistive matching network with crossed diodes for protection and an optional $\lambda/4$ phase shifter. DC voltage is stabilized to 5V preamplifier power supply by a voltage regulator. The necessary DC supply has to be injected in the output wire. Exemplarily a 20MHz and a 40 MHz version was built.

For the 20 MHz version, a noise figure of 1.7 dB with 20.5 dB gain was achieved, the 40MHz version showed a noise figure of 1.2 dB with a gain of 20 dB. Crucial for the noise figure is the arrangement of the coils. The best result was obtained with a dual layer board with the transistor on one side, and a ground plane and coils on the other side.
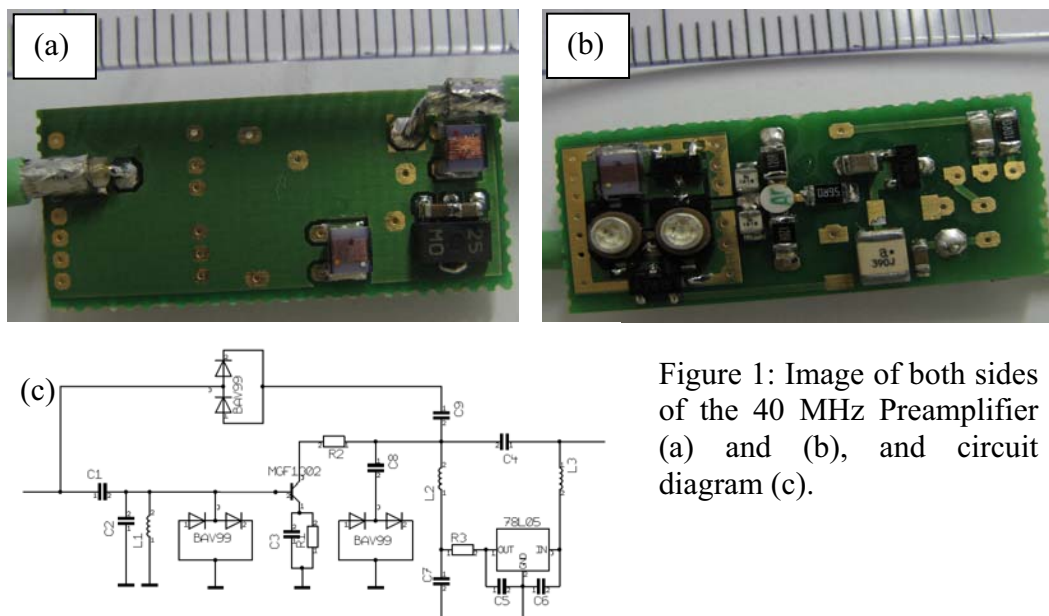

Figure 1: Image of both sides of the 40 MHz Preamplifier (a) and (b), and circuit diagram (c).

Conclusion: The preamplifier provides an excellent noise figure and high gain to conserve the SNR of the MRI experiment. Transmit receive coils equipped with this type of "plug and play" preamplifier behave similar to coils without preamplifier, but deliver optimized SNR.

Intraoral Receiver Coil for Dental Impression using MRI

Olga Tymofiyeva[1], Daniel Gareis[1], Kurt Rottner[2], Florian Schmid[1], Marcos Alonso Lopez[1], Ernst-Jürgen Richter[2] and Peter Michael Jakob[1]

[1] Dept. of Experimental Physics 5, University of Würzburg, Würzburg, Germany
[2] Dept. of Prosthodontics, Dental School, University of Würzburg, Würzburg, Germany

Abstract:

Introduction: The MRI-based contrast-enhanced method of tooth surface digitization [1, 2] provides an alternative technique of taking a dental impression. As recently reported [3], the precision of localization of 'signal/no signal' boundaries can surpass the nominal resolution by an order of magnitude. The achievable precision is limited by the signal-to-noise ratio (SNR) and can be extracted by Fourier interpolation. Thus, MR microscopy of the tooth surface can be performed *in vivo* using a clinical whole-body MRI scanner, provided a high SNR is achieved. The objective of this work was to develop a dedicated RF receiver coil which provides a high SNR in the complete region of the tooth rows and allows for application of the contrast medium into the mouth of the patient.

Concepts and Design: Intraoral application of the coil aimed at minimizing the distance to the teeth. A conductive loop (an ellipse of 3×8 cm) was incorporated into a flexible mouthpiece, adjustable to different curvatures of the tooth rows (Fig. 1). A plastic tube was incorporated into the mouthpiece allowing for application of the contrast medium after the coil is placed in the mouth.

Results and Discussion: *In vivo* images were acquired on a 1.5 T whole-body scanner (Magnetom Avanto) using the developed intraoral coil. Prone positioning and contrast medium described in [2] was applied. A 3D Turbo Spin Echo sequence with TR/TE = 400 ms/13 ms and turbo factor 5 was used. With the field of view of 58×30 mm^2, slab thickness of 16.8 mm and $192\times98\times48$ matrix, the nominal resolution was $300\times300\times350$ μm^3. The scan time was 8 min. The MR data were Fourier interpolated to a digital resolution of $57\times58\times66$ μm^3, segmented and the surface of the teeth was reconstructed using 3D visualization software (Amira). A reconstruction of one of the volunteers' front and distal teeth is shown in Fig. 2. The sensitivity of the coil allowed for measuring the complete tooth rows, providing SNR of 25-30 with the parameter given above. The developed intraoral RF receiver coil can be used for performing contrast-enhanced dental MRI *in vivo*.
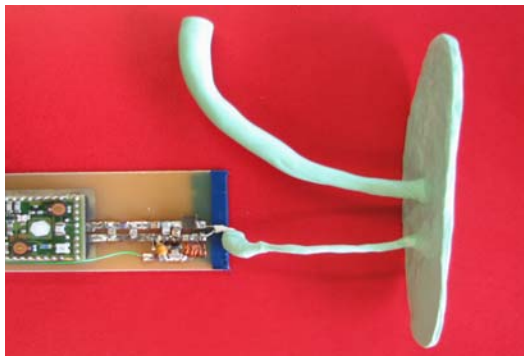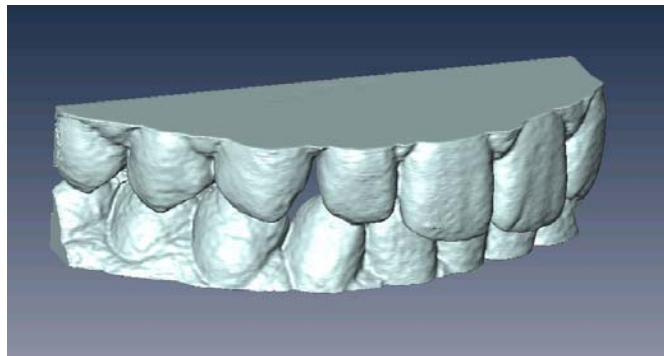
Fig. 1: Photo of the coil.   Fig. 2: Reconstructed dental impression.

1. S. Olt, P.M. Jakob, *Magn Reson Med* **52**(2004) 174-176.
2. O. Tymofiyeva, F. Schmid, K. Rottner, E.-J. Richter, P.M. Jakob, *Proc. ISMRM/ESMRMB, Berlin, Germany* (2007) Abstract 3007.
3. O. Tymofiyeva, K. Rottner, E. Richter, P.M. Jakob, *Proc. ESMRMB, Warsaw, Poland* (2006) Abstract 645.

Zero Mode TEM Parallel Plate for High Resolution Thin Film Depth Magnetic Resonance Imaging

Ziheng Zhang[1], Andrew E. Marble[1, 2], Rodney P. MacGregor[1], Bruce J. Balcom[1]

[1]MRI Centre, Department of Physics, [2]Department of Electrical Engineering, P. O. Box 4400, University of New Brunswick, Fredericton, New Brunswick, Canada E3B 5A3

Abstract:

A parallel plate radial frequency resonator has been designed for high resolution imaging of thin film samples. This novel frequency resonator, which is illustrated in Fig. 1, has two parallel conductive plates for sandwiching the sample of interest. When compared to a surface coil, which generates a B_1 field perpendicular to the sample surface [1], a parallel plate resonator permits lateral and homogeneous distribution of B_1 field across the sample plane. Lateral distribution of B_1 field has been found capable of avoiding the RF screening that is commonly encountered in imaging electrochemical cells like batteries and fuel cells, with conductive layers. Designing a parallel plate resonator to fit thin film samples automatically ensures the sample will experience effective excitation volume as well as high sensitivity for signal reception.

The B_1 field produced by the resonator was investigated by experimental and numerical simulations. SPRITE MRI technique was employed for the B_1 field mapping [2] and Double Half K-space Spin Echo (SE) Single Point Imaging (SPI) [3] was used to acquire high resolution water gradient 1D depth profiles of Nafion film as shown in Fig.2.

In order to observe dynamic phenomena like polymerization, and wetting and drying in thin film samples, parallel plate resonator can be fabricated to fit geometrical forms that would allow mass transport in and out of the sample.
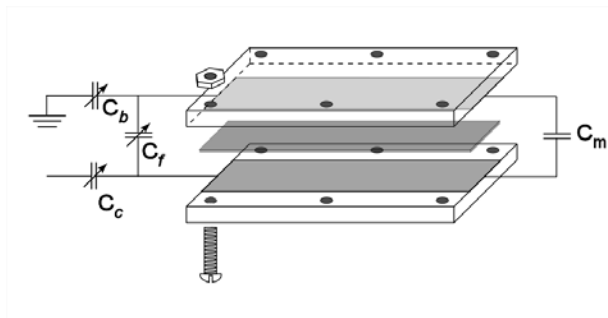
Fig. 1: Schematic of the zero mode parallel plate resonator. The resonating circuit consists of two plates and three tuning capacitor, C_c, C_f and C_b, which respectively implement adjustments on coupling, frequency, grounding, and another fixed capacitor, C_m, at the other side of the plates. The sample membrane was sandwiched by these plates.
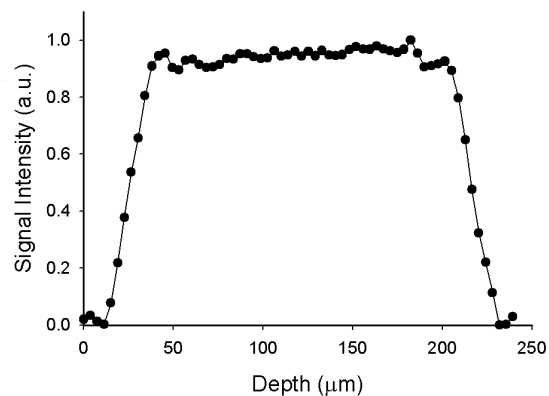

Fig. 2: Depth image of a static, hydrated nafion 117 film, 177 μm in thickness. The image was derived from the first echo. The desired resolution, 4.5 microns, was achieved by optimizing the combination of the primary and secondary phase encode gradients to orthogonalize the net encoding gradient to the sample plane.

1. B. Blumich, NMR Imaging of Materials, Clarendon Press, Oxford, 2000.
2. B. J. Balcom, etc. J. Magn. Reson. 123 (1996) 131.
3. A.V. Ouriadov,etc. J. Magn. Reson., 169 (2004) 174-186.

Earth's Magnetic Field NMR Using a SQUID Sensor

L. Q. Qiu[1,2], Y. Zhang[1], H.-J. Krause[1] and A. I. Braginski[1]

[1] IBN-2, FZ Juelich, D-52425 Juelich, Germany

[2] Pohl Institute, Tongji University, Shanghai 200092, P.R. China

Abstract:

High-resolution NMR spectroscopy is a powerful tool for non-destructive structural investigations of matter. The Earth's magnetic field (EMF, B_E), though weak, is appealing for NMR applications because it is highly homogeneous, globally available and free. As a NMR signal detector, a superconducting quantum interference device (SQUID) achieves a higher signal to noise ratio (S/N) than conventional Faraday detectors, especially in the low field regime. Here, we combine the EMF's homogeneity with the SQUID's sensitivity, demonstrating the feasibility of high-resolution NMR spectroscopy in the Earth's field using a radio-frequency (rf) SQUID operating at 77 K. The SQUID used in our work is of, so-called, substrate resonator type. Outdoors, it exhibited a magnetic field resolution of 70 fT Hz$^{-1/2}$ around 2 kHz.

The experiments were performed in a forest 100 m away from the nearest building. The setup was oriented such that the SQUID's sensitive direction was perpendicular to B_E. The liquid sample, nominally at room temperature, was located beneath the bottom of a Dewar finger. The distance between the sample and the SQUID was about 1 cm. The sample was polarized by a pulsed field (B_p) of about 10 mT for several seconds, which caused sample temperature increase by about 30 K. After switching off B_P, the free induction decay signal, perpendicular to B_P and B_E, was detected by the SQUID.

NMR spectra of some samples, for instance, water, benzene, fluorobenzene, and 2,2,2-trifluoroethanol were investigated. The Larmor frequency of proton was found to be about 2060 Hz. It was found that the Earth's field fluctuation will broaden the linewidth of the spectrum. To reduce the noise in EMF-NMR, the authors suggest to use frequency-adjusted averaging, which compensates line broadening due to EMF fluctuations. For benzene and water samples, a line-width of 0.034 Hz and 0.12 Hz, respectively, was observed at 330 K. High-resolution J-coupling spectra of fluorobenzene and 2,2,2-trifluoroethanol were also obtained.

Velocity maps measured in a single-shot using multi-echoes independently encoded

Andrea Amar, Federico Casanova, and Bernhard Blümich

Institut für Makromolekulare Chemie, RWTH-Aachen, Worringerweg 1, D-52056 Aachen, Germany

NMR velocimetry has proven to be a considerable useful tool for fluid dynamic investigations. Among the different approaches available nowadays to spatially resolve velocity distributions in a non-invasive fashion, one of the most powerful combines a first period where displacement is encoded in the signal phase with the successive application of a read-out imaging sequence. In order to speed up the acquisition time, a number of sequences have been reported in the last years, which exploit fast k-space scanning schemes like RARE or EPI. Although they have succeeded to produce reasonable velocity maps, they can be used to collect only a fraction of the available echoes generated under one T2. One of the main limitations to the use of the whole available echo trains comes from the fact that the velocity is encoded in a first period prior to the k-space sampling, and this information is not updated during the subsequent imaging sequence, time when spins are free to move and change their velocity. This problem is better observed in closed systems without in-out flow (a typical example is the flow in a couet cell). In these cases the liquid remains in the system during the whole experiment and the velocity variations observed in a time scale of T2 are of the order of the velocity range present in the sample (molecules can experience a complete turn to the couete cell). In this work we present a new sequence that encodes and decodes the velocity phase for each echo in an independent way, allowing us to use the complete echo train decay to sample the k-space. Besides tolerating higher velocities than the original sequences, the fact that the echoes are independently encoded along one train allows collection of all the information required to reconstruct the velocity maps along all three directions in a single shot (in general one experiment per direction plus one reference one are required). Moreover, as no phase needs to be preserved during the echo train, the sequence is highly immune to B1 inhomogeneities, an extremely critic source of distortions for conventional sequences.
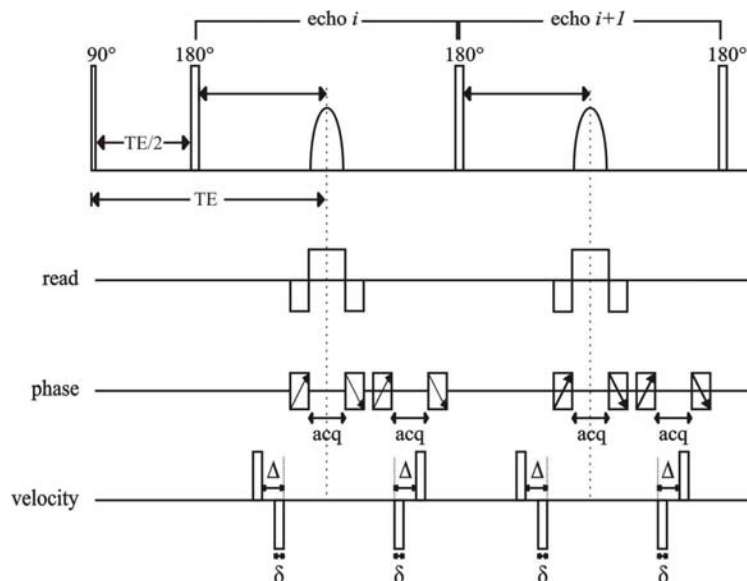

Fig. 1. Pulse sequence proposed to independently encode velocity for each echo. It uses two pair of velocity encoding gradients: one before and one after the echo (to rewind the phase shift proportional to the velocity introduced by the first one). Gradient pulses to sample the k-space are essentially applied as in the original RARE sequence, with the exception that along the phase direction the bipolar pulses are repeated with opposite sign to cancel the phase proportional to displacement accumulated after the first pair. Assuming the velocity does not change during T_E the magnetization phase before the pi pulses is the same as the one present in a CPMG sequence.

Combined Image Processing Tools for MRI- and PET-Data

Jonas Bühler[1], Peter Blümler[1], Hanno Scharr[1], Siegfried Jahnke[1] and Marion I. Menzel[1]

[1] ICG-3, Research Center Juelich, Germany

Abstract:

Tomographic imaging of non-medical subjects like soil or plants using MRI and PET often requires dedicated image processing and visualizations tools, which are not available off the shelf. A set of highly specialised image analysis methods, developed in C++, has been integrated into the object-oriented framework MeVisLab® [1]. The resulting image processing applications then offer these complex functionalities with user-friendly and intuitive graphical user-interfaces. The applications *TrajectoryInterpolation* and *PetTool* present our two latest achievements.
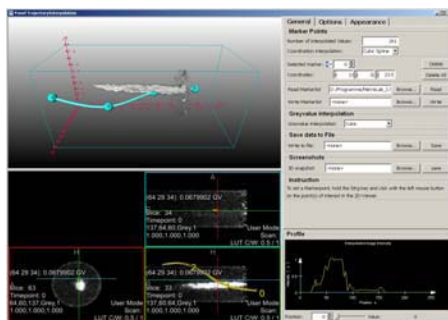
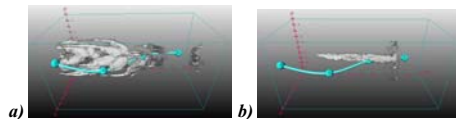Fig. 1: The *TrajectoryInterpolation* tool with PET-dataset of a wheat ear.

Fig. 2: a trajectory defined in MRI-image (*a*) transferred into the co-registered PET-dataset(*b*)

The *TrajectoryInterpolation* tool [2] allows **identifying a line-shaped or tubular structure** e.g. a phloem or xylem element of a plant by manual setting of seed points in an MRI-dataset. The resulting structural information can be transferred to the co-registered PET-dataset to receive the **allocation of a ^{11}C-Tracer along the plant organic structure**.

The calculation of the grey value profile takes place in two steps. In the first step, after defining the seed points in the 2D-viewer, the trajectory will be interpolated automatically, while there is a choice between linear and cubic spline interpolation [3]. In the second step the grey value profile along the trajectory is to be calculated using a choice of grey value interpolation methods. To this end the nearest neighbour-, linear- and cubic interpolation methods [4] are implemented. The resulting intensity profile can be previewed in the diagram down right in the application window (Fig. 1).

PetTool (Fig. 3) combines two main tasks: First it allows to generate **movie-sequences** of a preprocessed 3D-dataset (e.g. pseudo-colouring, highlighting volumes of interest, 3D-arrows, ...). The parameters of the rendering process are easy and intuitive but can also be hidden from the end-user for easy use. The second feature allows the fast and direct definition of a **Volume of Interest** (VOI). This VOI can be applied to a time series of any 3D-image to immediately obtain several temporal information of this region (e.g. the trend of the mean value or the integral). This tool is to be extended with an internal co-registration function in order to allow both MRI- and PET-datasets to be visualised in the same scene.
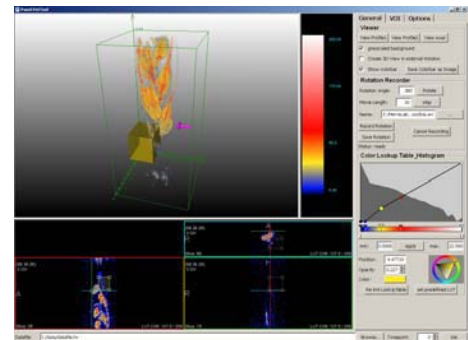

Fig. 3: Screenshot of *PetTool* with MRI-Dataset of a wheat ear

This set of applications is designed for scientists and technicians working in a broad area of scientific applications, who maybe are not too deep in digital image processing and visualisation.

[1] MeVis Research GmbH, Bremen, Webseite: www.mevislab.de
[2] Jonas Bühler, Diplomarbeit, Titel:"Entwicklung eines Werkzeugs zur Koordinaten- und Grauwertinterpolation von MRI- und PET-Daten in der objektorientierten Umgebung MeVisLab®", Fachhochschule Aachen, Abt. Jülich, 2007
[3] William H. Press, Saul A.Teukolsky, William T. Vetterling, Brian P.Flannery, "Numerical Recipes in C++: The Art of Scientific Computing", Second Edition, Cambridge University Press 2002
[4] Image processing library, Hanno Scharr, Forschungszentrum Jülich, ICG-3

Rheo-NMR micro-imaging in natural coordinates

Uri Nevo, Evren Özarslan, Peter J. Basser

Section on Tissue Biophysics and Biomimetics, NICHD, NIH, Bethesda, MD, USA

Abstract:

The Rheo-NMR is a unique device for non-invasive measurement of molecular displacements and spectra under controlled shear conditions [1]. By harnessing advantages of NMR spectroscopc methods and imaging, Rheo-NMR has found important niches in materials sciences and hydrodynamics [1].

An added benefit of Rheo-NMR is in imaging the medium under shear flow. Conventionally, MR images are sampled using a Cartesian k-space trajectory, and reconstructed in a Cartesian framework, (even if sampled in a non-Cartesian way). Here we suggest sampling and reconstructing the Rheo-NMR data in the natural coordinate system defined by the direction of fluid stream-lines, (i.e., cylindrical coordinates for the Couette cell and spherical coordinates for a cone-plate geometry).

In the Couette cell, the k-space samples, $M(k,\phi_k)$, are related to the local magnetization $M(r,\phi_r)$ by the Fourier relation:

$$M(k_r,\phi_k) = \int_{-\infty}^{\infty} dx \int_{-\infty}^{\infty} dy\, M(x,y)\, e^{-i(k_x x + k_y y)} = \int_0^\infty dr\, r \int_0^{2\pi} d\phi_r\, M(r,\phi_r)\, e^{-ikr\cos(\phi_r - \phi_k)}$$

$M(r,\phi_r)$ can be obtained by inversion and by expansion of the exponential factor, such that:

$$M(r,\phi_r) = \sum_{m=-\infty}^{\infty} i^m\, e^{im\phi_r} \int_0^\infty dk\, k\, J_m(kr) \int_0^{2\pi} d\phi_k\, M(k,\phi_k)\, e^{-im\phi_k}$$

where $J_m(kr)$ is the mth-order Bessel function of the first kind. This combined radial sampling and reconstruction scheme is advantageous over the Cartesian framework by providing: (a) similar partial volume artifacts in all voxels, (b) identical angular and linear resolution for all voxels and at all angles, (c) no ghosting artifacts in the velocity plane (no phase-encoding [2]), (d) homogeneous spatial frequency content in r and ϕ, (e) convenient presentation for further analysis. This framework is a particular case of the general concept by which the sampling and reconstruction parameters are uniquely tailored to exploit the specific symmetry, geometry and other characteristics of the sample.
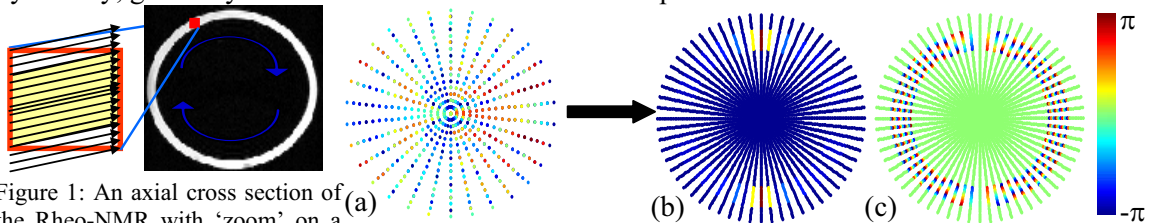

Figure 1: An axial cross section of the Rheo-NMR with 'zoom' on a Cartesian voxel. Notice that the partial volume of different stream-lines depends on the direction of flow within each voxel

Figure 2: Simulation of a micro-imaging experiment of a rotating Rheo-NMR. (a) The sampled cylindrical k-space data. (b) The resulting cylindrical magnitude image, and (c) phase images.

1. Callaghan P.T., Rep. Prog. Phys. 1999, Vol. 62, pp. 599-670.
2. Xia Y., Callaghan P.T., Jeffrey K.R. AICHE Journal 1992, Vol. 38(9), pp. 1408-1420.

On the Observation of (Remote) Anisotropy due to Macroscopic Restrictions

Evren Özarslan[1], Uri Nevo[1] and Peter J. Basser[1]

[1]Section on Tissue Biophysics and Biomimetics, LIMB, NICHD, NIH.

Introduction: Diffusing molecules in the proximity of restrictions are known to cause the 'edge enhancement' effect in NMR imaging [1]. In diffusion-weighted (DW) scans the edge enhancement effect is more pronounced and gives rise to an observable level of anisotropy when the DW acquisition is repeated with the diffusion gradients oriented along different directions. This anisotropy can be exploited to estimate the orientation normal to the nearby boundary [2]. In this work, using a simple geometry of a single infinite plane, we demonstrate that when the voxel is situated sufficiently close to a boundary, the diffusion signal is anisotropic even if the voxel itself contains no structure. The expected behavior is verified experimentally on samples of parallel planes and hollow cylinders. The method can be utilized to infer information from various tissues with macroscopic boundaries such as the cerebral cortex and the colon wall.

Simulations: We consider the geometry on the right, where the gray box depicts a representative voxel near the infinite plane. Starting from the propagator obtained using the method of images, we calculated the magnetization density and the total signal expected from the voxel. In our simulations we employ the following variables:

Fig. 1

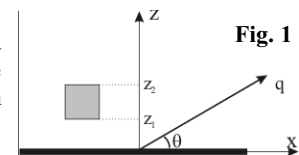$$u = \sqrt{4 D_0 \Delta} \quad , \quad \zeta = \frac{z}{u} \quad , \text{and} \quad \kappa = \pi q u$$
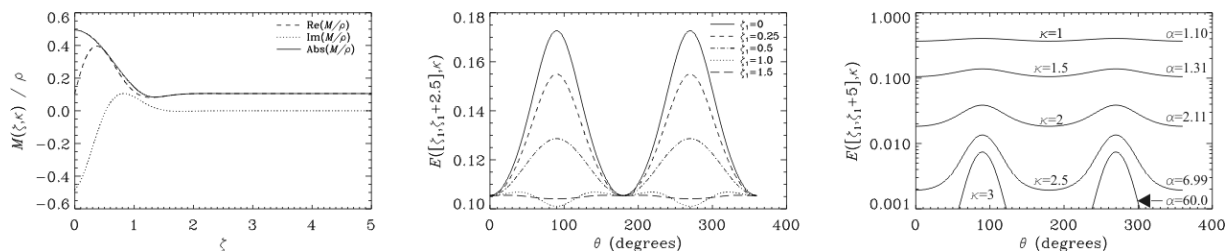

Fig. 2 The magnetization density profiles as a function of the distance from the infinite plane located at $\zeta=0$ with $\kappa=1.5$, $u=0.04$ (left panel). The signal attenuation values as a function of the angle between the infinite plane and the gradient direction (θ) where the length of the voxel along the z-direction ($\zeta_2-\zeta_1$ value) was taken to be 2.5 (middle panel). The signal attenuation values as a function of θ for various levels of diffusion weighting (κ varied between 1 and 3), with $\zeta_1=0$ and $\zeta_2-\zeta_1=5$. Here $\alpha=E(\theta=90°)/E(\theta=0°)$ is a measure of anisotropy (right panel).
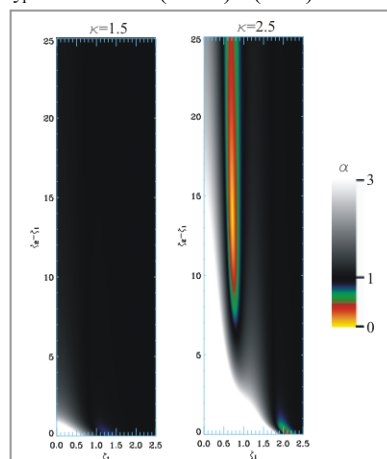

Fig. 3 Note that in the middle panel of Fig. 2, phase cancellations are responsible for E(θ=90°) to be even smaller than the free diffusion attenuation, E(θ=0°), resulting in $\alpha<1$ i.e., the 'edge detraction' effect. The figure above depicts the α values for a variety of ζ_1, $\zeta_2-\zeta_1$ and κ values. It is clear that for smaller values of κ and ζ_1, $\alpha>1$. In this regime, it is expected that the direction along which the signal is greatest is the surface normal.
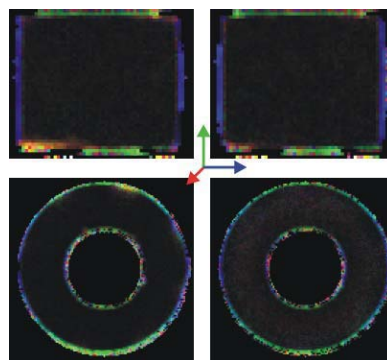

Fig. 4 Color orientation maps computed from the eigenvector of the diffusion tensor associated with the *smallest* eigenvalue hypothesized to yield the direction normal to the nearby boundary.
A cylindrical object with a rectangular void (top) was constructed in-house from Ultem 1000 (Boedeker Plastics Inc., Shiner, TX), whose susceptibility is similar to that of water. The resolution of the image was 78x 312.5μm^2 in-plane; the slice thickness was 1.5mm. Clearly, the eigenvectors in the voxels near the edges are coherently oriented perpendicular to the surface. A hollow cylinder (bottom) was also constructed in-house from Ultem 1000. The resolution of the image was 117x117μm^2 in-plane, and the slice thickness was 1.5mm. The orientation map computed from the third eigenvalue of the tensor accurately revealed the normal vectors on concave as well as convex surfaces.

Conclusion: We have shown that the effect of macroscopic boundaries on the nearby diffusing nuclei may lead to diffusion anisotropy. Further, this anisotropy was shown to be within observable limits.
This different notion of anisotropy can be exploited to infer information regarding the structure of nearby walls. Because many structures in human body (most organs of the GI tract, lungs, blood vessels, etc.) possess macroscopic boundaries, the method may be useful in examining many organs and diseases.

References: [1] Hyslop & Lauterbur, J Magn Reson 1991;94:501-510.
[2] Özarslan, Nevo & Basser, Proc Intl Soc Mag Reson Med, 2007;15:1516.

Charge determination by electrophoresis NMR

Ute Böhme[1] , Ulrich Scheler[,1]

[1] Leibniz Institute of Polymer Research Dresden, Germany

Abstract:

A combination of diffusion and electrophoresis NMR is applied to investigate the charge of molecules and complexes in solution. In the electrophoresis NMR a pulsed DC electric field is applied to the liquid sample simultaneous to the NMR experiment. Pulsed field gradient NMR is applied to monitor displacements from incoherent motion (diffusion) and coherent motion (electrophoresis).

The charge that is found for a protein in solution is significantly smaller, than that calculated or titrated, because during titration the condensed counterions are successively replaced.

As an example of ligand binding to macromolecules the interaction between glutamic acid and a polycation (PDADMAC) has been investigated. The charge of the strong polyelectrolyte is independent of pH, while that of glutamic acid increases by magnitude with pH. When the charge of glutamic acid increases, an increasing fraction binds to the polyelectrolyte, despite the fact, that the acid becomes more hydrophilic at the same time. That proofs, that glutamic acid binds to the polycation only via electrostatic interaction.

Towards the Design of PFG-NMR Experiments for Emulsion Droplet Sizing

T. C. Chandrasekera[1] and M. L. Johns[1]

[1] Magnetic Resonance Research Centre, Department of Chemical Engineering, University of Cambridge, Cambridge, United Kingdom

Abstract:

Emulsions (a dispersion of droplets of one liquid in another immiscible liquid) are found and used in food, biological fluids, agrochemicals, pharmaceuticals and cosmetics. The droplet size distribution of an emulsion is crucial in determining a number of physical attributes of the emulsion including stability.

Self-diffusion measurement using PFG-NMR has been widely used to measure droplet size distributions of emulsions. This method relies on the principle that self-diffusion of the liquid within droplets is restricted, which results in less signal attenuation during a PFG experiment compared to the corresponding pure liquid. This can be interpreted for an emulsion sample using Tikhonov regularisation techniques [1] to render the droplet size distribution. This relies on a mathematical description of the relationship between droplet size and signal attenuation, for which two alternative approximate series expressions are available: The Murday-Cotts equation [2], which assumes a Gaussian Phase Distribution (GPD) during the experiment; and the Short Gradient Pulse (SGP) equation [3,4], which assumes delta-function encoding and decoding gradient pulses. Both options result from the point-source solution of the diffusion equation bounded within a hard sphere, and therefore only differ in the treatment of the NMR phase distribution. Previous random walk simulations of self-diffusion bounded within a sphere have suggested that the true signal variation is more accurately interpreted by the GPD approximation [4], rather than the SGP approximation, in situations where the gradient encoding pulse length (δ) is not much smaller than the observation time (Δ).

This study extends sphere-bounded random walk simulations to yield signal-gradient curves for values of Δ/δ ranging from 1 to 20, repeated for different cases of $\delta D_0/a^2$ (where D_0 is the liquid self-diffusion coefficient and a is the droplet radius) ranging from 0.1 to 1. It is seen that the Gaussian approximation is sensible for $\delta D_0/a^2 < 0.1$, whereas the SGP can be used with comparatively greater accuracy if $\Delta/\delta > 10$. Simulation for enough values of $\delta D_0/a^2$ and Δ/δ can also allow for interpolation of the signal-gradient curve for any case, bypassing the need for either GPD or SGP approximations, and this option is explored. Alternatively, a numerical integration (which approximates the extension of the SGP method previously reported [5,6]) of the propagator solution of the diffusion equation can give sufficiently accurate signal-gradient curves to fit to the experimental data. However, considerations of the accuracy of measurement of D_0 (which will vary considerably with temperature) and the influence of numerical truncation error in calculating the series approximations show that care is required with respect to implementation.

References:
1. K. G. Hollingsworth, M. L. Johns, J. Colloid Interface Sci. **258** (2003) 383-389
2. J. S. Murday, R. M. Cotts, J. Chem. Phys. **48** (1968) 4938-4945
3. P. P. Mitra, P. N. Sen, Phys. Rev. B Condens. Matter **45** (1992) 143-156
4. B. Balinov, B. Jönsson, P. Linse, O. Söderman, J. Magn. Reson. A **104** (1993) 17-25
5. A. Caprihan, L. Z. Wang, E. Fukushima, J. Magn. Reson. A. **118** (1996) 94-102
6. P. T. Callaghan, J. Magn. Reson. **129** (1997) 74-84

Measurement of the spin-spin relaxation time T2 at very low magnetic field by means of the Fast Field Cycling NMR method

G.Ferrante[1], D.Canina[1], E.Bonardi[1], M.Polello[1], C. Vacchi[2], P.Golzi[2]

[1] Stelar s.r.l, via E.Fermi, 4 Mede (PV) Italy
[2] University of Pavia, Department of Electronics – Pavia, Italy

Field Cycling NMR is a reliable and powerful method used so far for measuring the spin-lattice relaxation time T1 at low fields as well as its dependence on the magnetic field strength. Moreover, the Field Cycling NMR is the only technique which allows to extend these measurements down to very low fields, typically close to hearth field or lower.

As far as the spin-spin relaxation time T2 is concerned, it was almost impossible till now to exploit the same advantages offered by the technique because of instrumental limits and the intrinsic problems you get with the acquisition and the accumulation of an echo (compared with the acquisition of an FID) in a fast field cycling experiment.

In this work we present new instrumental concepts and new NMR methods developed exactly on the objective to overcome these limits to allow the acquisition of a Hahn echo decay in the same magnetic field range used in the measurement of a T1 NMRD profile.

In case of experiment with lower S/N systematic errors are introduced. These errors can be removed using suitable acquisition procedures as well as proper weighting functions of the signal and noise during the accumulation process. Several T2 (spin-echo decay) profiles acquired on different samples by means of a Field Cycling Spin-echo experiment are presented and discussed.

Design of an acquisition-reconstruction algorithm for Magnetic Resonance surface Imaging

D. Franchi, A. Sotgiu and G. Placidi

Department of science and Biomedical Technologies, University of L'Aquila, via Vetoio 10, 67100, Coppito, L'Aquila, Italy

Abstract:

MRI surface scanners have been proposed both for spectroscopy and imaging purposes [1-3]. Acquisition-reconstruction techniques depend on the magnetic field shape. We describe an innovative technique for acquisition and reconstruction of images produced by an hand-size MRI surface scanner [3]. The considered magnet was optimized to guarantee field homogeneity in an approximately 20x2x4 mm^3 (x,y,z). The imaging is performed on the (x,y) plane (see Fig. 1a) by applying a single gradient G_x, allowing the acquisition of a 20x2xR mm^3 ROIs, with spatial resolution of $\Delta x=20/N$ mm, $\Delta y=2mm$ and R is the slice thickness along z. The imaging of wider ROIs can be accomplished by placing side by side contiguous strips collected by magnet displacement, but, in this way, the produced images will have low resolution in y direction (see Fig.1b). The proposed acquisition-reconstruction method is based on the acquisition of overlapping strips, distanced by Δy_{new} in order to obtain an improved resolution (Δy_{new}) along the y direction too. The algorithm is the following: **1)** Raw data are collected for all interleaved strips; **2)** Raw data of each interleaved strip are convolved with a localization function (*sinc function*); **3)** Results are added together; **4)** FFT was performed of the resulting matrix; **5)** The final image is obtained by deconvolving the previews image with the PSF due to magnet aperture along y. Figure 1c shows the results of the algorithm applied on a test image (Fig. 1a). The resolution improvement with respect to the image obtained by placing side by side contiguous strips (see Fig. 1b) is clearly evident.
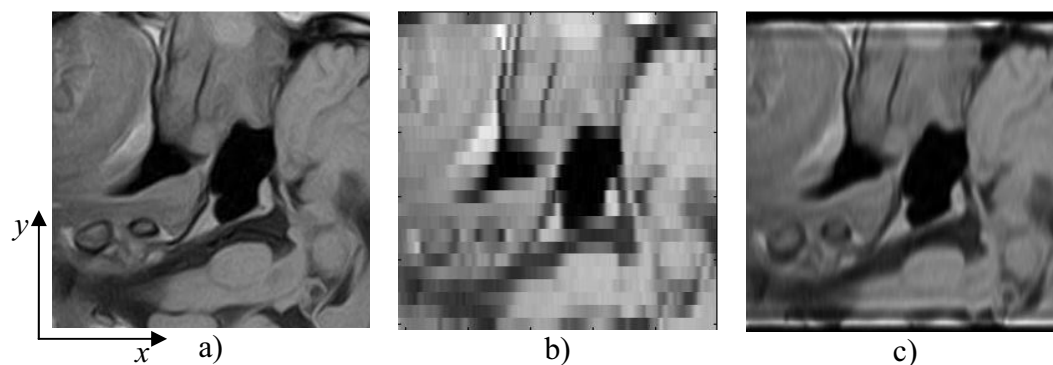
Figure 1: **a)** Test image; **b)** Image obtained by placing side by side contiguous strips; **c)** Reconstructed image obtained with the proposed method.

References:

[1]. G. Eidmann, R. Savelsberg, P. Blümler, And B. Blümich: *"The NMR MOUSE, a Mobile Universal Surface Explorer"*, J. Magn. Reson. A 122 **(1996)** 104-109;

[2]. Wei-Hao Chang, Jyh-Horng Chen and Lian-Pin Hwang: *"Single-sided mobile NMR with a Halbach magnet"*, 24 8 **(2006)** 1095-1102;

[3]. Ciarrocchi M. et al, *"Design of an Elliptical Permanent Magnet for Surface MRI"*, proceedings of the 9th International Conference on Magnetic Resonance Microscopy and 7th Colloquium on Mobile NMR, 3-7 Sept. 2007 (submitted).

Ex Situ Pulse Design and Implementation

J Franck, V Demas, L Bouchard, D Graziani, A Pines

July 31, 2007

Over recent years, researchers have demonstrated various pulse-based methodologies capable of selectively refocusing inhomogeneous evolution. These methods manipulate a very limited set of hardware components to narrow effective linewidths and to recover signal dispersed by imperfect fields. The earliest examples of such pulses manipulated a correlation, or "hardware matching" between RF and static field inhomogeneities to produce the desired correction. Simple composite pulses, like those of Meriles et al.[1], were the first type of pulses applied in such corrective schemes. In search of greater insensitivity to offset, these same authors demonstrated a scaled adiabatic double passage corrective pulse which also utilized hardware matching[2]. Later, Topgaard et al.[4] showed that an adiabatic double passage, coupled with time modulated imaging gradients, could generate similar corrective effects of a more general form. Most recently, Shapira et al.[3] demonstrated similar pulses – based on an adiabatic chirp pulse double passage in the presence of a constant gradient – which also refocus inhomogeneous signal dispersion.

Many of these methods manipulate adiabatic pulses to generate the desired correction. Despite this similarity, until now, no consistent model has successfully reproduced the advantages of these different techniques. We have shown that one can apply elementary approximation methods in the adiabatic limit to generate corrective pulses that exhibit any or all of the benefits of the previous types of pulses. Furthermore, such adiabatic ex-situ echo ("AXE") pulses exhibit specific improvements upon each of the previous methods.

This work includes an explanation of AXE pulse theory, along with experimental demonstrations that such pulses are, in fact, both robust and straightforward to implement.

The hope of acquiring meaningful signal from sample spread out over volumes comparable to the size of the magnet drive the progression of AXE pulses and similar corrective schemes. However, B_1 inhomogeneities complicate the excitation of such volumes. Therefore, we will also discuss the design and implementation of a pulse design method that allows efficient excitation in inhomogeneous fields. This method capitalizes on an RF / static field correlation in order to excite and refocus large volumes in a limited amount of time with limited B_1 power. To accompany this method, we have already demonstrated a new method for accurately mapping out such correlations (see Fig. 2.)

Inverse DESIRE: enhanced apparent longitudinal relaxation in thin excited slices

Achim Gädke[1] and Nikolaus Nestle[1,2]

[1] Institute of Condensed Matter Physics, TU Darmstadt, Darmstadt, Germany
[2] BASF Aktiengesellschaft, Ludwigshafen, Germany

Abstract:

NMR excitation of thin "open" slices is of interest both for conventional NMR microimaging and for mechanically detected magnetic resonance (MDMR). Especially in the latter case, the thickness of the excited slices may be well below 1 μm. In samples containing fast-diffusing components such as liquid water, the "open" (that means unrestricted) diffusive exchange of spin magnetization between such a thin excited slice and the surrounding material outside of the excitation zone on the time scale of the NMR experiments plays a major role [1, 2].

The resonant modulation of the nuclear spin magnetization in MDMR is achieved by periodic excitation schemes with periods in the ms range or less. In conventional NMR microimaging, the recovery times are also kept as short as possible (usually 50 ms to several 100 ms) in order to maximize signal accumulation in a short overall scanning time. In both cases, the diffusion balance between the excited slice and its surroundings becomes more complex as the effects of several excitation cycles have to be taken into account [2]. The resulting enhanced apparent relaxation inside the excited slice is the inverse effect to the Diffusion Enhancement of SIgnal and REsolution (DESIRE) concept suggested for the enhancement of details in NMR microimaging [3,4].

In our contribution, an experimental setup for inductive NMR experiments in a superconducting gradient magnet system with gradient strengths up to 200 T/m [5] will be presented along with the present stage of experimental results. Special experimental challenges include vertical positioning of the sample cells at μm precision relative to the magnetic field gradient and flat coil design for optimal signal filling factor. A novel experimental cell adapted to such a coil design will be shown and experimental options for manipulating diffusion and relaxation properties of the walls and the liquid in the cell while retaining the exact positioning with respect to the magnet will be discussed.

Consequences for further developments in micro-MRI and mechanically detected NMR will be addressed, too.

1. N. Nestle, B. Walaszek, M. Nolte, *Journal of Magnetic Resonance* **168** (2004) 46-52.
2. A. Gädke, N. Nestle, *Diffusion Fundamentals* **3** (2005) 38.1 - 38.12.
3. P.C. Lauterbur, W.B. Hyslop, H.D. Morris. NMR microscopy: old resolutions and new desires, in: XI International Society of Magnetic Resonance Conference, 1992, Vancouver, BC.
4. C.H. Pennington, *Concept. Magn. Res.* **19A** (2003) 71–79.
5. I. Chang, F. Fujara, B. Geil, G. Hinze, H. Sillescu, A. Tölle, *J. Non-Cryst. Sol.* **172-174** (1994) 674.

NMR Data Accumulation in Polar Coordinates Numerical Methods to minimize Systematic Errors

Paolo Golzi[1], Giuseppe Martini[1], Carla Vacchi[1], Davide Canina[2] and Gianni Ferrante[2]

[1] Department of Electronics, University of Pavia, Via Ferrata 1, 27100 Pavia, Italy
[2] Stelar s.r.l., Via Enrico Fermi 4, Mede (PV), Italy

Abstract:

In this paper, we discuss a hardware implementation of numerical methods to minimize Rician noise data contamination effects, during NMR signals magnitude accumulation.

The accumulation of signal magnitudes of NMR data in low signal-to-noise ratio (SNR) regimes produces signal-dependent noise bias that reduces the accuracy of the measurements. This is particularly important for T1 and T2 measurements when the relaxation curve are fitted by a multi-exponential acquisition from polar coordinates. In fact the white noise, with a Gaussian distribution, that affect the NMR signal, become a Rician noise, characterized from the Rayleight distribution, on the accumulated signal magnitudes resulting in a systematic error.

To apply the proposed numerical method we need to: acquire noise parameters such as mean and noise variance, estimate the signal-to-noise ratio and calculate the correction factor with dependences from signal amplitude.

We have developed the correction scheme on a reconfigurable digital hardware architecture, to apply the factor directly over the data-flow on our acquisition channel. In order to estimate noise parameters only a few phantom measures are needed and the technique is applied without any additional or external operation resulting in better than 1% signal correction on our tests.

Further developments are focused about the improved hardware implementation of numerical methods used to calculate the correction factor. We have also proposed a different technique in order to better evaluate SNR dependencies and extract the real signal intensity from noisy magnitude MNR signals. This alternative technique presumes the possibility of measuring the power of the noisy signals.

Several numerical approaches are been proposed in literature to de-noising NMR signals including a non-linear and wavelet transform. This methods are suitable to use in a post-processing process, used in conjunction with our hardware correction technique, becomes a complete tool to compensate and/or remove noise from digitalized NMR signals.

1. Cheng Guan Koay, Peter J. Basser, *Journal of Magnetic Resonance* **179** (2006) 317-322.
2. S.O. Rice, *Bell System Technical Journal - Mathematical Analysis of Random Noise* **23-24** (1944).

Magnetic Field Gradient Waveform Mapping and Shaping

Hui Han, Alexei V. Quriadov, Ziheng Zhang, Bruce J. Balcom

MRI Centre, Department of Physics, University of New Brunswick, Fredericton, N.B, E3B 5A3
Canada

Abstract:

Over the past two decades, great improvements in image resolution and speed have been achieved through improvements in gradient performance, in particular gradient amplitudes and rise times. Fast, high intensity gradients, however, are prone to waveform distortion, which leads to differences between the expected and actual k-space trajectories.

We have developed a method based on Fourier Transform to measure arbitrary magnetic field gradient waveforms. This method, a significant improvement on our previous work [1], is not only sensitive to low amplitude gradients (0.01G/cm~ 1 G/cm), but also can measure medium and high amplitude gradients (1 ~ 120 G/cm, see Fig. 1). A multiple FID point acquisition permits high temporal resolution of the gradient waveform.

Rather than a hardware based pre-emphasis concept, we employ a software compensation strategy to digitally correct the gradient waveforms. This active gradient waveform shaping compensates for the distortion arising in non-shielded gradient coils. As well, since PFG NMR diffusion measurements of short transverse relaxation time species with large gradient amplitudes are corrupted by the residual gradients which arise from eddy currents [2], gradient shaping will reduce this distortion by removing the residual gradients (see Fig. 2).
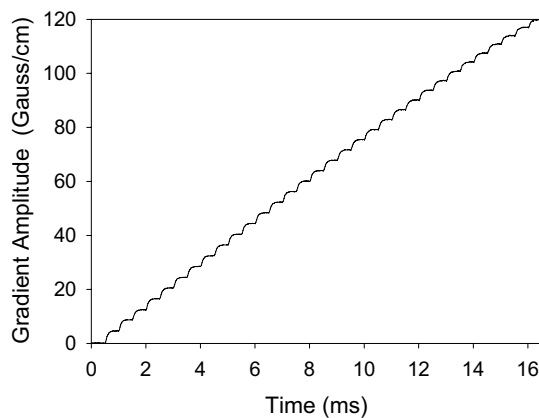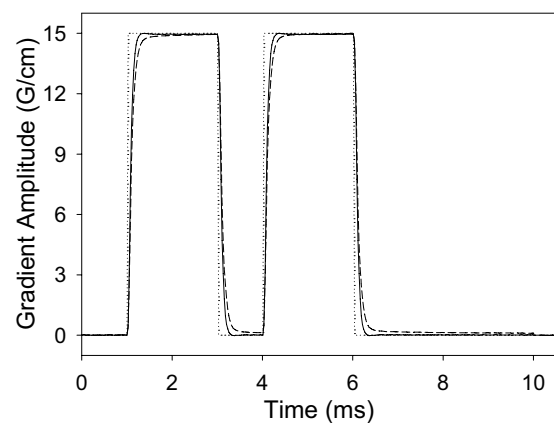
Fig. 1: Measured SPRITE waveform

Fig. 2: Adjusted PFG pulses: ideal (dotted), measured (dashed), shaped (solid)

1. D.J. Goodyear, M. Shea, B.J. Balcom, J. Magn. Reson. **163** (2003) 1-7.

2. E.V. Meerwall, M. Kamat, J. Magn. Reson. **83** (1989) 309-323.

Computation of inter and intra voxel diffusion using MC-simulations in frequency and spatial domain: a comparison

Thomas Kampf[1] , Christian Ziener[1], Xavier Helluy[1], Peter Jakob[1], Wolfgang Bauer[2]

[1]Experimental Physics 5, University of Wuerzburg, Wuerzburg, Germany,
[2]University Hospital, Internal Medicine, University of Wuerzburg, Wuerzburg, Germany

Abstract:

Susceptibility induced dephasing effects permits the detection of few to single iron oxide labeled cells using high resolution gradient echo sequences in MRI. As the voxel size is reduced to a scale below a few hundred microns, diffusion effects become important and significant influence on the signal attenuation caused by the labeled cell is observed [1]. To investigate such signal behavior, numerical simulations which include intra and inter voxel diffusion are required.

Recently Yang et al. [2] introduced a MC simulation of diffusion in the frequency domain [3] to avoid the long computation times of MC simulations in the spatial domain.

In this work we test the correctness and speed of this algorithm and investigate its potential to efficiently distinguish between inter and intra voxel diffusion. Test models are spherical and cylindrical magnetic field inhomogeneities.
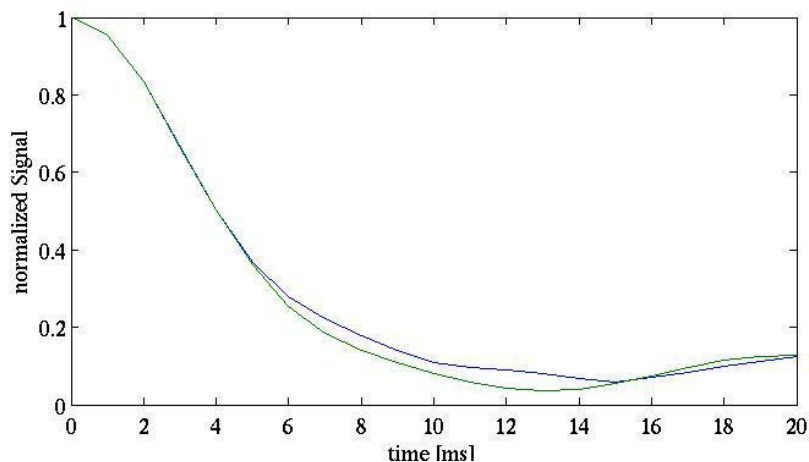
Fig. 1: Simulated time evolution of the signal decay around a capillary: green curve is obtained by MC simulation in spatial domain neglecting inter voxel diffusion, blue curve is obtained by the MC simulation in frequency domain, good agreement between MC simulations in spatial and frequency domain is found. (diffusion coefficient $5 \mu m^2/ms$, voxel size 100x100x100 μm, capillary radius $25 \mu m$, max. off-resonance frequency 2 kHz)

1. T. Wade, C. Heyn, D. Rutt, P.Foster, B. Rutt; Proc. Intl. Soc. Mag. Reson. Med. **14**: 1807 (2006)
2. X. Yang, P. Schmalbrock, M. Boss, B. Clymer, G. Mihai, M. V. Knopp; Proc. Intl. Soc. Mag. Reson. Med. **15**: 1779 (2007)
3. K. Schmidt-Rohr, H.W. Spiess; Multidimensional Solid-State NMR and Polymers Academic Press Ltd. (1994)

Solid state ^{27}Al MRI and its applications.

Khomichev A.V. , Koptyug I.V.

International Tomography Center, Siberian Branch of the Russian Academy of Sciences, Novosibirsk, Russia.

Abstract:

The MRI of rigid solid state samples is considered to be hard to realize using the standard tomographic instrumentation because of short relaxation times and line broadening. However, recently it was shown, that successful solid state MRI experiments using the liquid-phase instrumentation are possible. This clears the way for developing the new area of NMR applications.

One of the main problems on this way is poor signal to noise ratio. This problem can be partially solved by different ways. Specifically, for NMR experiments with quadrupolar nuclei with half-integer spin, we used the adiabatic inversion of the satellite transitions by applying the radiofrequency sweeps. This theoretically can lead to the NMR signal enhancement by the factor of 2I (where I is nuclear spin). For ^{27}Al (I=5/2) NMR experiments we reached the signal enhancement by the factor of 2.

Because of solid state NMR problems, most solid state mass transport observations were made indirectly, by using the liquid-phase NMR. Though, for many applications the direct registration of solid phase NMR signal is essential. In our experiments, the velocity maps of rotating Al_2O_3 powder sample and velocity propagator of freely falling Al_2O_3 powder was registered by the solid state ^{27}Al NMR signal.

One more situation, where direct registration of solid phase NMR signal could be essential is NMR thermometry of heterogeneous catalytic reactions. There is a set of temperature sensitive NMR parameters with known experimental dependence (e.g. ^{27}Al NMR signal intensity). Hence, by solving the inverse problem it is possible to obtain the local temperature maps of the sample. We investigated the hydrogenation of unsaturated hydrocarbons using the Pd/Al_2O_3 catalyst. The temperature maps in this heterogeneous reaction can be obtained by NMR signal registration of the solid phase (Al_2O_3 pellets). We observed prospective ^{27}Al NMR signal temperature dependence, and corresponding inhomogeneous 1D temperature distribution profile, which demonstrates an opportunity to get the 3D local temperature maps in the refined experiments in the future.

1. I.V. Koptyug, A.A. Lysova, A.V. Khomichev, *Magn. Reson. Imaging*, **2007, V. 25**, pp. 545-546.

^{1}H IP-DQF imaging on a clinical MR scanner

S. Kusmia[1], G. Guillot[2]

1-U2R2M UMR8081 CNRS Univ Paris-Sud, CIERM-Hôp Bicetre, 94275 Le Kremlin Bicetre, France
2-U2R2M UMR8081 CNRS-Univ. Paris-Sud, Bât 220, 91405 Orsay, France

MRI with Double-Quantum-Filtering (DQF) is a powerful technique for the characterization of connective tissues, giving information on the degree of order in macromolecules[1-2]. However its implementation on clinical scanners is complex due to the strong hard RF pulses needed, and also to their limited flexibility for sequence programming. We present the first implementation of the in-phase double-quantum filtered (IP-DQF) sequence combined with standard GE imaging on a clinical 1.5 T scanner. MRI combined with DQF has been already demonstrated in clinical scanners, but with a DQF sequence requiring a very short echo time. With the IP-DQF sequence, this constraint can be relaxed, which allows one to get higher spatial resolution. Equation (1) describes the different pulses and delays in the sequence.

$$90°(\phi 1) - \tau/2 - 90°(\phi 2) - t_{DQ} - 90°(\phi 3) - \tau/2 - 90°(\phi 3) - t_{LM} - 90°(\phi 4) – TE – AQ(\phi 5) \quad (1)$$

Images were obtained from a capillary filled with water (1.15 mm diameter) and a latex film rolled into a cylinder (4 mm diameter) to demonstrate the sequence efficiency. A home-made resonator (11.8 mm diameter) was used in combination with the whole-body transmit coil to get hard 90° pulses of 13 µs duration. With the 'research prepulse' available on the scanner (Philips Achieva) the 90° preparation pulses could be applied. Preliminary experiments on a 4.7 T scanner gave the influence of the different delays on the latex spectrum (Fig 1) so as to choose optimal delays (τ 1.8 ms, t_{DQ} 65 µs and t_{LM} 5 ms) in the imaging experiment. ^{1}H GE and DQF images (phase cycle of 32-steps[3], total of 128 acquisitions) of the phantom were taken with identical parameters (Fig 2). Slice selection was applied on the 5th 90° pulse (slice parallel to the resonator). We now plan to apply this method for the *in vivo* characterization of connective tissues (skin, tendon).
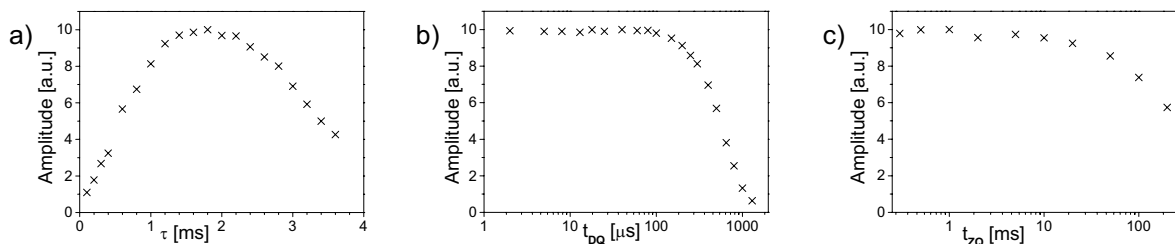
Fig.1. DQF spectrum amplitudes in latex as a function of the different delays: a) τ , b) t_{DQ} and c) t_{LM}.
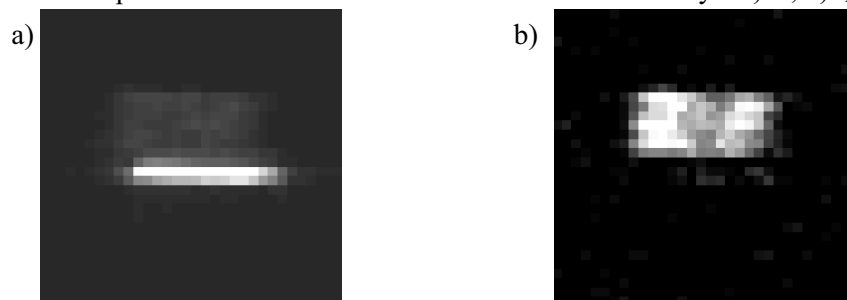
Fig.2. a) GE and b) DQF-MT MR images of a phantom consisting of latex (top) and capillary filled with water (bottom). FOV 16 mm x 16 mm, MTX 32 x 32, TR 1 s, TE 2.2 ms, slice thickness 2 mm

1. R. Fechete, D.E. Demco, B. Blümich J Magn Reson 165 (2003) 9-17
2. G. Navon, U.Eliav, D.E. Demco, B. Blümich J Magn Reson Imaging 25 (2007) 362-380
3. A. Neufeld, U. Eliav, G. Navon Magn Reson Med 50 (2003) 229-234

Evaluating and Avoiding Transient and Permanent Effects of Gradient Pulses on an NMR Permanent Magnet

Dirk Mertens[1,*] and Edme H. Hardy[1]

[1] IMVM, Universität Karlsruhe (TH), 76128 Karlsruhe, Germany

Abstract:

Transportable low-cost NMR systems are applied in an increasing number of industrial as well as research applications [1]. The need of pulsed magnetic-field gradients for the measurement of transport phenomena introduces new challenges on the design of gradient as well as magnet systems.

We already reported a scheme for evaluation of permanent gradients superimposed on the static magnetic field also enabling the determination of gradient pulse mismatch [2].

In our group we work on the development of pulse sequences enabling the evaluation as well as the compensation of effects interfering with the measurement of displacement using pulsed field gradients.

Pulse sequences are based on the PGSE-Massey [3] sequence proposed by Callaghan, an example is shown in fig. 1. The sequence and data analysis allows for the determination of permanent gradients as well as the gradient mismatch. Using the data obtained the problem of varying echo position, phase, and width can be overcome.
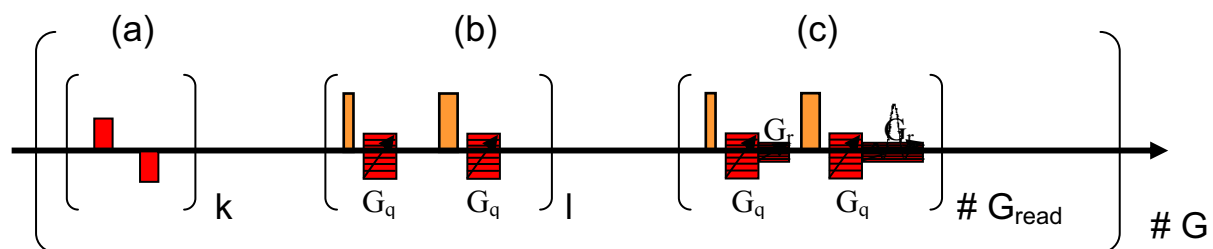
Figure 1 Pulse sequence applied for the evaluation of permanent gradients and gradient mismatch:
a) Gradient pulses of alternating polarity and high amplitude applied k times to set the system to a reproducible state even for following gradient pulses of low aplitude. **b)** Dummy PGSE sequences applied l times to generate a defined permanent gradient on the magnet system. **c)** PGSE Massey sequence using a read gradient G_r varied $\#G_{read}$ times for evaluating permanent and transient gradient effects. The whole sequence is repeated $\#G$ times each time using a different encoding gradient strength G_q.

In the pulse sequence used for the actual measurement of displacements the second PGSE gradient is modified to match the first and a read gradient compensating the permanent gradient is applied. Both corrections depend on the strength of the PGSE gradient.

Further on we design actively shielded gradient systems rendering the need for complex compensation schemes unnecessary therefore speeding up the measurement.
Application to NMR-based capillary rheometry will be presented.

1. DFG Project Hardy Hochstein, HA 2840/4-1
2. CMMR6, Aachen,September 6-8, Poster presentation, „Compensation of Permanent Gradients and PGSE-Gradient Mismatch Generated in a Permanent Magnet"
3. P.T. Callaghan, *J. Magn. Reson*. **88** (1990) 493

*Dirk.Mertens@mvm.uni-karlsruhe.de

Enhanced BOLD Effect with iMQCs at High Fields

Johannes T. Schneider[1], Benjamin Zahneisen[1], Cornelius Faber[1]

Department of Experimental Physics 5, University of Würzburg, Würzburg, Germany

Signal originating from intermolecular multiple-quantum coherences (iMQC) has been demonstrated to show enhanced BOLD effect [1] in fMRI studies in human subjects. The problem of inherently low SNR of iMQC signal is less pronounced at high magnetic fields and can be reduced by the use of a RARE acquisition scheme. For fMRI or oxygenation studies in small animals, iMQC methods potentially provide a suitable alternative to gradient echo methods. We have assessed the BOLD effect in mice at 17.6 T using conventional and iMQC experiments.

Measurements were carried out on a Bruker Avance 750 WB spectrometer at 17.6 T. Breathing gas for spontaneously breathing, anesthetized mice was switched between medical air (21% O_2) and carbogen (95% O_2, 5% CO_2) to achieve different blood oxygenation. The CRAZED sequence [2], selecting signal from iDQC, was combined with a RARE acquisition module [3] with optimized k-space sampling and phase cycling of the refocusing pulses. The timing was chosen to fully refocus magnetization, avoiding T_2^* weighting. iDQC images were obtained with TR=5 s, TE=10.5 ms, RARE-factor 8, averages 4, matrix 32^2, acq-time 1:20 min. For comparison, conventional RARE images (parameters equal to CRAZED but averages 1, acq-time 0:20 min) and GE images (TR=100ms, TE=5ms, acq-time 0:03 min, geometry equal to CRAZED) were acquired. Signal in a ROI in the brain was averaged over five consecutively acquired images before breathing gas was changed.

The optimized CRAZED sequence produced iDQC images with a resolution of (600 μm)^2 and a slice of 2 mm in 1:20 min (Fig. 1), which were suitable to observe the BOLD effect (Fig. 2). Upon gas change, significant signal differences of 5%, 6%, and 3% were observed for CRAZED, FLASH, and RARE images, respectively.

The refocused CRAZED sequence showed more pronounced signal changes than RARE, but smaller changes than observed with FLASH. Since the signal change in CRAZED does not result from T_2^* weighting, it is possible to combine both effects and obtain higher signal changes. CRAZED can be applied, not fully refocusing transverse magnetization, or in combination with a GE read out. Signal changes beyond 10% may become possible, rendering iMQC methods interesting for small animal studies at high magnetic fields.
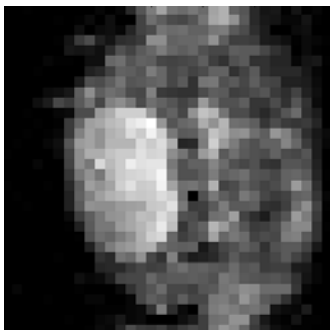

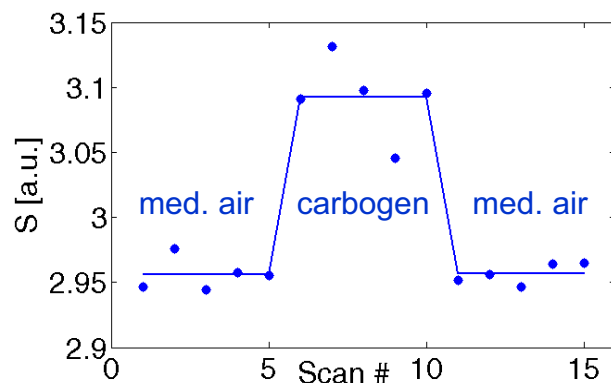Fig. 1: CRAZED image of mouse brain, acquired in 1:20 min (see text for parameters)

Fig. 2: CRAZED-signal of mouse brain; dots: measurement; drawn line: mean of 5 points in each case

1. Ogawa S. et al., *MRM* **14** (1990) 68-78.
2. Warren W. et al., *Science* **265** (1993) 2005-2009.
3. Hennig J. et al., *MRM* **3** (1986) 823-8

A Closer Look into DESIRE for NMR Microscopy

<u>Markus Weiger</u>[1] , Yi Zeng[,1] and Michael Fey[1]

[1] Bruker BioSpin AG, Faellanden, Switzerland

Abstract:

NMR microscopy at a spatial resolution of a few micrometers is not only limited by low SNR due small voxel volumes but also by diffusion effects [1]. Therefore, with conventional Fourier encoding techniques the true spatial resolution is reduced by the associated filtering in *k*-space. Using very strong gradients to overcome this problem leads to a further SNR decrease in case of frequency encoding.

Here, the DESIRE approach (Diffusion Enhancement of SIgnal and REsolution) offers an attractive alternative by utilising diffusion to increase the SNR [2]. Being a real-space imaging method, spatial localisation is accomplished by saturation pulses while diffusion continuously replaces the saturated by unsaturated spins. For this technique a signal enhancement of up to three orders of magnitude has been predicted [3] and initial experimental data have provided a proof of principle [4].

In this work, a detailed investigation of one-dimensional (1D) DESIRE is presented including simulations of a real implementation of the method, a quantitative experimental analysis, and basic 1D imaging. The simulations reveal the importance of carefully ensuring the true spatial resolution of this particular approach and enable the selection of useful experimental parameters. Experimental data were obtained with resolutions down to 3 μm and DESIRE enhancement up to 25 that are in good agreement with the simulation results (Fig. 1). However, 1D images taken from a sharp edge show considerable smoothing of the latter caused by the diffusion being spatially restricted. This observation opens a fundamental discussion about the localisation of the signal acquired with DESIRE imaging, as features of the surrounding area can mitigate the value of the obtained information.
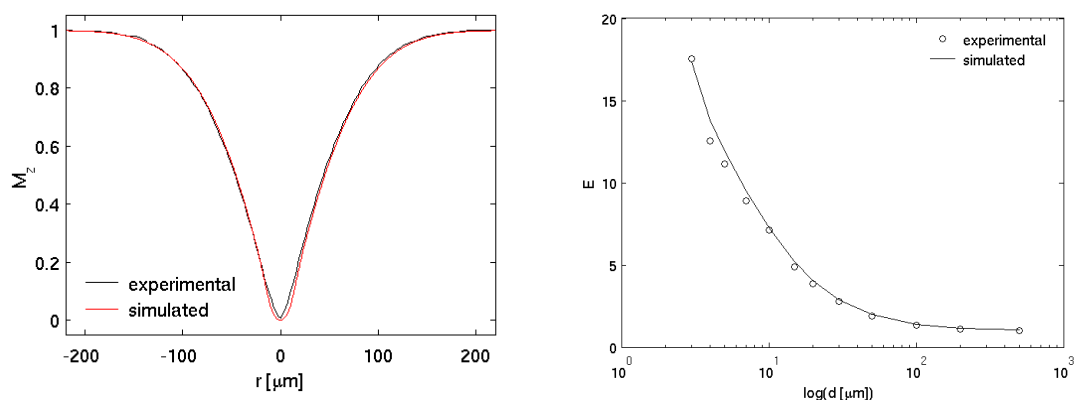
Fig. 1: Measured and simulated DESIRE data. <u>Left:</u> Spatial profiles after a 20 μm DESIRE saturation of 50 pulses applied every 20 msec. <u>Right:</u> DESIRE enhancement E as a function of the spatial resolution d.

1. P.T. Callaghan, C.D. Eccles, *J. Magn. Reson.* **78** (1988) 1-8
2. H.D. Morris, W.B. Hyslop, P.C. Lauterbur, *Proc. Soc. Magn. Reson., San Francisco* (1994) 376
3. C.H. Pennington, *Concept. Magn. Reson.* **19A** (2003) 71-79
4. L. Ciobanu, A.G. Webb, C.H. Pennington, *J. Magn. Reson.* **170** (2004) 252-256

Accurate Spin-Echo Inversion in Imaging with Inhomogeneous B_1 Fields

Klaus Woelk[1] , Emma T. Satterfield[,1] , and Steffen J. Glaser[2]

[1] Department of Chemistry, University of Missouri-Rolla, Rolla, MO 65409, USA
[2] Department Chemie, Technische Universität München, 85747 Garching, Germany

Abstract:

Materials NMR investigations and MR microscopy methods are most often based on spin-echo (SE) techniques. For optimum performance, these SE experiments require accurate in-plane 180° flip angles that invert the magnetization whilst preserving their transverse phase information, i.e., that invert the x to $–x$ magnetization component while the y component stays untouched (or vice versa). Unfortunately, such in-plane inversion pulses are hard to achieve with the strong B_1 gradients of surface coils and toroid cavities [1], or within the fringe field of other, more standard coil geometries. Strong B_1 gradients are generally useful for rotating-frame imaging (RFI) but SE experiments often fail therein or suffer from severe artifacts.

We have applied both conventional and newly developed concepts for SE experiments in strong B_1 gradients and evaluated their performance through T_2-relaxation and molecular-diffusion experiments on polymeric or polymer-stabilized aerogel materials.

In a conventional CPMG sequence, up to half the signal intensity may be lost because of a strong B_1 gradient. Still, accurate T_2 times may be obtained if the experiment is appropriately set up. In a new concept, the RFI capability of B_1 gradients is utilized together with the SE measurement. Magnetization data are spatially resolved along the B_1 gradient (Fig.), and only those data are evaluated for which the flip angle in the SE sequence is effectively ±180°. By synchronizing the RFI sequence with the SE pulses, T_2 relaxation times are measured very accurately and, if desired, spatially resolved. A third concept employs composite pulses that are computer-optimized for the particular coil geometry and the material under investigation. These so-called pattern pulses [2] perform like single 180° pulses in homogeneous B_1 fields; thus, they are directly substituted in the SE sequence.

Since molecular motion is a concern in all of the abovementioned concepts, the influence of diffusion is particularly examined in their application. Other limitations are also assessed.
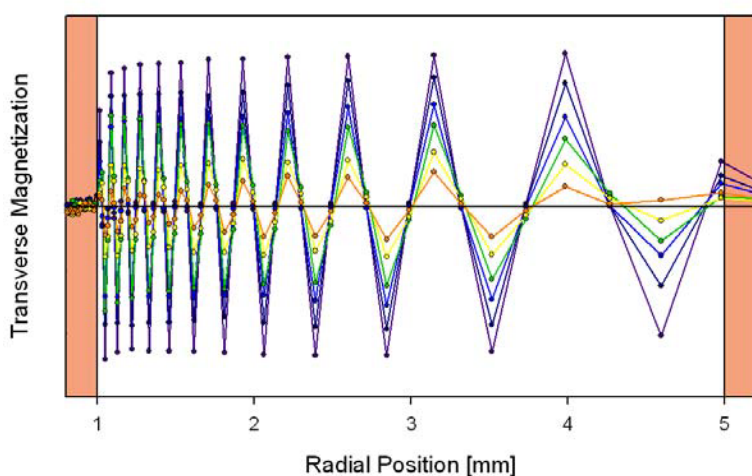
Fig: RFI-SE profiles of polyethylene (MW: 2.5 kg/mol) obtained at 180 °C in the strong B_1 gradient of a toroid cavity probe after different evolution times (1 ms, 3 ms, 5 ms, 7 ms, 9 ms, and 12 ms). Only maxima and minima of the grating profile are evaluated for T_2 relaxation. At these locations, the effective pulse widths in the SE sequence is 180° or -180°, respectively.

1. K. Woelk, J. W. Rathke, and R. J. Klingler, *J. Magn. Reson. A* **109** (1994) 137.
2. K. Kobzar, B. Luy, N. Khaneja, and S. J. Glaser, *J. Magn. Reson.* **173** (2005) 229-235.

Centric Scan MR T_1 Contrast Imaging

Ziheng Zhang[1], Bruce J. Balcom[1]

[1]MRI Centre, Department of Physics, University of New Brunswick, Fredericton, New Brunswick,
Canada E3B 5A3

Abstract:

In MRI, when a sample exhibits multi-component relaxation behavior, image contrast is not easily quantifiable [1]. Additionally, in a magnetization prepared imaging sequence, a short spin-lattice relaxation time, T_1, facilitates a rapid return to equilibrium, which could result in edge enhancement artifacts.

We report a study on two sampling techniques with short trajectories (see figure 1). Radial SPRITE has the shortest interleaves, and is most effective when T_1 is short. Spirally winding interleaved (SWIRL) SPRITE was specifically developed as a more flexible sequence for contrast MRI.

SWIRL SPRITE combines radial and spiral trajectories in a manner similar to TWIRL and WHIRL [2, 3]. Being a SPRITE sequence, however, it isn't affected by gradient slew rate limitations. It is designed to give a higher sampling efficiency with considerable flexibility in resolution.
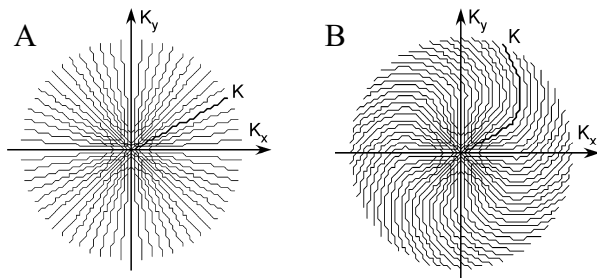
Fig. 1: A: The sampling diagram for Radial SPRITE. B: The sampling diagram for SWIRL SPRITE. The trajectories begin to curve at the jointing point at 16th point.

In this study, we demonstrate that with Radial and SWIRL SPRITE, signal nulling can be achieved with no obvious edge enhancement artifacts provide, $\ln 2 \cdot T_1 \geq (1/2) \cdot T_{acq}$, where T_{acq} is the acquisition time of one interleaf. An application SWIRL SPRITE in suppressing the high spin density species in a hydride-hydrogen is shown below (figure 2).
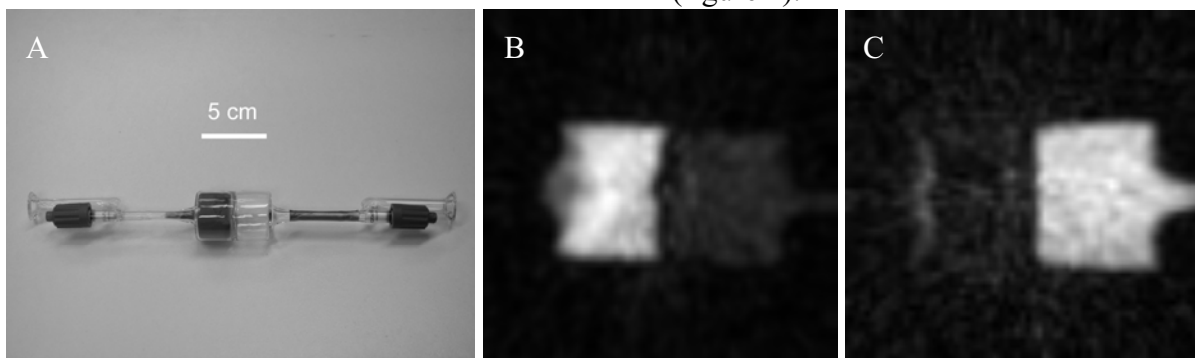
Fig. 2: A: A photograph of a model multi-component system. A specially designed glass chamber was divided into two equal cells with a glass partition. The left hand chamber contains Lithium Aluminum Hydride (LiAlH$_4$) powder, while the right hand chamber hydrogen gas at 1 atmosphere. B: A 2D slices from a 3D SWIRL SPRITE image. The signal from powder is 6 times as strong as the gas, making visualization of the gas difficult. C: The same 2D slice from a 3D SWIRL SPRITE image where the hydride signal has been suppressed. The gas is now clearly visible.

1. E.M. Haacke, et al. Magnetic resonance imaging: physical principles and sequence design, John Wiley & Sons, Inc., 1999.
2. J. I. Jackson, D. G. Nishimura and A. Macovski, Magn. Reson. Med. 25 (1992) 128-139.
3. J.G. Pipe, Magn. Reson. Med. 42 (1999) 714-720.

Diffusion Dependent Frequency Distribution

Christian H. Ziener[1], Thomas Kampf[1], Wolfgang R. Bauer[2], and Peter M. Jakob[1]

[1] Experimental Physics 5, University of Wuerzburg, Wuerzburg, Germany
[2] University Hospital, Internal Medicine, University of Wuerzburg, Wuerzburg, Germany

Abstract:

The aim of this work is to give a rigorous description of magnetic resonance imaging experiments in the presence of field inhomogeneities. Shapes such as cylinders and spheres are often used to describe the signal formation in a capillary network or around magnetically labelled cells. To describe the signal formation process around a field inhomogeneity, a single voxel in which a field inhomogeneity is embedded is considered. The inhomogeneity generates a local frequency ω at different positions in the voxel. The diffusion around the field inhomogeneity is characterised by the correlation time $\tau = L^2/D$, where L is the characteristic length of the field inhomogeneity (in our case, the radius of the sphere or the cylinder), and D is the diffusion coefficient. To extend the results of the static dephasing regime [1,2], the *strong collision approximation* [3] is applied. This approximation interpolates relaxation rates coming from very long (static dephasing regime) and short (motional narrowing regime) correlation times. The inhomogeneity generates a frequency shift on the surface of $\delta\omega \propto \gamma \, \Delta\chi \, B_0$, where η is the volume fraction of material inside the voxel and $\Delta\chi$ is the susceptibility difference between the inhomogeneity and the surrounding tissue. For the diffusion-dependent frequency distribution $p(\omega)$, the following expression can

$$p(\omega) = \frac{\tau}{\pi} \left| \Re \frac{G\left(\frac{1+i\tau\omega}{\eta\,\tau\,\delta\omega}\right) - \eta\, G\left(\frac{1+i\tau\omega}{\tau\,\delta\omega}\right)}{\frac{1-\eta}{\rho_0}(1+i\tau\omega) - G\left(\frac{1+i\tau\omega}{\eta\,\tau\,\delta\omega}\right) + \eta\, G\left(\frac{1+i\tau\omega}{\tau\,\delta\omega}\right)} \right|$$

$$G_S(y) = \frac{1}{3} + \frac{2}{3}\left(1-\frac{2i}{y}\right)\sqrt{\frac{1-iy}{3}}\,\mathrm{arccoth}\sqrt{\frac{1-iy}{3}}$$

$$G_C(y) = \sqrt{1+\frac{1}{y^2}}$$

be written, where the function G depends on the geometry of the field inhomogeneity. For cylinders, the function G_C is obtained, and for spheres, the function G_S. In Figs. 1 and 2, the frequency distribution for cylinders and spheres is shown for different values of the diffusion coefficient D. Using this frequency distribution $p(\omega)$, we are able to describe sequences such as SSFP in the case of capillaries or magnetically labelled cells.
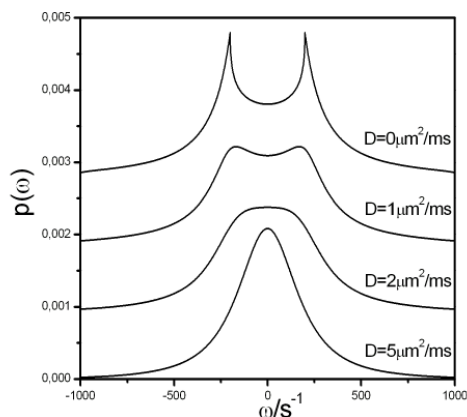

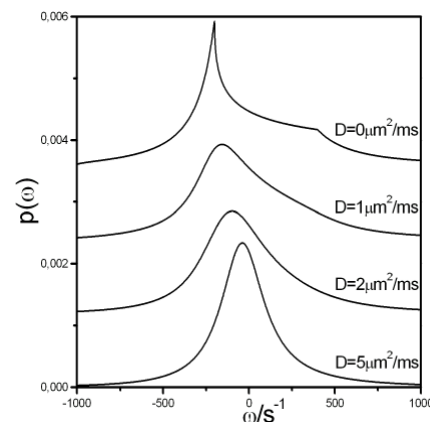Fig. 1: Frequency distribution around a capillary.

Fig. 2: Frequency distribution around a sphere.

1. Ziener CH, Bauer WR, Jakob PM. *Magn. Reson. Mater. Phy.* **18** (2005) 225-230.
2. Cheng YC, Haacke EM, Yu YJ. *Magn. Reson. Imag.* **19** (2001) 1017-1023.
3. Bauer WR, Nadler W. *Phys. Rev. E* **65** (2002) 066123.

NMR of Geophysical Drill Cores with

a Mobile Halbach Magnet

S. Anferova[1], V. Anferov[1], E. Talnishnikh[1], and B. Blümich[1]

[1] RWTH Aachen University, Aachen, Germany

Abstract:

NMR is an analytical method most sensitive to protons of water, oil, and gas. It has become a valuable tool in Oil Well Logging and Geophysics. A particular milestone in mobile NMR for geophysical applications was the development of the Halbach core scanner. The Halbach scanner provides good sensitivity due to a large sensitive volume and a low gradient of the magnetic field. It is light-weight and mobile, which allows nondestructive measurements of the most important core properties at full fluid saturation directly after drilling [1, 2]. Measurements with the Halbach scanner can be related to pore-size distribution and, thus, used for permeability estimation. Moreover, effective porosity of the porous media can be measured directly with the current technique.

Based on the last version of the improved Halbach magnet, a new NMR scanner has been designed and tested for on-line studies of water saturated long cylindrical or semi-cylindrical drill cores with diameters up to 60 mm [3]. The measurement time of porosity at each point of the core is about 30 s. The signal-to-noise ratio of the Halbach scanner is enough to measure porosity values less than 1 %. The Halbach scanner is suitable of demonstrating the principles of non-destructive on-line measurements of porosity at different axial positions along water-saturated large-size IODP drill cores with minimal human interaction and without prior preparation of the core.

The NMR techniques and existing software were refined and extended to provide 2D correlation experiments to probe influence of diffusion on transverse relaxation. A methodology is proposed to estimate permeability from NMR T_2 relaxation data in the presence of internal gradients of the magnetic field in samples with high micro-porosity. PFG experiments were arranged with the same Halbach magnet to evaluate inhomogeneity, tortuosity and anisotropy of the selected sediments.

1. S. Anferova et.al., *Magn.Reson.Eng.,* **23B** (2004) 26-32.
2. J. Arnold et.al., *Petrophysics*, **47** (2006) 306-314.
3. S. Anferova et.al., *MRI*, **25** (2007) 474-480.

Surface effects on the dynamics of molecules confined in core – shell nanocapsules

Ioan Ardelean[1], Mircea Bogdan[2], Adrian Parnau[2,3] and Vasile Pop[1]

[1]Technical University from Cluj-Napoca, Department of Physics, 400020,
Cluj–Napoca, Romania (ioan.ardelean@phys.utcluj.ro)
[2]National R&D Institute for Isotopic and Molecular Technologies,
400293 Cluj–Napoca, Romania
[3]Babeș-Bolyai University, Faculty of Physics, 400084 Cluj-Napoca, Romania

Abstract:

Understanding the surface effects on dynamics of molecules confined in nanocapsules is important both for obtaining of theoretical scientific knowledge and for designing of new nanocapsules to be used in controlled drug delivery [1]. Obtaining of information about the surface effects on confined molecules and the molecular exchange through capsules membrane can be favorably accomplished using nuclear magnetic resonance diffusometry and relaxometry techniques [2].

In our contribution time dependent diffusion studies were performed on miglyol and hexadecane molecules encapsulated in polymeric nanocapsules of different dimension. The nanocapsules were prepared by two different methods based on emulsification – diffusion technique as described in detail in Refs. [3,4]. The diffusion experimental data obtained with a high field instrument (9.4T) using the fringe field stimulated echo (FFStE) technique [5] were compared with those obtained with a low field instrument (0.47 T) by using the well known pulsed field gradient stimulated echo (PFGStE) technique. The proton relaxation data were obtained at 20 MHz using the CPMG technique. The apparent diffusion coefficient extracted from the first part of echoes decay allowed us to evaluate the capsules dimension. The coincidence with the dimension observed from electron micrograph is remarkable. In order to obtain a correct interpretation of the experimental data these were also compared with Monte Carlo simulations.

[1]. V.R. Kumar, J.Pharm. Pharmaceut Sci. **3**, 234(2000)
[2]. C. Mayer, Prog. Nucl. Magn. Reson. Spectroscopy, **40**, 307(2002)
[3]. H.Wassenius, M.Nyden, and B.Vincent, J.Coll.Interf.Sci.**264**, 538(2003)
[4]. D.Quintanar, H.Fessi, E.Allemann, and E.Doelker, Int.J.Pharm.**143**, 133(1996)
[5]. G. Farrher, I. Ardelean, and R. Kimmich, J. Magn. Reson. **182**, 215 (2006)

Spatially Resolved Tracer Distributions in a Rock Core Diffusion Experiment

<u>Bruce Balcom</u>[,1] , Florea Marica[,1] and Tom Al[2]

[1] MRI Centre, University of New Brunswick, Fredericton, Canada
[2] Department of Geology, University of New Brunswick, Fredericton, Canada

Abstract:

A non-invasive MRI method using molecular labelling for measuring transport of H_2O in a stationary D_2O pore-water solution has been presented.

By employing the SPRITE MRI technique, we have performed macroscopic measurements of the spatially resolved diffusion coefficient for water in sandstone cores.

The value of the pore water diffusion coefficient for a representative homogeneous core of calcium silicate was found to be 1.75×10^{-9} m^2/s. This coefficient is independent of the observation time, as it should be in the case of unrestricted diffusion. The results demonstrate that the transport process is well described by the analytical solution of Fick's 2nd law.

The second sample was a heterogeneous bedded Locharbriggs sandstone core. The spatial distribution of water concentration at various diffusion times was obtained based on the spatial distribution of porosity. The highest water concentration, and the regions with the most rapid rates of diffusion are those that also display the highest porosity. The application of a numerical transport model, designed to investigate reactive or non-reactive transport in saturated and unsaturated porous media in partial equilibrium systems, for obtaining the diffusion maps, is in progress.

(a)   (b)
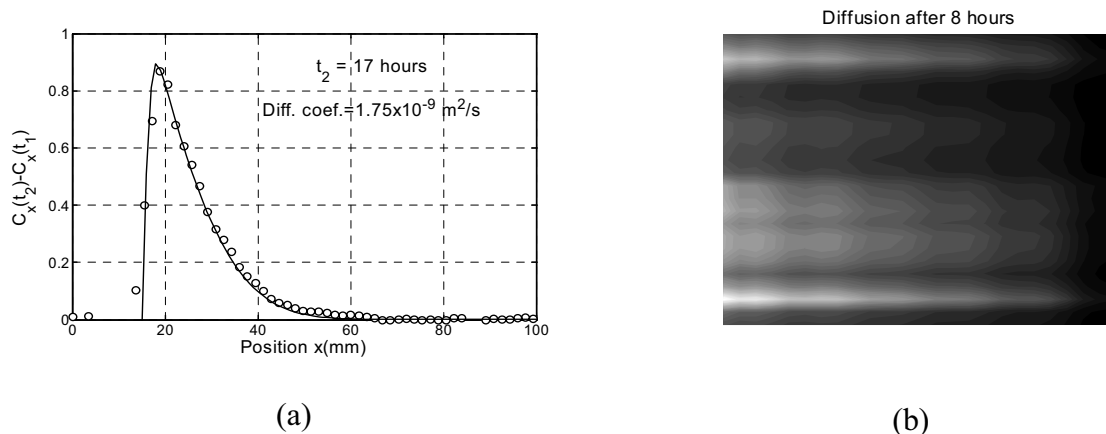
Fig. 1: (a) The difference diffusion ^{1}H MRI profiles acquired after t_2 of 17 hours of H_2O diffusion into a D_2O-saturated calcium silicate and the corresponding analytical fitting curves (continous line). The time reference t_1 was 10 min. (b) A 2D ^{1}H concentration map acquired after 8 hours of H_2O diffusion into a D_2O-saturated Locharbriggs core. The H_2O-filled reservoir (not shown) was placed on the left side.

1. Balcom, B.J. MacGregor, R.P., Beyea, S.D., Green, D.P., Armstrong, R.L., Bremner T.W., *Journal of Magnetic Resonance* **A 123** (1996) 131-134.
2. Marica, F., Chen, Q., Hamilton, A., Hall, C., Al, T., Balcom, B.J., *Journal of Magnetic Resonance* **178** (2006) 136–141.
3. Mayer, K. U., Frind, E. O., and Blowes, D. W., *Water Resour. Res*. **38** (2002) 1174-1187.

NMR relaxation in natural soils: Fast Field Cycling and T_1-T_2 Determination by IR-MEMS

<u>S. Haber-Pohlmeier</u>[1], A. Pohlmeier[2] and S. Stapf[3]

[1] ITMC, RWTH-Aachen, Germany
[2] ICG-4, Research Centre Jülich, Germany
[3] Inst. Physics, Technical University Ilmenau, Germany

Abstract:

Soils are natural porous media of highest importance for food production and sustainment of water resources. For these functions, prominent properties are their ability of water retainment and transport, which are mainly controlled by pore size distribution. The latter is related to NMR relaxation times of water molecules, of which the longitudinal relaxation time can be determined non-invasively by fast-field cycling relaxometry (FFC) and both are obtainable by inversion recovery – multi-echo- imaging (IR-MEMS) methods. The advantage of the FFC method is the determination of the field dependent dispersion of the spin-lattice relaxation rate, whereas MRI at high field is capable of yielding spatially resolved T_1 and T_2 times.

Here we present first results of T_1- relaxation time distributions of water in three natural soils, obtained by the analysis of FFC data by means of the inverse Laplace transformation (CONTIN)[1]. The example in Fig. 1 (Kaldenkirchen soil) shows relatively broad bimodal distribution functions $D(T_1^{-1})$ which shift to higher relaxation rates with increasing relaxation field. These data are compared to spatially resolved T_1- and T_2 distributions, obtained by IR-MEMS. As an example from the same sample, Fig. 2 shows an IR-MEMS image. The obtained intensities vary strongly through the whole sample, although it is visually homogeneous. The next steps consist of the clarification whether the relaxation time distributions are mainly controlled by the surface relaxivities or the pore size distributions.

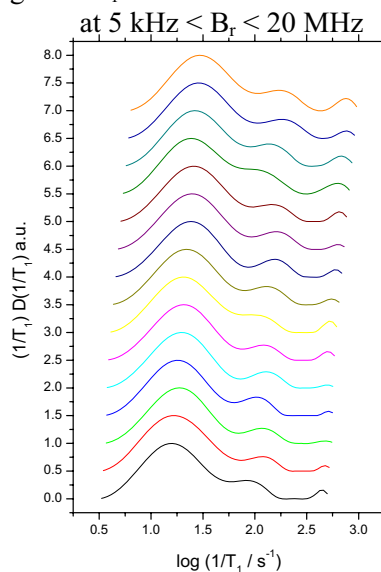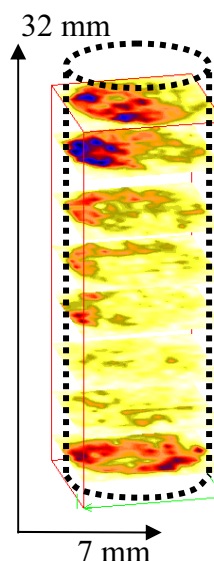Fig. 1: $1/T_1$ relaxation distribution functions at $5\ kHz < B_r < 20\ MHz$

Fig. 2: IR-MEMS image at 300 MHz

Measuring Flow Propagator Moments using DiffTrain

J. Mitchell, A. J. Sederman, E. J. Fordham[1], M. L. Johns, and L. F. Gladden

Department of Chemical Engineering, University of Cambridge, Cambridge, UK.
[1] Schlumberger Cambridge Research Ltd, Cambridge, UK.

Flow propagators [1] are a probability distribution of the displacement ζ of molecules in a flowing fluid and can be acquired with NMR diffusion measurements such as the established alternating pulsed gradient stimulated echo (APGSTE) sequence, or the rapid DiffTrain sequence [2, 3]. The determination of propagators is important in reservoir engineering as the flow of liquids through rocks is a factor in determining the efficiency of oil recovery. Of interest is the advective dispersion of the fluid as this relates to the heterogeneity of the rock structure [4]. In the case of a fluid undergoing Stokes flow through a porous matrix, a relative measure of the advective dispersion can be obtained from a power law relation between the standard deviation σ and mean $\langle\zeta\rangle$ of the displacement [5], i.e. the second and first moments of the propagator. The third moment, or skewness, reveals the progress of the probability distribution as it approaches a Gaussian shape at the asymptotic limit. Rather than sample a full spread of q-space points (where q is the magnitude of the magnetisation wave vector) to reproduce accurately the probability distribution, the moments can be obtained from relatively few sparsely distributed data points around $q = 0$ [4].

A DiffTrain measurement can be used to acquire 8 propagators with 128 q-space points in about 60 minutes; see Fig. 1. The same measurement performed using the APGSTE technique would take in excess of 7 hours. If only the moments are required, the sparse q-space acquisition can be combined with DiffTrain to provide a further reduction in measurement time. In the examples presented, the moments from 8 propagators were obtained from 16 q-space points in under 10 minutes. These rapid techniques will allow for time sensitive measurements, such as dissolution or deposition in rocks and other porous systems.
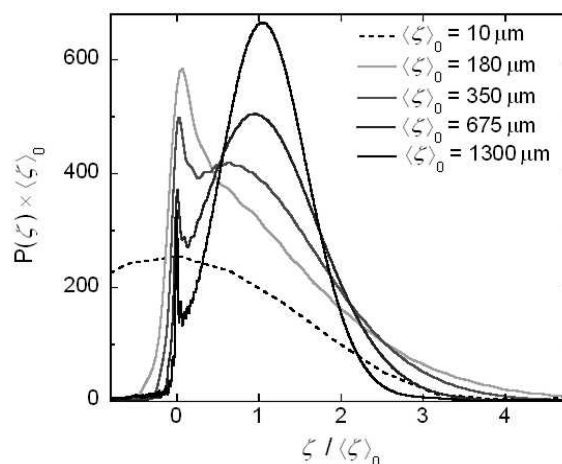
Fig. 1: Flow propagator probability distributions obtained from a single DiffTrain experiment on brine flowing through Bentheimer sandstone, where $\langle\zeta\rangle_0$ is the expected displacement.

1.   J. Karger and W. Heink, *J. Magn. Reson.* **51** (1983) 1-7
2.   J. P. Stamps*, et al.*, *J. Magn. Reson.* **151** (2001) 28-31
3.   C. Buckley*, et al.*, *J. Magn. Reson.* **161** (2003) 112-117
4.   U. M. Scheven*, et al.*, *Phys. Fluids* **17** (2005) 117107
5.   P. G. de Gennes, *J. Fluid Mech.* **136** (1983) 189-200

Ultra-fast quantitative MRI of novel advection-free polysaccharide preparations, retaining high sensitivity to local fluid pressure using gas filled liposomes

<u>R. Morris</u>[1], M. Bencsik[1], N. Nestle[2], A. Vangala[3], Y. Perrie[3]

1 School of Biomedical and Natural Sciences, Nottingham Trent University, UK. **2** BASF Aktiengesellschaft, Ludwigshafen, D.

3 Medicines Research Unit, School of Life and Health Sciences, Aston University, Birmingham, UK.

Abstract:

Until recently, the measurement of the pressure experienced by a porous medium could only be measured with conventional sensors at its surface. In 2001 it was found that the pressure within samples with low permeability could be measured using MRI by saturating them with gas[1]. In 1996 Alexander published a method[2] which utilises gas filled liposomes in a viscous medium to yield contrast to pressure. A similar fluid was then used in 2007 to determine the 3 dimensional pressure within a sandstone like sample[3]. Unfortunately the use of gas filled liposomes is inherently accompanied by a rapid signal drift due to buoyancy driven liposome advection upwards through the fluid as noted in both publications. A method for reducing this advection by using highly viscous polysaccharide gels has been found and tested with MRI. High sensitivity to pressure is retained in such gels as the diffusion of water within the gel matrix is relatively unhindered[4] despite their high viscosity.

The gas filled liposomes are prepared by homogenising an aqueous solution of 1,2-Distearoyl-*sn*-Glycero-3-Phosphocholine (DSPC, C18:0, M_R: 790.16) at standard temperature and pressure [5] which produces a broad size distribution centred around 3μm. These are then suspended at a concentration of 2.5% in 2% polysaccharide gel solutions. Ultra fast EPI-RARE imaging (RARE factor = nb of lines in the image, imaging time < 1s, T_E^{eff} = 144ms) is performed on a system comprised of a multi-well vessel for simultaneous application of identical pressures to 4 individual fluids whilst the pressure is controlled and monitored with a PC connected to a syringe pump and pressure sensors at either side of the vessel. To determine if advection is present, axial images at each pressure are divided by the mean over all pressures. If advection has occurred, a horizontal gradient will appear across the image (see Fig. 1), whereas no gradient is indicative of an advection free preparation (see Fig. 2). By comparing the difference in signal intensities between the two preparations we found that the sensitivity to pressure change around 20% per bar has been preserved whilst advection has been prevented.

This work leads to an entire new range of MRI experiments exploiting rapid quantitative maps of fluid pressure in porous media. The strengths and limitations of the technique will be discussed.
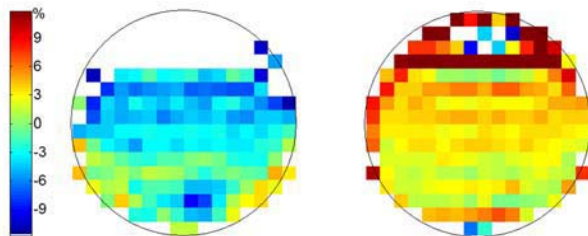
Fig 1: Methyl cellulose at 0.95 and 1.4 bar   Fig 2: Polysaccharide gel at 0.95 and 1.4 bar
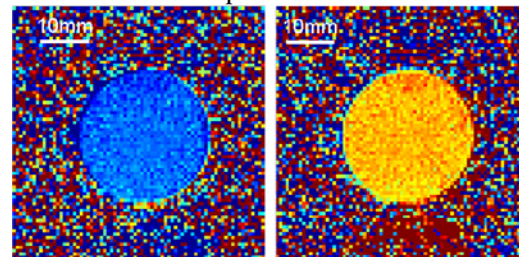
[1] Bencsik M., Ramanathan C., *Magn. Reson. Imaging* **19** (2001) 379-383 **[2]** Alexander A.L. et al., *Mag. Res. Med.* **35** (1996) 801-806 **[3]** Morris R.H. et al., *Magn Reson Imaging,* 25 (2007) 509-512 **[4]** Nestle N, et al. *Proceedings of the 15th European Experimental NMR Conference* (2000) **[5]** Vangala A.K. et al., *Journal of liposome research*, submitted May 20 2007

Pore Geometry from Internal Magnetic Fields. Simulations and Experiments of CPMG Trains

Alexander Sagidullin[1], István Furó[1]

[1] Division of Physical Chemistry and Industrial NMR Centre, KTH – Royal Institute of Technology, Stockholm, Sweden

Abstract:

The echo-time (t_E) dependence of Carr-Parcell-Meiboom-Gill (CPMG) spin-echo decays [1] was experimentally and numerically studied for liquid diffusing in the inhomogeneous magnetic field [2] inside controlled-pore glasses (CPGs). In the two limiting cases of short and long t_E the relaxation curves are, as required [3], close to single-exponential functions. The shape of CPMG decays becomes significantly non-exponential in the intermediate range of echo-times [3, 4]. This latter phenomenon was the subject of our research.

In order to provide a simple but robust measure of the non-exponentiality of CPMG curves we use the function $E_2(t_E) = T_{e2}(t_E)/[2T_e(t_E)]$, where $T_e(t_E)$ and $T_{e2}(t_E)$ are the characteristic times at which the spin-echo amplitude decreases by factors e and e^2, respectively [4]. If the relaxation decay is single-exponential we obtain $E_2 = 1$ from which value we deviate for non-exponential decays. We have found that the E_2-function obtained for water imbibed into CPGs reaches its maximum at t_E^* where the mean-square molecular displacement is on order of two pore diameters. This characteristic was closely reproduced by computer simulations [5] performed for two-dimensional model geometries which closely resembled of that of our porous materials. Thus, CPMG relaxometry of liquids diffusing in the internal magnetic field inside porous solids may, in combination with appropriate numerical simulations, provide information about the morphology of porous networks having pores in the sub-micron range or above.

1. H.Y. Carr, E.M. Parcell, *Phys. Rev.* **94** (1954) 630-638; S. Meiboom, D. Gill, *Rev. Sci. Instrum.* **29** (1958) 688-691
2. D.L. VanderHart, "Magnetic Susceptibility & High resolution NMR of Liquids and Solids", in *Encyclopedia of Nuclear magnetic Resonance*, edited by D.M. Grant and R.K. Harris (John Wiley & Sons, Chichester, 1996), V. 5, 2938-2946; J.F. Schenck, *Med. Phys.* **23** (1996) 815-850
3. G.Q. Zhang, G.J. Hirasaki, *J. Magn. Reson.* **163** (2003) 81-91; L.J. Zielinski, P.N. Sen, *J. Magn. Reson.* **147** (2000) 95-103
4. A.I. Sagidullin, I. Furó, *Magn. Reson. Imag.* **25** (2007) 580-581; V. Skirda, A. Filippov, A. Sagidullin, A. Mutina, R. Archipov, G. Pimenov. "Restricted Diffusion and Molecular Exchange Processes in Porous Media as Studied by Pulsed Field Gradient NMR", in *Fluid Transport in Nanoporous Materials*, edited by W.C. Conner and J. Fraissard, NATO Science Series. Series II: Mathematics, Physics and Chemistry (Springer Netherlands, 2006), 255-278.
5. C. Mayer, *J. Magn. Reson.* **138** (1999) 1-11; C. Mayer, *J. Chem. Phys.* **118** (2003) 2775-2782

NMR measurement of magnetic field correlation function in porous media

H. Cho and Yi-Qiao Song

Schlumberger-Doll Research, Cambridge, MA 02139 USA

Abstract:

In porous and granular media, the structure factor provides fundamental characterization of such materials. Here, we use the pulsed field gradient nuclear magnetic resonance (PFG-NMR) method to demonstrate that the structure factor of the granular and porous media can be approximated by the pair correlation function of the inhomogeneous magnetic field, which arises from the susceptibility difference between the pore filling liquid and the solid matrix.

First, we employ PFG NMR to select spins by their translational diffusion displacement. For this experiment, the effect of the internal field is nullified. Then, we perform a similar experiment but with the internal field effect. The field difference across the displacement causes a signal decay that is related to the magnetic field correlation at that displacement. We show that the method is robust for different grain sizes, diffusion, encoding times and resolution and reliably obtain the surface-to-volume ratio of the sample.
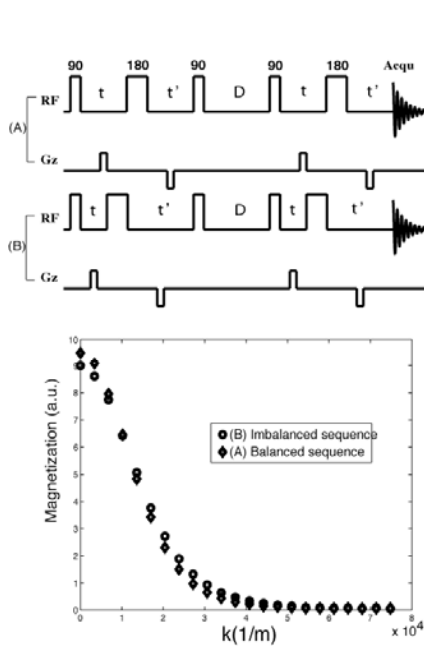
Figure 1: Pulse sequences and raw data.
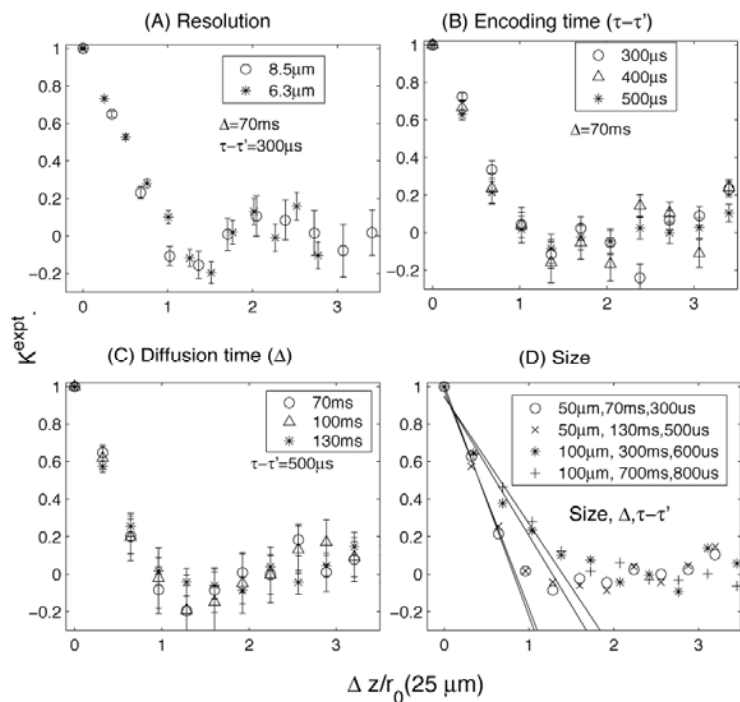
Figure 2: NMR derived field correlation functions for different resolutions, encoding times, diffusion times and grain sizes.

Relaxation Measurements and Water Flux Imaging in Sand/Clay Phantom

L. Stingaciu[1], A. Pohlmeier[1], D.van Dusschoten[2], M.I. Menzel[2], P. Blümler[2], H. Vereecken[1], S. Stapf[3]

[1] Forschungszentrum Jülich, ICG-4, Germany, l.stingaciu@fz-juelich.de
[2] Forschungszentrum Jülich, ICG-3, Germany
[3] Inst. Physics, Technical University Ilmenau, Germany

Abstract

This poster reports two NMR studies at 7 tesla and 0.5 tesla (NMR-CUFF) on model soil samples. First, we determined T_1 and T_2 relaxation times of a number of sand/clay phantoms with different water contents down to 10% relative saturation by means of the IR-CPMG sequence. Bimodal T_2 relaxation processes (T_2 appr. 20 and 200 ms at TE = 1 ms) were observed, which decrease slightly with decreasing water content. T_1 relaxation was monomodal in the range between 1.7 and 1 s. The magnetisation M_0 was found to be proportional to the mean water content in the samples.

In order to map slow and fast water flow in the sample, we imaged water infiltration into a coaxial heterogeneous sand-sand/clay phantom using the 7 tesla scanner and employing a multi-echo-multi-slice (MEMS) sequence.
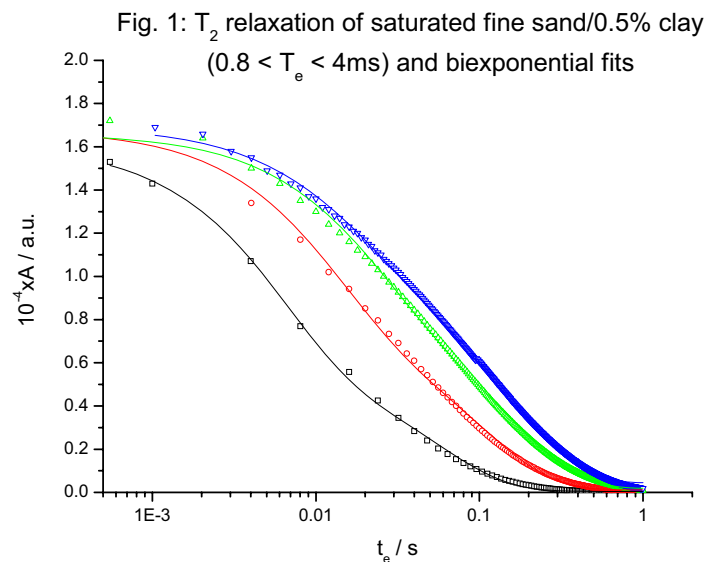
Fig. 1: T_2 relaxation of saturated fine sand/0.5% clay (0.8 < T_e < 4ms) and biexponential fits

NMR diffraction in partially ordered lattices – towards detection of Alzheimer plaques in the brain

Volker Sturm, Faber Cornelius

Dept. of Experimental Physics 5, University of Würzburg, Würzburg, Germany

Abstract:

In periodic structures, NMR diffraction effects can be observed when the nonlinear echo formed by the action of the distant dipolar field (DDF) is detected [1-3]. Such diffraction experiments provide structural information on the lattice, and have been discussed to be useful for the investigation of porous material or trabecular bone. However, theoretical description of signal formation is only available for well defined geometries. Partially ordered structures, such as depositions of Alzheimer plaques in the brain may be detectable through diffraction. Acquisition of global signal greatly enhances the sensitivity of this approach. Here, we investigate the influence of deviations from periodicity in the lattice on diffraction peaks.

Lattice phantoms were realized by arranging glass capillaries (0.7/0.85 mm ID/OD), filled with DMSO, on a Cartesian grid (2.5 mm) inside a 20 mm NMR tube. For negative lattices, empty capillaries were used in a 20 mm NMR tube filled with DMSO. Experiments were performed on a Bruker Avance 750WB spectrometer with a 20 mm birdcage coil. The CRAZED sequence [4] was applied with different values for the coherence selection gradient along the x-axis. Plotting the total signal as a function of the gradient area ($\lambda_m = 2\pi/(\gamma GT)$) diffraction peaks were observed.

Further lattice geometries (3D and deviations from periodicity) were investigated with computer simulations. CRAZED was simulated for different geometries, calculating the DDF in k–space with MATLAB (*ode45 solver*) [5] for a matrix size of (256^2 x 32) representing (20^2 x 10) mm^3.

Results of the simulations reproduced both theoretical predictions and experimental data. Diffraction peaks were observed for both 2D and 3D, in both positive and negative lattices. In perfectly periodic lattices diffraction peaks provided information about the lattice constant and the radius of the lattice points. In lattices with random deviation from the grid positions with a variance of up to (0.7 mm)^2, the major diffraction peak remained observable. Such geometries provide models for tissue with neurodegenerative plaques or scaffolds in tissue engineering, which may become accessible for NMR investigation with the diffraction approach.
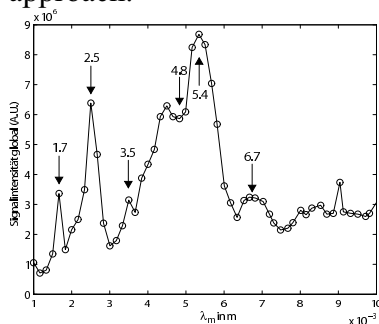
Array of capillaries measured at 17.6 Tesla
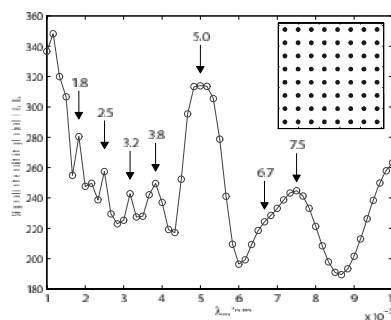
Simulation of the equivalent array
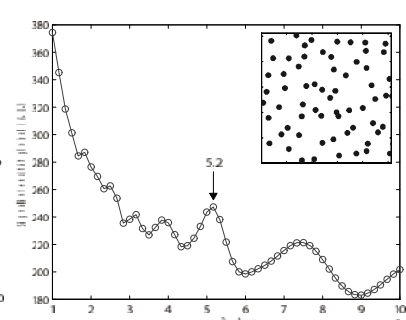
Simulation with variance (0.7mm)^3

[1] de Sousa P.L. et al., *Compt. Rend Chim* **7** (2004).   [2] Tang X.P. et al., *Phys. Lett. A* **326** (2004).
[3] Kirsch S. and Bachert P., *J. Magn. Reson.* **184** (2007). [4] Warren W.S. et al., *Science* **262** (1993).
[5] Enss T. et al., *Chem. Phys. Lett.* **305** (1999).

Investigation of ancient mummies and bones by NMR and CT

Maria Baias[1], Juan Perlo[1], Federico Casanova[1],
Kerstin Münnemann[2], Frank Rühli[3], Bernhard Blümich[1]

[1] Institute for Technical and Macromolecular Chemistry, RWTH-Aachen, Germany
[2] Mainz University Medical School, Department of Radiology, Mainz, Germany
[3] Institute of Anatomy, University of Zürich, Switzerland

The natural glacier mummy Iceman, a mummified recent cadaver, a peruvian mummy, historic mummified body parts, historic bones, and living volunteers have been analyzed by non-invasive, single-sided NMR with the NMR-MOUSE®.

We aquired high-resolution depth profiles and T_2 relaxation curves of the head region of the Iceman mummy *in situ* in the storage room at the Museum and of a cadaver in the hospital. A spatial differentiation of surface ice layer, cutis, and skull bone up to a depth of 5 mm was possible. In ancient Egyptian mummified specimens, the thickness of a fingernail and a differentiation of a single bandage layer versus the skin underneath were possible. Depth profiles were aquired for the head, tibia and suprascapula of a Peruvian mummy as well as different historical tibiae and compared with CT images. A comparison of depth profiles through different foreheads of mummies, skulls, and living people gives strong evidence, that single-sided NMR with the NMR-MOUSE is a non-invasive technique to determine bone density. Our results demonstrate for the first time the feasibility of non-clinical MRI to visualize historic human tissue in a non-invasive approach.

We show for the first time completely non-invasive ^{1}H and ^{23}Na imaging of an ancient Egyptian mummified finger by NMR. Protons could be visualized by NMR only in the tissue close to surface and sodium primarily in the bone, while computer tomography images both, tissue and bone.

References:
Frank Rühli, Thomas Böni, Juan Perlo, Federico Casanova, Maria Baias, Eduard Egarter, Bernhard Blümich, *J. Cult. Heritage* – in press
Kerstin Münnemann, Thomas Böni, Giovanni Colacicco, Bernhard Blümich, Frank Rühli, *Magn. Reson. Imag.* – in press

Unilateral and conventional NMR relaxation studies on hydrating gypsum: Experimental evidence for vapour phase diffusion in strong gradients and signal/noise benefits in a sensor with reduced gradient

Nikolaus Nestle[1], Andrew E. Marble[2], Achim Gädke[3], Rüdiger Völkel[1], Michael Schinabeck[4], Konrad Wutz[4], Klaus Prosiegel[4], Igor Mastikhin[2], Bruce J. Balcom[2]

[1] BASF Aktiengesellschaft, Ludwigshafen, Germany
[2] MRI Centre, University of New Brunswick, Fredericton NB, Canada
[3] Institute of Condensed Matter Physics, TU Darmstadt, Darmstadt, Germany
[4] BASF Construction Chemicals, Trostberg, Germany

Abstract:

Compared to other mineral binders such as Portland cement or geopolymers, gypsum pastes exhibit quite long water transverse relaxation times [1-3]. While the transverse relaxation of the water bound by the actual hydration process is a very short, solid-state type signal (which is very well-fitted for the determination of the degree of hydration from the NMR data), the relaxation times of the remaining liquid water remain in the same order of magnitude throughout the hydration process.

In a series of TD-NMR studies on hydrating gypsum pastes, unilateral NMR data obtained in the relatively strong gradient of a Bruker profiler and conventional NMR results obtained in a homogeneous magnet at 20 MHz were recorded and led to a surprizing and seemingly contradictory result: While the average relaxation time of the water phase in the homogeneous magnet remained almost the same during the first hours of hydration, it was found to decrease by almost a factor of 2 in the unilateral NMR measurements. The hydration degrees extracted from the overall signal amplitudes showed almost the same behaviour for both measurement conditions.

In a third series of experiments, a low-background-gradient magnet with a large sensitive volume was used [4]. With this sensor, the relaxation times found in the liquid phase were well comparable to those in the conventional NMR system, furthermore, the signal/noise ratio was considerably better than in the strong-gradient system.

While conventional liquid phase diffusion effects provide an explanation for the shorter relaxation times found for freshly prepared gypsum pastes in the strong-gradient sensor, they can't explain the further reduction of the relaxation times after the onset of the hydration reaction. For this, much larger diffusion coefficients than in free water would be needed. In recent experiments on partially saturated micrometer porosity model materials, a strong increase of the self-diffusion coefficients due to vapour phase diffusion was reported [5]. Our experimental findings suggest that this effect is responsible for the decreasing relaxation rates in the hydrating gypsum, too.

1. H. Jaffel, J.P. Korb, J.P. Ndobo-Epoy, V. Morin, Guicquero, *J. Phys. Chem. B* 110 (2006) 7385-7391.
2. J. Boguszynska, M.C.A: Brown, P.J. McDonald, J. Mitchell, M. Mulheron, J. Tritt-Goc, D.A. Verganelakis *Cement and Concrete Research* **35** (2006) 2033 – 2040.
3. N. Nestle *Re/views in Environmental Biotechnology* **1** (2002) 215-225.
4. A.E. Marble, I.V. Mastikhin, B.G. Colpitts, B.J. Balcom *Journal of Magnetic Resonance* **186** (2007) 100-104.
5. I. Ardelean, G. Farrher, C. Mattea, R. Kimmich 2005 Magnetic Resonance Imaging 23 (2005) 285–289

Study of Aging Process in Polyethylene

Alina Adams[1], Annemarie Piechatzek[2], Michael Adams[1], Crisan Popescu [3], and Bernhard Blümich[1]

[1]Institute for Macromolecular Chemistry, Aachen University of Technology, Worringerweg 1, D-52074 Aachen, Germany

[2]University of Applied Science, Frauenstuhlweg 31, D-58644 Iserlohn, Germany

[3]Deutsches Wollforschungsinstitut an der RWTH Aachen e.V., Pauwelsstraße 8 D-52056 Aachen, Germany

In the present work we investigate the changes in microscopic and macroscopic properties of a special grade of silane crosslinked polyethylene PEXb during accelerated aging by a combination of analytical and physical methods. This material is intended to be used for pipeline applications and therefore the study of the time-dependent behaviour of its properties under defined conditions is of fundamental importance for determining the origin of potential failure. Accelerated aging was induced at 60^0C and 24 bar pressure in contact with different media such as methanol and oil for a time of up to several months. In a first step, the changes in the microscopic properties were followed by high- and low-field NMR measurements. Whereas the high-field measurements allow the detection of degradation products by ^{13}C spectroscopy, the low-field NMR experiments were conducted with an NMR-MOUSE® (Nuclear Magnetic Resonance **MO**bile **U**niversal **S**urface **E**xplorer) to investigate the polymer morphology in a non-destructive way. The changes in phase composition, chain dynamics, and fluid uptake were followed as a function of the aging time. The NMR results were correlated with DSC measurements from which the crystallinity and the melting temperature were estimated. Changes in crosslink density were evaluated according to DIN EN 579, and variations in material density and elongation at break measured. The time-dependence of the microscopic and macroscopic properties are analyzed towards a better understanding of the aging process of this class of materials. The presented results demonstrate that a simple and low cost device as the NMR-MOUSE® can be used for state assessment of polyethylene pipes.

Studies on Hydration of Leather: One and Two Dimensional NMR using Mobile NMR MOUSE[®]

N. N. Fathima[1], M. Bais[2], E. Talnishnikh[2], T. Ramsami[1], and B. Blümich[2]

[1] Central Leather Research Institute, Chennai, India
[2] RWTH Aachen University, Aachen, Germany

Abstract:

Leather is a commodity, which connects the common man to fashion world. The uniqueness of leather stems from its pore structure and connectivity. Collagen is the main leather making protein. Raw hide/skin is converted into leather after treating with small molecules known as 'tanning agents'. The way the skin interacts with various tanning agents differs. This also leads to changes in the final properties of the leathers. Three different and widely used tanning agents namely chromium, polyphenols and aldehyde have been employed in this study. The changes brought about by these small molecules in the hydration structure of leather have been studied using Nuclear Magnetic Resonance (NMR) relaxometry, which is a non-invasive technique and offers an opportunity to gain insights into the hydration network of leather.

Both 1D and 2D NMR measurements on wet and dry leather samples treated with chromium, polyphenols and aldehyde were studied using mobile NMR (NMR MOUSE)[®]. Magnetisation was measured using inversion recovery and CPMG for T_1 and T_2 in 1D, respectively. The multidimensional NMR relaxation measurements were measured using 2D T_1- T_2 correlation. The 2D distribution map was obtained by 2D inverse Laplace transformation. The T_1 and T_2 relaxation measurements show the existence of two or more different types of water molecules i.e. the bound, free and the intermediate water. It has been found that water molecules exist in a continuum than as separate distinct entities. The influence of the small molecules on the T_1 and T_2 relaxation is well characterised. Deeper insight into the hydration network of leather was obtained using 2D experiments.

Relaxation Anisotropy of Tendon and Strained Rubber

A. Blümich, B.Blümich

Institute of Technical and Macromolecular Chemistry RWTH Aachen University, Germany

Abstract:
Single-sided NMR sensors with the field parallel to the surface are well suited to study angle dependences of NMR parameters in large objects, in particular of relaxation rates, which are difficult to study by conventional medical MRI as the patient is difficult to reorient perpendicular to the magnet axis [1].

Tendon

Tendon is a high performance biological material of exceptional strength with a high degree of macroscopic molecular order. It consists mainly of collagen triple helices which are arranged in bundles in a hierarchical structure with crimps and twists to provide optimum mechanical stability [2].

The anisotropy of human Achilles tendon was studied *in vivo* and compared to that of sheep Achilles tendon and a rat tail [3]. To account for the crimps and twists in the collagen fibrils, a weighted sum of two second order Legendre polynomials phase shifted by 90° was used [4],

$$1/T_{2\text{eff}} = 1/ T_{2\text{eff},0} \{C + [½(3\cos^2(\theta) - 1)]^2 + R (C + [½(3\cos^2(\theta + 90°) - 1)]^2)\}.$$

The weight C of the isotropic relaxation rate is the larger, the more disordered tissue is in the sensitive volume. Interestingly, both, the rat tail and the sheep Achilles tendon can be fitted reasonably well with a predominantly uniaxial fiber orientation as the R values are low while the anisotropy pattern of the human Achilles tendon is much more star like and is biaxial with both orthogonal orientations nearly equally populated ($R = 1.2$). A possible explanation is that the tendon structure has changed upon sacrificing the animals.

Strain

Multi-quantum coherences can be generated in elastomer networks, because a residual dipolar interaction between neighboring spins in the chain remains due to the anisotropic motion of the chain segments between the cross-links. The residual dipolar interaction also defines the relaxation times. All kinds of relaxation rates and multi-quantum signals in strained samples depend on the orientation angle θ of the magnetic field $\boldsymbol{B}_0$ with respect to the strain direction $\boldsymbol{n}$ similar to the transverse relaxation rate of tendon and can be measured with the NMR-MOUSE [5, 6]. The anisotropic transverse relaxation rate can be fitted by a distribution $P(\theta)$ of second order Legendre Polynomials,

$$R_{2\text{eff}}(\theta) = R_{2\text{eff,iso}} + R_{2\text{eff,aniso}} \int P(\theta\text{-}\theta') [(3 \cos^2\theta' - 1)/2]^2 \, d\theta'$$

With increasing sample elongation Λ, the orientation distribution of chain segments narrows and the angular dependence of the transverse relaxation rate $R_{2\text{eff}} = 1/T_{2\text{eff}}$ becomes more pronounced [7]. The dependences of the isotropic and anisotropic relaxation rates on elongation Λ are approximately linear for natural rubber (NR), but change differently in the vicinity of $\Lambda = 3$, where NR is known to crystallize reminiscent of second and first order phase transitions, respectively.

1. G. Eidmann, R. Savelsberg, P. Blümler, B. Blümich, J. Magn. Reson. A122 (1996) 104-109.
2. J. Kastelic, A. Galeski, E. Baer, Connective Tissue Research 6 (1978) 11-23.
3. G. Navon, U. Eliav, D.E. Demco, B. Blümich, Magn. Reson. Imag. 25 (2007) 362-380.
4. Y. Xia, Magn. Reson. Med. 39 (1998) 941-949.
5. A. Wiesmath, C. Filip, D.E. Demco, B. Blümich, J. Magn. Reson. 149 (2001) 258-263.
6. A. Wiesmath, C. Filip, D.E. Demco, B. Blümich, J. Magn. Reson. 154 (2002) 60–72.
7. K. Hailu, R. Fechete, D.E. Demco, B. Blümich, Solid State Nucl. Magn. Reson. 22 (2002) 327–343.

Mobilization of Drug and Polymer During Dissolution of Pharmaceutical Tablets

Carina Dahlberg [1,3], Anna Fureby [1], Michael Schuleit [2], Sergey V. Dvinskikh [3], István Furó [3]

[1] YKI, Institute for Surface Chemistry, Stockholm, Sweden
[2] Novartis Pharma AG, Pharmaceutical and Analytical Development, Basel, Switzerland
[3] Division of Physical Chemistry and Industrial NMR Centre, Department of Chemistry, Royal Institute of Technology, Stockholm, Sweden

Abstract:
Designing controlled release systems with desired properties demands an understanding of molecular factors affecting the release profile. Here we present our observations with nuclear magnetic resonance (NMR) microimaging which reveal *in situ* the swelling behaviour of tablets prepared from a hydrophilic polymer, commonly used in controlled delivery systems, when exposed to water. In parallel, ^{1}H NMR spectroscopy provided the concentration of the drug released into the aqueous phase above the swelling tablet. The novelty of this work is that, by using deuterated water and a one-dimensional constant time imaging (CTI) sequence, the spatial distribution and molecular dynamics of the polymer carrier and their kinetics during swelling could be observed selectively and in parallel to drug release. The ability of monitoring those two processes using the same experimental setup has important advantages when evaluating the drug-polymer-solvent interactions and their affects on drug release on a molecular scale.

The evolution of the distribution and hydration of the polymers is illustrated by images recorded as the tablets undergo D_2O penetration, see Fig.1. As the polymers hydrate, their molecular mobility increases, resulting in higher image intensity. The release occurred at a similar rate as the swelling, suggesting that the rate-determining step of release is the polymer swelling. The different NMR parameters such as ^{1}H density, and T_1 and T_2 relaxation times contributing to the image density can also be deconvoluted into distinct profiles allowing one to obtain more accurate information about penetration kinetics and about polymer dynamical regimes arising with increasing hydration.
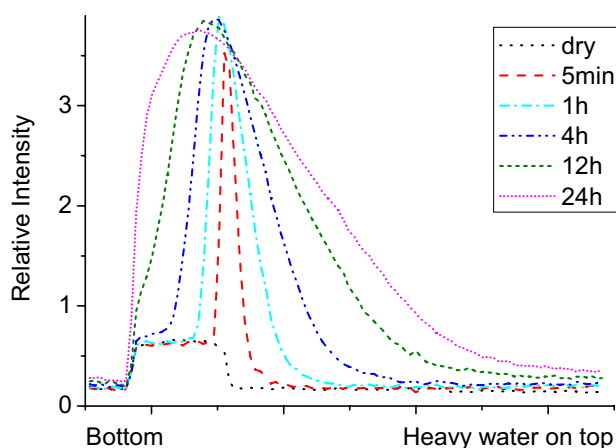
Fig. 1: 1D ^{1}H images illustrating the evolution of the distribution of the hydrated and therefore mobilized hydroxypropyl methylcellulose polymers during the swelling process of a tablet undergoing D_2O penetration from the top. The polymer profiles are shown for different times after the initiation of hydration.

NMR cryoporometry and imaging of swelling clays

Sergey V. Dvinskikh, Oleg V. Petrov and István Furó

Division of Physical Chemistry and Industrial NMR Centre, Department of Chemistry, Royal Institute of Technology, Stockholm, Sweden

Abstract:

Compacted bentonite is attracting attention as cut-off wall material to build in-ground barriers for the encapsulation of radioactive waste. As such it must have suitable swelling characteristics and is expected to fill up the space between material and surrounding ground by swelling. In the present study the swelling properties of bentonite clays of different compositions and compactness are studied by using magnetic resonance imaging.

The MR images recorded during swelling on the time scale from seconds to days can be contributed either by water molecules originally present in dry clay or by the added water. In addition to conventional imaging of water density, images with dynamic contrast were acquired to evaluate the spatial variation of the molecular mobility of water. Dynamic contrast was introduced by implementing T_1 and T_2 relaxation time filters. Solid-state imaging techniques, such as CTI (constant time imaging [1]), also modified to accommodate for dynamic filters, were applied as they allow for acquiring images of both immobilized and mobile water molecules.

During swelling, the clay expands by adsorbing water into the interlayers of bentonite particles and also fills possible voids between the particles. To characterize the porosity of the bentonites of different compactness a cryoporometric study [2] has also been performed.

[1] S. Emid, J. H. N. Creyghton. *Physica*, **128B**, (1985) 81-83.
[2] J. H. Strange, M. Rahman, E. G. Smith, *Phys. Rev. Lett.* **71**, (1993) 3589.

Determination of load influenced mean collagen fiber orientation by means of NMR microscopy

Nikita Garnov[1], Wilfried Gründer[1]

[1] Institute of Medical Physics and Biophysics, University of Leipzig, Germany

Abstract:

Collagen, a fiber protein, is one of the major constituents of cartilage. It forms a three-dimensional network and thus lends the cartilage form, stability and (in conjunction with the water absorbing ability of the charged proteoglycans of the cartilage matrix) tensile strength and resistance to shear forces. These special properties are substantially influenced by the spatial organization of the collagen fibers.

Imbalances between load and resilience may cause cartilage degradation and the development of osteoarthritis. As a result, morphological and structural alteration occur, leading to drastic changes in viscoelastic properties and progressive cartilage destruction. Thus, non-invasive techniques able to evaluate intracartilagenous structures and elastic cartilage properties can be an essential tool for a diagnosis of early arthritic changes.

Recently it has been shown that MRI is potentially suited to detect collageneous cartilage structures and their load-influenced and age-related or arthritic changes. Based on NMR microscopic data, new methods of MRI for quantitative assessment of collagen structuring and intracartilagenous load distribution was proposed [1]. Alternatively to the determination of mechanical parameters from cartilage deformation, these methods use MR intensity changes caused by alteration of the mean fiber orientation under pressure (Fig.1). Here we demonstrate that the variation of the mean fiber orientation of the collageneous network could be determined from load influenced MR intensity variations.
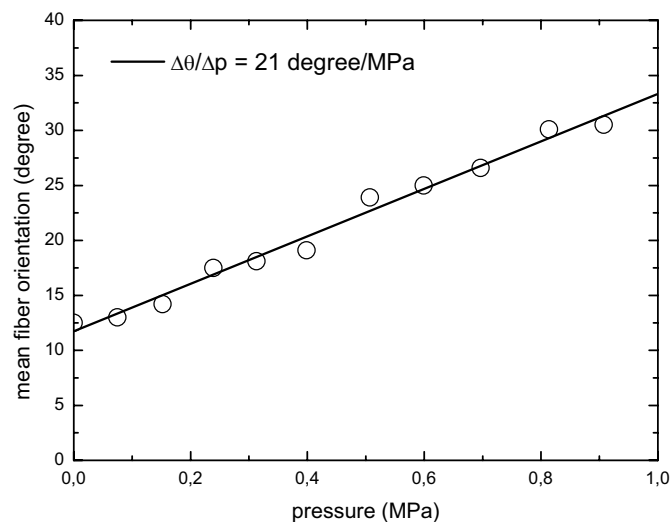
Fig.1: Change of mean fiber orientation under pressure

1. Gründer W, *NMR Biomed.* **19** (2006) 855-876.

Surface UV aging of elastomers investigated with microscopic resolution by single-sided NMR

N. O. Goga, D. E. Demco, J. Kolz, R. Ferencz, F. Casanova, and B. Blümich

Institut für Technische Chemie und Makromolekulare Chemie, Rheinisch-Westfälische Technische Hochschule, Worringerweg 1, D-52072 Aachen, Germany

Abstract:

Depth profiles taken from the surface of UV-irradiated natural rubber have been measured with microscopic resolution using a high-precision-profile NMR-MOUSE®. An NMR observable related to the sum of the spin echoes in the Carr-Purcell-Meiboom-Gill pulse sequence was used to characterize the cross-link density changes produced by the action of UV radiation at each position along the depth direction. The aging process was investigated as function of the irradiation time and penetration depth (Fig. 1). An exponential attenuation law with an exponentially varying space dependent absorption coefficient describes the change in the NMR observable with penetration depth. An Avrami-like model is used for the first time to describe the dependence of the absorption coefficient on the aging time. The method can be applied to investigate the effect of other aging agents on the surfaces of elastomers.
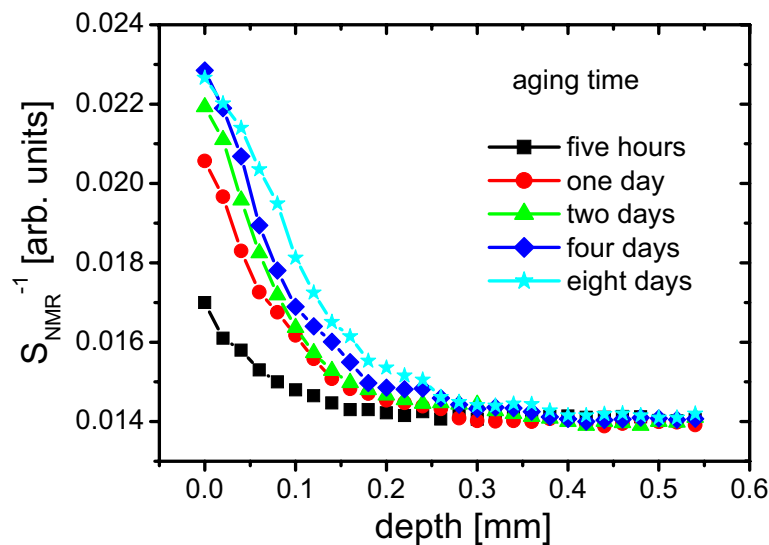
Fig. 1. The inverse sum of the echoes as a function of depth for different aging times.

Water percolation studied in hydrogel filled elastomer matrices using fast imaging techniques

Katharina Hunger[1] , Jürgen Kolz[,1,2], Thomas Mang[2], and Bernhard Blümich[1]

[1] Institute for Technical and Macromolecular Chemistry, RWTH Aachen, Germany
[2] Institute for Applied Polymer Chemistry, FH Aachen, Germany

Abstract:

Besides their use as smart polymers in pharmaceutical and biomedical applications hydrogels are used as absorbers in sanitary products and sealing materials, due to their ability to absorb tremendous amounts of water. Sealing rubber bands, which are used to seal buildings from pressing ground water, consist of an elastomer foam matrix in whose pores crosslinked polyacrylate particles are embedded. When exposed to water the hydrogel particles inside the foam matrix start to swell resulting in an overall extension of the elastomer foam. However, this only happens when the amount of polyacrylate incorporated into the rubber matrix is high enough. This observation led to the assumption, that a critical concentration exists, above which percolation clusters can be formed, that are big enough to achieve an overall swelling of the rubber band. The aim of this work is to study the effect of the hydrogel concentration on the swelling behaviour of the rubber band, as well as the visualization of the percolation pathways using fast magnetic resonance imaging techniques. Furthermore the swelling behaviour is investigated for different pH-values to take the variable environments that can appear under field conditions into account.

For this purpose a set of polymer foams containing different amounts of polyacrylate hydrogels were prepared. Cylindric samples were put in a 10 mm tube and treated with water and solutions of hydrochloric acid and sodium hydroxide. Since samples and tube had the same diameter, the liquid only could invade the sample from one side. Also, the swelling was restricted through the tube walls in x- and y-direction, but unrestricted in the z-direction. The ingress of the water was followed using a 3D-RARE [1] sequence of 30 minutes duration with a resolution of 190*160*160 μm^3.

The experiments show that percolation channels can be visualized by fast imaging techniques. Furthermore the growth of pore clusters could be followed, as well as their combination with clusters in their immediate vicinity. The speed of swelling depends on the hydrogel concentration as well as on the pH of the swelling medium. The sample with the highest amount of hydrogel was almost completely swollen after 12 hours, while the other samples still had a dry core. The presumption, that a higher amount of hydrogel increases the speed of the swelling, could be corroborated. The influence of the pH was investigated by swelling one sample with water, HCl and NaOH. The swelling with HCl was the fastest, the swelling with NaOH the slowest. The difference in pH leads to a different concentration of ionized carboxylate groups in the hydrogel. Less ionized carboxylate groups lead to a smaller repulsion of the polymer chains, the swelling gets slower.

1.   Hennig et al, *Magnetic resonance in medicine* **3** (1986) 823-833.

Investigation of water dynamics and diffusion processes in polyacrylate hydrogels using low-field NMR techniques

Jürgen Kolz[1,2], Katharina Hunger[1], Bernhard Blümich[1], and Thomas Mang[2]

[1] Institute for Technical and Macromolecular Chemistry, RWTH Aachen, Germany
[2] Institute for Applied Polymer Chemistry, FH Aachen, Germany

Abstract:

Hydrogels consist of polymer networks that are able to absorb water to a multiple of their own weight. They are used as absorbers in a variety of products, like, for example, diapers and sealing materials in the building industry. Since a few years they have also attracted the attention to fields like biomedicine and sensor technology due to their stimuli responsive properties. Nevertheless, processes like swelling, water binding, and diffusion taking place in hydrogels, especially in non-equilibrium swollen states, are not fully understood. In this work we present studies on the dynamics of water in polyacrylate hydrogels by means of self diffusion measurements and NMR-relaxometry. Furthermore the swelling process in a hydrogel was followed by measuring the ingress of water into a dry specimen in order to obtain information about the characteristics of the transport diffusion of water.

Self diffusion coefficients were determined in dependence on the degree of swelling as well as on the crosslink density. The results show that the self diffusion coefficients are lower than the one of free water. This can be explained by water bound to polar carboxylate groups which is in fast exchange with free water surrounding the polymer chains. The self diffusion coefficient increases asymptotically to a value close to the one of free water with increasing degree of swelling, while no dependence on the crosslink density is observed. Measurements of the relaxation times T_1 and T_2 conducted as a function of the degree of swelling show a similar behavior since the relaxation times increase with higher degree of swelling approaching to the ones of free water. The T_2 decays show also a second shorter component, which is assigned to the polymer chains. The short T_2 increases with the degree of swelling proving the higher mobility of the polymer in the swollen state.

The swelling kinetics of the polyacrylate gels were investigated by measuring 1D profiles through a hydrogel tablet exposed to water. A numerical model based on simple Fickian diffusion is used to describe the ingress of the water into the hydrogel tablet. To take the different mobility of bound and free water inside the hydrogel matrix into account a concentration dependent diffusion coefficient is introduced.

NMR and MRI measurements of stable, surfactant-free emulsions

Igor Mastikhin, Andrew King, Ben Newling.

It has been recently demonstrated that thorough degassing of water has a dramatic effect upon its efficacy as a solvent of *non-polar* molecules [1,2]. For the effect to be manifest, the water must be freeze-thaw degassed under vacuum, four or five times. So changed are the physical properties of the water by this process, that stable emulsions can be created by simple hand-shaking with no surfactant.

Recent refinements to MR diffusion measurements [3] have allowed a reduction in acquisition times by a factor of 4. We have taken advantage of this time saving in a study of emulsion stability and droplet size distributions of mixtures of thoroughly degassed water and dodecane. Our 2D SPRITE MRI kinetic measurements confirmed a remarkable stability of the formed emulsion, with little or no creaming over several hours after the emulsion preparation. NMR diffusion data provided information on droplet size distribution in emulsions as a function of both a number of degassing cycles and time after the emulsion preparation (up to several weeks).

1. R.M.Pashley, M.Rzechowicz, L.R.Pashley, M.J.Francis. De-gassed water is a better cleaning agent. J.Phys.Chem.B. 109, 1231-1238 (2004)
2. M.J.Francis, N.Gulati, R.M.Pashley. The dispersion of natural oils in de-gassed water. J.Coll. Interface Sci. 299, 673-677 (2006)
3. A.Jerschow and R.Kumar. Calculation of coherence pathway selection and cogwheel cycles. J. Magn. Reson. 160, 59-64 (2003)

Quantitative relaxation time measurements on aqueous polymer solutions by unilateral NMR

Nikolaus Nestle[1], Andrew E. Marble[2], Harald Nissler[1], Igor Mastikhin, Bruce J. Balcom[2]

[1] BASF Aktiengesellschaft, Ludwigshafen, Germany
[2] MRI Centre, University of New Brunswick, Fredericton NB, Canada

Abstract:

Many industrial polymers are produced by solution-phase polymerizations. For sales or further processing purposes it is often necessary to determine the solids content of these products. The conventional gravimetric approach to do this involves rather long drying times and only will lead to the polymer content but not provide any further information on the properties of the polymeric product.

In some cases, NMR relaxometry provides an alternative approach to the determination of the solids content in polymer solutions: The transverse relaxation times of the dissolved polymer and the solvent phase are often order of magnitude apart from each other. By analyzing transverse magnetization decay curves (e.g. from CPMG measurements), this can be used to determine the polymer content in a solution sample.

In the practical implementation of this approach, the high viscosities of many polymer solutions may pose a serious problem in sample preparation for conventional NMR as it takes some time to get such samples into an NMR sample tube with a well defined degree of filling.

Therefore, measurements on large bottles would me much easier to perform than experiments on aliquots filled into standard NMR tubes. We have explored the possibilities of polymer content determination in conventional TD-NMR on small sample tubes and in unilateral NMR on large-scale samples on the example of polyvinylpyrrolidon (PVP) solutions.

Our results indicate that unilateral NMR measurements on large bottles may provide a valid approach for PVP determination in aqueous solutions. The applicability of the same approach to other polymers will be discussed, too.

Local water-content measurement of PEM
for fuel cell applications using planar surface coils

Kuniyasu Ogawa [1] , Tomoyuki Haishi [2] and Kohei Ito [3]

[1] Keio University, 3-14-1 Hiyoshi, Kohoku-ku, Yokohama, Japan
[2] MRTechnology, Inc., 169-1 Kouya, Tsukuba, Japan
[3] Kyushu University, 744 Motooka, Nishi-ku, Fukuoka, Japan

Abstract:

A real-time monitoring method of local water content in polymer electrolyte membrane (PEM) is required to achieve higher current density operation of a polymer electrolyte fuel cell. Based on signal intensity and T_2(CPMG) relaxation time of NMR, water content in a PEM can be obtained. In order to localize the measurement area in the PEM, a use of planar surface coil of about 1 mm outside diameter is effective.

The distribution-measurement system with 8 channel transceivers and planar surface coils of 1.3 mm outside diameter for monitoring water content distribution in PEM was developed. The system consisted of a permanent magnet (NEOMAX Co., Ltd.) and an MRI console (MRTechnology, Inc.). The permanent magnet had a static magnetic field of 1.0 Tesla and a 45 mm air gap. Using the CPMG method, water content in PEM can be obtained from echo-signal intensity and T_2 (CPMG) relaxation time.

MEA (Membrane Electrode Assembly) was put in the cell controlled at the cell temperature of 75 ºC and the vapor concentration of 0.14 kg/m^3 in N$_2$ gas. The arrangement of coils and MEA is illustrated in Fig. 1. Time-dependence changes of echo-signal intensity of MEA under water electrolysis condition were obtained as shown in Fig.2. It can be seen that the water content in the area near the cathode electrode increases once immediately after the DC voltage is applied.
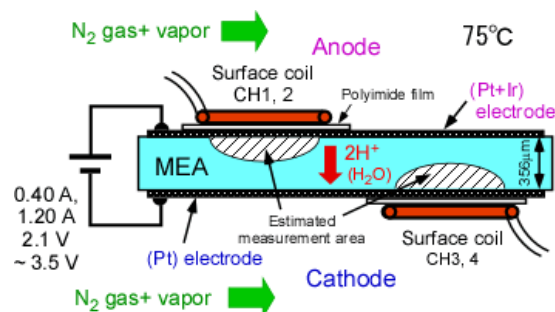
Fig. 1: Schematic draw of MEA applied DC voltage and positions of the planar surface coils on the MEA
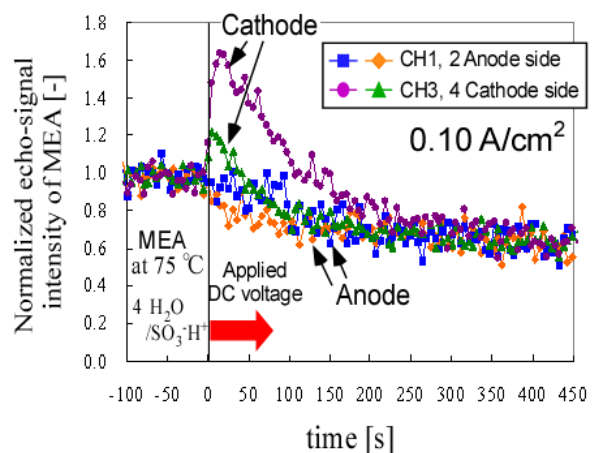
Fig. 2: Time-dependence changes of echo-signal intensity of MEA under water electrolysis condition at 75 ºC obtained by the planar surface coils on the anode and cathode electrodes

Diffusion profiles to study reactions in solvent-gel systems

Andrea Amar, Federico Casanova, and Bernhard Blümich

Institut für Makromolekulare Chemie, RWTH-Aachen, Worringerweg 1, D-52056 Aachen, Germany

Abstract:
Fluid organic-aqueous two phase systems play an important role in industrial production processes, particularly in organic chemistry and biotechnology, where isolated biocatalysts can be used for the synthesis of fine chemicals. As the enzymes as well as the essential cofactors are unstable in the presence of organic solvents. they are immobilized in a hydrogel matrix that protects the enzyme efficiently against detrimental effects of the organic phase, while the organic phase set at the gel interface facilitates the supply with hydrophobic substrates and extraction of products. For an optimal application of immobilized enzymes in industrial processes, profound knowledge about the physical and chemical processes occurring inside the stabilized water phase (gel-stabilized beads and rods) is required [1].

Unfortunately, the phenomena occurs inside the gel (e.g. mass transfer and enzymatic reaction) and cannot be directly accessed with standard optical methods. Thus, only integral information obtained from the gel surrounding bulk phase is used to draw conclusions about intra-particle processes. However, the insights gained by this approach are rather limited. Therefore, a new methodology for the investigation of intra-particle processes has to be developed which allows obtaining reliable mechanistic information about these processes.
In this work we show that magnetic resonance imaging with chemical shift resolution provides detailed information about molecular transport on the macroscopic scale [2,3]. The concentration of species of different spectral lines can be quantified from high-resolution ^{1}H spectra, and these can also be acquired with spatial resolution. One-dimensional images with spectral resolution were obtain from 10mm NMR tubes filled up to 5cm with a k-carrageenan hydrogel (stabilized aqueous phase - bottom) and a stable solution of hexane and 3,5-dimethoxy-benzaldehyde (DMBA) (organic bulk phase - top). Concentration profiles of DMBA over time were obtained by integrating the different spectral lines of this compound. This slow inter-diffusion process was monitored for at least 24hs and the data was used as input to calculate the kinetic constants of the system via mathematical model fitting.

1. M. Küppers, C. Heine, S. Han, S. Stapf, and B. Blümich. In-situ observation of diffusion and reaction dynamics in gel microreactors by chemically resolved NMR microscopy. *Appl. Magn. Reson.*, **22** (2002) 235 - 246.
2. D. Papadopoulos, M. A. Voda, S. Stapf, F. Casanova, M. Behr, B. Blümich. Magnetic Field Simulations in Support for Interdiffusion Quantification with NMR. *Chemical Engeneering Science* (2007), submitted.
3. A. Salvati, I. Lynch a, C. Malmborg, D Topgaard. Chemical shift imaging of molecular transport in colloidal systems: Visualization and quantification of diffusion processes. *Journal of Colloid and Interface Science.*, **308** (2007) 542-550.

Quantifying Mass Transfer & Velocity in Two Phase Taylor-Couette Flow

Amber L. Broadbent[1], Joseph D. Seymour[1], Sarah L. Codd[2], and Jennifer R. Brown[1]

[1] Department of Chemical and Biological Engineering, Montana State University, Bozeman, Montana

[2] Department of Mechanical and Industrial Engineering, Montana State University, Bozeman, Montana

Abstract:

The understanding of hydrodynamics and rheology are critically important to the success of modern pharmaceutical, food and cosmetic manufacturing processes that rely on dispersions. Interactions between organic and aqueous phases in a manufacturing process govern dispersion formation, phase continuity, droplet size, droplet size distribution and dispersion stability. In order to meet stringent product specifications, it must be understood how the fluid properties, namely viscosity, surface tension and density, affect the mixing and formation of an emulsion. Additionally, a thorough understanding of how the process equipment and energy inputs affect mixing and transport is crucial to the transformation of raw materials into an exact and reproducible final product. Pulsed NMR has been applied extensively to study droplet sizes in emulsions [1] and rotationally compensated magnetic resonance imaging techniques used to determine droplet motion in Couette flow [2]. In this work PGSE and RARE are used to investigate and quantify the interactions between silicone oil and water in a Couette system with a 1 mm gap and a rotating inner cylinder. The flow regime analyzed is the Taylor regime of hydrodynamic instability for which vortices form in the axial direction. Kinematic viscosity and rotation rate play a critical role in the degree of mixing between the organic and aqueous phases. Additionally, the presence of a surfactant to reduce the amount of interfacial tension between the liquid phases greatly increases the interfacial surface area and thus the degree of interaction between the two phases.

[1]   B. Balinov and O. Soderman, Diffraction-like effects observed in the PGSE experiment when applied to a highly concentrated water/oil emulsion, *Journal of Physical Chemistry*, **98** (1994), 393-395.

[2]   K.G. Hollingsworth and M.L. Johns, Droplet migration in emulsion systems measured using MR methods, *Journal of Colloid and Interface Science*, **296** (2006), 700-709.

NMR velocity phase encoded measurements within unidirectional tapered-pore ceramic structures

T. R. Brosten[1], K. V. Romanenko[1,2], S. L. Codd[1], J. D. Seymour[2] and S. W. Sophie[1]

[1] Department of Mechanical and Industrial Engineering, Montana State University, Bozeman, Montana

[2] Department of Chemical and Biological Engineering, Montana State University, Bozeman, Montana

Tape cast freezing of ceramics allows the opportunity for tailored control of ceramic pore structure [1]. In order to utilize the ability to control pore structures to design ceramics with specific transport properties for fuel cell or filtration applications, the connection between pore structure and transport function must be established. Magnetic Resonance Microscopy techniques have been used to obtain pore scale resolution images averaged over a range of slice thicknesses to assess the depth alignment of the tapered pores. The complementary nature of the MRM and other imaging techniques in understanding complex structures is apparent. The high resolution spin density images obtained with varying spatial resolution indicate the pore structure is highly anisotropic (see figure 1). This work also applies pulsed gradient spin echo (PGSE) techniques to obtain spatially resolved velocity measurements of a newtonian fluid (Octane) flowing through the tapered-pore ceramic structure. Two dimensional velocity profiles of the pressure driven liquid are obtained at various slice locations in the ceramic structure. The velocity profiles reveal transport heterogeneities (in contrast to the spin density homogeneity) occurring at a scale exceeding the average pore size in the slice plane. The volumetric flow rate calculated from experimental PGSE data reveals a one dimensional variation in the porosity between the slice planes. Furthermore, propagator studies are carried out to develop an understanding for the transport of momentum occurring within these novel porous structures. The results are discussed in the context of porous media transport models.
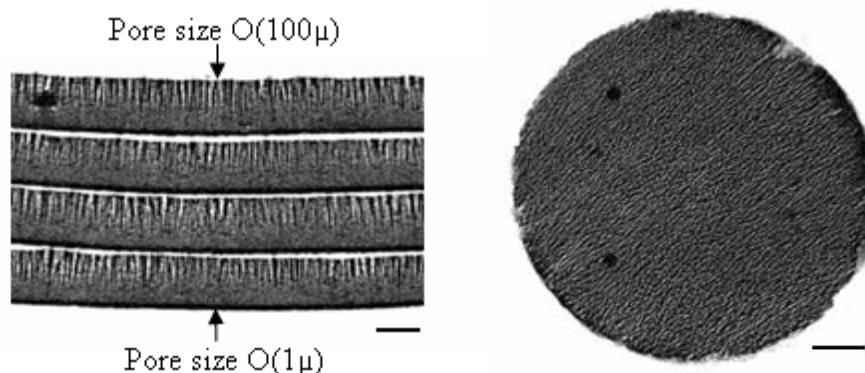
Figure 1: High resolution spin density images, bar=1.0mm, 0.5mm & 0.64mm slice thickness, left and right image respectively

References:

1. S.W. Sofie, "Fabrication of functionally graded and aligned porosity in thin ceramic substrates with the novel freeze-tape casting process," J. Amer. Ceram. Soc., 90 [7], 2007

Investigation of H_2O_2 decomposition in heterogeneous catalysts

L. Buljubasich[1], Thomas Oehmichen[,2], Leonid B. Datsevich[2], A. Jess[2], B. Blümich[1] and S. Stapf[3]

[1] Dept. of Macromolecular Chemistry, ITMC, RWTH Aachen, 52074 Aachen, Germany
[2] Dept. of Chemical Engineering, University of Bayreuth, 95447 Bayreuth, Germany
[3] Dept. of Technical Physics II, TU Ilmenau, PO Box 100565, 98684 Ilmenau, Germany

Abstract:

Heterogeneously catalysed reactions mostly take place in the presence of finely dispersed catalysts (i.e. metals such as Ni, Pt, Pd, …), these in turn are localized in materials of large internal surfaces, i.e. porous media (typically, pellets of Al2O3 of several mm in size). The reaction efficiency then depends on parameters such as internal surface area; homogeneity of metal distribution; porosity and tortuosity of the pellet; transport of the reactants and products between the pellet (flow, diffusion) and inside the pellets (diffusion). It is known that the pore space of catalyst pellets is complex, usually bimodal, i.e. having pores in the nm and um range – it is also known that the presence of um scale pores ("macropores") have a strong influence on the reaction efficiency, without them the reaction would mostly take place at the outer edge of the pellet, and the core would remain useless.

In most technically interesting reactions, gas occurs as one of the involved components; furthermore, steam may be generated in exothermic reactions. For not too small pores, this leads to the generation of gas or steam BUBBLES (dependent on the surface tension, for instance). Bubbles grow and eventually leave the pore; just like the dissolution of an aspirin tablet in water, bubbles form more or less at regular intervals provided that the pores have the same size. In other words, each pore generates bubbles at a certain rate or frequency; large pores lead to large bubbles at a low frequency and vice versa.

On the other hand, pure Hydrogen Peroxide solution is stable with weak decomposition, but when it comes in contact with heavy metals, produces oxygen gas and decomposition heat.

The aim of this work is monitoring the Hydrogen Peroxide decomposition. During the reaction, some NMR parameters like T_1 or T_2 change over the time. On the other hand, using NMR Imaging it is possible determine T_1, T_2 in different regions inside and outside the pellets. We will present some results obtained with High Resolution NMR.

1. L. Datsevich, *Appl. Cat. A* **247** (2003) 101.
2. L. Datsevich, *Appl. Cat. A* **262** (2004) 149.

Velocity Imaging of Two-Phase Flow in Microchannels

Colin J Davies[1] and Lynn F Gladden[1]

[1] Department of Chemical Engineering, University of Cambridge, Pembroke Street, Cambridge CB2 3RA UK.

Abstract:

Two-phase flows within microchannels are of interest in the production of food and cosmetic products. They are also used in microchannel reaction engineering, as reducing the length scale of reactors increases the driving force for heat and mass transfer, thereby allowing more efficient operation. Understanding the nature of these flows is obviously critical to harnessing them for industrial operation. In particular, knowledge of variables such as the position of the interface between the two phases, the velocity profile across the channel (including its value at the interface) and also the shape of the interface are key to understanding both these flows and to processes taking place within them. Magnetic Resonance Imaging (MRI) has been used increasingly in the context of imaging flows within microchannels [1,2]. One key benefit of using MRI is that distortion of the shape of the interface due to varying refractive indices, as found with optical techniques such as confocal microscopy, does not occur. MRI has been used as a non-invasive tomography to map both the spatial distribution of fluid within a two-phase microchannel flow and also to measure the velocity distribution within the channel.

Time-averaged velocity images of single and two phase flow within microchannels have been acquired for flows of PDMS and water within a 100 μm × 250 μm microchannel. Within the regime investigated, a stable flow of two parallel streams is formed. Changing the relative velocity of the streams changes the position of the point of maximum velocity in the channel. Changing the viscosity of the oil phase changes the relative pressure drops along the channel of the two phases and hence the proportion of the cross-sectional area of the channel that is occupied by each phase changes also.

One of the aims of this work is to compare the experimental measurements with commonly used simulation techniques. Three different modeling techniques have been investigated. The first is a numerical solution of the Stokes equation for both single and two-phase flow within a microchannel. The second is a single-phase lattice-Boltzmann code used to simulate low Reynolds number flows within channels [3]. Lastly, a CFD code [4] specially designed to simulate two phase dynamic flows in small geometries, that models the discontinuity in fluid properties using a phase field method, was applied [4]. The extent to which these methods can be used to model flows of both single and two phases in microchannels has been investigated.

1. Harel E, *et al.*, *Phys. Rev. Lett.*, **98** (2007) 017601
2. Akpa BS, *et al.*, *Anal. Chem.,* in press.
3. Sullivan S, *et al.*, Electro. Comm., **7** (2005) 1323-1328
4. De Menech M., *Phys. Rev. E*, **73** (2006) 031505

NMR-Imaging at µ-Mixers

Sven Englert[1], Siegfried Stapf[2] and Bernhard Blümich[1]

[1] Institute for Macromolecular Chemistry, RWTH Aachen, Germany
[2] Institute for Polymer Physics, TU Ilmenau, Germany

Abstract:

The development of µ-devices is advancing at high speed and is of much interest for chemical engineering [1]. Therefore data for the optimization of these devices should be provided. The NMR technique is predestinated for this purpose because of its non-invasive character. In this work, conventional NMR methods [2] like chemical shift imaging (CSI) and the application of soft pulses for selective excitation with the combination of velocity compensation [3] have been used to obtain valuable data of processes inside a µ-mixer. A quite simple system of two mixing components, water and acetone, has been choosen. The mixing characteristics of an interdigital µ-mixer at low flowrates could be enlightened.

The methods which have been applied are the foundation for investigations of a vesicle formation process inside various types of µ-mixers. This work is part of the IMPULSE (Integrated Multiscale Process Units with Locally Structured Elements) project funded by the European Union.

1. W. Ehrfeld, V. Hessel, H. Löwe, „Microreactors", Wiley-VCH, Weinheim(2000)
2. B. Blümich, "NMR-Imaging of Materials", Clarendon Press, Oxford(2000)
3. S. Laukemper-Ostendorf, K. Rombach, P. Blümler, B. Blümich, „3D-NMR-Imaging of Flow in Stationary Systems", *Bruker Note* (1998).

Investigation of shear banding fluctuations in wormlike micelles using rapid NMR velocimetry

Kirk W. Feindel[1], María R. López-González[1], William M. Holmes[2], and Paul T. Callaghan[1]

[1] MacDiarmid Institute, Victoria University of Wellington, Wellington, New Zealand
[2] Wellcome Surgical Institute, University of Glasgow, Glasgow, United Kingdom

Abstract:

Complex fluids exhibit a combination of solid- and liquid-like properties. Such fluids are encountered everyday; common examples include foods (e.g., milk, cheese), detergents, and biological fluids such as blood and synovial fluid found in joints. Whilst the macroscopic behaviour of complex fluids is often readily observable, the flow and deformational (i.e., rheological) properties and their molecular origin are, in general, not well understood.

During the past two decades numerous advances have been made in the development of experimental and theoretical methodologies for the study, characterization, and understanding of complex fluids [1]. One of the objectives of our research is to improve the understanding of complex fluids via experimental investigation of model systems, such as solutions of wormlike micelles. The flow curves (log-log plot of shear stress vs. shear rate) of shear-thinning wormlike micellar systems, above a critical shear rate, often exhibit a stress plateau [2]. This stress plateau has been associated with the spatial separation of the system into regions of differing local shear rate (i.e., viscosity), a phenomenon termed shear banding. A multitude of techniques have been applied to the study of shear banding including NMR velocimetry, particle image velocimetry, particle tracking velocimetry, dynamic light scattering, ultrasonic velocimetry, and small angle neutron scattering. NMR techniques are particularly attractive as they are non-invasive and enable spatial localization of specific areas of interest.

By combining conventional rheological methodology with magnetic resonance techniques (rheo-NMR), previously elusive information about the properties and behaviour of complex fluids can be garnered. The model system investigated here is a shear-thinning solution of 10 w/w% cetylpyridinium chloride and sodium salicylate in 0.5 M NaCl (far from the isotropic-to-nematic phase transition). Previous NMR velocimetry studies of this system revealed shear banding fluctuations by imaging velocity profiles across the gap of a Couette cell (i.e., concentric cylinders) [3].

Here we present results that highlight our recent progress in the development of rapid NMR velocimetry techniques for real-time investigations of shear banding fluctuations in wormlike micelle solutions. Steady shear deformation was performed using a Couette cell with an inner- and outer-diameter of 17 and 19 mm, respectively. We have developed rapid 2D slice selective EPI- and RARE-type imaging sequences that are preceded by a PGSE encoding period to yield 2D velocity maps. Inspired by recent theoretical results which suggest a novel mechanism for the emergence of stress bands and Taylor-like velocity rolls in the vorticity direction [4], we also present our results from preliminary experiments that investigate velocity fluctuations along the vorticity direction of the Couette cell gap.

1. M. E. Cates, S. M. Fielding. *Adv. Phys.*, **55** (2006) 799.
2. H. Rehage, H. Hoffmann. *J. Phys. Chem.*, **92** (1988) 4712.
3. M. R. López-González, W. M. Holmes, P. T. Callaghan. *Soft Matter*, **2** (2006) 855.
4. S. M. Fielding. arXiv:cond-mat/0703151v1

Study of flow and particle distribution in a bifurcation using dynamic NMR Microscopy

E.O. Fridjonsson [1], J.D. Seymour [1], S.L.Codd [2] and G.R. Cokelet [1]

[1] Department of Chemical and Biological Engineering, MSU, Bozeman, USA
[2] Department of Mechanical and Industrial Engineering, MSU, Bozeman, USA

The flow and distribution of Newtonian, polymeric and colloid suspension fluids at low Reynolds numbers in bifurcations has importance in a wide range of disciplines, including microvascular physiology (1) and microfluidic devices (2). A bifurcation consisting of circular capillaries laser etched in a hard polymer with inlet diameter 2.64 ± 0.06 mm, bifurcating to a small diameter outlet of 0.76 ± 0.06 mm, and a large outlet of 1.35 ± 0.06 mm diameter is examined using four distinct fluids (Water, $0.25\%(^w\!/_w)$ Xanthan Gum, 8% and 22% (v/v) polydisperse oil inside core-shell latex particles (3)) at different flow rates from 5mL/hr to 30mL/hr covering a range of Reynolds numbers based on the entry flow from 0.3 to 8. A Bruker DRX250 NMR system is used with PGSE techniques to obtain dynamic images of the fluids inside the bifurcation with spatial resolution of 58.6 x 58.6 µm/pixel in plane over a 200 µm thick slice (see Fig 1). Velocity in all three spatial directions is examined to determine the impact of secondary flows and characterize the transport in the bifurcation. The velocity data provide direct measurement of the volumetric distribution of the flow between the two channels. For the colloidal particle flow the distribution of colloid particles down the capillary is determined by examining the spectrally resolved propagator for the oil inside the core-shell particles in the direction perpendicular to the axial flow. Using dynamic NMR Microscopy the potential for using magnetic resonance for "particle counting" in a microscale bifurcation is thus demonstrated.
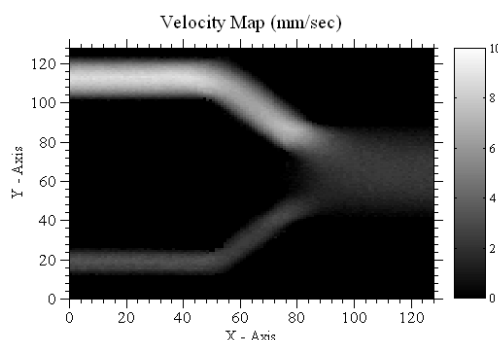
Fig 1: Velocity Map for water flowing in the axial direction
from right to left at a flow rate of 20mL/hr

1. A.R. Pires, K.Ley, M. Claassen, P. Gaehtgens, *Microvasc. Res.*, **38** (1989) 81-101.
2. B.W. Roberts, W.L. Olbricht, *AICHE Journal* **52** (2006) 199-206.
3. A. Loxley, B. Vincent, *J. Colloid Interface Sci.* **208** (1998) 49-62.

Diffusion Studies on the Ionic Liquid-CO$_2$ System

Qingxia Gong, Tobias Höfener, Jürgen Klankermayer, Walter Leitner, Bernhard Blümich

Institut für Technische und Makromolekulare Chemie , RWTH Aachen, Germany

qgong@mc.rwth-aachen.de

Room temperature ionic liquids (ILs) have been considered as novel "green" reaction media for a wide range of chemical processes.[1] The advantageous application of ILs as solvents in metal catalyzed reactions involving gaseous substrates have been demonstrated recently.[1] In 1999, Brennecke and co-workers showed for the first time that compressed CO$_2$ is the *predestined partner solvent* for ILs.[2] The high solubility of CO$_2$ in ILs induces substantial changes in the physico-chemical properties of the liquid phase as compared to the neat IL. The compressed CO$_2$ greatly decreases the viscosity of the ionic solution thus facilitating mass transfer during catalytic reactions.[3,4,5] Much effort has been made to investigate the temperature-dependence of ionic liquid's properties at atmospheric pressure, but so far there exists no data about the factors which control the gas solubility in the ILs in the presence of compressed CO$_2$ and any underlying structure-function relationship.

In order to obtain data which allow a correlation of the gas solubility to the structure of the ILs, we studied a matrix of imidazolium, pyridinium and ammonium cations in combination with [TF$_2$N]$^-$ and [BF$_4$]$^-$ anions. The main focus in this investigation was the solubility of hydrogen in the IL-compressed CO$_2$ system. To better understand the effect of pressure on the interactions in the ILs and between the gases and the ILs, we determined the self-diffusion coefficients of the IL and hydrogen by PGSE diffusion studies in CO$_2$ with and without hydrogen at 25°C up to a maximum pressure of 136 bar.

[1] P. Wasserscheid, T. Welton, *Ionic liquids in synthesis, Wiley-VCH* **2003**.
[2] L. A. Blanchard, D. Hancu, E. J. Beckman, J. F. Brennecke, *Nature* **1999**, *399*, 28.
[3] W. Leitner, *Acc. Chem. Res.* **2002**, *35*, 746.
[4] M. Solinas, A. Pfaltz, P. G. Cozzi, W. Leitner, *J. Am. Chem. Soc.* **2004**, *126*, 16142.
[5] P. J. Dyson, G. Laurenczy, C. A. Ohlin, J. Vallance, T. Welton, *Chem. Commun.* **2003**, 2418

Measurement of Granular Temperature in Gas-Solid Systems

Daniel J. Holland[1], C.R. Müller[1], J.S. Dennis[1], L.F. Gladden[1], A.J. Sederman[1]

[1] Department of Chemical Engineering, University of Cambridge, Pembroke Street, Cambridge CB2 3RA, United Kingdom

Abstract:

Owing to its complex behavior, granular matter has attracted considerable interest among physicists and engineers. Under certain conditions, granular systems may behave as a continuum fluid. To model the flow of granular material two key characteristics have been identified. Firstly, the mechanism by which momentum is transmitted through a granular system. Secondly, collisions between granular particles are inelastic and therefore result in a loss of energy from the system as heat. These features are both related to the distribution of particle velocities, which is characterized by the "granular temperature". Thus, the measurement of granular temperature is critical to continuum modeling of granular media. However, due to their opaque nature, conventional optical techniques for studying granular systems are restricted to 2D geometries or observations at the wall.

Magnetic resonance provides a useful tool to study motion in optically opaque systems, and therefore is ideally suited to studying granular temperature in 3D geometries. However, the application of MRI to granular systems is complicated by the very fast relaxation time constants typical of solid materials and the rapidly changing velocities and spin density distribution often encountered in granular systems. This is particularly true of gas-solid granular flows. This work will demonstrate the particular MR approaches required to obtain quantitative measurements of the granular temperature. In particular, it will discuss the artifacts that arise from insufficient spatial resolution of the measurement and due to the time-variant velocity and spin density distribution in the system. This last point has implications to the wider field of MR measurements on time-dependent systems, such as gas-liquid flows.

Figure 1 shows the granular temperature measured in both 2D and 3D systems, emphasizing the importance of the physical geometry on granular flow problems – a point often underestimated in optical studies. The granular temperature measurements will also be used to demonstrate that an anisotropic granular temperature may even exist in dense phase systems, which suggests that the mechanism of stress transmission must be re-examined in modeling these systems. Finally, the unique properties of the system studied enable the direct measurement of the dissipation of granular temperature. In contrast to previous findings, the dissipation of granular temperature is demonstrated to follow Haff's Law.
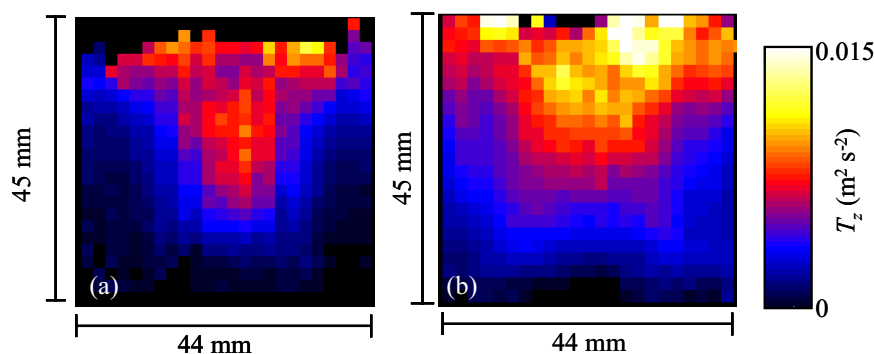
Fig. 1: Granular temperature measurement in (a) 3D and (b) 2D geometries

Analysis of Biofilm Extracellular Polymeric Substance (EPS) Diffusion

Jennifer A. Hornemann[1,2], Sarah L. Codd[2,3], Anna A. Lysova[4], Joseph D. Seymour[1,2], and Jennifer R. Brown[1]

[1]Department of Chemical and Biological Engineering, Montana State University
[2]Center for Biofilm Engineering, Montana State University
[3]Department of Mechanical and Industrial Engineering, Montana State University
[4]International Tomography Center, Novosibirsk, Russia

From water service utilities to pharmaceutical processing, biofilms occur and create havoc in almost every water-based industrial process. Thus, there is an urgent need to better understand the internal behavior, transport and activities of these biofilms. The primary objective of this research is to acquire Magnetic Resonance Microscopy (MRM) data for the predictive modeling of momentum and mass transport in biofilm systems, and determine structure-function relationships over a hierarchy of scales from macroscale clusters to the molecular structure of the EPS hydrogel. MRM is noninvasive and nondestructive tool able to access several observable quantities in biofilms such as chemical composition [1, 2], diffusion [2, 3], and macroscale structure and transport [4-7]. The study presented here extends the work published earlier by Veeman et al [2] where spectrally resolved diffusion was measured in biofilm. This study measures spatially resolved mass transfer in biomass, determines material content and estimates the percentage of fast and slow diffusing components of specific spectral peaks. Using pulsed field gradient NMR techniques, the signal from free water is crushed in order to view the spectra of components such as carbohydrate, DNA and proteins. The diffusion data demonstrate that biofilm EPS contains both a fast and slow diffusion component for the major constituents. The dependence of the diffusion on antimicrobial and environmental factors suggests the polymer molecular dynamics measured by NMR are a sensitive indicator of the biofilm function.

References:
1. Majors, P.D., McLean, J.S., Fredrickson, J.K., and Wind, R.A., *HMR methods for in-situ biofilm metabolism studies: spatial and temporal resolved measurements.* Water Science and Technology, 2005. **52**(7): p. 7-12.
2. Vogt, M., Flemming, H.-C., Veeman, W. S., *Diffusion in Pseudomaonas aeruginosa biofilms: a pulsed field gradient NMR study.* Journal of Biotechnology, 2000. **77**: p. 137-146.
3. Hornemann, J.A., Lysova, A. A., Codd, S.L., Seymour, J.D., Brown, J.R., Stewart, P.S. and Busse, S.C., *Analysis of Biofilm Extracellular Polymeric Substance (EPS) Diffusion.* Biotechnology and Bioengineering, To be submitted.
4. Manz, B., Volke, F., Goll, D., Horn, H., *Investigation of biofilm structure, flow patterns and detachment with magnetic resonance imaging.* Water Science and Technology, 2005. **52**(7): p. 1-6.
5. Seymour, J.D., Codd, S.L. , Gjersing, E.L. and Stewart, P.S. , *Magnetic resonance microscopy of biofilm structure and impact on transport in a capillary bioreactor.* Journal of Magnetic Resonance, 2004. **167**: p. 322-327.
6. Seymour, J.D., Gage, J. P., Codd, S.L., and Gerlach, R., *Anomalous fluid transport in porous media induced by biofilm growth.* Physical Review Letters, 2004. **93**(19): p. 198103.
7. Gjersing, E.L., Codd, S.L., Seymour, J.D. and Stewart, P.S., *Magnetic resonance microscopy analysis of advective transport in a biofilm reactor.* Biotechnology and Bioengineering, 2005. **89**(7): p. 822-834.

Visualization of Polymer Flooding in Heterogeneous Cores by SPRITE Imaging Methodology

Linqing Li[1,2], Sureerat Ongsurakul[1,3,4], Laura Romero-Zerón[4], Bruce J. Balcom[1,2]

[1] Department of Physics, MRI Centre, University of New Brunswick, Fredericton, Canada
[2] Department of Chemistry, MRI Centre, University of New Brunswick, Fredericton, Canada
[3] The Petroleum and Petrochemical College, Chulalongkorn University, Bangkok, Tailand
[4] Department of Chemical Engineering, University of New Brunswick, Fredericton, Canada

Abstract:

MRI has considerable potential as a non-destructive probe for visualizing and quantifying the microscopic displacement efficiency of polymer flooding processes (EOR) in rock core plugs, allowing rapid quantification of local fluid content. Realistic rocks are challenging samples with traditional MRI methods due to their very short signal life times which arise from inhomogeneities in the microscopic magnetic susceptibility. Specialized MRI imaging techniques are therefore required.

In this work we have developed two methodologies to quantify and spatially resolve water flooding in core plugs. One involves observing the displacement by water of isotopic substances, such as fluorinated oil, in core plugs with centric SPRITE sequences[1]. We also explore another general method to discriminate water and oil in rock via the molecular diffusion coefficient. This measurement utilizes a diffusion weighted centric-scan SPRITE sequence[2].

These methods are illustrated below with the displacement of fluorolube oil and mineral oil through core plugs. Both spatially resolved 3D images and local fluid content distributions can be acquired.
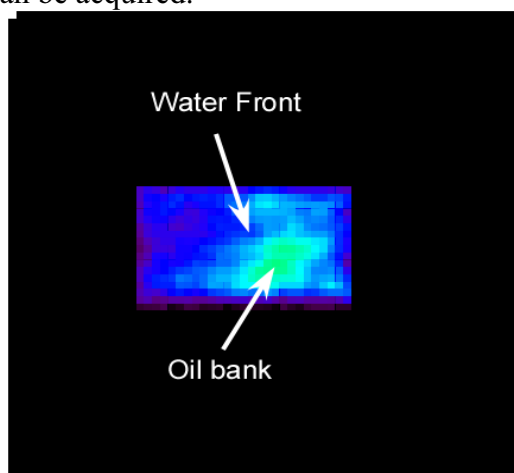
Fig. 1: A 2D slice of fluorolube oil spin density, (fluorine resonance), extracted from 3D conical SPRITE image. Image was acquired after 6 ml of water was injected into an oil- sturated sandstone
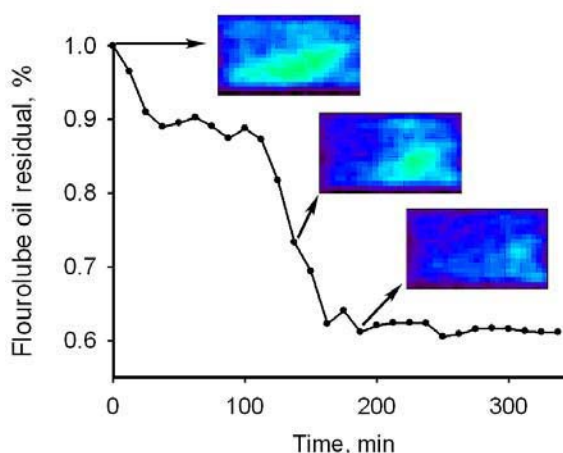
Fig. 2: Residual fluorolube oil in rock at different time of water flooding. Each point was obtained by integrating and normalizing the signal intensity from individual images. The water flow rate was maintained at 0.055 ml/min. Images was acquired without stopping the water injection.

1. Laura Romero-Zerón, et al., Journal of Peroleum Science and Engineering , submitted.
2. Linqing Li, et al., et al., J. Mag. Res., 186, 2, 282-292, (2007)

Velocity Imaging of Single Phase Flow in Porous Media by Magnetization Prepared Centric-scan SPRITE[1]

Linqing Li[1,2] , Ben Newling[1], Bruce J. Balcom[1,2]

[1] Department of Physics, MRI Centre, University of New Brunswick, Fredericton, Canada
[2] Department of Chemistry, MRI Centre, University of New Brunswick, Fredericton, Canada

Abstract:

  MRI has considerable unrealized potential as a non-destructive probe of porous media, offering the possibility of rapid quantification of local fluid content, diffusion and flow. Realistic porous media are challenging samples for traditional MRI methods since they are characterized by very short signal life times. Novel applications of MRI imaging techniques are therefore required.

  In recent work[2] we have developed methodologies to spatially resolve molecular diffusion coefficients allowing us to differentiate water and oil in realistic porous media. In the current work we extend these ideas to measurements of flow velocity in porous media (specifically petroleum reservoir core plugs) by combining Cotts PFG flow preparation with a centric scan SPRITE MR imaging readout methodology[3].

  The combination of these two techniques permits facile flow velocity and dispersion coefficient measurements in porous media. This new approach has proven to be very robust in characterizing fluid behavior and may be applied to very large range of flow problems.

   This method is illustrated through flow measurements in pipes, sand packs, bead packs and ultimately porous reservoir rocks. Both spatially resolved flow maps and local fluid velocity distributions can be acquired.
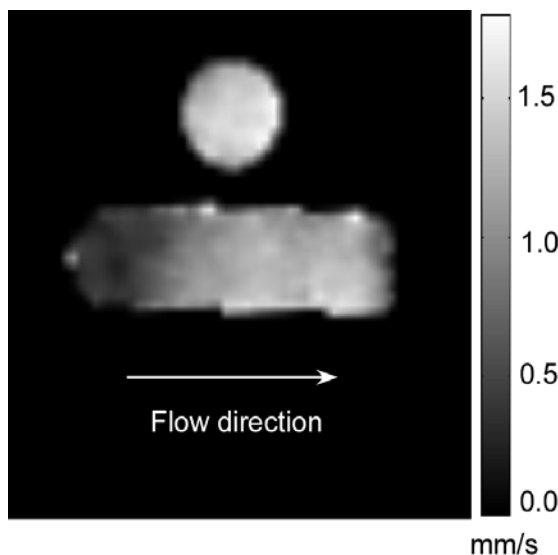
Fig. 1: 2D slices from 3D Flow velocity map of Ottawa sand in a cylindrical holder, $u_{avg} = 0.89$ mm/s, Re=0.135.
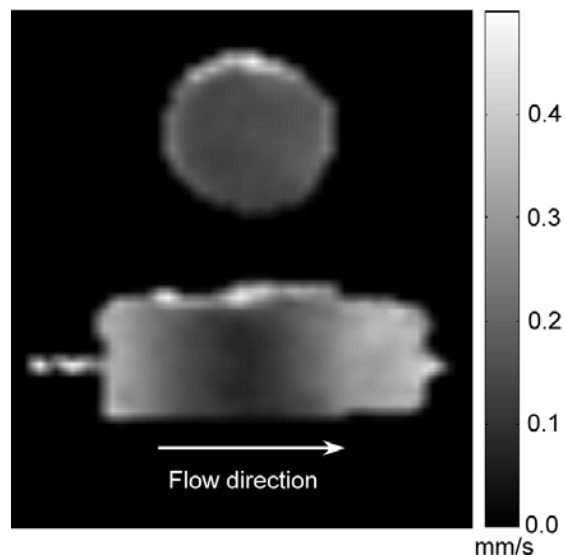
Fig. 2: 2D slices from a 3D Flow velocity mapping in carbonate limestone rock, $u_{avg} = 0.246$ mm/s.

1. Linqing Li, et al., J. Mag. Res., manuscript in preparation.
2. Linqing Li, et al., J. Mag. Res., 186, 2, 282-292, (2007).
3. Alexandre A. Khrapitchev, et al., J. Mag. Res., 181, 271-279 (2006).

Investigation of Biofilm Detachment Using MR Microscopy and ^{13}C-MAS NMR Spectroscopy

B. Manz[1], F. Volke[1], K. Garny[2,3], M. Haesner[2], Th. R. Neu[2] and H. Horn[3]

[1] Fraunhofer-Institute for Biomedical Engineering, Ensheimer Str. 48, 66386 St. Ingbert, Germany
[2] Department of River Ecology, Helmholtz Centre for Environmental Research – UFZ, 39114 Magdeburg, Germany
[3] Institute of Water Quality Control, Technische Universität München, Am Coulombwall, 85748 Garching, Germany

Abstract:

Biofilms are microorganisms and their extracellular polymeric substances associated with interfaces in environmental, technical and medical habitats. The function of biofilms in all of these systems is strongly related to their structure, whilst the biofilm structure in turn is again determined by nutrient availability as well as hydrodynamic conditions. Recent studies have shown that MR microscopy is a perfect tool to investigate structure and dynamics of biofilm systems in their natural habitats [1, 2, 3]. Structural information can be obtained by mapping the T_2 relaxation times, and flow maps provide information about transport properties as well as the forces acting on the biofilm surface.

In the study presented here, detachment from a heterotrophic biofilm, which was grown in a tube reactor, was investigated. The biofilms were cultivated in a test segment (diameter 7 mm) at a constant Reynolds number and a well-defined substrate load. For the MRI experiments, the test segments with the biofilms were placed inside the NMR magnet and connected to the flow loop. Spatially resolved maps of flow velocity and T_2 were recorded at laminar flow conditions. After each set of experiments, the flow rate was increased for two minutes (Reynolds number Re: 1000, 2000, 3000, 4000, 5000) in order to force biofilm detachment from the reactor. The resulting images show the increasing detachment of biomass from the biofilm surface with increasing shear forces (Fig 1).

Additionally, biofilms were cultivated in a RAR reactor with ^{13}C-labelled glucose as a substrate. The ^{13}C-MAS spectra of the biofilm and detached biomass show peaks at identical positions, indicating identical chemical composition. However, the T_1 relaxation time of most peaks is increased in the detached biomass, suggesting increased molecular mobility compared to the more strongly cross-linked biofilm matrix.
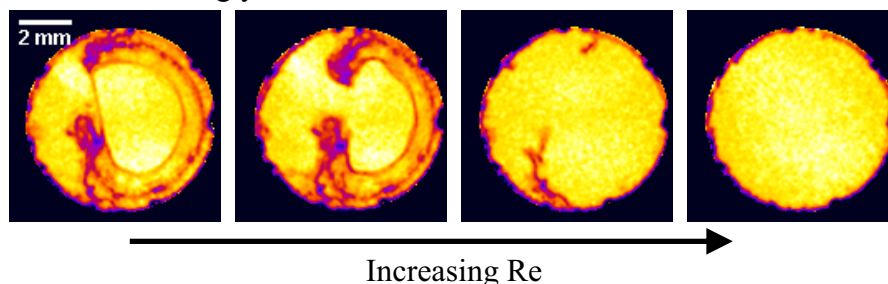
Increasing Re

Fig. 1: T_2 maps characterizing the biofilm structure with increasing detachment.

1. B. Manz, F. Volke, D. Goll, H. Horn, *Biotechnol. Bioeng.* **84** (2003) 424-432.
2. J. D. Seymour, S. L. Codd, E. L. Gjersing, P. S. Stewart, *J. Magn. Reson.* **167** (2004) 322-327.
3. U. Metzger, U. Lankes, E. H. Hardy, B. C. Gordalla, F. H. Frimmel, *Biotechnol. Lett.* **28** (2006) 1305-1311.

MRI study of complex flows of viscoelastic fluids

<u>G. Maddinelli</u>**,** A. Guarneri[±] and S. Carminati[#]

*Eni S.p.A., R&M Division, via F. Maritano 26, 20097, S. Donato Mil., Milan, Italy
[±]Eni S.p.A., E&P Division, via Emilia 1, 20097 S. Donato Mil., Milan, Italy
[#]Eni S.p.A., E&P Division, via dell'Unione Europea, 20097, S. Donato Mil., Milan, Italy

In the oil and petrochemical industry there is a need of understanding the complex flow dynamics involved in several engineering problems, particularly when multiphase systems, such as gas, oil and water together with solid particles are involved. To address these aspects one of the most promising NMR applications are certainly velocity measurements methods based on the combination of pulsed field gradients spin-echo (PGSE) and imaging experiments[1]. The advantage of MRI techniques, compared to other conventional techniques (e.g. ultrasound and laser Doppler methods), is the great potential in discriminating the different fluids and especially in measuring velocity profiles over a wide range of values avoiding any interference with the flowing system. In this work, we report some of the results obtained in our flow dynamics studies (see Fig.1) performed on a viscosified water dispersion of polymers, widely applied in drilling mud operations, by using a flow loop with a horizontal section inside a 2 T, 31 cm horizontal-bore magnet. Flow was maintained in a velocity range of 10-100 cm/sec. The viscosified fluids were water solution with different concentration of polysaccharides (Xanthan

Fig. 1 Experimental velocity profiles at different Reynolds Numbers
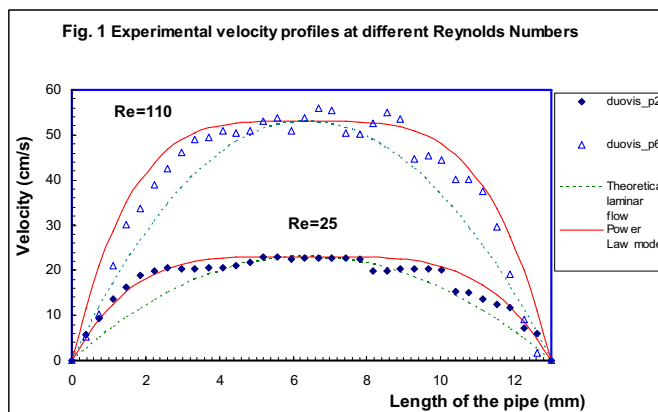
gum 0.3-0.5 % in water, w/w). FLASH imaging and double PGSE (VEXY) based techniques[2] were alternatively applied to evaluate transient phenomena and fluctuations induced in the flow line at high flow rates.

In a previous work[3], early transitions from laminar to turbulent regime were observed even at very low Reynolds number (Re comprised between 300 and 500 compared to the theoretical transition value Re ~ 2300). In this work the rise of fluctuations (and turbulence) was confirmed by the determination of the velocity distribution function, and associated to the elastic properties of the large polymeric molecules and their conformation in solution. The application of the FLASH imaging technique allowed also a useful visualization of solid particles movement and deposition in the horizontal section of the flow loop inside the bore magnet.

References

1. Callaghan P.T., Eccles C.D. and Xia Y. J. Phys. Sci. Instrum. 21, 820-822, 1988;
2. Callaghan P.T., Codd S.L., Seymour J.D. Concepts in Magn. Resonance,11, 181-202, 1999.
3. Maddinelli G. Carminati S. and Guarneri, A, abstracts of the 8th ICMRM, Mibu, 22-26 August 2005.

Turbulent, Two-Phase Flow Measurements

Yang Zhi[1], Mark Sankey[2] and <u>Ben Newling</u>[1]

[1] UNB MRI Centre, Department of Physics, University of New Brunswick, PO Box 4400, Fredericton, NB E3B 5A3, Canada.
[2] Magnetic Resonance Research Centre, Department of Chemical Engineering, University of Cambridge, Pembroke St., Cambridge, CB2 3RA, UK.

Abstract:

Most of the beautiful fluid flow phenomena which occur in nature and technology are turbulent, and to understand the behaviour of such flows in pollution, erosion, corrosion, processing, and mixing, there is still a need for new, quantitative measurement methods. Techniques such as laser Doppler and hot wire/film anemometries, while rapid, are sometimes invasive and sometimes hampered by optical opacity. Sounds like a job for MRI.

Turbulent flows can be awkward to quantify by MRI. There is considerable mixing of the fluid during each MR encoding time, which can lead to signal cancellation or geometrical distortion of the image. However, techniques in which the encoding time is deliberately kept short (such as those used in materials MRI) have been shown to be quite robust to fast, turbulent flows. In particular, we have developed a motion-sensitised version [1] of the purely phase-encoded SPRITE technique [2].

Short encoding times and pure phase encoding have some other benefits, including near immunity to magnetic susceptibility artifacts [3]. This makes our technique an attractive option in turbulent gas/liquid flows, in which bubble boundaries can be another awkward source of imaging artefact.

In this paper, we will present a discussion of the implementation and interpretation of our turbulent flow measurements, and demonstrate their use in dispersed bubbly pipe flow, which is important in studies of flow-accelerated corrosion.
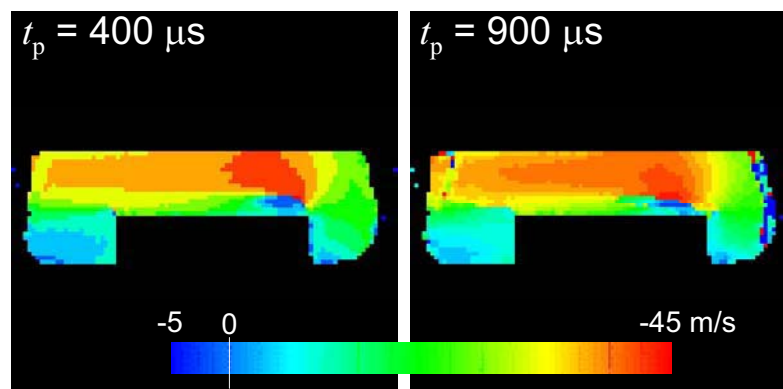
Effects of variation in encoding time (t_p) on velocity mapping in turbulent gas flow (Re > 200 000) past a bluff obstruction in a cylindrical tube. Flow is from right to left, and the scale refers to the component of velocity along the pipe axis.

1. B. Newling, C. C. Poirier, Yang Zhi, J. A. Rioux, A. J. Coristine, D. Roach, and B. J. Balcom, *Phys. Rev. Lett.* **93** (2004), 154503.
2. A. A. Khrapitchev, B. Newling and B. J. Balcom, *J. Magn. Reson.* **178** (2006), 288-296.
3. B. J. Balcom, R. P. MacGregor, S. D. Beyea, D. P. Green, R. L. Armstrong and T. W. J. Bremner, *J. Magn. Res. A* **123** (1996), 131-134.

MR velocimetry of liquid flow in trickle-bed reactors

Mark Sankey[1], Christopher Dunckley[1], Andrew Sederman[1] and Lynn Gladden[1]

[1] Department of Chemical Engineering, University of Cambridge, Cambridge, UK

Abstract:

The most common 3-phase reactor in industry is the trickle-bed reactor (TBR), used to generate products worth hundreds of billions of US dollars per annum. It is a column filled with a fixed unstructured packing, often catalyst coated, over which liquid and gas phases flow co-currently downwards. At low flow-rates the bed operates in the steady-state trickle flow regime in which the liquid trickles over the surface of the solid and the gas fills the remaining void space. Our current understanding of TBRs is mainly based on spatially-averaged properties; however, the local fluid flow distribution is spatially heterogeneous which influences local rates of heat and mass transfer. It has not previously been possible to obtain an accurate non-invasive measure of local velocities in a TBR.

Spatially-resolved spin-warp PFG has been used to map liquid fluid velocities in model TBRs. A slice of thickness of 1 mm is selected with an in-plane spatial resolution of 176 μm. The data are time-averaged but a short echo time of ~5 ms is used to prevent loss of signal from fast-moving fluid elements. The technique has been applied in two cases: (i) an idealised system of glass spheres, water and air; and (ii) a system of porous Pd/alumina catalyst pellets, 1-octene liquid and nitrogen gas which is used to run a hydrogenation reaction when hydrogen is added to the gas stream.

The quantitative nature of the results has been demonstrated by calculating volumetric flow-rates at a range of superficial velocities. They show significant heterogeneity in the flow field which has been analysed by examining velocity distributions and performing a pore scale comparison of single phase and two-phase flow fields. The data offer the ability for improved analysis and operation of TBRs. From a theoretical point-of-view the results improve our understanding of hydrodynamics in reactors and provide data against which numerical models can be validated. At a more practical level, the results improve our ability to select packing elements and loading procedures to optimise reactor operation.

Flow NMR of complex fluids

Frank Bagusat[,1] Ute Böhme[1] Ulrich Scheler[1]

[1] Leibniz Institute of Polymer Research Dresden, Germany

Abstract:

Flow NMR imaging, a combination of NMR imaging and pulsed field gradient (PFG) NMR, is applied to investigate complex flow. As a model geometry a Couette cell with an additional area of high shear is used. NMR relaxation is used to generate contrast in binary systems. The spatial distribution as well as the flow pattern for each component is investigated separately. NMR relaxation times are used to generate contrast. If applicable T_1 contrast from inversion recovery is idea, since it provides suppression of one component at its zero crossing. A combination of NMR-imaging experiments subsequently suppressing either component yields the spatial distribution of the components providing non-destructive insight into mixing. Shear-induced mixing and emulgation are followed. The difference in viscosity is the origin of the deformation of the interface. That becomes visible in the flow images resolving velocity by magnitude and direction for each pixel. The flow pattern differ significantly in the bulk of each component due to their different viscosities. In the vicinity of the interface a separate pattern is established, significant axial flow is the origin of the bending of the interface and subsequent emulgation. The difference in the tangential components leads to deformation of the interface. The approach is demonstrated in a system of paraffin oil and water and subsequently applied to polymer melts of polybutyrate and polyethylene.

Biofilm-mediated Ion Exchanger Optimisation using MRI

D.A. Graf von der Schulenburg*, Marion Patterson-Beadle[+], Lynne Macaskie L.F.[+] Gladden* and M.L. Johns,*

*Department of Chemical Engineering, University of Cambridge, UK
[+]School of Biosciences, University of Birmingham, Edgbaston, Birmingham, UK

The purification of heavy or radioactive metal polluted water is of great concern. One possible and highly selective method of water purification is the use of ion exchangers. In this study a biofilm-mediated ion exchanger is used for the purification of Co^{2+} and Sr^{2+} contaminated water. *Serratia* sp. NCIMB 40259, grown on a polyurethane foam support, enzymatically mediates a hydrogen uranyl phosphate (HUP) surface nano-layer, which exchanges H^+ with the contaminant. The exchanger is contained in a cylindrical vessel and operates under continuous flow.

In this study MRI is used to track the Co^{2+} concentration in the column, using RARE techniques and interpreting ^1H T_2 relaxation effects in terms of local Co^{2+} concentration. The column design was gradually optimised, using this detailed 3D MRI, such that its full exchange capacity is maximally used before significant breakthrough of the contaminant. Figure 1 presents a time resolved series of images tracking the migration of un-exchanged Co^{2+} through the column and as such represents the front position behind which the exchangeable materials is exhausted; the white bar indicates where the front would have reached in the absence of exchange.
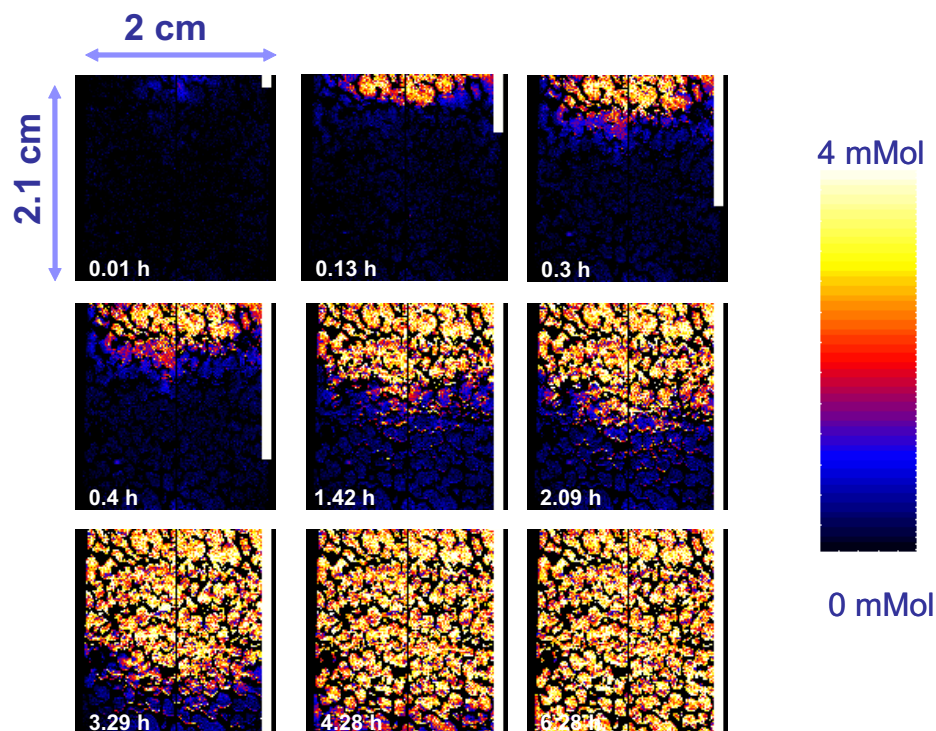
Figure 1

Impact of biofilm growth on displacement statistics studied using enhanced ^{13}C PFG-NMR

Daniel A.W. Graf von der Schulenburg[1], B.S. Akpa[1], L.F. Gladden[1] and M.L. Johns[1]

[1]Department of Chemical Engineering, University of Cambridge, Pembroke Street, Cambridge CB2 3RA, UK

Biofilms consist of micro-organisms, which are surrounded by an extracellular polymeric matrix (EPS) and are attached to a surface by van der Waal forces and adhesion molecules. They grow in a variety of systems and are of importance in medical, environmental, ecological and engineering processes [1]. Displacement statistics of fluids and nutrients through biofilm-containing systems is both heterogeneous and complex due to the presence of biofilm regions, which allow for diffusion of fluid molecules into them but not for advection. Conventional ^{1}H PFG-NMR was applied previously to measure displacement propagators in biofilm-modulated systems up to observation times (Δ) of 0.3 s [2]. Such observation times are typically constrained to less than 1-2 s by signal loss due to ^{1}H T_1 relaxation.

In the current study, longer values of Δ are achieved in realistic total experimental times by application of ^{13}C PFG-NMR, in the process exploiting the typically longer value of T_1 for ^{13}C. The pulse sequence used is a composite of a distortionless enhancement by polarisation transfer (DEPT) from ^{1}H to ^{13}C (hence improving the overall signal-to-noise) and an alternating pulsed gradient stimulated echo (APGSTE) where magnetisation is preserved on the ^{13}C during Δ [3]. This technique was applied to a *Serratia* sp. NCIMB 40259 biofilm grown on a polyurethane foam support [4]. Fig. 1 shows a ^{1}H cross-sectional image of the biofilm covered foam support; dark regions correspond to biofilm due to T_2 signal loss. Propagators for a range of Δ up to 30 s were successfully measured for a range of flow rates using methanol (at natural ^{13}C abundance) as the probe fluid, no measurable ^{13}C signal was detected from the biofilm material. A transition from pre-asymptotic to normal Gaussian displacement dynamics was observed to occur significantly later than for the clean foam support. The transition occurred via a bimodal shape. Simulation of this propagator data was achieved using a directed random walk algorithm and a lattice Boltzmann method [5], with the lattice being provided by 3D pore-scale images of the support and biofilm. Agreement between the experimental data and simulation results was very good.

The pre-asymptotic evolution of the displacement statistics were shown to be compatible with anomalous transport equations derived from the continuous time random walk (CTRW) theory.
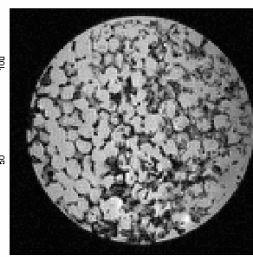
Figure 1: Cross-sectional ^{1}H image of the biofilm covered foam support. Biofilm appears dark due to its lower T_2.

1. H.M. Lappin-Scott and J.W. Costerton, Microbial biofilms (CUP, Cambridge, 2003).
2. J.D. Seymour *et al.*, Phys. Rev. Let. **93**, 1 (2004).
3. B.S. Akpa *et al.,* J Magn. Reson. **186**, 123 (2007).
4. J.A. Finlay *et al.,* Biotechnol. Bioeng. **63**, 87 (1999).
5. D.A.Graf von der Schulenburg *et al*., Water Sci. Technol. **55**, 275 (2007).

MRI-based D_2O/H_2O-Contrast Method to Visualize Membrane Hydration Path in a Temperature-Controlled Polymer Electrolyte Membrane Fuel Cell

Shohji Tsushima[1] , Toshikazu Kotaka[1] and Shuichiro Hirai[1]

[1] Research Center for Carbon Recycling and Energy, Tokyo Institute of Technology, Tokyo, Japan

Abstract:

Polymer electrolyte membrane fuel cells (PEMFC) are attracting great attention as future power sources for vehicles and on-site power generation due to their high power density and low temperature operation. However, Water management in polymer electrolyte membrane (PEM) is a major issue because PEMs must be well hydrated to maintain high proton conductivity (1). Consequently, it is of great interest to water content and water transportation in PEMs during fuel cell operation. In our previous studies, we introduced magnetic resonance imaging (MRI) technique to measure a transversal water distribution in PEM under fuel cell operation and revealed that PEM was dehydrated partially in the anode due to the electro-osmotic effect (2, 3). Demonstrated in our previous studies with MRI, transversal water content distribution of PEM varies greatly by operating condition, cell temperature and humidifying condition. However, the effect of water vapor on hydration of PEM under fuel cell operation is not well understood.

In this study, D_2O/H_2O-contrast method by a nuclei-labeling magnetic resonance imaging (NL-MRI) technique is applied to investigate the effect of water vapor and generated water on hydration of polymer electrolyte membrane (PEM) separately in polymer electrolyte membrane fuel cell (PEMFC) during operation. As shown in Fig.1, it was successfully visualized that the membrane hydration path (i.e. anode humidification, cathode humidification or generated water) could be distinguished in an operating PEMFC. From visualization results, it was found that water vapor from the anode and the cathode has little effect on the membrane hydration. This indicates that most membrane hydration came from water generated by the electrochemical reaction.

1. T. A. Zawodzinski et al., *J. Electrochem. Soc.* **140**(1993) 1041.
2. S. Tsushima et al., *Electrochem. Solid-State Lett.* **7**(2004), A269.
3. S. Tsushima et al., *ECS Transaction* **3**(2006), 91.
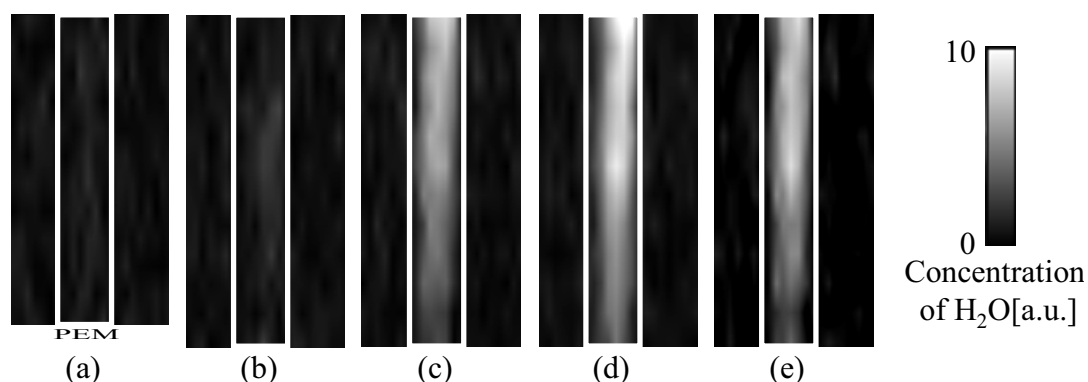
Fig.1: Result of separation analysis of the effect on hydration of PEM by nuclei-labeling MRI technique. White box denotes membrane and the anode is on the left side. (a) effect of anode humidification (b) effect of cathode humidification (c) effect of supplied hydrogen (d) normal operation (e) summation of (a), (b) and (c).

Counter Hagen-Poiseuille flow of two liquids

F.J. Vergeldt[1], E. Spruijt[2], W.J. Wolferink[2], R.H. Tromp[3], H. Van As[1] and S. Lindhoud[4]

[1] Laboratory for Biophysics, Wageningen University, Wageningen, the Netherlands
[2] MSc Molecular Sciences, Wageningen University, Wageningen, the Netherlands
[3] NIZO Food Research BV, Ede, the Netherlands
[4] Laboratory of Physical Chemistry and Colloid Science, University, Wageningen, the Netherlands

Abstract:

Mixtures of equally charged and/or uncharged polymers will separate in two coexisting phases, each being rich in one type of polymer. Mixtures of aqueous solutions of gelatin and dextran are an example where such segregative phase separation takes place. These are interesting model systems to study both their static behavior in confined geometries like capillaries, where they form a meta-stable system of plugs, as well as their dynamic properties in larger tubes. This behavior might be relevant in micro-analyses systems, e.g. lab-on-a-chip.

At equal concentration (% w/w) of polymer there exists a density difference between the aqueous dextran and gelatin phase. In a NMR tube this can results in two layers, aqueous dextran on top of the heavier gelatin solution. When this tube is turned, the dextran solution rises through the centre, while the gelatin solution sinks along the edge, to restore the stable starting situation. Here MRI flow imaging is used to study in detail how the two liquids flow along each other.

MRI flow imaging was done using Pulsed Field Gradient (PFG) spin echo NMR for q-space imaging in combination with a Turbo Spin Echo imaging sequence (PFG-TSE) [1].

The central column of the rising dextran phase shows a clear Hagen-Poiseuille flow profile. The outer ring of sinking gelatin solution also shows a Hagen-Poiseuille-like pattern, as through a hollow pipe. In one experiment the repetition time was chosen short, resulting in a T_1 weighted image where the two phases could be distinguished (Fig. 1a). A map of the mean velocity per pixel (Fig. 1b) is used to separate rising from the sinking fraction. In Fig. 1c it is clearly shown that boundaries of the two phases don't coincide with the boundary between the rising and sinking fraction. From this it is concluded that part of the central dextran phase is dragged downwards by the gelatin solution.
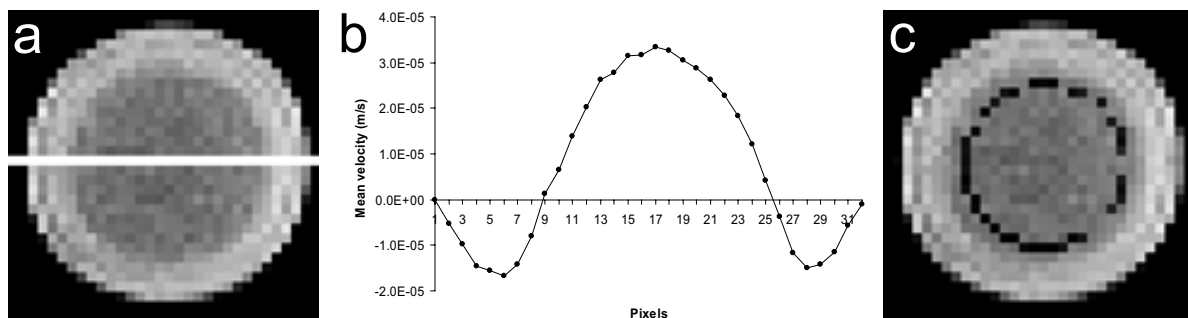
Fig. 1: Results from a PFG-TSE experiment of 12% w/w aqueous gelatin and dextran at 0.72 T, resulting in a 32*32 image of 4.5*4.5 mm^2 with a slice thickness of 4 mm. Q-space imaging was done with 16 PFG steps of 9 ms ranging from -0.085 to 0.074 T/m, with a displacement encoding time of 0.3 s. Using turbo factor 32, 256 averages and repetition time 1.0 s., the experiment lasted 1 hour and 8 minutes. a) T_1 weighted image b) Cross section (marked by the white line in Fig. 1a) of the mean velocity map c) T_1 weighted image; the black pixels mark zero velocity (-2.5 μm/s < v_{mean} < 2.5 μm/s)

1. T.W.J. Scheenen, D. van Dusschoten, P.A. de Jager and H. Van As, *JMR* **142** (2000) 207-215.

Quantitative analysis of interdiffusion in a binary liquid system

Mihai A. Voda, Federico Casanova, Siegfried Stapf, Bernhard Blümich

Institut für Technische Chemie und Makromolekulare Chemie, RWTH University of Aachen, Germany

Modeling the mixing process of multicomponent liquids is still an open problem. The possibility of using NMR to measure with high accuracy concentration profiles during interdiffusion of multicomponent systems is discussed. The accuracy of the experimental data is mandatory when the results are used for model discrimination. This work presents the difficulties that appear when measuring concentration profiles of two mixing liquids with low viscosities and similar densities. During the mixing process of different liquids, the concentration gradient leads to a time-dependent distribution of magnetic susceptibility within the sample. NMR experiments as well as numerical simulations are used to show the magnetic field distortions introduced by the susceptibility of pure liquids as well as their mixture in the sample. The field distortion due to the interface between the two liquids is also discussed. A chemical shift imaging method is used to measure the concentration profiles of water-acetone system during mixing. The resultant profiles are processed in order to compute the interdiffusion coefficients.

Spatial and Temporal Mapping of Water Content across Nafion Membranes under Wetting and Drying Conditions

Ziheng Zhang[1], Andrew E. Marble[1,2], Bryce MacMillan[1], Keith Promislow[3], Bruce J. Balcom[1]

[1]MRI Centre, Department of Physics, [2]Department of Electrical and Computer Engineering,
  University of New Brunswick, Fredericton, New Brunswick, Canada E3B 5A3
[3]Department of Mathematics, Michigan State University, East Lansing, MI 48824, USA

Abstract:

   Water transport and water management are fundamental to polymer electrolyte membrane fuel cell operation. Accurate measurements of water content within and across the nafion layer are required to elucidate water transport behavior and validate existing numerical models [1].

   We report here a direct measurement of water content profiles across a nafion layer under wetting and drying conditions, using multi-echo double half k-space spin echo single point imaging. Based on a pure phase encode spin echo, it is purposely designed for high resolution 1D depth imaging of thin film samples. The method generates high resolution (< 8 μm) depth images with an SNR greater than 20 with an image acquisition time of less than two minutes.

   A mock fuel cell was custom designed, removing the complications associated with an operating fuel cell. Three different, well-controlled, boundary conditions were established for studying the water gradient across nafion membrane samples: (A) Passive drying. (B) Active drying. (C) Wetting and drying boundary conditions. The corresponding resultant profiles are shown in Fig. 1.
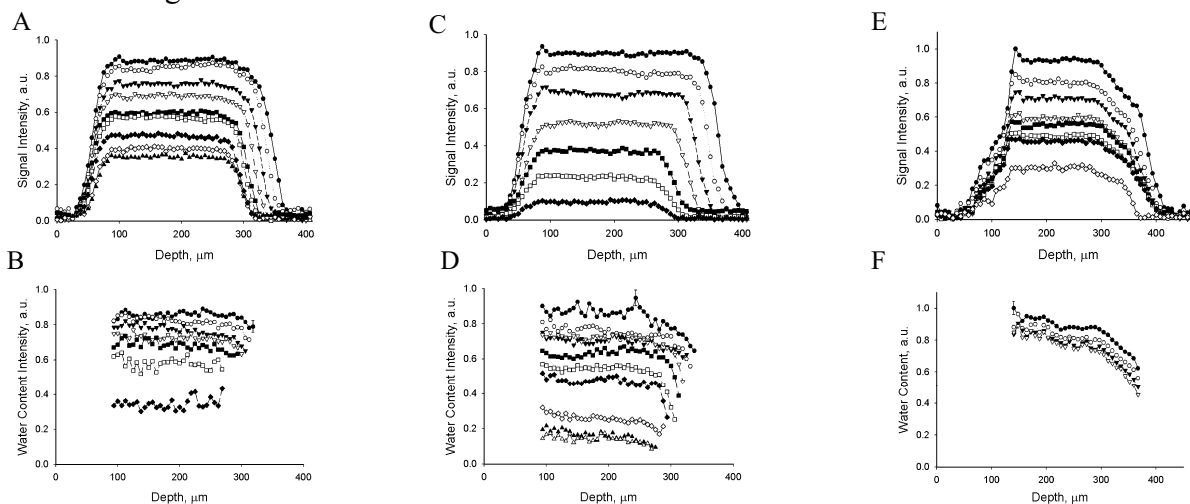
Fig 1: (A), water content across the nafion membrane undergoing passive drying. The sample shrinks in thickness (B), true water content maps of the drying profiles, determined by relaxation time mapping. The water content is quasi uniform and decreases with time. (C), water content across the nafion membrane undergoing active drying. The membrane shrinks as it dries, while the profile intensity is quite uniform, although the intensity decreases with time. (D), the water content of active drying. At right of the profiles, there may be an indication of the development of a drying front as the membrane shrinks. (E), water content across the nafion membrane undergoing wetting/drying. At the left bottom of the profiles, there exists some residual signal from the water in perforations. At the right top corner, the 'shoulders' are pronounced. (F), 4 averaged water content profiles. Water content decreases in over 20 hours, due to the aging effect of the membrane. A clearly declining water content is present at the drying side.

1. R.A. Lemons, Fuel cells for transportation, J. Power Sources, 29 (1990) 251-264.

Transport influence on chemical waves: an MRM study

Vladimir V. Zhivonitko and Igor V. Koptyug

International Tomography Center SB RAS , Novosibirsk, Russia

Abstract:

An autocatalytic reaction in an unstirred medium can provide a constantly propagating wave front resulting from the coupling of diffusion to the chemical reaction. Similar interface motion and front propagation occur in many different areas of interest to science and technology. Among the most interesting instances one can be mentioned population dynamics of ecological communities (e.g., plankton), atmospheric chemistry (ozone hole), flame propagation in gases, biological systems (bacteria colonies morphology, calcium waves in cells). MRM provide great possibility to investigate such chemical systems in optically opaque media without invasive penetration and distortion of its intrinsic structure. Moreover, acquired data allow gaining information about various parameters changing during the front motion such as concentration, temperature and flow velocity.

The present work deals with MRM investigation of advection (transport in a fluid) or convection influence on chemical waves in different environment such as packed bed (PB) or thin capillary. MRM has been already employed in investigations of various modifications of oscillating Belousov-Zhabotinsky reaction in the presence of advective flow, but never for non-oscillating autocatalytic reactions [1]. Three non-oscillating reactions were examined in order to get *wave Front Velocity-Flow Rate* (FVFR) dependencies.

$$2CoEDTA^{2-} + nOH^- + H_2O_2 = 2CoEDTA^- + (n+2)OH^- \qquad R1$$

$$2Fe^{2+} + HNO_3 + nHNO_2 + 2H^+ = 2Fe^{3+} + (n+1)HNO_2 + H_2O \qquad R2$$

$$S_2O_3^{2-} + 2ClO_2^- + nH^+ + H_2O = 2SO_4^{2-} + 2Cl^- + (n+2)H^+ \qquad R3$$
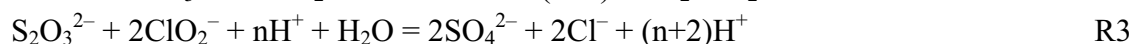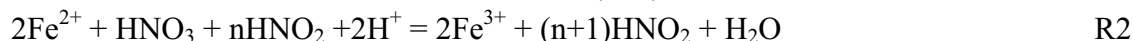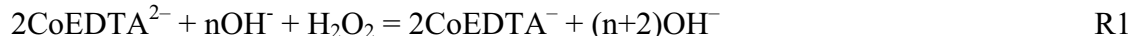
As distinct from the first two reactions, where contrasted images and/or one-dimensional profiles were acquired basically by differences in paramagnetic properties of oxidation states of metal-ions, contrast for the third system was performed by measuring temperature changes during the course of this strongly exothermal reaction using spatially resolved water chemical shift NMR-thermometry. As it has been found the formation of considerable amount of gaseous oxygen during the side reaction determined by scanning time resolved 2D images of propagating wave in PB makes it impossible to derive quantitative conclusions in the case of the R1. Meanwhile, linear FVFR dependence obtained for the R2. Also oscillating convective instability has been found for the latter system at low rates of advective flow by acquiring 1D profiles of moving front. The FVFR dependence for different initial concentrations in the case of R3 shows that by adjusting chemical composition it is possible to control evaluation of stationary ascending in the flow chemical waves that previously was observed only in oscillating Belousov-Zhabotinsky reaction system [2]. Acquired temperature maps in addition to visualization of wave propagation (R3) allow one to judge about directions of arising convective flows [3].

1. M. M. Britton, A. J. Sederman, A. F. Taylor, S. K. Scott, L. F. Gladden, *J. Phys. Chem. A* **109** (2005) 13209-13214.
2. M. Kaern, M. Menzinger, *J. Phys. Chem. B* **106** (2002) 3751-3758.
3. V. V. Zhivonitko, I. V. Koptyug, R. Z. Sagdeev *J. Phys. Chem. A* **111** (2007) 4122-4124.

Detecting Magnetic Nanoparticles that Selectively Bind to Cancer Cells: the complementary aspects of SQUID Magnetometry and Magnetic Resonance Imaging

Natalie L. Adolphi[1] , Edward R. Flynn,[2] Howard C. Bryant,[2] Richard S. Larson,[3] Laurel O. Sillerud,[3] and Debbie Lovato[3]

[1] New Mexico Resonance, Albuquerque, New Mexico, USA
[2] Senior Scientific LLC, Albuquerque, New Mexico, USA
[3] Health Sciences, University of New Mexico, Albuquerque, New Mexico, USA

Abstract:

It is well-known in the MRI community that superparamagnetic iron oxide nanoparticles (SPIONs) can be used as MR contrast agents, due to their effects on the relaxation rates of nuclei in the vicinity of the particles. Recently, there has been considerable interest in attaching antibodies or other recognition ligands to the SPIONs, such that they bind selectively to particular cell types (such as cancer) *in vivo* to enable the specific, non-invasive detection of disease. In addition to MR, another possibility for detecting SPIONs is to directly measure their magnetic moments. Recently, Flynn and Bryant [1] have shown that SQUID (superconducting quantum interference device) magnetometry has the necessary sensitivity to detect the magnetization of SPIONs bound to just a few thousand cells at distances of several centimeters, appropriate for *in vivo* detection of magnetically-labeled cancer cells in humans.

To detect SPIONs using SQUID magnetometry, the particles are magnetized by a pulse of magnetic field (35 Gauss for 300 ms, in our case), after which the SQUID sensors measure the decaying magnetization (for 2 s, digitizing at 1 kHz). A significant advantage of the SQUID technique is the possibility of detecting only those SPIONs bound to the cells of interest, even in the presence of a large background of unbound particles, because of differences in the relaxation mechanisms of bound and unbound particles. Another advantage of the SQUID technique is the simplicity of the interpretation – the measured magnetic moment is simply proportional to the number of bound SPIONs. By using an array of SQUID sensors, both the magnetic moment and spatial coordinates of a magnetic source may be determined; however, a potential disadvantage of SQUID "imaging" is that the background anatomy is not depicted. **Thus, co-registery of SQUID and MR images is an attractive possibility for optimizing localization and quantitation.**

Preliminary data (see below) indicate that SPIONs suitable for SQUID detection also give rise to easily-detected contrast changes in MRI. Additional data illustrating the complementary features of SQUID and MRI will be presented. Progress towards optimizing detection, quantitation, and co-registration will also be discussed. [1] ER Flynn and HC Bryant, *Phys. Med. Biol.* **50** (2005) 1273-1293.

Fig. 1 MR images (spin echo, TE = 10 ms , TR = 1500 ms, B_0 = 1 T) of test tubes containing agarose gel. In samples B-D, the dark bands are a layer of agarose gel containing human ovarian cancer cells (TOV112D) labeled with SPIONs (SiMag 1411, Chemicell, Berlin) bearing antibodies to the CA125 antigen expressed by the cells. The nominal number of cells in each sample is given on the figure.
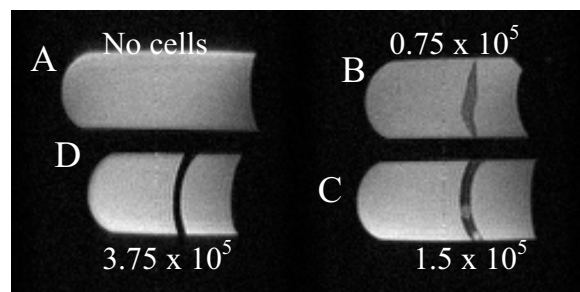
Fig. 2: Comparison of MR contrast with the SQUID-determined magnetic moment for each sample shown in Fig. 1. While the SQUID signal is linear in the number of nanoparticles, the T_2 contrast saturates when the concentration of nanoparticles becomes too high.

MR Microscopy of Resorbable Polymeric Bioceramics

Josh M. Bray[1,2], Carl Petrone[3], M. Filiaggi[3] and Steven D. Beyea[1,2,4]

[1] Institute for Biodiagnostics (Atlantic), National Research Council, Halifax, Nova Scotia, Canada
[2] Department of Physics, [3] School of Biomedical Engineering, [4] Department of Radiology, Dalhousie University, Halifax, Nova Scotia, Canada

Abstract:

While novel and innovative interventions in regenerative medicine hold great promise, such methods are only as effective as the ability to develop an empirical and mechanistic understanding of how/why they work. One such example is the use of resorbable bioceramics, which have potential to provide large, sustained concentrations of therapeutic agents to a specific tissue, while not exceeding the minimum toxic concentration in other tissues.

Optimization of resorbable bioceramic design requires methods that will permit the non-invasive and non-destructive study of the spatially and temporally varying physicochemical changes that occur due to material degradation. The study of drug delivery biomaterials using MRI therefore has the potential to significantly improve the understanding of the performance of such devices.

The current study focuses on the use of MR imaging and relaxometry at 11.7 Tesla to characterize the spatial-temporal evolution of amorphous Calcium Polyphosphate (CPP) bioceramics, intended for implantation into bone fractures for treatment of osteomyelitis. The ability of MR microscopy to resolve the internal network reorganization will be demonstrated by comparing the results obtained as a function of initial biomaterial processing.

Fig. 1: Data extracted from a single pixel internal to a CPP disk, shown as a function of time during 1D fluid transport into the material. Plots of Fluid Saturation, T1 relaxation time, and T1 component relative amplitude are shown. Data for CPP disks produced using two different processes are shown, with the "G2" disks having undergone a secondary re-compaction/gelling step.

Dynamic *in vivo* GARField Magnetic Resonance Profiling of Skin Hydration

E. Ciampi[1], S. Singleton[1], M. van Ginkel[1], S. Pitts[2] and P. J. McDonald[2]

[1] Measurement Science Unit, Unilever R&D, Colworth Science Park, Sharnbrook, Bedford, U.K.

[2] Department of Physics, University of Surrey, Guildford, Surrey, U.K.

Abstract:

Ageing and stress effects on skin ultimately correlate to changes in skin properties and hydration status. To optimise delivery of positive skin benefits to consumers, such as improved hydration to deeper layers, it is important to understand the complex interplay between the applied material and the underlying system response. The challenge for skin is particularly severe as it is a highly differentiated and complex structural and biological system.

In this work we describe progress we have made in exploiting non-invasive *in vivo* GARField Nuclear Magnetic Resonance Profiling applied to human skin to investigate product delivery to the skin and its response to stimulus. We demonstrate that GARField NMR offers quantification of spatio-temporal dynamics *in vivo* that allows us to assess the impact of applied materials on skin hydration and molecular mobility in terms of e.g. self-diffusivity and NMR relaxation times.

Our work has been applied to components typical of skin care formulation systems. Hence, we show how different materials penetrate and indeed fundamentally impact diffusion and mobility properties throughout skin for considerable periods after application. As these properties are ultimately related to molecular and water transport mechanisms, we gain a further insight into permeation mechanisms into skin and underlying barrier functions.

We believe our findings will begin to offer improved understanding of skin behaviour and hence ultimately to optimise skin care product design delivering moisturisation and functional actives.

Characterization by MRI of glenoid trabecular bone

G. Guillot[1], S Abdelmoumene[2], I Kalouche[2], J Crépin[3], O Gagey[2]

1-U2R2M UMR8081 CNRS-Univ. Paris-Sud, Bât 220, 91405 Orsay, France
2-Service d'Orthopédie-Traumatologie, Hôpital de Bicêtre, 94275 Le Kremlin-Bicêtre, France
3-Solid Mechanics Laboratory, CNRS UMR 7649, École Polytechnique, 91128 Palaiseau , France

Replacement arthroplasty for gleno-humeral osteoarthritis faces problems of long-term stability, especially concerning the fixation of the glenoid component[1]. In this work, high resolution MRI and image analysis were used to evaluate the general patterns and possible variability of trabecular bone architecture of the glenoid. Images were acquired from 20 fresh frozen specimens, with a thickness of about 2 cm from the articular surface, in a clinical 1.5 T scanner. A home-made coil with the Helmholtz configuration was used as receiver. Trabeculae appeared thicker with 3D GE than with 3D SE, as well as with 3D SE multi-echo than with 3D SE single echo, in agreement with previous findings[2]. Images were acquired with a resolution of 0.1 mm x 0.1 mm x 0.25 mm, the coarser resolution being along the left-right anatomical axis which also corresponded to the main direction of the trabecular structure (Fig 1), then interpolated to an isotropic resolution of 0.1 mm. Fig 1 shows the three orthogonal 2D sections across a 3D volume, and the positioning of 6 ROIs chosen to match those of cubes taken from each specimen for later mechanical testing. Architecture parameters (bone volume fraction BV/TV, bone surface to volume BS/TV, Euler number, anisotropy ratios) were computed from these ROIs with home-developed software[2] running with Matlab, after data binary segmentation adapted to the local gray-level. Signal-to-noise between bone marrow and background was in the range of 10 to 20, and trabecular bone pixels were about 2 times lower than marrow ones, indicating partial volume effects. The architecture parameters were in the same range as those measured at other anatomical sites[3]. While BV/TV, BS/TV and Euler number were significantly different between the specimens, from the anisotropy factor, the posterior superior ROI was significantly more anisotropic than the 5 others. The last result was in fair qualitative agreement with the anisotropy observed on Young modulus.
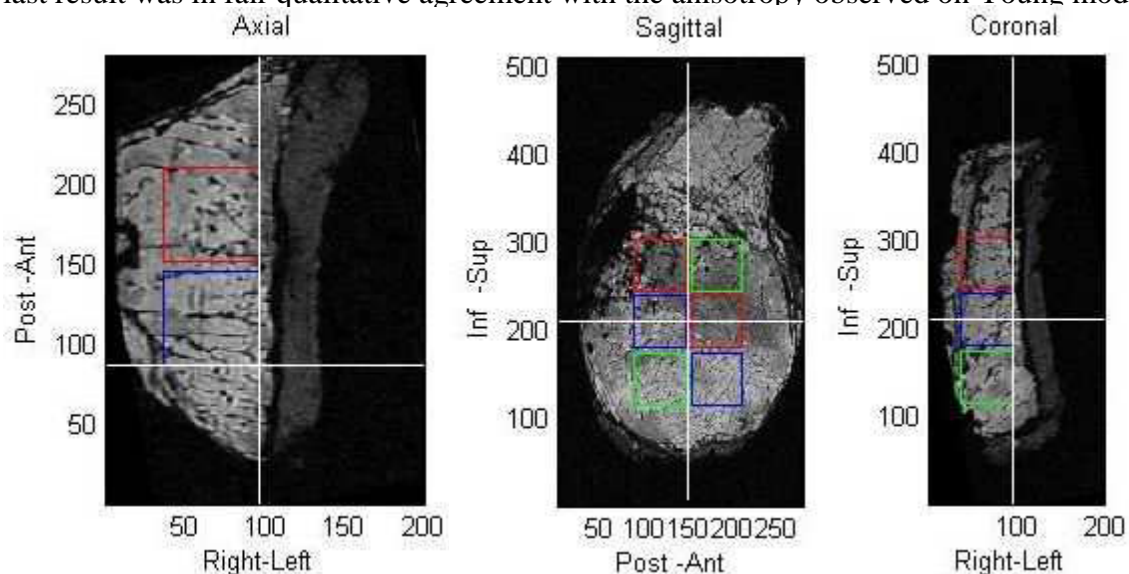
Fig.1. Three orthogonal sections across one glenoid specimen, at an isotropic resolution of 0.1 mm. The white lines represent the positions of the other sections. FOV 51 x 28 x 20 mm³, matrix 512 x 280 x 80, TE/TR 24/100 ms, bandwidth/pixel 120 Hz, Nacc 3.

1. C. S. Neer Replacement arthroplasty for glenohumeral osteoarthritis. J Bone Joint Surg Am 56 (1974):1-13.
2- F. Wehrli J Magn Reson Imaging 25 (2007) 390–409.
3- D. Last, F. Peyrin, G. Guillot MAGMA 18 (2005) 26–34.

Assessing the detection sensitivity of iron loaded cells in spoiled gradient echo imaging

Xavier Helluy[1] , Wing Chow[2] and Peter M. Jakob[1]

[1] Department of Experimental Physics 5 ,University of Würzburg, Würzburg, Germany
[2] University of Toronto, Toronto, Canada

Abstract:

Susceptibility inhomogeneities induced by iron particles affect the magnitude and phase of gradient echo images (GE) [1], facilitating the detection of iron-loaded cells with MR [2,3]. The goal of this work is to quantify the iron detection sensitivities of spoiled GE phase and magnitude images or of a combination of both informations. To this end, the sensitivity of various complex image filters on the detection of isolated iron loaded cells in spoiled GE imaging is assessed based on a statistical analysis of filtered numerical simulations images in the static dephasing regime [4] (figure 1). Magnitude, phase, phase masks [1], commutator [1] and bivariate filters are considered. The influence on the sensitivity of signal to noise ratio, voxel size, T2*, echo time and GE bandwidth is investigated and numerical predictions are compared to a phantom experiment.
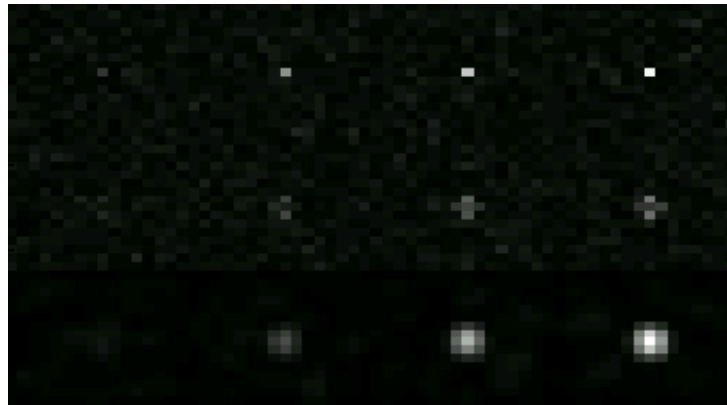
Fig. 1: simulations in the static dephasing regime of 16x16 magnitude (up), phase (middle) and commutator (bottom) GE images for iron concentrations of 4, 8, 12, and 16 pgFe/cells [5] at a SNR of 50. Voxel size: 100µm, TE/TR[ms]=10/20, T1/T2/T2*[ms]=1000/300/50.

1. Reichenbach JR et al, *J Magn Reson Imaging* **7**(1997) 266-279 – 2. Dahnke H et al, *Proc 15th Scientific Meeting ISMRM Berlin (*2007) p1228 - 3. Mills PH et al, *Proc 15th Scientific Meeting ISMRM Berlin* (2007) p525- 4. Yablonskiy DA, *Magn Reson Med* **32**(1994) 749-763 - 5. Heyn C et al., *Magn Reson Med* **53**(2005) 312-20

In vivo intra-oocyte NMR spectroscopy

Verena Hoerr, Armin Purea and Cornelius Faber

Dept. of Experimental Physics 5, University of Würzburg, Würzburg, Germany

Abstract:

In vivo intracellular NMR spectra were acquired from Xenopus laevis oocytes, either using PRESS localization in single cells, or using a novel approach, which combines solvent-localized (SOLO) NMR [1] with chemical shift reagents.
Measurements were performed on a Bruker Avance 750 MHz wide bore spectrometer equipped with a 1 T/m gradient system. Oocytes were incubated for 3 hours in Barth medium containing 125 mM choline. Press spectra (fig.1) from $(250 \ \mu m)^3$ voxels in different intracellular regions (vegetal and animal cytoplasm, and nucleus) were acquired using a 1 mm microcoil to verify the choline uptake. While in the vegetal hemisphere no choline was found, high choline concentrations were observed in animal hemisphere and nucleus. SOLO NMR (fig.2) allows separating NMR spectra of solutes in different solvents, based on selective excitation of the solvent. 2 ppm difference in chemical shift between intra- and extracellular water was achieved by doping the medium with Tm-DOPT. SOLO spectra were acquired on a sample of about 100 oocytes in a 5mm NMR tube using a 5 mm Birdcage coil. Upon selective excitation of either intracellular or extracellular water, only intracellular or extracellular choline was observed, respectively.
SOLO spectra were intrinsically averaged over all oocytes in the sample, compensating for the low sensitivity of the method. Since SOLO requires only a one-axis gradient, it can be performed on a standard high-resolution NMR spectrometer. Experiments were also performed on a 700 MHz system equipped with a cryo-probe. Measurements detecting tetracycline indicated that SOLO is a promising method for studying pharmacokinetics of cellular uptake of drug molecules.
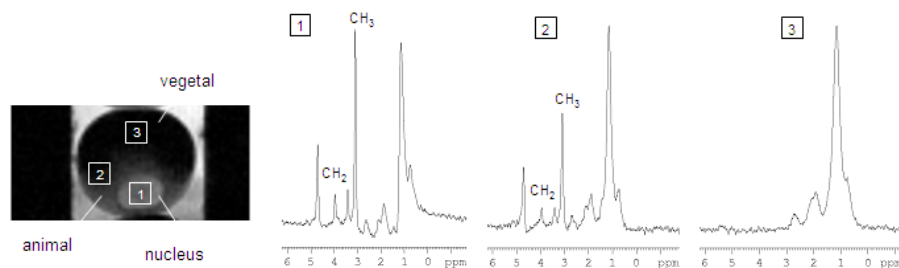
Fig.1: Choline uptake into cellular compartments. Localized PRESS spectra from a voxel size of $(250 \ \mu m)^3$ of nucleus (1), and animal (2) and vegetal (3) cytoplasm.
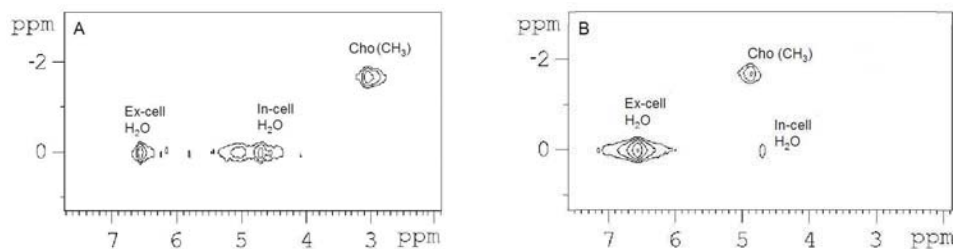
Fig.2: SOLO spectra with selective excitation of intracellular (A) or extracellular (B) water. Only intracellular (A) or extracellular (B) choline was observed.

1. C. Faber, J. Magn. Reson. **176** (2005) 120-124

Rapid 3D MR Histology on Murine Embryos using a Contrast Agent

Esra Lang[1], Andreas Fischer[2], Manfred Gessler[2], Peter M. Jakob[1]

[1]Department of Experimental Physics 5, University of Würzburg, Würzburg, Germany
[2]Department of Physiological Chemistry, Biocenter, University of Würzburg, Würzburg, Germany

Abstract

As congenital heart defects (CHD), such as ventricular septum defects (VSD) or dysplastic valves, are the most common human congenital malformations [1], locating the origin of these malformations is quite important. Despite its time consuming and invasive properties, histology is still the gold standard for phenotyping gene mutations. Nevertheless, MRI has started to become an alternative [2]. Here a 3D MRI microscopy set up which uses a contrast agent to study heart developmental failures in the knockout mouse embryo in approximately 6 hours total measurement time is presented.

MRI measurements were performed on a Bruker Avance 500 spectrometer (11.7T, 500MHz), equipped with a gradient unit with 0,6T/m, and a quadrature-driven birdcage coil with an inner diameter of 20 mm (Rapid Biomedical, Rimpar, Germany). A 3D-FLASH sequence (TE 5.9ms, TR 50ms, 30º hermite excitation pulse, SW 40kHz) was used. The field of view was 13 x 10 x 10 mm^3, with a matrix size of 648 x 256 x 256, resulting in a nominal resolution of 20 x 39 x 39 μm^3. The total experimental time was less than 4h, including averaging four times. Data sets were reconstructed and zero-filled to a matrix size of 648 x 512 x 512, yielding an isotropic voxel size of 20 x 20 x 20 μm^3.

Wild-type (WT) mouse embryos were fixed in 4% paraformaldehyde (either non-doped or doped with 2mM Magnevist (Schering, Germany)) and embedded in 2ml syringes using 1.5% agarose gel. The CNR (atrium-ventricle contrast) of the images with the non-doped embryos (Fig.1) was lower by a factor of 2-3 compared to the doped embryos. Subsequently, doped WT and two different knockout type mouse embryos (six of each, stage 15.5 dpc) were screened and investigated for CHDs (Fig.2). The findings were verified by histology. For a better illustration of the complexity of the CHDs, datasets were reconstructed in 3D and surface views were created (Fig.3) using a commercial software package (Amira 3.1, Mercury Computer Systems, USA).

By using a MRI contrast agent during fixation, the total operator time is hours compared to days in histology and the resolution and contrast achieved were sufficient to identify CHDs. Thus, MR histology is capable of screening and phenotyping large numbers of small samples in a suitable time.
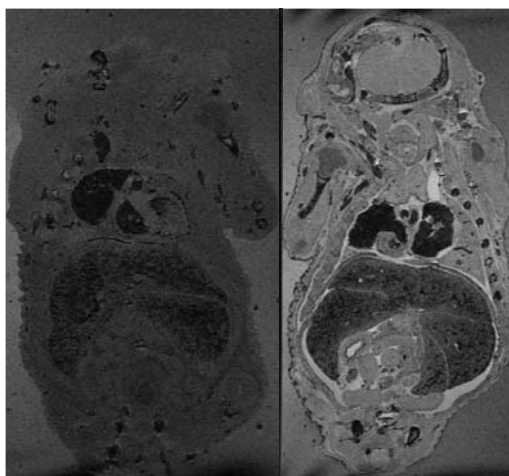
Fig.1: *Coronal view of murine embryo fixed in PFA non-doped (left) and doped (right) with Magnevist*
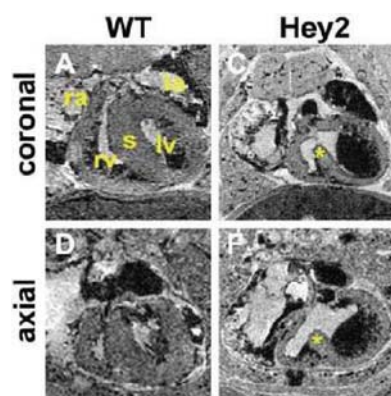
Fig.2: *Murine embryo hearts magnified, wildtype and knockout with VSD (*)*
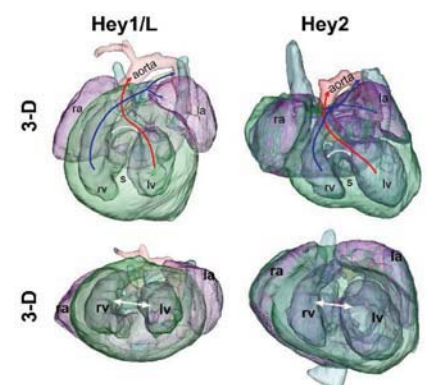
Fig.3: *Murine embryo heart 3D reconstruction of MRI images, arrows indicate bloodflow*

[1] Hoffman JI et al.; J Am Coll Cardiol. 2002; 39:1890-900.
[2] Schneider JE et al.; J Mol Cell Cardiol. 2003; 35:217-222

Morphological imaging of the *in vivo* mouse eye: application to diabetic retinopathy.

T.Neuberger[1], S.Aussenhofer[1], M.Kennett[2], T.Gardner[3], A.Barber[3], N.B.Smith[1], A.G.Webb[1]

[1] College of Engineering, [2] Veterinary Medicine, [3] Hershey Medical School, Penn State University, University Park, PA, USA

Abstract:
As a leading cause of blindness, diabetic retinopathy is a severe complication in which blood vessels and neuroglial cells in the retina are damaged. In mild nonproliferative retinopathy areas of retina blood vessel swelling (microaneurysms) occur, moderate nonproliferative retinopathy is characterized by blocked vessels, severe nonproliferative retinopathy leads to abnormal vessel growth, and in proliferative retinopathy fragile vessels can leak which can lead to vision loss and blindness. The goal of the project is to determine whether MRI techniques can be used for future clinical diagnosis and therapy in humans by evaluating techniques developed on diabetic mice. Diabetic retinopathy is being studied using the C57BL/6J Ins2Akita mouse model. The first step has been to image the morphology and vascularity of normal mice. Although extensive work has been performed on rat eyes [1-3] these are some of the first images from the *in vivo* mouse eye. Experiments were performed at 600 MHz using an 8 mm diameter surface coil with balanced impedance matching. Mice were anesthetized using an isoflurane/oxygen mixture. In order to minimize the effects of the curvature of the mouse eye on spatial resolution, ten thin slices (200 μm) were acquired with an in-plane spatial resolution of 30 x 30 μm^2 in an acquisition time of 8 mins. Figure 1 shows that several thin layers can be distinguished within and at the back of the eye. Upon administration of Gd-DTPA (i.v. or i.p.) both vascular and avascular layers at the back of the eye can be visualized. Current research is underway to compare the morphology, relaxation times and vascularity of the Akita mouse model with the corresponding wild types.
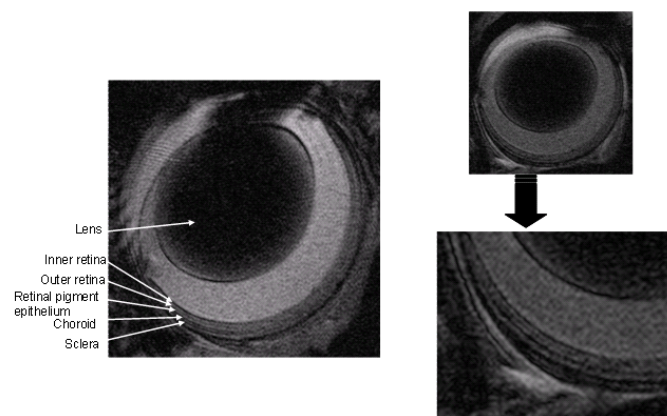
Fig. 1: (left) Image of in vivo mouse eye acquired in 8 minutes (200 x 30 x 30 μm). (right) Images acquired after i.v.administration of Gd-DTPA.

1. Cheng H, Nair G, Walker TA, Kim KM, Pardue MT, Thule PM, Olson DE, Duong TQ, *Proc.Natl.Acad.Sci.* 2006, **103**, 17525-17530. .2. Luan H, Roberts R, Snlegowski M, Goebel DJ, Berkowitz BA. *Inv.Opth.Vis.Sci.* 2006, **47**, 320-328. 3. Berkowitz BA, Roberts R, Luan H, Peysakhov J, Mao X, Thomas K.A., *Inv.Opth.Vis.Sci.* 2004, **45**, 2391-2398.

Morphometric and air flow analysis of the nasal airways of the dog using magnetic resonance microscopy.

T.Neuberger[1], B.A.Craven[1], G.S.Settles[1], E.G.Patterson[1], E.M.Josephson[2], E.E.Morrison[2], A.G.Webb[1]

[1] College of Engineering, Penn State University, University Park, PA, USA
[2] Department of Anatomy, Auburn University, Auburn, GA, USA

Abstract:

The canine nasal airway is one of nature's most complicated anatomic structures and has been proposed as a model for designing chemical sensors for narcotics and explosives detectors. Previous non-invasive studies [1, 2] have not been able to show bone and soft-tissue interfaces of the ventral and ethmoidal conchae. Partially overlapped composite scans (950 slices) were acquired using a Varian 7T magnet and a 14 cm i.d. quadrature birdcage coil. The slice thickness used was 200 μm, with an in-plane resolution of 180 x 180 μm^2. The specimen was placed in a plastic cylinder: trapped air was removed with a vacuum pump and water introduced into the sample. After image segmentation, morphometric analysis of the canine nasal airway was performed, in which airway perimeter, cross-sectional area, cumulative surface area, and cumulative internal volume were calculated as functions of axial location. The fractal dimensions of the perimeter were also calculated. Figure 1 shows a three-dimensional reconstruction of the airwaves, together with a plot of the flow characteristics. Further three-dimensional scans were performed at a spatial resolution of 62.5 x 62.5 x 62.5 μm^3 through selected volumes which were characterized by very complicated morphology. The data provided some unexpected results. For example, the dorsal meatus of the canine was shown to function as a partial bypass for odorant-bearing inspired air, around the complicated ventral concha during sniffing for olfaction. Thus, a majority of the airflow may be reaching the ethmoidal region (where olfactory reception occurs) directly via the dorsal meatus, rather than filtering through the scrolls of the ventral concha as was previously thought.
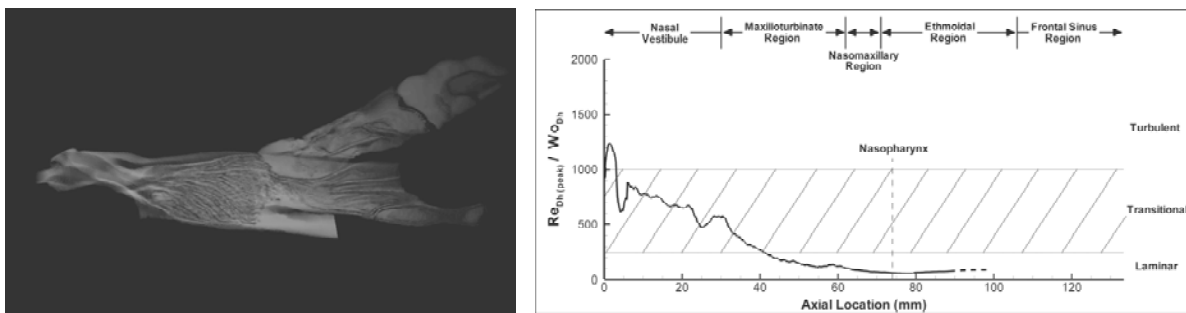
Fig. 1: (left) Three-dimensional reconstruction of the canine nasal cavities. (right) Nature of pulsatile flow represented by the ratio of the Reynolds to Wormesley number.

1. Stitzel SE, Stein DR, Walt DR. 2003. *J.AmChem.Soc.* **125** 3684-3685. 2. Hahn, I., Scherer, P.W., Mozell, M.M. 1994. *J. Theor. Biol.* **167** (1994)115-128.

Measurements of NMR parameter weighted images in chemically fixed human embryos

K.Oya[1], K.Kose[1], K.Shiota[2]

1 Graduate School of Pure and Applied Science, University of Tsukuba

2 Graduate School of Medicine, Kyoto University

Introduction Our group has acquired about 1,200 3D MR microscopic images of chemically fixed human embryos (Kyoto Collection of Human Embryos (1)) using a super-parallel MR microscope to construct an anatomical database for human embryos (2-4). In this project, only T_1 weighted 3D images were acquired. However, because T_2 and the diffusion constant will give us different and valuable image contrasts, their measurements are highly desired. In this study, we measured 2D or 3D distribution of T_1, T_2, diffusion constant and proton density (PD) of a chemically fixed human embryo to clarify the relation between the NMR parameters.

Materials and Method A chemically fixed human embryo (CS 21) was used for NMR parameter measurements. A homebuilt MR microscope with a 4.74 T vertical bore superconducting magnet and a gradient probe was used for 3D SE image acquisition. A dual scan method, in which k space NMR signal was separately acquired for the low and high spatial frequency datasets with different receiver gain, was used to overcome the limitation of the receiver dynamic range. 3D SE image acquisitions were repeated for various TR, TE, and b values. After the 3D image datasets (matrix:128^3) were extended to 256^3 image datasets through a zero-filled Fourier interpolation, mid-sagittal planes were extracted by 3D image rotation. T_1, T_2, and diffusion constant images were calculated for the mid-sagittal plane using a nonlinear regression method. The PD image was calculated by correcting the PDWI (TR/TE=2000ms/10ms) using T_1 and T_2 images.

Results and discussion Figure 1 shows distributions of T_1, T_2, diffusion constant and PD in the mid-sagittal plane. As shown in the figure, images of T_1 and T_2 give similar image contrast. Table 1 shows R^2 between NMR parameters. Because R^2 between T_1 and T_2 is about 0.88(Fig.2), this result suggests that T2WI of the fixed embryo give identical (but reversed) image contrast with that of T1WI. However, because R^2 values between relaxation times and diffusion constant are relatively low, DWI may give different image contrast from that of T1WI or T2WI.

Conclusion Distributions of T_1, T_2, and diffusion constant of a chemically fixed human embryo were calculated in the mid-sagittal plane using 3D datasets of T_1, T_2 and diffusion weighted SE images. The correlation between T_1 and T_2 was very high but those between diffusion constant and relaxation times were not high. Therefore, if we take another image in addition to T1WI for chemically fixed human embryos, DWI should be preferred to T2WI.
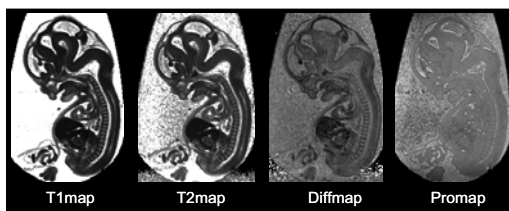
Fig.1 T1 map, T2 map, diffusion map and proton map
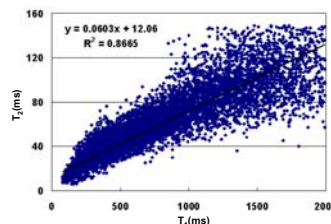
Fig.2 Correlation between T_1 and T_2

	T_1	T_2	D	PD
T_1		0.8665	0.4415	0.0864
T_2			0.5069	0.1362
D				0.1462
PD				

Table.1 Correlation coefficient between NMR parameters

References
1. Nishimura H, Takano K, Tanimura T, Yasuda M. Teratology 1968; 1:281-290
2. Matsuda Y, et al. 12th ISMRM Pro, Kyoto, 2004, p61
3. Matsuda Y, et al. 13th ISMRM Pro, Miami, 2005, p534
4. http://mrlab.frsc.tsukuba.ac.jp/human_embryos/index.html

Using MR Elastography to Image Force Chains in a Quasi-Static Granular Assembly

L. Sanfratello[1], S.A. Altobelli[1], E. Fukushima[2]

[1] New Mexico Resonance, Albuquerque, USA
[2] ABQMR, Albuquerque, USA

Abstract:

Granular materials abound in nature and industry. Understanding the behavior of these materials under a variety of conditions is important, for example, for avoiding landslides. However, numerous questions about the behavior of dense granular assemblies and flow remain unanswered. One important reason is the lack of experimental data of the internal structure of these systems. It is known from 2D observations as well as from the boundaries of 3D systems that non-uniform stresses are present on the sides of containers as well as at the bottom of granular piles. These forces are distributed by what have been termed "force chains" where most of the stress is transmitted through only a few of the chains with much of the assembly bearing little or none of the force. Force chains can be studied in 2D by optical methods but they have yet to be seen in 3D due to the lack of a technique to do so. Therefore, it has not been possible to directly confirm the statistics of 3D force chains, an important variable when modeling how these systems are organized. We propose a variation of magnetic resonance elastography (MRE) imaging to visualize 3D force chains within a densely packed granular assembly.

MRE is a technique whereby small periodic displacements within an elastic material can be measured. Multiple bipolar motion encoding gradients incorporated into a typical spin-echo or gradient-echo pulse sequence, applied at the frequency of the mechanical oscillations, are used to detect the displacements. MRE can be used in medical MRI to discern discontinuities of Young's modulus to distinguish different types of tissue, for example, cancerous versus healthy. In some systems motion amplitudes as small as 1 micron have be detected using this technique. We verified our MRE technique using a gel (PermaGel) being sheared by a rod that is driven by a speaker. We propose to expand this method to image force chains within a 3D packed granular assembly of soft solid particles under a weak stress, i.e. enough for some chains to form. On top of this initial static stress we will superimpose a small-amplitude vibrational stimulus. The data will be collected in much the same way as typical MRE but with the difference that the wavelength of the mechanical oscillation will be longer than the sample, thereby having the force chains always oscillating in phase with the bipolar motion encoding gradient pulses. It is our hypothesis that significant coherent displacements will be found only along force chains while the majority of particles will move randomly if at all and spin phase will accumulate solely along these chains.

Dental Impression using MRI

F. Schmid[1], O. Tymofiyeva[1], K. Rottner[2], E.-J. Richter[2] and P. M. Jakob[1]

[1] Dept. of Experimental Physics 5, University of Würzburg, Würzburg, Germany
[2] Dept. of Prosthodontics, Dental School, University of Würzburg, Würzburg, Germany

Abstract:

For the production of dental restorations by CAD/CAM techniques, digital surface data are required. One way of gaining these data is using contrast-enhanced MRI [1]. The precision of the digital surface is required to be at least 100 µm. Under clinical conditions, resolution is limited and images with a nominal resolution of less than 100 µm can not be achieved due to the lack of signal-to-noise ratio (SNR) and long measurement times. Our purpose was to investigate if sufficiently accurate surfaces can be obtained from in-vitro measurements under clinical conditions.

Measurements were made on a whole-body MR scanner at 1.5 T (Magnetom Avanto). Extracted and prepared human teeth (Fig. 1) embedded in a MR signal-giving contrast medium (solution of 1.5% agar and 0.15% Magnevist, Schering, in water) were used as phantoms. Images were taken using a 3D-TSE sequence with an isotropic resolution of 300 µm using a surface coil with a diameter of 4 cm. Measurement parameters were: TR 400ms, TE 13ms, turbo factor 5, matrix size 192x100x52, FOV 60x31x16 mm^3, TA 8:34min. It has been shown that object boundaries can be detected with an accuracy surpassing the nominal resolution [2]. Images were Fourier-interpolated to a matrix size of 2048x1024x512. The surface of the tooth was reconstructed (Fig. 2) and compared to an optical reference.

A map showing the distance between the MR surface and the reference surface is shown in Fig. 3. The mean distance between the surfaces was (26 ± 21) µm. The results show that it is possible to detect object boundaries with an accuracy of one order of magnitude below the nominal resolution. We could show that object surfaces with an accuracy in the range of tens of micrometers can be obtained using a whole-body MR scanner at 1.5 T.

Fig. 1: a prepared human tooth used as a phantom
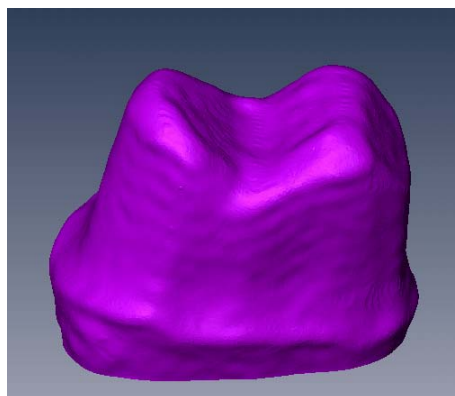
Fig. 2: surface reconstructed from MR data
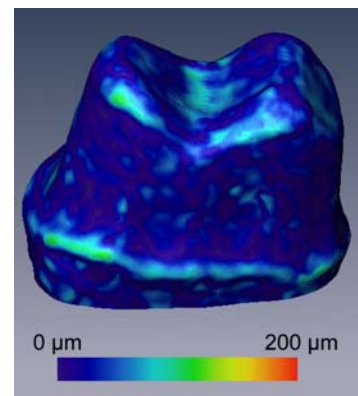
Fig. 3: difference map, scale from 0 µm (blue) to 200 µm (red)

[1] Olt S, Jakob PM, *Magn Reson Med* **52(1)** (2004) 174-176.
[2] Tymofiyeva O, Rottner K, Richter E, Jakob PM, *Proc. ESMRMB, Warsaw, Poland,* (2006) Abstract 645.

Evaluation of Scars and Skin Tissue using the new NMR Mouse® Technology

Schroeder M.[1] , Oppell P.[2] Demir E. [1], Bluemich B. [2] and Pallua N.[1]

[1] Plastic and reconstructive surgery, RWTH Aachen, Germany
[2] Institute of technical and macromolecular chemistry, RWTH Aachen, Germany

Abstract:

For the very first time biomedical sciences have been successful in utilizing the NMR MOUSE® Technology with regard to a highly sensitive and long discussed field in medicine: a clinical procedure for an objective evaluation in scar therapy came into reach.

The present study will enable to survey reliable results allowing not only for a precise assessment of scar and skin tissue, but moreover for a specific and well suited therapy.

Although silicon and compression therapy are recognized methods in plastic and reconstructive surgery, an objective evaluation within the therapy of scars enabling to determine the most favourable treatment for the patient has always proven to be difficult so far.

With the aid of the new designed NMR MOUSE® (Mobile Universal Surface Explorer), a sensor of the size of a hand, excellent ascertainment of skin and scar tissue based upon an authentic data acquisition of the T2 relaxation time and density will be possible. Scar and skin elements will be able to be gauged and compared up to a depth of 5 mm by a precise correlation of the gathered measurement results and the respective local anatomy.

The sensor, composed of a complex arrangement of several magnetic fields, affords information with respect to consistence of the tissue structure, inter alia density, hardness and water content from different skin layers. The maximum resolution of up to 4μm delivers a microscopic profile of the skin which pinpoints progress as well as alterations throughout the entire healing process of the patients.

One of the main findings that could be revealed until now was that a low relaxation time relates to a more dense tissue.

The device might further be a decisive step towards scientific proof of the so far unexplained effects of compression and silicon-sheet therapy on scarring and the gestation of scar tissue. Finally, further fields of application as to wound healing, burn evaluation and skin alterations are conceivable.

Lateral diffusion of Mn^{2+} ion in the brain determined by T_1 relaxation time measured by ^1H MRI

Y. Seo[1], H. Wakamatsu[1], Y. Imaizumi[1], M. Yokoi[1], A. Takamata[2], T. Ogino[3] and Murakami[4]

[1] Dept. of Regulatory Physiology, Dokkyo Medical University School of Medicine, Mibu

[2] Dept of Environmental Health, Nara Women's University, Nara

[3] Dept. of Biochemistry and Cellular Biology, National Institute of Neuroscience, National Center of Neurology and Psychiatry, Tokyo

[4] Dept. of Nano-Structure Physiology, Center for Integrative Bioscience, National Institute for Physiological Sciences, Okazaki, Japan

Abstract:

1. Interstitial application of Mn^{2+} ion can be used to visualize neural activities in the brain by using T_1-weighted MRI. When we infuse Mn^{2+} in the cerebrospinal fluid (CSF), Mn^{2+} can be transferred into the interstitial space of brain through the ependymal cells. In order to optimize this entry process, we have analyzed diffusion process of Mn^{2+} into the parenchyma.

2. Mn^{2+} solution infused from the lateral ventricle of the rat brain, diffusion of Mn^{2+} was measured perpendicular direction from the third ventricle. T_1 relaxation times were measured at 4.7 T MR imaging system. Relaxivity of Mn^{2+} was used to convert T_1 relaxation time to Mn^{2+} concentration.

3. On an assumption of the simple diffusion process, apparent diffusion coefficient (D_{ap}) of Mn^{2+} ion in the interstitial space is 2.5×10^{-3} mm^2/min. However, the Dap tends to decrease when the distance from the third ventricle increased.

4. It might be possible that i) Mn^{2+} ion is trapped by neural cells during diffusion, and/or ii) Mn^{2+} ion efflux from the brain by veins.
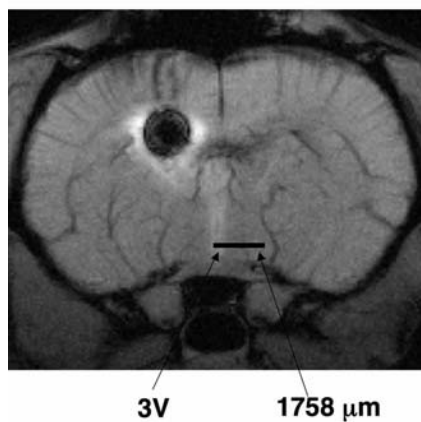
Fig. 1 Diffusion of Mn^{2+} from the 3rd ventricle to brain parenchyma. The black bar indicate position of ROIs.
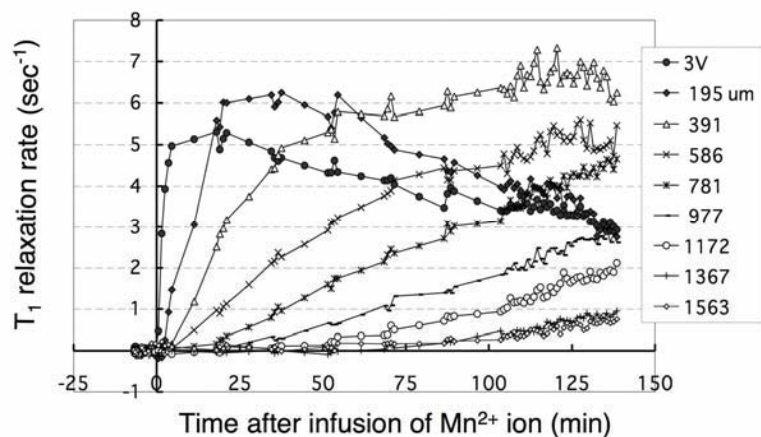
Fig. 2 Increase of T_1 relaxation rate ($1/T_1$) by continuous infusion of Mn^{2+} in the 3rd ventricle.

MR Microscopy of Blood Clot Dissolution

Igor Serša[1], Gregor Tratar[2], and Aleš Blinc[2]

[1] Condensed Matter Physics Department, Jožef Stefan Institute, Ljubljana, Slovenia
[2] Department of Vascular Diseases, University of Ljubljana Medical Centre, Ljubljana, Slovenia

The aim of thrombolytic therapy is to dissolve blood clots and restore normal vessel function. It is important in treating myocardial infarction, acute ischemic stroke, and pulmonary embolism. Thrombolysis is a biochemical process in which plasminogen is activated by a thrombolytic agent into active plasmin that cleaves the fibrin network and so dissolves the clot. Often blood clots only partially occlude the vessel. In dissolution of these non-occlusive blood clots blood flow through the clot plays essential role not only because it increases delivery of the clot dissolution agent into the clot, but also because viscous forces introduce a shear force on the wall of the clot. This shear force promotes clot degradation by removing relatively large partially chemically degraded parts of the clot from its surface.

MR microscopy is a convenient tool for studying blood clot dissolution in-vitro. For this study, we made an artificial blood circulation system that consisted of a pump that could generate a constant pressure difference of 15 kPa (fast flow) or 3 kPa (slow flow), plastic hoses, half a liter of human blood plasma and an artificially made blood clot. The clots were prepared from venous blood of a healthy volunteer in 3 mm diameter and 30 mm long glass tubes. Blood clotting was initiated by adding calcium and thrombin and clot retraction was inhibited by the phosphodiesterase inhibitor UDCG 212. The clots were inserted in the circulation system and then into the RF coil in the center of the magnet. After adding the thrombolytic agent rt-PA and MRI contrast agent Gd-DTPA to the plasma the circulation system was started simultaneously with dynamic MR imaging. Clots were imaged dynamically in 2D by T1-weighed spin-echo method at a resolution of 80 μm and TE/TR = 8/400 ms in a transverse slice across the center of the clot, or in 3D by the 3D-RARE method at isotropic resolution of 200 μm, matrix 32 by 32 by 128 points, RARE factor of 32 and inter-echo-time/TR = 3.3/3000 ms. In 40 minutes 20 images of the clot were acquired. The sequence of 2D images in Fig. 1 shows a typical clot dissolution process. Clot permeation with Gd-DTPA (white regions), which was used to identify clot permeation with the thrombolytic agent, was much faster in fast flow than in slow flow. The results confirm our hypothesis that fast flow promotes clot dissolution. Based on these results we developed a consistent analytical mathematical model for clot dissolution [1].
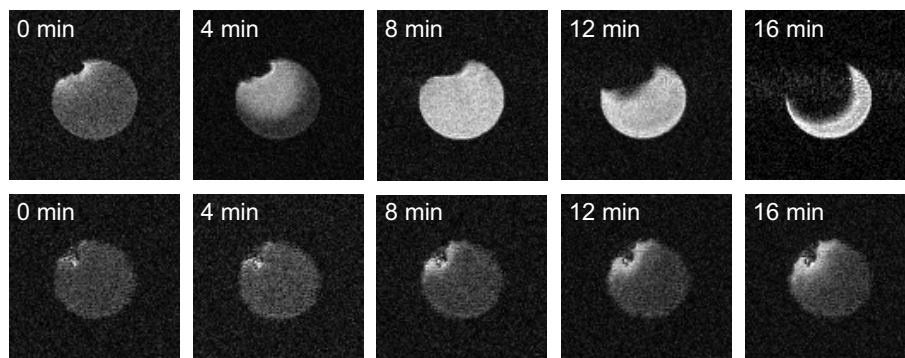
Fig. 1: Clot dissolution process in fast-flow (top) and in slow-flow (bottom).

1. I Serša, et al., *Phys. Med. Biol.* **52** (2007) 2969-2985.

Imaging of bound water in the frozen rat brain

A.M. Oros-Peusquens and N.J. Shah

Institute of Medicine, Research Centre Jülich, Germany

Introduction

Evidence has accumulated in the past 40 years for the existence of an important proportion of highly structured water in biological samples. The term 'bound water' is generally used for this component which is believed to consist of water molecules in a thin hydration layer around biological macromolecules. This layer is in intimate contact with the macromolecules and moderates the transfer of relaxation from the solid-like protons 'frozen' in the macromolecules to the bulk water. This study shows that imaging of bound water is feasible.

Materials and methods

Measurements were performed on a 4T whole-body scanner (Varian UnityInova). We investigated the changes in the NMR response with a simple pulse-acquire sequence. A square pulse of 4μs duration was applied corresponding to an angle of 25°, and 2048 complex points were acquired for the FID. SPRITE images with 1 mm resolution were obtained from a FOV of 64x64x32 mm and matrix size 64x64x32, TR of 4 ms, TE=0.3ms, 1 average. The total acquisition time for SPRITE was 5 ½ min, and 200s for each set of 20 FIDs. The imaging and NMR sequences were alternately applied and the evolution of the frozen samples was monitored over a period of 3-6 hrs.

Results

Changes in the position, intensity and shape of the different proton lines were monitored as a function of time. The dependence of the intensity of the proton peak on time is shown in Fig.1 The broad peak in both spectra was identified as belonging to ice (frozen 'free' water). Melting in the ice phantom was identified as the time interval where the linewidth of the ice peak is close to that of water; the peaks coexist and practically no changes in the NMR lines were observed. Analogously, in the rat brain, melting was presumed to take place after the two lines merged. The narrow peak, before melting starts, is expected to consist either entirely of, or have a very large component from, the bound water. By dividing the intensity of the narrow peak just before melting starts to the total intensity of the free water (the plateau seen on the plot of intensity vs. time), the amount of bound water can be estimated. It is roughly 6% in the ice sample and 12% in the rat brain.
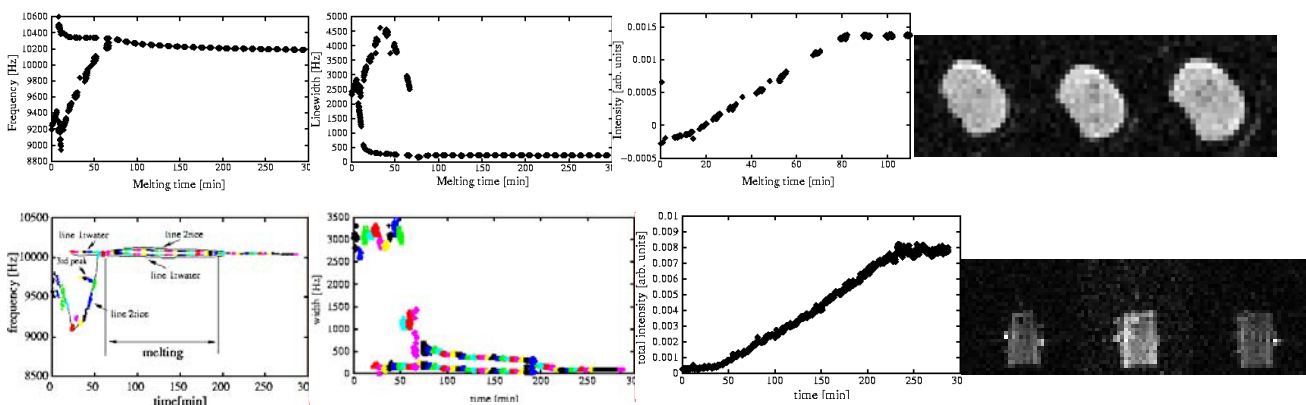
Conclusions

Imaging of bound water in the frozen rat brain has been demonstrated using SPRITE – an imaging sequence for fast relaxing species. The bound water was identified as being the unfrozen water component and the temperature was inferred by comparison with a water phantom. The amount of bound water in both samples was estimated to be approximately 6% for the ice sample and 12% for the rat brain.

Imaging the Molecular Concentrations in Articular Cartilage

Yang Xia, ShaoKuan Zheng, Aruna Bidthanapally
Department of Physics and Center for Biomedical Research,
Oakland University, Rochester, MI 48309, USA
Phone: (248) 370-3420; Fax: (248) 370-3408; Email: xia@oakland.edu

Introduction

Covering the load-bearing ends of bones in joints, articular cartilage is a thin layer of specialized tissue consisting of at least three sub-tissue structural zones, each defined by its collagen fibril orientation [1,2]. Trapped among the fibrils are the proteoglycans that have a central protein core and glycosaminoglycan (GAG) side-chains. The heavily sulfated GAG chains preferentially attract positive ions and the water protons to ensure electroneutrality. This water-binding ability of GAGs is closely related to the mechanical integrity of cartilage as a load-bearing tissue. The reduction of GAGs in the tissue will result in a weakened cartilage, eventually a clinical disease such as osteoarthritis. In this work, μMRI T_1-$Gd(DTPA)^{2-}$ approach is used to monitor the GAG content in cartilage.

Methods

Canine cartilage from healthy humeral heads was imaged using a Bruker AVANCE II console with a 7T/89mm vertical magnet. These specimens were T_1-imaged before and after the $Gd(DTPA)^{2-}$ immersion at 14μm pixel resolution and 1mm slice thickness. At high field, the relaxivity and T_1 without contrast agent are approximately independent of tissue composition so the conversion from T_1 to $[Gd(DTPA)^{2-}]$ is possible [3]. Then, together with information about $[Gd(DTPA)^{2-}]$ in the equilibrating solution, $[Gd(DTPA)^{2-}]$ in the tissue can be used to calculate [GAG] in tissue. After the tissue has been T_1 imaged, the specimens were sectioned into 40μm parallel slices. Each slice was numbered and digested with enzyme to determine the [GAG] by binding the cationic dye 1,9-dimethylmethylene blue (DMMB) using a Shimadzu UV-Visible spectrophotometer at 656nm (model UV-1650).

Results

The specimens were T_1 imaged using different inversion time points. Several experimental issues such as the treatment times and concentrations of the $Gd(DTPA)^{2-}$ solution were investigated. The results were consistent. Several tissue blocks have been sectioned to determine the GAG concentration biochemically. The following figure shows one set of preliminary results, which demonstrates the good agreement between the MRI and biochemistry methods. Quantitative and statistical calculations are currently in progress.
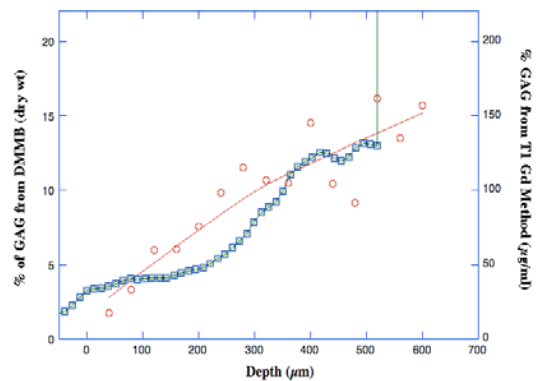
Discussion and Conclusion

This is one part of the on-going project in our lab that aim to determine the correlations among the physical, optical, chemical, and structural parameters in cartilage using microscopic MRI (μMRI), polarized light microscopy (PLM), and Fourier-transform infrared imaging (FTIRI). The goal of our project is to develop molecular-level markers that are sensitive to a small set of early changes that signal the on-set of the tissue degradation.

References

[1] Maroudas A, Bayliss MT, Venn M, *Ann Rheum Dis*, **39**, 514-534 (1980).
[2] Xia Y, *Investigative Radiology*, **35**(10), 602-621 (2000).
[3] Bashir A, Gray ML, Burstein D, Magn Reson Med, 36, 665-673 (1997).

Probing the meso- and microstructural heterogeneity of low dense networks with dendrimer probes and NMR/MRI diffusometry

Gert-Jan W. Goudappel[1], Magnus Nydén[2], John P.M. van Duynhoven[1]

[1] Unilever Food and Health Research Centre, Unilever R&D, PO Box 114, 3130 AC Vlaardingen, The Netherlands
[2] Applied Surface Chemistry, Chalmers University of Technology, SE-412 96 Göteborg, Sweden

Abstract:

The functionality of most food materials is determined by their meso- and microstructure. Structural characterisation at these length scales is challenging and requires the deployment of complementary microscopic and spectroscopic techniques. For porous materials with dense networks, probing the diffusion behaviour of water by NMR and MRI is an established approach for obtaining descriptive meso- and microstructural parameters.

For low dense networks, however, water is not a suitable probe, hence recently the use of macromolecular probes has been proposed. So far this approach was only demonstrated for homogeneous low dense networks. Thus we embarked on a feasibility study to explore whether this approach could also be applied to systems which display meso- and microstructural heterogeneity. As a model system we used alginate networks, which can be prepared as homogeneous gels, as well as beads which display a radial crosslink density gradient. First, a homogeneous alginate gel was prepared and characterised by probing the diffusion behaviour of dendrimer probes by NMR. By monitoring the diffusion behaviour of the dendrimer probe with a range of sizes, the mesostructural heterogeneity of alginate networks could be established. Subsequently, the diffusion behaviour of dendrimers in heterogeneous alginate beads was probed.

Positron Emission Tomography of Plants meets NMR Imaging

Siegfried Jahnke[1], Gerd Roeb[1], Dagmar van Dusschoten[1], Marion I. Menzel[1], Senay Minwuyelet[1], Jonas Bühler[1], Peter Blümler[1], Matthias Streun[2], Simone Weber[2], Karl Ziemons[2], Ulrich Schurr[1]

[1] Institute für Chemie und Dynamik der Geosphäre, ICG-3: Phytosphäre, Forschungszentrum Jülich, Germany; [2] Zentralinstitut für Elektronik, ZEL, Forschungszentrum Jülich, Germany

Abstract:

Plant growth and transport processes in plants are highly dynamic and strongly interrelated. They are characterized by plant-internal control processes and by strong interactions with the spatially and temporally varying environment. Analysis of structure-function relations of growth and transport in plants will strongly benefit from the development of non-invasive techniques.

Fig. 1: The PlanTIS setup mounted on a turning table. On the left, one detector block is opened showing the electronics.

A new measuring system called **Plan**TIS (= **Plan**t **T**omographic **I**maging **S**ystem) has been designed for non-destructive 3D-imaging of positron emitting radiotracers in plants (Fig. 1). This PET scanner is dedicated to monitor the dynamics of the allocation of ^{11}C labelled photoassimilates in a plant after photosynthetic uptake of $^{11}CO_2$ by a green leaf. Front end electronics and data acquisition architecture of the scanner are based on the ClearPET(TM) system [1]. Four detector modules form one of two opposing detector blocks. Optionally, a hardware coincidence detection between the blocks can be applied. The scan duration is rather long (approx. 2 hours) compared to the decay time of ^{11}C (20.4 min) thus the count rates vary over a wide range and accurate dead time correction is necessary.

PlanTIS will permit functional investigations on carbon distribution in living plant organs which hitherto were not accessible. Fig. 2A shows an image of ^{11}C-isolines obtained from a wheat root system embedded in soil. Such images obtained sequentially in time will allow us to analyse the dynamics of long-distance transport processes with both spatial and temporal resolution. Co-registration with NMR-imaging (Fig. 2B) will supplement the functional PlanTIS data by showing the anatomical traits of a root system with higher spatial resolution and, with NMR, it will become possible also to measure the water flow in a given plant.

Both PET and NMR are supposed to become applicable for low-throughput screening of transport properties of plants to evaluate e.g. chilling or drought stress adaptation of genetically modified plants.

Fig. 2: (A) ^{11}C isolines of wheat roots obtained 90 min after labeling the flag leaf with $^{11}CO_2$. (B) Finally, the upper and lower parts of the same root system were imaged using ^{1}H-MRI.

1. K. Ziemons et al., *Nucl. Instr. Meth.* **A537** (2005) 307-311.

MR Study of Moisture Content and Water Distribution in Tree Tissues

Urša Mikac[1], Ana Sepe[1], Igor Serša[1], Maks Merela[2], and Primož Oven[2]

[1]Jožef Stefan Institute, Ljubljana, Slovenia
[2]University of Ljubljana, Biotechnical faculty, Department of Wood Science and Technology, Ljubljana, Slovenia

Abstract:

Wood properties are a function of wood structure and most importantly moisture content (MC) [1]. Large variability in wood structure and therefore distribution of MC is expected in the same tree and among different trees of the same species from the same and from different growth sites. Secondary changes (heartwood, discolorations) and other growth features that represent defects (juvenile wood, compression wood, mechanical injuries, etc.) enhance variability of the material. Calsically MC is determined by gravimetric method, that is an invasive method and gives only an average MC value for the whole sample. Magnetic resonance (MR) on the other hand, is a non-invasive method that enables water distribution determination *in vivo* for different tree tissues.

Wood has two main components: solid wood material and water that can be in the cell cavities as lumen water or bound in the cell walls. Relaxation times of lumen water depend on cell sizes and since wood generally contains a continuous distribution of cell sizes, a multiexponential analysis of relaxation times were used. The correlation between the MC and relaxation times was measured on samples of beech (*Fagus sylvatica* L.) branches from different trees at different MC. In order to better understand the relaxation processes in tree tissues T_1-T_2 correlation experiments [2] were also performed for the samples. To obtain relaxation times distributions inverse Laplace transformation (ILT) was used [3]. Finally, relaxation times mappings were used to determine the MC on pixel-by-pixel basis in a MR image of a wood sample (Fig. 1).
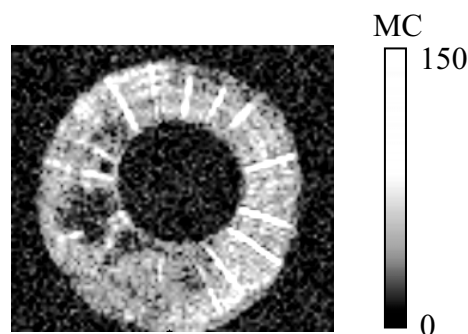
Fig. 1: MC determined from T_1 and T_2 maps of a sample with an average MC = 45 %.

1. J.F. Siau, Wood: Influence of moisture on physical properties. New York, Polytechnic Institute and State University, 1995.
2. Y.-Q. Song, L. Venkataramanan, M. D. Hürlimann, M. Flaum, P. Frulla, and C. Straley, *J. Magn. Reson.* **154** (2002) 261-268.
3. For multiexponential analysis a 2DILT program provided by Professor P. T. Callaghan, Victoria University of Wellington, New Zealand was used.

MR microscopy of lipid depositions in developing seeds.

T.Neuberger[1,3], M. Rokitta[3], H. Rolletschek[2], T. Rutten[2], P. Jakob[3], L. Borisjuk[2], A.G.Webb[1]

[1] College of Engineering, Penn State University, University Park, PA, USA,
[2] Leibniz-Institut für Pflanzengenetik und Kulturpflanzenforschung (IPK), Gatersleben, Germany,
[3] Institute of Experimental Physics V, University of Würzburg, Würzburg, Germany,

Abstract:

Oil storage in plants is developmentally regulated, and undergoes multiple modulations within particular tissues. Understanding of the regulatory networks requires quantitative visualisation data on storage lipid at a variety of stages and scales. In this study we explore a rapid and non-invasive detection, visualization and quantification of triacyl glycerol in living seeds using magnetic resonance microscopy. Lipid deposition was followed in two contrasting subjects: barley grains with a low, but highly compartmentalized, oil deposition, and soybean with a rather high amount of oil as an example of an economically important oilseed. Steep gradients in lipid content were established within individual grains and followed during seed development. In both cases, lipid mapping coupled with biochemical measurements and electron microscopy, demonstrated a high tissue-specificity of oil storage *in vivo*. Developmental distribution of oil accumulation was closely coordinated with seed maturation and the acquisition of desiccation tolerance. Lipid mapping depicts regions of maximum oil accumulation capacity in the context of the surrounding plant structure without interrupting the developmental process. Thus, it can conveniently define areas appropriate for biotechnological manipulation of different plant tissues.
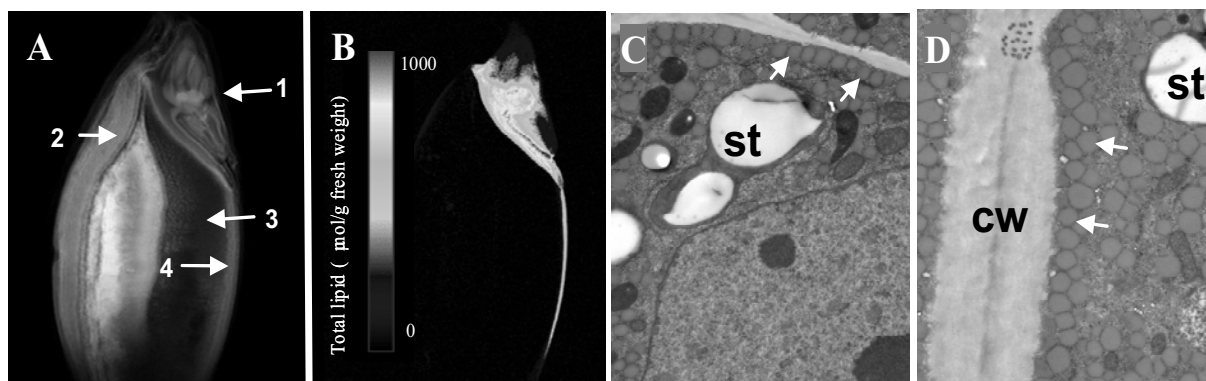
Figure 1: Examples of a living barley seed at the main storage stage.
The left images are the water (A) and the right images the corresponding lipid distributions (B). EM image of intracellular distribution of lipid (arrows) in aleuron (C) and scutelum (D). The typical experiment time needed to create one high resolution, frequency selective *in vivo* lipid image was 1h 8min, using a field of view of 8 mm, a data matrix of 256 x 256 complex points, an in-plane resolution of 31 μm, slice thickness 0.75 mm, and TR/TE = 1000/12.1 ms. Abbreviations: 1-embryo, 2-pericarp, 3-endosperm, 4-aleuron, st-starch, cw-cell wall.

MRI studies of moisture absorption of food wafers

P. Parasoglou[1], M.L. Johns[1], J. Rasburn[2] and H. Powell[2]

[1]Department of Chemical Engineering, University of Cambridge, Cambridge, UK
[2]Nestlé Product Technology Centre, York, UK

Abstract:

Magnetic Resonance Imaging has been used to visualise moisture absorption from humid air, and subsequent diffusion of this absorbed water, in initially dry samples of wafer. Such phenomena are part of the wafer conditioning process. Wafer is a thin cereal-based biscuit often combined with chocolate to form confectionery products. Imaging these processes is extremely challenging as the signal-to-noise ratio is poor – the porosity of the wafers is typically 80-90 % and the absorbed moisture is typically only 2 wt %. In addition, the low moisture content means that the water has restricted mobility and the highly porous structure results in significant magnetic susceptibility variations. These collectively result in short spin-spin relaxation constants, T_2^*, typically of the order of 50 μs. Consequently, conventional MRI, with sufficient temporal resolution to follow the moisture absorption, is not possible and faster techniques (e.g. *RARE* [1]) are precluded due to the unfavourable signal relaxation properties.

Consequently, Single Point Imaging (SPI)[2] is the main MRI technique used in the current study. To overcome its main disadvantage, a long acquisition time, this method was combined with the Multiple Point Acquisition technique (MPA)[3, 4], which can either increase the signal to noise delivered by SPI or shorten the total acquisition time. MPA works by acquiring more points of the free induction decay (FID) following each excitation pulse. At the end of the experiment the number of images acquired will be equal to the number of points acquired from the FID. These images will have a different field of view which has to be corrected with the use of the so-called Chirp z-Transform. Single-Point Ramped Imaging with T_1 Enhancement (SPRITE)[5], a faster form of SPI, was also used in order to decrease acquisition times further. This was combined with a centric **k**-space acquisition following a spiral-like sampling trajectory. As a result the signal to noise was improved significantly.

From the results obtained so far MRI, based on the acquisition of selected points from the FID, is a promising technique to follow moisture absorption and diffusion in the wafer samples. 2D images of the wafer with sufficient spatial resolution have been acquired in less than 1 minute allowing the absorption process, which typically occurs over 10s of minutes, to be followed adequately *in situ*. The absorption process was shown to be linear with respect to time for all wafer samples considered, whilst diffusion of absorbed moisture into the centre of the water was successfully imaged. MPA can also be used to create T_2^* maps of the samples and, after extrapolating to the signal origin, to quantify local moisture content.

1. Hennig, J.*, et al.*, *Magnetic Resonance in Medicine* **3** (1986) 823-833.
2. Emid, S.*, et al.*, *Physica B & C* **128** (1985) 81-83.
3. Halse, M.*, et al.*, *Journal of Magnetic Resonance* **169** (2004) 102-117.
4. Kaffanke, J.*, et al.*, *Journal Of Magnetic Resonance* **178** (2006) 121-128.
5. Balcom, B.J.*, et al.*, *Journal of Magnetic Resonance Series A* **123** (1996) 131-134.

The fat content determination with unilateral NMR

Oleg V. Petrov[1] , Igor V. Mastikhin[1], Bruce J. Balcom[1]

[1] MRI Centre, Department of Physics, University of New Brunswick, Fredericton, Canada

Abstract:

An aim of this work was to demonstrate an applicability of portable unilateral NMR systems, recently built in our laboratory[1,2], for determining the fat content in food. We primarily focused on the diffusion-weighted CPMG experiments previously employed for the fat/water discrimination on bench-top NMR analyzers with a pulsed field gradient[3,4].

The steady-gradient version of those experiments was performed on two magnets. One, designed with a constant gradient of 0.3 T/m over a 0.8 cm depth, was employed for accurate determination of relaxation and diffusion parameters. 2D-SGSE-CPMG experiments with variable SGSE inter-pulse intervals τ for diffusive attenuation were conducted on test samples of cod liver oil dispersed in a water/agar gel, with the oil content 10-50%. Back-extrapolated CPMG amplitudes plotted against $\sim\tau^3$ provided us with a well-resolved biexponential decays. A good correlation was found between the decay components and the oil/water composition. No such resolution could be achieved in a 1D CPMG experiment. Measurements on ground beef samples of different fat content showed that the fat and moisture components in beef could be resolved by the above technique.

These results were utilized for rapid measurements of fat content with the other system, designed to have a high SNR due to a large sensitive spot. Taking into account the system's gradient distribution, we found a good correlation of our measurements with an analytically measured fat percentage. The fat content can be determined within several minutes provided that a post-experimental computational routine is automatized.

1. Marble AE, Mastikhin IV, Colpitts BG, Balcom BJ. *Journal of Magnetic Resonance* **183** (2006) 228-234.
2. Marble AE, Mastikhin IV, Colpitts BG, Balcom BJ. *Journal of Magnetic Resonance* 186 (2007) 100-104.
3. Pedersen HT, Berg H, Lundby F, Engelsen SB. *Innovative Food Science & Emerging Technologies* **2** (2001) 87-94.
4. Sørland GH, Larsen PM, Lundby F, Rudi A-P, Guiheneuf T. *Meat Science* **66** (2004) 543-550.

Root water uptake and root system architecture monitored by MRI-MSME and RARE

A. Pohlmeier[1], F. J. Vergeldt[2], E. Gerkema[2], J. Vanderborght[1], M. Javaux[1], H. Vereecken[1], H. Van As[2], M. I. Menzel[3], D. van Duschoten[3]

[1] ICG-4, Research Centre Jülich, Germany
[2] Wageningen NMR Centre, Wageningen University, The Netherlands
[3] ICG-3, Research Centre Jülich, Germany

Abstract:

We investigated root water uptake by ricinus in a fine sand using MRI. Before starting the experiments the plants germinated and grew for 3 weeks in a cylindrical container with a diameter of 9 cm. Immediately before the MRI experiments started, the containers were water-saturated and sealed, so water content changes were only caused by root water uptake. In continuation of a preceding work, where we applied SPRITE[1, 2] we tested a multi-echo multi-slice sequence (MSME) In this approach, the water content was imaged by setting $T_E = 6.76$ ms and $N_E = 128$ with an isotropic resolution of 3.1mm. This protocol turned out to be less sensitive to artefacts than SPRITE and yielded comparable results. We calculated the water content maps by i) biexponential fitting of the multi-slice echo train data[3] and normalisation on reference cuvettes filled with glass beads and 1 mM $NiCl_2$ solution. The water content determination was compared to mean gravimetric water content measurements.

By co-registration with the root architecture, visualised by a 3D fast spin echo sequence (RARE), one may conclude that the largest water content changes occurred in the neighbourhood of the roots and in the upper layers of the soil. The study will be continued by investigation of the water uptake by maize roots.
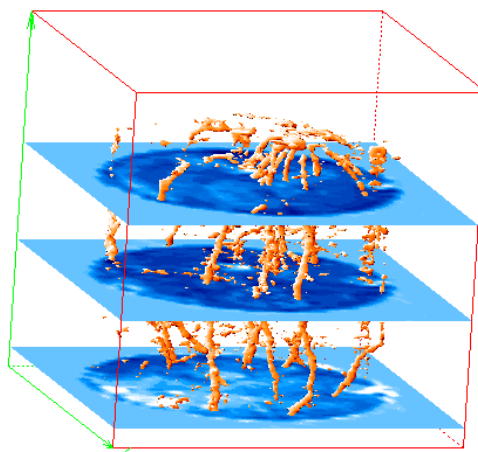
Fig. 1: Water content changes and root system

1. Pohlmeier, A., A.M. Oros-Peusquens, M. Javaux, M.I. Menzel, V. H., and N.J. Shah. Magnetic Resonance Imaging **25** (2007). 579-580.
2. Pohlmeier, A., A.M. Oros-Peusquens, M. Javaux, J. Lindenmair, M.I. Menzel, H. Vereecken, and N.J. Shah. Vadose Zone Journal (2007). submitted.
3. Edzes, H.T., D. van Dusschoten, and H. Van As. Magnetic Resonance Imaging **16** (1998). 185-196.

Imaging of water transport in Coffee Beans after roasting and quenching

Thomas D Schulze-Till[1] , Claudia Fischer[2], Heiko K Cammenga[2] and Peter M Jakob[1]

[1] Lehrstuhl für Experimentelle Physik 5, Bayerische Julius-Maximilians-Universität, Würzburg, Germany

[2] Institut für Physikalische und Theoretische Chemie, Technische Universität Braunschweig, Braunsschweig, Germany

Abstract:

After roasting and cooling with water (so called quenching), industrially processed coffee beans cannot be milled immediately but have to be stored for about ten hours [1]. Starting too early, the beans would glue the mill. This study shows how water transport processes explain this behaviour.

All experiments were performed on a Bruker AMX500 system, with a maximal gradient strength of 660 mT/m, and a homebuild probehead. A Helmholtz coil (diameter 1cm, wire distance 5mm) was used. 300 g of green Arabica Santos coffee beans were roasted in a home roasting system (Dieckmann Aroma Kaffee GmbH und Co. KG, Bremen) at 242°C for 50 seconds [2]. After that, they were put in a glass tube and quenched with 100 ml water to stop the roasting process at a well defined point. The beans took up water until about 20 % of the weight consisted of water. Above all available water in the tube was removed. Then repeatedly different beans were put into the magnet and a FLASH image was acquired. Every ten minutes a new coffee bean was imaged until 14 hours after quenching.

FLASH images of roasted coffee beans showed mostly signal from water applied by quenching. Images taken over the time showed, that highly concentrated water near the hull was distributed all over the coffee bean within about 10 hours.

Since it is known that the water content of the tissue affects the behaviour during milling, probably this study explains why coffee beans can't be milled immediately after roasting and quenching. Further studies could be made with MRI to evaluate new coffee processing methods.
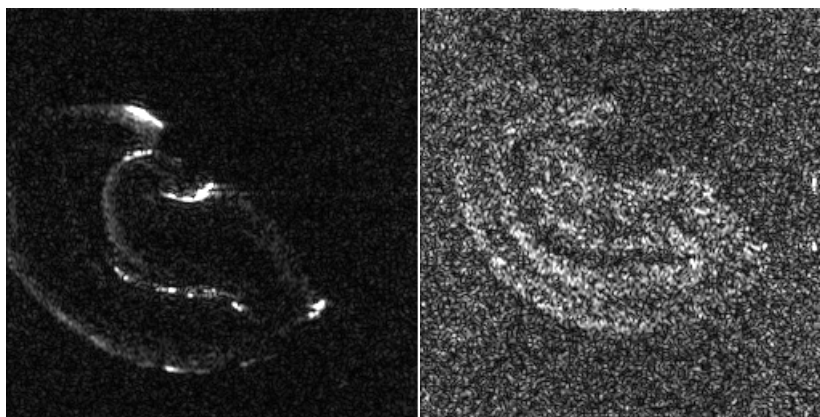
Fig. 1: FLASH images of two coffee beans 40 minutes (left) and 13 hours (right) after quenching (FoV 1 mm x 1mm, matrix = 128 x 128, TE 1.5 ms, TR 10 ms, 32 averages)

1. R. J. Clarke and O. G. Vitzthum, eds., Coffee - Recent developments, New York, Blackwell Science, 2001
2. C. Fischer and H.K. Cammenga, *Proc. IXX Int. Coll. on Coffee Science ASIC*, Trieste/Italia (2001)

Slow flow quantification using the inflow effect

Thomas D. Schulze-Till[1] and Peter M. Jakob[2]

1 Lehrstuhl für Experimentelle Physik 5, Bayerische Julius-Maximilians-Universität, Würzburg, Germany

Abstract:

Flow measurement at high fields using phase contrast methods is difficult in plants due to inhomogeneities and slow flow velocities [1]. To overcome this, a new method for flow quantification [2] using the inflow effect [3] is presented.

Three pieces of information have to be known to quantify flow velocities: (1) T1 of the flowing medium, (2) a spin-echo image containing two slice selective pulses and (3) a spin-echo image containing one global and one slice selective pulse. Theoretical considerations lead to

$$v = \frac{M_{sel} - M_{glob}}{M_{glob}} \cdot \frac{\Delta z}{T_R} \cdot \left(\exp(T_R / T_1) - 1\right) \qquad (1)$$

where v is the flow velocity, T_R the repetition time, Δz the slice thickness, M_{sel}, M_{glob} the signal from the image with 2 slice selective pulses and the image with a global and a slice selective pulse respectively.

The method was validated on a flow phantom showing a maximum flow velocity of 0.80 mm/s where 0.77 mm/s were expected. Flow in the roots of a zea maize plant was measured, including velocities down to 0.2 mm/s.

Using this flow quantification method, a complete flow image for functional imaging can be obtained within 2 minutes, given that T_1 and M_{glob} are known as previous knowledge. This is especially interesting for measuring series of flow images with high temporal and spatial resolution, since T_1 and M_{glob} remain approximately constant during measurement without external influences. Also high resolution inflow images can be acquired within 17 minutes see Fig. 1.
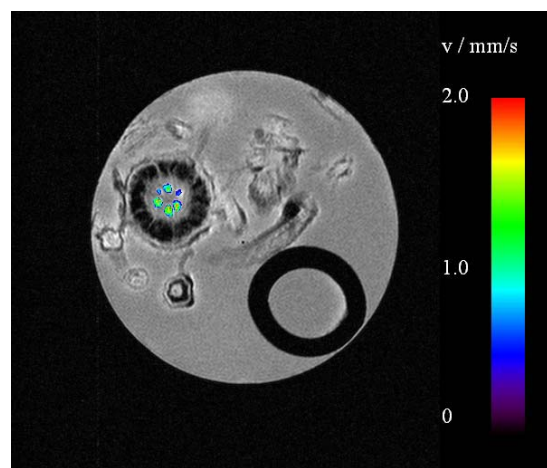
Fig. 1: Flow velocity map (colored) of a *zea mays*-root superimposed on a spin-echo image (FoV 0.5 x 0.5 mm², matrix = 256², zerofilled to 512², TE 6.5 ms, TR 0.5 s (inflow), TR 2 s (reference))

1. Rokitta M., Zimmermann U. and Haase A., *JMR* **137** (1999) 29-32.
2. Schulze-Till T.D. Rokitta M. and Jakob P.M., Flow quantification using the inflow effect, Proceedings of the 23rd ESMRMB, September 21 – 23, 2006: MR Microscopy Session 326
3. Suryan J. R., *Proceedings of the Indian Academy of Science Section A*, **33** (1951) 107-111.

High resolution NMR Imaging and Relaxation Mapping to study the transition of activity of wood garlic (*Allium ursinum)* in natural soils: A Feasibility Study

Natascha Spindler[1], Dagmar van Dusschoten[1], Reiner Almstedt[2], Andreas Ulbrich[1,2], Heike U. Schneider[1], Marion I. Menzel[1]

[1]Institute for Chemistry and Dynamics of the Geosphere: ICG-3, Research Center Jülich, Germany; [2]Institut für Nutzpflanzenwissenschaften und Ressourcenschutz: INRES, Bonn, Germany

Successful growing of wood garlic is a consequence of the comprehension of its vegetative and generative propagation. High resolution NMR imaging was used to study the internal anatomy of wood garlic by short TE spin-echo sequences and the transitional period was examined with relaxation mapping by multi-slice-multi-echo sequences.

Wood garlic (*Allium ursinum*) has recently become an important life style herb and carrier of aroma. As there is no adequate crop system available for growing wood garlic in cultivation, we aim to understand the underlying cause for the insufficient vegetative and generative propagation. Furthermore there is only little known on wood garlic´s internal anatomy and water status of the transitional periods [1]. As NMR has recently been applied to study *Alliaceae* [2-5], it seems to be a method of choice to tackle these questions. The approach presented here is twofold: First we studied the internal anatomy of wood garlic with high resolution MRI and compared it to classical thin sections. Second we monitored water content of the bulb using NMR relaxation mapping, in order to identify changes prior and during induced physiological transition of the bulb.

For all investigations we used one year old wood garlic bulbs cultivated in Einheitserde Typ 0. For investigation by NMR the wood garlic bulb and root system was carefully transferred to the three different cultivation substrates and well watered. All NMR imaging was performed using a 7 T vertical magnet system (Varian), equipped with micro imaging system (max grad strength 300mT/m) and 38 mm inner diameter birdcage resonator. Anatomical images were acquired using a short TE spin-echo sequence and a multi-slice-multi-echo sequence was used for relaxation mapping.

Prior to the investigation of structure and function of wood garlic in natural soils, suitable cultivation conditions needed to be identified. So first we needed to identify which of the culture soil is most suitable for NMR investigation. We compared cultures of wood garlic in three different substrates (Rockwool (Grodan® Classic), Perlite®, white peat) to select the one having the smallest impact on NMR signal homogeneity and the lowest image distortion, while satisfying the cultivation prerequisites.

White peat and rock wool turned out to be most suitable, while Perlite® lead to image distortions. In order to study induced transition, we first acquired images at high resolution. Fig. 1 depicts the inner anatomy of the wood garlic internal structure, the initiation of a new spear was visible.
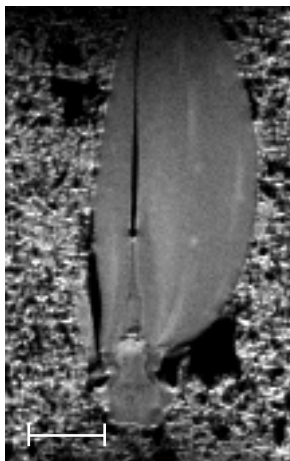
Figure 1: High resolution image of wood garlic in white peat as visualized by a longitudinal slice of spin-echo multi-slice dataset. The following parameters were used: field of view: 50.0 mm x 50.0 mm, image matrix 512 x 512, repetition time 1.5 s, echo time 9.7 ms, 4 averages. Bar = 1 cm.

[1] Ernst; WHO, *J Ecology* **67** (1979) 347– 62.
[2] Bendel P et al, *Magn Reson Imag* **19** (2001) 857-865.
[3] Van Kilsdonk MG et al, *J Exp Bot* **374** (2002) 1603-1611.
[4] Van der Torn A et al, *J Exp Bot* **348** (2000) 1277-1287.
[5] Zemah H et al, *Plant Sci* **147** (1999) 65-73.

Rapid Determination of the Fat Content in

Packaged Dairy Products by Unilateral NMR

E. Veliyulin[1], I.V. Mastikhin[2], A.E. Marble[2] and B.J. Balcom[2]

[1] SINTEF Fisheries and Aquaculture, N-7465 Trondheim, Norway
[2] MRI Centre, Department of Physics, University of New Brunswick, Fredericton, NB, Canada E3B 5A3

Abstract:
Knowledge of the fat content in dairy products is important for both industry and consumers. A new procedure for rapid and non-destructive determination of the fat content in dairy products in commercial packages using a unilateral NMR was proposed. Rapid accumulation of the NMR signal was achieved by the use of a newly developed unilateral magnet array with a well-controlled magnetic field and optimized for sensitivity [1]. The sample magnetization was prepared using either T_1 suppression or diffusion editing and read out via a CPMG pulse sequence (Fig.1). A linear correlation between the measured NMR signal from the fat component and the declared fat content in the tested products validated both approaches as viable instrumental methods. The shortest measurement time was about 7 s.

Advantages of the unilateral NMR method, including hardware simplicity and accommodation of commercially packaged products make it attractive for routine use in industry.
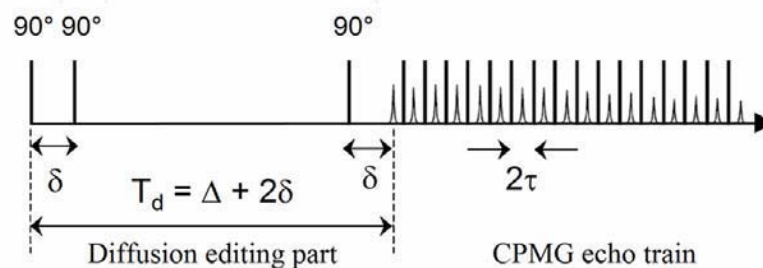
Fig.1: Diffusion edited CPMG pulse sequence [2] effectively suppressing the contribution of the water component in the dairy products

1. Marble, A.E., Mastikhin, I.V., Colpitts, B.G., Balcom, B.J., A compact permanent magnet array with a remote homogeneous field. *J Magn Reson* **186** (2007) 100-104.

2. Rata, D.G., Casanova, F., Perlo, J., Demco, D.E. and Blümich, B., Self-diffusion measurements by a mobile single-sided NMR sensor with improved magnetic field gradient, *J Magn Reson* **180** (2006) 229-235.

Rapid Determination of the Moisture Content in Wood Shavings Using Time Domain NMR

E. Veliyulin[1], I.V. Mastikhin[2], A.E. Marble[2], G.M. Jenkins[3] and B.J. Balcom[2]

[1] SINTEF Fisheries and Aquaculture, N-7465 Trondheim, Norway
[2] MRI Centre, Department of Physics, University of New Brunswick, Fredericton, NB, Canada E3B 5A3
[3] Wood Science and Technology Centre, Faculty of Forestry and Environmental Management, University of New Brunswick, Fredericton, NB, Canada E3C 2G6

Abstract:

A new procedure of rapid and non-destructive determination of the moisture content in wood shavings based on time domain NMR is proposed. The solid echo NMR technique [1] was implemented in the on board NMR analyzer (Bruker the minispec mq10), allowing information concerning rapidly relaxing hydrogen atoms from the cellulose, as well as from the hydrogen in the water phase, to be obtained.

Linear correlation (Fig.1) between the latter component and the gravimetrically determined moisture content in the tested samples has been observed. Speed and simplicity of the time domain NMR method make it attractive for routine use in the wood industry.
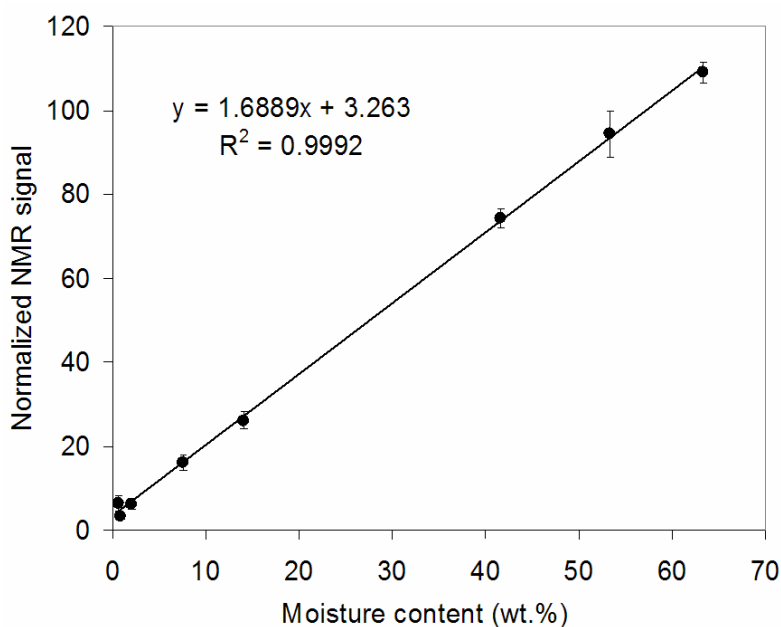
Fig.1: NMR signal from the shaving samples normalized with sample weight as a function of the gravimetrically determined moisture content

1. Slichter, C.P. 1990. Principles of Magnetic Resonance, Springer-Verlag, New-York, pp. 371-379.

Quantitative ^{23}Na MRI of muscle foods

E. Veliyulin[1], B. Egelandsdal[2], F. Marica[3] and B.J. Balcom[3]

[1] SINTEF Fisheries and Aquaculture, N-7465 Trondheim, Norway
[2] Institute of Food Research, University of Agriculture, N-1432, Ås, Norway
[3] MRI Centre, Department of Physics, University of New Brunswick, Fredericton, NB, Canada E3B 5A3

Abstract:

Quantitative sodium analysis in muscle foods by ^{23}Na MRI is traditionally considered problematic because of the well-known partial MRI sodium "invisibility" phenomenon reported earlier [1,2]. Partial ^{23}Na "invisibility" is often referred to as an inherent drawback of the MRI technique, impairing the quantitative sodium analysis.

Several model samples were designed to simulate muscle foods with a broad variation in the protein, fat, moisture and salt content. Spin-echo MRI technique and a recently developed SPRITE MRI approach [3,4] were applied for quantitative sodium imaging. Typical sodium images generated by these two methods from the same sample are shown in Fig. 1. Substantial underestimation of the salt content by the spin-echo technique and good correspondence between the SPRITE MRI sodium content and that determined by the reference chemical method were found. Thus the applicability of SPRITE MRI approach for accurate sodium quantification was demonstrated. ^{23}Na free induction decay and CPMG relaxation experiments were performed on the same sample set as well, additionally confirming that the sodium "invisibility" is rather a methodological problem that can easily be circumvented by using SPRITE MRI technique.

(a)   (b)
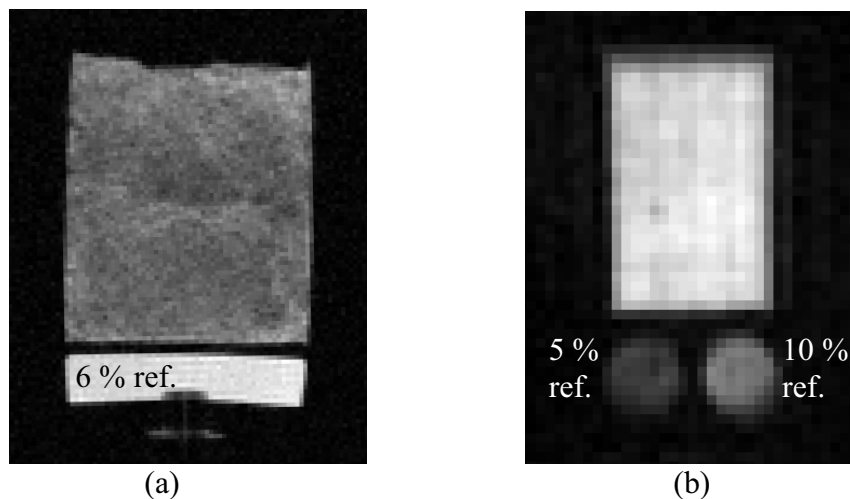
Fig.1: (a) Spin-echo MRI and (b) SPRITE MRI image of the same sample.
Salt content determined chemically was 15.8 %.

1. Springer, C.S., Ann. Rev. Biophys. Biophys. Chem., **16** (1987) 375-399
2. Shapiro, E.M., Borthakur, A., Dandora, R., Kriss, A., Leigh, J.S. and Reddy, R., J. Magn. Res., **142** (2000) 24-31
3. B.J. Balcom, R.P. MacGregor, S.D. Beyea, D.P. Green, R.L. Armstrong and T.W. Bremner, *J. Magn. Reson. Series A* **123** (1996) 131-134
4. M. Halse, D.J. Goodyear, B. MacMillan, P. Szomolanyi, D. Matheson and B.J. Balcom, *J. Magn. Reson.* **165** (2003) 219-229

Investigating cheese pressing by NMR and MRI.

B.B. Venne, D. Polders, F. Vergeldt and H. Van As

Lab. of Biophysics, Wageningen University, Wageningen, the Netherlands

Abstract:

There is a strong need for non-destructive analytical methods to characterise the relation between composition (e.g. water, fat, protein content), processing and structure of complex biopolymer food systems. NMR and MRI methods can fulfil (at least part of) this need.

An interesting example of such a food system is (Dutch, e.g. Gouda) cheese. During the processing pressing step, pieces of curd are collected and pressed (0.1-0.3 bar during 80 min) into the desired shape resulting in more whey removal from the cheese, and fusion of the curd pieces. This pressing step also forms the rind surrounding the cheese, and determines the homogeneity and hardness of the cheese.

Understanding this step is of great importance, as it is considered a critical step in the production of cheese. Pressing gives cheese its specific structure, and partly determines the moisture content. Rind formation is of interest because it protects the cheese from external influences such as microbiological organisms that might infect (and spoil) the cheese. It is also suspected that in this step small air bubbles are introduced in the cheese, particularly near the rind of the cheese. As this can result in complications for rind formation, the origin of these bubbles are under much scrutiny from industry. Limited research on the fusion of curd particles has been conducted. To our best knowledge, there has not been any previous research on the fusion of curd particles using a non-invasive technique.

In order to investigate this important processing step a cheese pressing set up was developed for a cheese of 10 cm diameter and 10 cm height, which can be inserted inside a 10 cm birdcage coil in the cavity of our vertical bore 3T MRI system.

While pressing a number of T2 measurements have been done. The T2 signals have been analysed using CONTIN and SPLMOD. The distributions show two fractions determined as water and fluid fat. The spatial information can be used to follow the fat and water distribution in the process. The distributions also give an useful tool to investigate the structure on the cheese. One typical T2 measurement of the quality needed to do this analysis takes about 7 min. Thus the different measurements can be used to follow these distributions in time with a time resolution of 7 min using a spatial resolution of $3*7.8*7.8$ mm^3. This can provide a good tool to investigate the process of pressing.

Single-shot depth profiling with a single-sided NMR sensor: Application to skin measurements

Ernesto Danieli[1] , Juan Perlo[1], Federico Casanova[1], and Bernhard Blümich[1]

[1] ITMC - RWTH-Aachen Worringerweg 1, D52056 Aachen, Germany

Abstract:

Portable open NMR probes built from permanent magnets offer several advantages over conventional NMR systems, they are small in size, low in cost and robust. However, the open geometry of the magnets brings associated a number of challenging limitations. The strong stray field gradient of such sensors limits the thickness of the sensitive slice to be much below one millimeter, imposing an important restriction to the experimental time required to profile large depth ranges into the sample [1]. In this work we exploit the concept of field shimming by means of a shim unit based on permanent magnet blocks [2] to strongly reduce the magnetic field gradient along the depth direction while keeping under control the lateral components. Under these conditions depth profiles over a range of some millimeters are measured with a resolution of 50 μm in a single-shot as the Fourier transform of the echo signal acquired in the presence of a static gradient of about 1 T/m. The increment in the thickness of the sensitive volume eliminates the need for repositioning the sensor with respect to the object allowing us to cover the whole depth range in a single measurement. An important advantage of this new magnet design is that - by proper design of the shim unit- the reduction in the static gradient is not achieved at expenses of a strong reduction in the magnitude of the average field, a price usually paid in conventional designs. The field of the first prototype is about 0.3 T, which is comparable to the field generated by a previous sensor of the same size [3].

1. J. Perlo, F. Casanova, and B. Blümich, Profiles with microscopic resolution by single-sided NMR, *J. Magn. Reson.* **176** (2005) 64.
2. J. Perlo, F. Casanova, and B. Blümich, Ex Situ NMR in Highly Homogeneous Fields: [1]H Spectroscopy, *Science* **315** (2007) 1110.
3. J. Perlo, F. Casanova, and B. Blümich, 3D imaging with a single-sided sensor: an open tomograph, J. *Magn. Reson.* **166** (2004) 228.

Improving the field homogeneity of a Halbach array using an efficient shim unit based on permanent magnets

Ernesto Danieli, Jörg Mauler, Juan Perlo, Federico Casanova, and Bernhard Blümich

Institut für Makromolekulare Chemie, RWTH-Aachen, Worringerweg 1, D-52056 Aachen, Germany

The practice of NMR usually involves the use of large magnets producing homogeneous static magnetic fields suitable to obtain information about the spatial distribution, molecular structure and dynamics for a wide range of materials. For many applications, however, it would be useful to carry out magnetic resonance spectroscopy and imaging on small mobile NMR devices. Among the different alternatives, the Halbach geometry is particularly convenient because it generates a considerable strong magnetic field keeping at the same time a large bore size to positioning the sample [1,2]. Moreover, it generates a magnetic field transverse to the longitudinal axis allowing the use of sensitive solenoid radiofrequency coils to excite and detect NMR signals. Although, in theory, this magnet geometry should provide a quite homogeneous field, in practice, the inhomogeneity of the magnetic material (hardly better than one per cent), plus the inaccuracy in the size and positioning of the pieces in the final array, lead to important field distortions.

Recently, we have shown that the important field inhomogeneities present in single-sided magnets can be compensated by means of a shim unit built from movable permanent magnet blocks [3]. This approach has proven to give enough degree of control to shim the field even to the sub ppm limit. In this work we exploit this concept to correct the field of a Halbach array in order to extend the working volume size. In particular, we show that using four pairs of relatively small blocks placed inside the magnet bore and next to the main rings, the size of the sensitive volume can be increased up to two orders of magnitude. The magnet was equipped with a three-axis gradient coil system to provide the sensor with imaging capabilities. The 32 cm in diameter and 30 cm long portable tomograph uses is suitable to study samples up to 4 cm in diameter and 4 cm long.

1. K. Halbach, Design of permanent multipole magnets with oriented rare earth cobalt material, Nucl. Instr. Meth. 169, 1 (1980).

2. H. Raich, P. Blümler, Design and construction of a dipolar Halbach array with a homogeneous field from identical bar magnets: NMR mandhalas, Concepts Magn. Reson. B 23B (1) 16 (2004).

3. J. Perlo, F. Casanova, and B. Blümich, Ex Situ NMR in Highly Homogeneous Fields: [1]H Spectroscopy, Science 315, 1110 (2007).

Investigation of coated particle boards with the *profile* NMR-MOUSE

Wolfgang Schoefberger[2], Primoz Petek[1], Jürgen Kolz[3], Bernhard Blümich[3], and Andreas Kandelbauer[1]

[1] Wood Carinthian Compentence Center (W3C), St. Veit/Glan, Austria
[2] Institute Organic Chemistry, Johannes Kepler Universität, Linz, Austria
[3] Institute for Technical and Macromolecular Chemistry, RWTH Aachen, Germany

Abstract:

Particle boards coated with MF resin impregnated paper sheets are used in the wood based panel industry as decorative surfaces for construction and furniture in interior and exterior applications. For interior use, besides having an appealing surface they must be resistant towards chemicals and display high abrasion and scratch resistance. Furthermore, they must be easy to clean. For exterior use, additional properties such as weatherability, light stability and durability are required. These properties are strongly related to the curing degree of the resin and the structure of the interface paper/board. In order to analyse the structure of the joint and the effect of different process parameters on its properties a set of boards with systematically varied curing degree was analysed using the *profile* NMR-MOUSE.

Due to its specially designed magnet geometry the *profile* NMR-MOUSE provides a technique that enables one to achieve high resolution depth profiles, that can be used to study the structure of the joints. Figure 1 shows the *profile* MOUSE mounted in a high precision lift, which is used to move the sensitive volume of the sensor through the object under investigation. The lift is equipped with a stepper motor and fully automated, so that a manual repositioning between measurements at different depths is not required.

Using this set up a set of paper coated particle boards with different concentrations of hardener in the resin, was investigated. Figure 2 shows the achieved profiles. From the profiles three different layers, paper, wood, and interphase can be distinguished as well as their thickness can be determined. Furthermore the effect of different hardener concentrations can be observed by introducing a T_1- contrast into the profiles. Since a higher hardener concentration results in a higher crosslink density of the resin, the longitudinal relaxation time T_1 decreases with increasing amount of hardener.
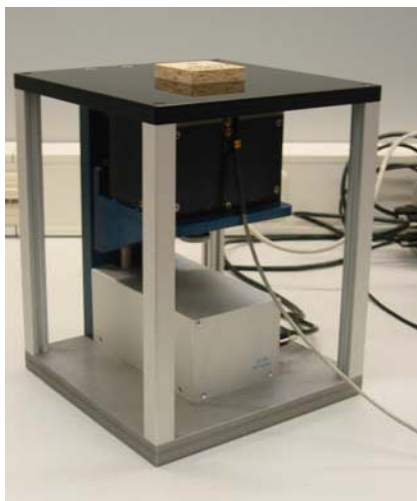
Fig. 1. Profile MOUSE mounted in automated lift.
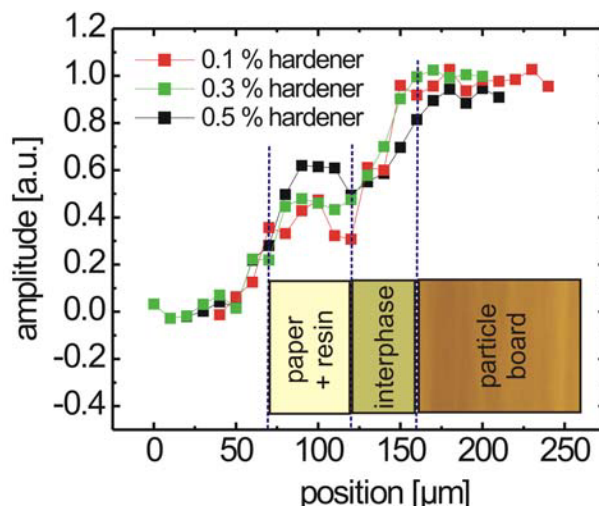
Fig. 2. Profiles through particle board samples with different amount of hardener.

Authors ICMRM 2007

T# = Talk, P# = Poster

Name	Initials	Contribution
Abdelmoumene	S.	P95
Acosta	R. H.	T43, T65
Adachi	S.	P16
Adams	A.	P55
Adams	M.	P55
Adolphi	N. L.	P92
Adriaensen	H.	T29
Agulles Pedrós	L.	T43, T65
Akpa	B. S.	P86
Al	T.	P45
Alecci	M.	P2
Almstedt	R.	P118
Alonso Lopez	M.	P19
Altobelli	S. A.	P102
Amar	A.	P22, P67
Anadon	L. D.	T56
Anferova	S.	P43
Anwar	M. S.	T61
Appelt	S.	T69
Aptaker	P. S.	T17
Ardelean	I.	P44
Armstrong	B.	T62
Arns	C. H.	T14
Aussenhofer	S.	P99
Bagusat	F.	P84
Baias	M.	T8, P53, P56
Baker	A.	P15
Balcom	B. J.	T28, P12, P13, P20, P33, P41, P45, P54, P65, P78, P79, P90, P114, P119, P120, P121
Barber	A.	P99
Barlow	M. J.	T63
Basser	P. J.	P24, P25
Bauer	W.	P34, P42
Beckham	H. W.	T32
Behr	V. C.	P1, P8
Bencsik	M.	T29, P48
Benecke	M.	P11
Bernhardt	A.	T24
Beyea	S. D.	T34, P93
Bidthanapally	A.	P108
Blinc	A.	P106
Blümich	A.	P57
Blümich	B.	T1, T8, T10, T12, T38, T69, P14, P22, P43, P53, P55, P56, P57, P61, P62, P63, P67, P70, P72, P75, P89, P104, P123, P124, P125

Name	Initials	Contribution
Blümler	P.	T16, T65, P23, P110
Bogdan	M.	P44
Böhme	U.	P26, P84
Bonardi	E.	P28
Borisjuk	L.	T55, P112
Bouchard	L. S.	T12, T61, P31
Braginski	A. I.	P21
Bray	J. M.	T34, P93
Breuer	F.	P10
Brewer	S.	T29
Britton	M. M.	T58
Broadbent	A. L.	P68
Brosten	T. R.	P69
Brown	J. R.	T41, P68, P77
Bryant	H. C.	P92
Budker	D.	T67
Buhai	B.	T26
Bühler	J.	P23, P110
Buljubasich	L.	P70
Burt	S. R.	T61
Bussandri	A.	T15
Callaghan	P. T.	T3, T9, T14, T37, T42, T44, T70, P6, P73
Cammenga	H. K.	P116
Canina	D.	P28, P32
Capitani	D.	T6
Carminati	S.	P81
Casanova	F.	T10, T38, P53, P14, P22, P61, P67, P89, P123, P124
Centeno	S.	T5
Chandrasekera	T. C.	P27
Cho	H.	T13, P50
Choi	Y. J.	T23
Chow	W.	P96
Ciampi	E.	P94
Ciarrocchi	M.	P2
Ciobanu	L.	T20
Clarke	J.	T66
Codd	S. L.	T31, T41, P68, P69, P74, P77
Cokelet	G. R.	T41, P74
Collienne	C.	P4
Collins	S. D.	T23
Cornelius	F.	P52
Coy	A.	T37
Cozzolino	S.	T6
Craven	B. A.	P100
Crawford	C.	T67
Crépin	J.	P95

Authors ICMRM 2007

T# = Talk, P# = Poster

Name	Initials	Contribution
Dahlberg	C.	P58
Danieli	E.	P123, P124
Darrasse	L.	P9
Datsevich	L. B.	P70
Davies	C. J.	T33, P71
de Ropp	J. S.	T23
Del Federico	E.	T5
Demas	V.	T12, T24, P31
Demco	D. E.	P61
Demir	E.	P104
Dennis	J. S.	P76
Denoth	S.	T36
Di Miccoli	V.	P2
Doraisamy	L.	T15
Dunckley	C. P.	T56, P83
Dvinskikh	S. V.	P58, P59
Dvoyashkin	M.	T27
Dykstra	R.	T19, T37, T70
Eccles	C. D.	T37, T70
Egelandsdal	B.	P121
Ehses	P.	P10
Englert	S.	P72
Espy	M. A.	T68
Evans	L.	T24
Faber	C.	T11, P8, P38, P97
Fathima	N. N.	P56
Feindel	K. W.	P73
Ferencz	R.	P61
Ferrante	G.	P28, P32
Fey	M.	T36, P39
Fidler	F.	P18
Filiaggi	M.	T34, P93
Fischer	A.	P98
Fischer	C.	P116
Flentje	M.	T55
Flynn	E. R.	P92
Fordham	E. J.	P47
Franchi	D.	P29
Franck	J.	T12, T24, P31
Fridjonsson	E. O.	T41, P74
Fukushima	E.	T2, T18, P102
Fureby	A.	P58
Furó	I.	P49, P58, P59
Gädke	A.	P3, P30, P54
Gagey	O.	P95
Galante	A.	P2
Galvosas	P.	T9
Garcia	S.	T22
Gardner	T.	P99
Gareis	D.	P10, P19
Garnov	N.	P60
Garny	K.	P80
Gerkema	E.	T40, P115
Gessler	M.	P98
Ginefri	J.-C.	P9
Girard	O.	P9
Gladden	L. F.	T56, P47, P71, P76, P83, P85, P86
Glaser	S. J.	P40
Glückler	H.	P4, P5
Goga	N. O.	P61
Goloshevsky	A. G.	T23
Golzi	P.	P28, P32
Gong	Q.	P75
Goudappel	G. J. W.	P109
Granwehr	J.	T22
Gratz	M.	T9
Graziani	D.	P31
Graziani	N.	T12
Griffith	J.D.	T33
Gross	D.	T35
Gründer	W.	P60
Guarneri	A.	P81
Guillot	G.	P9, P36, P95
Haber-Pohlmeier	S.	P46
Haesner	M.	P80
Haishi	T.	T45, T46, P7, P16, P66
Halse	M. E.	T37, T44, P6
Han	H.	P33
Han	S.-I	T22, T62
Handa	S.	T45, T46, P7, P16
Hardy	E. H.	P37
Harel	E.	T22
Häsing	F. W.	T69
Helluy	X.	P34, P96
Herberg	J.	T24
Hilty	C.	T22
Hippmann	T.	P18
Hirai	S.	P87
Hoerr	V.	P97
Höfener	T.	P75
Holland	D. J.	T56, P76
Holmes	W. M.	P73
Homan	N.	T40
Horn	H.	P80
Hornemann	J. A.	P77
Huang	Z.	T56
Hunger	K.	P62, P63
Hunter	M. W.	T14, T37, T42, T70, P6
Hürlimann	M. D.	T52
Imaizumi	Y.	P105
Ito	K.	P66
Jackson	A. N.	T42

Authors ICMRM 2007

T# = Talk, P# = Poster

Name	Initials	Contribution	Name	Initials	Contribution
Jahnke	S.	P23, P110	Lysova	A. A.	T64, P77
Jakob	P. M.	T50, T55, P1, P10, P18, P19, P34, P42, P96, P98, P103, P112, P116, P117	Macaskie	L.	P85
			MacGregor	R. P.	P20
			MacMillan	B.	P90
			Maddinelli	G.	P81
Javaux	M.	P115	Mair	R. W.	T63
Jenkins	G. M.	P120	Malba	V.	T24
Jerschow	A.	T5	Mang	T.	P62, P63
Jess	A.	P70	Mantle	M. D.	T56
Johns	M. L.	T33, P27, P47, P85, P86, P113	Manz	B.	T7, P11, P80
			Marble	A. E.	P12, P13, P20, P54, P65, P90, P119, P120
Josephson	E. M.	P100			
Kalouche	I.	P95	Marica	F.	P45, P121
Kampf	T.	P34, P42	Martin	J.	T28
Kandelbauer	A.	P125	Martini	G.	P32
Kärger	J.	T27	Massin	C.	T36
Kennett	M.	P99	Mastikhin	I. V.	T60, P12, P13, P54, P64, P65, P114, P119, P120
Khokhlov	A.	T27			
Khomichev	A. V.	T64, P35			
Kimmich	R.	T26	Matlashov	A. N.	T68
King	A.	P64	Mauler	J.	P14, P124
Klankermayer	J.	P75	Maxwell	R.	T24
Koen	K.	T22	Mc Hale	G.	T29
Köllisch	U.	P8	McCarney	E.	T62
Kolz	J.	T38, P61, P62, P63, P125	McCarthy	M. J.	T23, T54
			McDonald	P. J.	T17, P94
Koptyug	I. V.	T61, T64, P35, P91	McDonnell	E. E.	T22
Kose	K.	T45, T46, P7, P16, P101	McDowell	A.	T21
			Melkus	G.	T55
Kotaka	T.	P87	Menzel	M. I.	P23, P51, P110, P115, P118
Kovtunov	K. V.	T61, T64			
Kraus	R. H. Jr.	T68	Mercier	O.	T70
Krause	H.-J.	P21	Merela	M.	P111
Kühn	H.	T69	Mertens	D.	P37
Kusmia	S.	P9, P36	Michalak	D.	T67
Lanagan	M.	P15	Mietchen	D.	T7
Lang	E.	P98	Mikac	U.	P111
Larson	R. S.	P92	Milczarek	R.	T54
Lasič	S.	T59	Minwuyelet	S.	P110
Ledwig	M.	P18	Mitchell	J.	P47
Lehmann	V.	T35	Mohoric	A.	T51, T59
Leisen	J.	T32	Morris	R.	P48
Leitner	W.	P75	Morrison	E. E.	P100
Li	C.-H.	T63	Mosher	J. C.	T68
Li	L.	P78, P79	Müller	C. R.	T56, P76
Li	Y.	T26	Münnemann	K.	T8, P53
Lindhoud	S.	P88	Murakami		P105
Lingwood	M.	T62	Nestle	N.	P3, P30, P48, P54, P65
Lizhi	X.	T4			
Lopez	M.A.	P10	Neu	T. R.	P80
López-González	M. R.	P73	Neuberger	T.	P15, P99, P100, P112
Lovato	D.	P92			

Authors ICMRM 2007

T# = Talk, P# = Poster

Name	Initials	Contribution	Name	Initials	Contribution
Nevo	U.	P24, P25	Qiu	L. Q.	P21
Newling	B.	T60, P64, P79, P82	Quriadov	A. V.	P33
Nguyen	T.	T56	Ramos Cabrer	P.	T51
Niendorf	T.	T48	Ramsami	T.	P56
Nissler	H.	P65	Rasburn	J.	P113
Nydén	M.	T41, P109	Reimer	J. A.	T24, T30
Oehmichen	T.	P70	Ren	X.	T13
Oerther	T.	T35	Richter	E.-J.	P19, P103
Ogawa	K.	P66	Roa	A.	T23
Ogino	T.	P105	Roeb	G.	P110
Ongsurakul	S.	P78	Rokitta	M.	P112
Oppell	P.	P104	Rolletschek	H.	T55, P112
Oros-Peusquens	A. M.	P107	Romanenko	K. V.	P69
Ortmanns	T.	P5	Romero-Zerón	L.	P78
Oven	P.	P111	Rommel	E.	P17
Oya	K.	P101	Rosen	M. S.	T63
Özarslan	E.	P24, P25	Rosenstihl	M.	P3
Ozeki	T.	P16	Rottner	K.	P19, P103
Pallua	N.	P104	Rühli	F.	T8, P53
Parasoglou	P.	P113	Rutten	T.	P112
Parkinson	B.	T37	Sagdeev	R. Z.	T61
Parnau	A.	P44	Sagidullin	A.	P49
Patterson	E. G.	P100	Sanfratello	L.	P102
Patterson-Beadle	M.	P85	Sankey	M.	P82, P83
Patz	S.	T63	Satterfield	E. T.	P40
Paulsen	J. L.	T12	Scharr	H.	P23
Peerenboom	H.	P4	Scheidegger	R.	T63
Perlo	J.	T8, T10, T38, P53, P123, P124	Scheler	U.	P26, P84
			Schenkel	M.	T36
Perrie	Y.	P48	Schinabeck	M.	P54
Petek	P.	P125	Schmid	F.	P19, P103
Petrone	C.	T34, P93	Schmidig	D.	T36
Petrov	O. V.	P59, P114	Schmidt	J.	T43
Piechatzek	A.	P55	Schmiedeskamp	J.	T43, T65
Pierce	K. L.	T22	Schmitt	C.	P3
Pines	A.	T12, T22, T24, T61, T67, P31	Schmitz	H. M.	P4
			Schneider	H. U.	P118
Pitts	S.	P94	Schneider	J. T.	T11, P38
Placidi	G.	P29	Schoefberger	W.	P125
Planinšič	G.	T59	Schönhoff	M.	T9
Pohlmeier	A.	P46, P51, P115	Schröder	M.	P104
Poirier-Quinot	M.	P9	Schuleit	M.	P58
Polders	D.	P122	Schulze-Till	T. D.	P116, P117
Polello	M.	P28	Schurr	U.	P110
Pop	V.	P44	Sederman	A. J.	T33, T56, P47, P76, P83
Popescu	C.	P55			
Powell	H.	P113	Segre	A. L.	T6
Prado	P. J.	T15	Seiberlich	N.	P10
Proietti	N.	T6	Sell	J.	P18
Promislow	K.	T28, P90	Semouchkina	E.	P15
Prosiegel	K.	P54	Seo	Y.	P105
Purea	A.	P97	Sepe	A.	P111
Qiao	Y.	T9			

Authors ICMRM 2007

T# = Talk, P# = Poster

Name	Initials	Contribution	Name	Initials	Contribution
Serša	I.	T59, P106, P111	Veliyulin	E.	P119, P120, P121
Settles	G. S.	P100	Venne	B. B.	P122
Seymour	J. D.	T41, T70, P68, P69, P74, P77	Vereecken	H.	P51, P115
			Vergeldt	F. J.	T40, T53, P88, P115, P122
Shah	N. J.	P107	Vincent	F.	T36
Shiota	K.	P101	Voda	M. A.	P89
Sieling	U.	T69	Volegov	P. L.	T68
Sigmund	E. E	T13	Volke	F.	T7, P11, P80
Sillerud	L. O.	P92	Völkel	R.	P54
Singleton	S.	P94	Voll	S.	P10
Smith	N. B.	P99	von der Schulenburg	D. A. G.	P85, P86
Soltner	H.	T16, P5	von Waldburg	H.	T8, P53
Song	Y.-Q.	T13, T25, P50	Wakamatsu	H.	P105
Sophie	S. W.	P69	Wald	L. L.	T47
Sotgiu	A.	P2, P29	Walsworth	R. L.	T63
Southern	T.	T19	Walton	J. H.	T23
Speck	O.	T49	Wang	H.	T28
Spiess	H. W.	T43, T65	Washburn	K. E.	T14
Spindler	N.	P118	Webb	A. G.	P15, P99, P100, P112
Spruijt	E.	P88			
Stapf	S.	T57, P46, P51, P70, P72, P89	Weber	S.	P110
			Weglarz	W.	T51
Stepišnik	J.	T59	Weiger	M.	T36, P39
Stingaciu	L.	P51	Weisser	A.	T39
Stork	H.	P3	Wiggins	G. C.	T47
Streun	M.	P110	Windt	C.	T51
Sturm	V.	P52	Woelk	K.	P40
Takamata	A.	P105	Wolferink	W. J.	P88
Talnishnikh	E.	P43, P56	Wutz	K.	P54
Telkki	V.-V.	T22	Xia	Y.	P108
Tratar	G.	P106	Xu	S.	T67
Tromp	R. H.	P88	Yamazaki-Kleps	A.	T5
Tsai	L. L.	T63	Yokoi	M.	P105
Tsushima	S.	P87	Zahneisen	B.	P38
Tyagi	V.	P15	Zänker	P. P.	T43
Tymofiyeva	O.	P19, P103	Zeng	Y.	P39
Ulbrich	A.	P118	Zhang	Y.	P21
Utsuzawa	S.	T18	Zhang	Z.	T28, P20, P33, P41, P90
Vacchi	C.	P28, P32			
Valiullin	R.	T27	Zheng	S.K.	P108
Van As	H.	T40, T51, T53, P88, P115, P122	Zhi	Y.	P82
			Zhivonitko	V. V.	T64, P91
Van Der Werff	M.	T19	Zick	K.	T35
van Dusschoten	D.	T53, P51, P110, P115, P118	Zielinski	L.	T25
			Ziemons	K.	P110
van Duynhoven	J. P. M.	T51, P109	Ziener	C.	P34, P42
van Ginkel	M.	P94	Zotev	V. S.	T68
Vanderborght	J.	P115			
Vangala	A.	P48			

Participants ICMRM 2007

Name	Firstname	University / Institute	Country	email
Adams	Alina	RWTH Aachen	Germany	aadams@mc.rwth-aachen.de
Adams	Michael	RWTH Aachen	Germany	adams@mc.rwth-aachen.de
Adriaensen	Hans	Nottingham Trent University (NTU)	United Kingdom	hans.adriaensen@ntu.ac.uk
Agulles Pedrós	Luis	Max Planck Institut for polymer research	Germany	agulles@mpip-mainz.mpg.de
Alexey	Khomichev	International Tomographic Center	Russia	khomichev@tomo.nsc.ru
Amar	Andrea	ITMC, RWTH-Aachen	Germany	aamar@mc.rwth-aachen.de
Amber Broadbent	Amber	Montana State University	United States	amber.broadbent@coe.montana.edu
Andrei Matlashov	N.	Los Alamos National Laboratory	USA	matlachov@lanl.gov
Anferova	Sophia	ITMC, RWTH Aachen University	Germany	sanferova@mc.rwth-aachen.de
Appelt	Stephan	Forschungszentrum Jülich	Germany	st.appelt@fz-juelich.de
Aptaker	Peter	Lapalcian Limited	UK	psa@laplacian.co.uk
Ardelean	Ioan	Technical University from Cluj-Napoca	Romania	ioan.aredelean@phys.utcluj.ro
Arns	Christoph	Australian National University	Australia	christoph.arns@anu.edu.au
Baias	Maria Antoaneta	RWTH-Aachen	Germany	mbaias@mc.rwth-aachen.de
Balcom	Bruce	University of New Brunswick	Canada	bjb@unb.ca
Basser	Peter	NIH / NICHD	USA	pjbasser@helix.nih.gov
Behr	Volker	Experimental Physics 5, University of Würzburg	Germany	behr@physik.uni-wuerzburg.de
Bencsik	Martin	Nottingham Trent University (NTU)	United Kingdom	martin.bencsik@ntu.ac.uk
Beyea	Steven	NRC, Institute for Biodiagnostics	Canada	steven.beyea@nrc.gc.ca
Blümich	Bernhard	RWTH Aachen University	Germany	bluemich@mc.rwth-aachen.de
Blümich	Adrian	RWTH Aachen	Germany	adrian@bluemich.net
Blümler	Peter	Research Center Jülich	Germany	p.bluemler@fz-juelich.de
Böhme	Ute	Leibniz Institute of Polymer Research Dresden	Germany	boehme-ute@ipfdd.de
Bouchard	Louis	Institut: University of California-Berkeley	USA	louis.bouchard@gmail.com
Breuer	Felix	Research Center Magnetic Resonance Bavaria (MRB)	Germany	breuer@mr-bavaria.de
Britton	Melanie	Birmingham University	United Kingdom	m.m.britton@bham.ac.uk
Brosten	Tyler	Montana State University	USA	tyler.brosten@coe.montna.aedu
Brown	Jennifer	Montana State University	USA	jbrown@coe.montana.edu
Buljubasich	Lisandro	RWTH-Aachen	Germany	lbuljubasich@mc.rwth-aachen.de
Callaghan	Paul	MacDiarmid Institute	New Zealand	paul.callaghan@vuw.ac.nz
Capitani	Donatella	Institute of Chemical Methodologies	Italy	donatella.capitani@imc.cnr.it
Casanova	Federico	RWTH-Aachen	Germany	fcasanova@mc.rwth-aachen.de
Chandrasekera	Thusara	University of Cambridge	United Kingdom	tcc23@cam.ac.uk
Ciampi	Elisabetta	Unilever	United Kingdom	Elisabetta.Ciampi@unilever.com
Ciarrocchi	Manola	University of l'Aquila	italy	manola.ciarrocchi@univaq.it
Ciobanu	Luisa	Pfizer Inc.	USA	luisa.ciobanu@gmail.com
Clarke	John	University of California	USA	jclarke@berkeley.edu
Codd	Sarah	Montana State University	USA	scodd@coe.montana.edu

Participants ICMRM 2007

Name	Firstname	University / Institute	Country	email
Coy	Andrew	Magritec Limited	New Zealand	andrew@magritek.com
Cross	David	RototecSpintec GmbH	Germany	cross@rototec-spintec.com
Dahlberg	Carina	Institute for Surface Chemistry	Sweden	carina.dahlberg@surfchem.kth.se
Danieli	Ernesto	RWTH-Aachen	Germany	edanieli@mc.rwth-aachen.de
Danilo	Franchi	University of L'Aquila	Italy	franchi.danilo@yahoo.it
Davies	Colin	University of Cambridge	UK	cjd46@cam.ac.uk
Del Federico	Elenora	Pratt Institute/ Math and Science	USA	edelfede@gmail.com
Demas	Vasiliki	Lawrence Livermore National Labs	USA	demas2@llnl.gov
Demco	Dan Eugen	RWTH Aachen	Germany	demco@mc.rwth-aachen.de
Dvinskikh	Sergey	Royal Institute of Technology	Sweden	sergey@physchem.kth.se
Englert	Sven	RWTH Aachen	Germany	senglert@mc.rwth-aachen.de
Feindel	Kirk	Victoria University of Wellington	New Zealand	kfeindel@gmail.com
Ferreira Martins	Joao	RWTH-Aachen	Germany	jmartins@mc.rwth-aachen.de
Fey	Michael	Bruker BioSpin AG	Switzerland	michael.fey@bruker-biospin.ch
Fidler	Florian	Forschungszentrum Magnet-Resonanz-Bavaria	Germany	fidler@mr-bavaria.de
Fordham	Edmund	Schlumberger Cambridge Research	England	fordham1@slb.com
Franck	John	UC Berkeley	USA	franck@berkeley.edu
Fridjonsson	Einar Orn	Montana State University	USA	efridjonsson@coe.montana.edu
Fukushima	Eiichi	ABQMR	USA	eiichi@abqmr.com
Gädke	Achim	Institute of Condensed Matter Physics	Germany	achim.gaedke@physik.tu-darmstadt.de
Garnov	Nikita	University of Leipzig	Germany	nikita.garnov@medizin.uni-leipzig.de
Giuseppe	Maddinelli	ENI Spa	Italy	giuseppe.maddinelli@eni.it
Gladden	Lynn	University of Cambridge	United Kingdom	Gladden@cheng.cam.ac.uk
Glückler	Harald	Forschungszentrum Jülich GmbH	Germany	h.glueckler@fz-juelich.de
Goga	Nicolae	RWTH Aachen	Germany	ngoga@mc.rwth-aachen.de
Gong	Qingxia	RWTH-aachen	germany	qgong@mc.rwth-aachen.de
Graf von der Schulenburg	Daniel	MRRC, Cambridge University	UK	dawg2@cam.ac.uk
Green	Dan	Varian, Inc.	United Kingdom	dan.green@varianinc.com
Grinberg	Farida	University of Leipzig	Germany	grinberg@uni-leipzig.de
Grodjinejad	Ali	Forschungszentrum Jülich	Germany	a.gardiinejad@fz-juelich.de
Gross	Dieter	Bruker-Biospin GmbH	Germany	dieter.gross@bruker-biospin.de
Guillot	Genevieve	CNRS, U2R2M, UMR8081	France	genevieve.guillot@u-psud.fr
Guthausen	Gisela	Bruker Optik	Germany	gisela.guthausen@bruker.de
Haber-Pohlmeier	Sabrina	RWTH Aachen	Germany	s.haber-pohlmeier@fz-juelich.de
Halse	Meghan	Victoria University of Wellington	New Zealand	meghan@magritek.com
Hardy	Edme Horst	Universität Karlsruhe	Germany	Edme.Hardy@mvm.uni-karlsruhe.de
Harel	Elad	UC Berkeley		

Participants ICMRM 2007

Name	Firstname	University / Institute	Country	email
Harms	Silke	RWTH Aachen	Germany	sharms@mc.rwth-aachen.de
Häsing	Wolfgang	Forschungszentrum Jülich	Germany	f.haesing@fz-juelich.de
HATTORI	Mineyuki	National Institute of Advanced Industrial Science and Technology	Japan	mineyuki.hattori@aist.go.jp
Helluy	Xavier	University of Wuerzburg	Germany	xavier.helluy@physik.uni-wuerzburg.de
Herberg	Julie	Lawrence Livermore National Laboratory	USA	herberg1@llnl.gov
Hill	Stefan	Scion	New Zealand	stefan.hill@scionresearch.com
Hilty	Christian	Texas A&M University	USA	chilty@mail.chem.tamu.edu
Hippmann	Toni	FH Würzburg-Schweinfurt	Germany	tonihippmann@web.de
Holland	Daniel	University of Cambridge	United Kingdom	djh79@cam.ac.uk
Hopper	Tim	Schlumberger	USA	thopper@boston.oilfield.slb.com
Hornemann	Jennifer	Montana State University	USA	jhornemann@erc.montana.edu
Hörr	Verena	University of Würzburg	Germany	verena.hoerr@mail.uni-wuerzburg.de
Hörr	Verena	University Würzburg	Germany	
Hunger	Katharina	RWTH Aachen	Germany	khunger@mc.rwth-aachen.de
Hunter	Mark	MacDiarmid Institute	New Zealand	mark.hunter@vuw.ac.nz
Hurlimann	Martin	Schlumberger -Doll Research	USA	hurlimann@slb.com
Jaehyuk	Lee	University of Cambridge	United Kingdom	jl446@cam.ac.uk
Jakob	Peter	University of Würzburg	Germany	ep5-sek@physik.uni-wuerzburg.de
Johns	Michael Leslie	University of Cambridge	UK	mlj21@cam.ac.uk
Kampf	Thomas	University of Wuerzburg	Germany	thomas.kampf@physik.uni-wuerzburg.de
Kimmich	Rainer	Bureau NMR-Ulm	Germany	rainer.kimmich@nmr-ulm.de
Köllisch	Ulrich	University of Würzburg	Germany	uli.koellisch@web.de
Köllisch	Ullrich	University of Würzburg	Germany	
Kolz	Jürgen	RWTH Aachen	Germany	jkolz@mc.rwth-aachen.de
Koptyug	Igor	International Tomography Center	Russia	koptyug@tomo.nsc.ru
Kose	Katsumi	University of Tsukuba	Japan	kose@bk.tsukuba.ac.jp
Kovtunov	Kirill	International Tomography Center	Russia	kovtunov@tomo.nsc.ru
Kueppers	Markus	RWTH Aachen	Germany	mkueppers@mc.rwth-aachen.de
Kusmia	Slawomir	U2R2M UMR8081 CNRS	France	slawomir.kusmia@u-psud.fr
Lang	Esra	University of Wurzburg	Germany	esralang@physik.uni-wuerzburg.de
Langlais	Denis	TECMAG	USA	dlanglais@tecmag.com
Ledwig	Michael	University of Würzburg	Germany	michael.ledwig@physik.uni-wuerzburg.de
Leisen	Johannes	Georgia Institute of Technology School of Polymer	USA	johannes.leisen@ptfe.gatech.edu
Li	Linqing	University of New Brunswick	Canada	z51he@unb.ca
Lopez Terrones	Marcos Alonso	Universirty of Wuerzburg	Germany	mslopez@physik.uni-wuerzburg.de

Participants ICMRM 2007

Name	Firstname	University / Institute	Country	email
Manz	Bertram	Fraunhofer-IBmT	Germany	bertram.manz@ibmt.fraunhofer.de
Marble	Andrew	University of New Brunswick	Canada	andrew.marble@unb.ca
Marica	Florea	University of New Brunswick	Canada	fmarica@unb.ca
Marrufo Melendez	Oscar Rene	University of Würzburg	Germany	omm_oscar@yahoo.com
Martin	Dave	AstraZeneca	UK	dave.martin@astrazeneca.com
Mastikhin	Igor	University of New Brunswick	Canada	mast@unb.ca
Mauler	Joerg	RWTH Aachen	Germany	jmauler@mc.rwth-aachen.de
McCarthy	Michael	University of California	USA	mjmccarthy@ucdavis.edu
McDonald	Peter	University of Surrey	UK	p.mcdonald@surrey.ac.uk
McDowell	Andrew	ABQMR, Inc.	USA	mcdowell@abqmr.com
Melian Flamand	Claudiu	RWTH Aachen	Germany	cmelian@mc.rwth-aachen.de
Melkus	Gerd	University of Würzburg	Germany	melkus@physik.uni-wuerzburg.de
Mertens	Dirk	Universität Karlsruhe	Germany	dirk.mertens@mvm.uni-karlsruhe.de
Mikac	Urša	Jožef Stefan Institute	Slovenia	Urska.mikac@ijs.si
Milczarek	Rebecca	University of California	USA	rmilczar@ucdavis.edu
Milczarek	Rebecca	University of California	USA	rmilczar@ucdavis.edu
Mitchell	Jonathan	University of Cambridge	UK	jm600@cam.ac.uk
Morris	Robert	Nottingham Trent University (NTU)	United Kingdom	rob.morris@ntu.ac.uk
Neuberger	Thomas	Penn State University	USA	tneu@engr.psu.edu
Newling	Ben	University of New Brunswick	Canada	bnewling@unb.ca
Ogawa	Kuniyasu	Keio University	Japan	ogawa@mech.keio.ac.jp
Oya	Kazuki	University of Tsukuba	Japan	ohya@mrlab.frsc.tsukuba.ac.jp
Ozeki	Toshihiro	Hokkaido University of Education	Japan	oze@iwa.hokkyodai.ac.jp
Perlo	Juan	ITMC, RWTH-Aachen	germany	jperlo@mc.rwth-aachen.de
Petrov	Oleg V.	University of New Brunswick	Canada	opetrov@unb.ca
Pirnau	Adrian	Babes-Bolyai University	Romania	apirnau@phys.ubbcluj.ro
Pitts	Simon	University of Surrey	United Kingdom	s.pitts@surrey.ac.uk
Pohlmeier	Andreas	Forschungszentrum Jülich	Germany	a.pohlmeier@fz-juelich.de
Prado	Pablo	GE Security	USA	pablo.prado@ge.com
Prodromos Parasoglou	Prodromos	University of Cambridge	UK	pap31@cam.ac.uk
Qiu	Longqing	Forschungszentrum Juelich	Germany	l.qiu@fz-juelich.de
Ren	Xiaohong	Schlumberger-Doll Research	USA	xren@boston.oilfield.slb.com
Robin	Dykstra	Massey University	New Zealand	R.Dykstra@massey.ac.nz
Rommel	Eberhard	Universität Würzburg	Germany	rommel@physik.uni-wuerzburg.de
Sagidullin	Alexander	Royal Institute of Technology (KTH)	Sweden	alexandr@physchem.kth.se
Sankey	Mark	University of Cambridge	UK	mhs28@cam.ac.uk
Scheler	Ulrich	Leibniz Institute of Polymer Research Dresden	Germany	scheler@ipfdd.de

Participants ICMRM 2007

Name	Firstname	University / Institute	Country	email
Schmid	Florian	University of Würzburg	Germany	florian.schmid@physik.uni-wuerzburg.de
Schneider	Johannes	University of Wuerzburg	Germany	Johannes.T.Schneider@physik.uni-wuerzburg.de
Schroeder	Martin	RWTH Aachen	Germany	schroeder-martin@gmx.de
Schulze-Till	Thomas	University of Würzburg	Germany	tschulze@physik.uni-wuerzburg.de
Sell	Johannes	University of Würzburg	Germany	johannes.sell@physik.uni-wuerzburg.de
Seo	Yoshiteru	Dokkyo Medical University School of Medicine	Japan	yseo@dokkyomed.ac.jp
Sersa	Igor	Jozef Stefan Institute	Slovenia	igor.sersa@ijs.si
Seymour	Joseph D.	Montana State University	USA	jseymour@coe.montana.edu
Shah	N. Jon	Forschungszentrum Jülich GmbH	Germany	n.j.shah@fz-juelich.de
Shinya Handa	Shinya	University of Tsukuba	Japan	handa@mrlab.frsc.tsukuba.ac.jp
Shoujun Xu	Shoujun	University of Houston	USA	shoujunxu@yahoo.com
Song	Yi-Qiao	Schlumberger-Doll Research	USA	ysong@slb.com
Stapf	Siegfried	TU Ilmenau	Germany	siegfried.stapf@tu-ilmenau.de
Stepisnik	Janez	University of Ljubljana, FMF,	Slovenia	Janez.Stepisnik@fmf.uni-lj.si
Stingaciu	Laura-Roxana	Forschungzentrum	Germany	l.stingaciu@fz-juelich.de
Sturm	Volker	University of Würzburg	Germany	vrsturm@physik.uni-wuerzburg.de
Szabo	Laszlo	Babes-Bolyai University	Romania	szabolaci81@yahoo.com
Talnishnikh	Elena	RWTH Aachen	Germany	telena@mc.rwth-aachen.de
Tyler	Brosten	Montana State University	USA	tyler.brosten@coe.montana.edu
Tymofiyeva	Olga	University of Würzburg	Germany	oltymofi@physik.uni-wuerzburg.de
Utsuzawa	Shin	New Mexico Resonance	USA	shin@nmr.org
Vadim	Zotev	Los Alamos National Laboratory	USA	vzotev@lanl.gov
Valiullin	Rustem	University of Leipzig	Germany	valiullin@uni-leipzig.de
Van As	Henk	Wageningen University	The Netherlands	henk.vanas@wur.nl
van Dusschoten	Dagmar	Forschungszentrum Juelich	Germany	d.van.dusschoten@fz-juelich.de
van Duynhoven	John	Unilever Food and Health Research Institute	The Netherlands	john-van.duynhoven@unilever.com
Veliyulin	Emil	SINTEF Fisheries and Aquaculture	NORWAY	emil.veliyulin@sintef.no
Veliyulin	Emil	SINTEF Sealab, Fisheries and Aquaculture	Norway	emil.veliyulin@sintef.no
Venne	Bart	WUR	netherlands	bart.venne@wur.nl
Vergeldt	Frank	Wageningen University	The Netherlands	frank.vergeldt@wur.nl
Vladimir	Zhivonitko	International Tomography Center	Russia	v_zhivonitko@tomo.nsc.ru
Voda	Mihai Adrian	RWTH Aachen	Germany	mvoda@mc.rwth-aachen.de
Wald	Lawrence	Massachusetts General Hospital	USA	wald@nmr.mgh.harvard.edu
Walton	Jeffrey	University of California, Davis	USA	jhwalton@ucdavis.edu
Weiger	Markus	Bruker BioSpin AG	Switzerland	markus.weiger@bruker-biospin.ch

Participants ICMRM 2007

Name	Firstname	University / Institute	Country	email
Xia	Yang	Oakland University	USA	xia@oakland.edu
Xiao	Lizhi	China University of Petroleum	China	xiaolizhi@cup.edu.cn
Zänker	Paul P.	Max Planck Institut for polymer research		-
Zhang	Shelley		USA	midori2@gmail.com
Zhang	Ziheng	University of New Brunswick, MRI Centre, Dep. Of Physics	Canada	ziheng.zhang@unb.ca
Zick	Klaus	Bruker-Biospin GmbH	Germany	klaus.zick@bruker-biospin.de
Ziener	Christian	University of Würzburg /Dept. of Experimental Physics 5	Germany	ziener@physik.uni-wuerzburg.de